The Effect of Stress Changes on Wave Velocity:

Application of Stress Measurement in a Concrete Medium

M. Ouali

MSc Thesis

Structural Engineering
Concrete Structures
Delft University of Technology

Faculty of Civil Engineering and Geosciences

TU Delft ARUP

The Effect of Stress Changes on Wave Velocity:

Application of Stress Measurement in a Concrete Medium

by

M. Ouali

to obtain the degree of Master of Science
at the Delft University of Technology,
to be defended publicly on Wednesday August 11, 2021 at 02:30 PM.

Student number:	4239199	
Project duration:	January 1, 2020 – August 11, 2021	
Thesis committee:	Dr. ir. Y. Yang,	TU Delft, Chair
	Dr. D. Draganov,	TU Delft
	Dr. C. Weemstra,	TU Delft
	Ir. M. Aurik,	Arup, company supervisor

This thesis is confidential and cannot be made public until August 11, 2021.

TU Delft Delft University of Technology ARUP

Acknowledgements

بِسْمِ ٱللَّهِ ٱلرَّحْمَٰنِ ٱلرَّحِيمِ

In the name of Allah, the Most Gracious and the Most Merciful.

All praises to Allah for blessing me with the patience to persevere during these uncertain times and for granting me the strength to complete this thesis.

Working on my thesis during the pandemic has been challenging. Luckily, I have been fortunate to have had the right people around me which aided me throughout the process. First, I would like to express my gratitude to Yuguang Yang, the chair of my committee. Your guidance as well as your enthusiasm for the research topic has helped me to stay motivated during this thesis. Due to the pandemic, our meetings were less frequent than usual. Nevertheless they were always beneficial and contributed greatly to the quality of my report. I would also like to thank Deyan Draganov and Kees Weemstra for their supervision and their expertise. I really appreciate your efforts of helping me to understand the various mathematical derivations as well as your additional aid with regard to the signal processing. In addition, I would like to acknowledge the staff of the Geoscience & Engineering Laboratory, in particular Karel Heller for the support with the experiments.

After the first wave of the COVID-19 pandemic, I started an internship at Arup. I would like to express my gratitude to Daan Boddeke and Paul van Horn for offering me the possibility to complete my thesis at Arup. Special thanks to Mike Aurik for his excellent supervision and constructive feedback. Our weekly meetings have benefited the quality of my work greatly. Further, I would like to extend my thanks to the colleagues from Arup for their interest and involvement in my thesis as well as for making me feel like part of their team.

Last but certainly not least, I would like to express my appreciation and gratitude to my family. To my parents, I can not thank you enough for the great job of raising me to be the person I am today. Despite of having come from humble beginnings yourselves, you have never made me feel like I fell short of something. This milestone is as much yours as it is mine. I have to mention my fun-loving little sister. Your positive distractions have contributed to a healthy work-life balance. Finally, I would like to thank my entire family for always believing in me and for their unwavering support. I hope I have made you proud and that I will continue to do so in the future.

فَإِنَّ مَعَ العُسرِ يُسرًا ﴿٥﴾

“For indeed, with hardship will be relief”

– The Holy Qur’an [94:5]

M. Ouali
Assendelft, August 2021

Abstract

The Dutch infrastructure counts many bridges, the majority of which are built in concrete. These bridges have been designed and constructed according to safety codes. A lot of these bridges date from the previous century and have been designed conform outdated safety codes. Therefore, the main problem of these bridges is the uncertainty with regard to their structural health as well as their performance under the current loading conditions.

The application of 'smart aggregates' could potentially solve these issues. Smart aggregates refer to a network of sensors that emit and receive wave signals inside the concrete structure. These sensor are embedded within the concrete and can be implemented in both new and existing structures. The changes in the medium with regard to the stresses are reflected by the phase changes of the wave signal measured by the smart aggregates. This information allows for the monitoring of the conditions of the bridge during its lifespan. The magnitude of the stress in certain parts of the structure could then indicate the need for maintenance at an early stage, thus preventing unnecessary maintenance while preserving the safety of the bridge. This method, however, requires a thorough understanding of the wave propagation inside a concrete medium subjected to a stress state. This thesis investigates how the relative wave-velocity change of a concrete-like medium is influenced by the stresses to which it is subjected. Throughout the report this relation is referred to as the acoustoelastic effect.

The first part of the thesis is centered around the theoretical formulation of the acoustoelastic effect. During this study, the models of Murnaghan and Biot have been studied. Subsequently, their differences with respect to the fundamental assumptions have been indicated. Here, it has been found that the main difference between the two models is demonstrated by the way they regard the second-order deformation terms. Murnaghan assumed that these terms are significant and has included them in the constitutive relation. From the latter, Hughes and Kelly have derived expression for wave velocities of a stressed medium, which have been verified with experimental results. On the other hand, Biot adopted the theory of infinitesimal deformations which omits the second-order deformation terms. In addition he based his theory around the wave propagation of a bending rod and extended this model to a three-dimensional medium subjected to initial stresses. This generalisation of an approximated model has led to analytical expressions for the wave velocity of a stressed solid which are contradicted by experiments. From this comparison, it has been concluded that Murnaghan's model results in the most accurate representation of the acoustoelastic effect.

The second part of the thesis focuses on the verification of the theoretical acoustoelastic effect through experimental research. For the purpose of verifying the acoustoelastic effect as well as determining the third-order elastic coefficients of a concrete-like medium, four specimens have been tested. In order to investigate the influence of the inhomogeneity of the material on the changes in the wave velocity, two different material compositions have been investigated. The first type consists of a homogeneous cement paste, whereas the second type represents heterogeneous concrete including aggregates. During the experiment, the different waveforms have been repeatedly emitted through a specimen subjected to an uniaxial compression. The relative wave-velocity change has then been obtained by post-processing the acquired data, which has been compared with Murnaghan's model.

The conclusion of this research is that Murnaghan's theory can be used to accurately predict the relative wave-velocity changes of the cement-paste specimens, and in particular the relative P-wave velocity changes. The results have shown that the radial recordings yield inconsistencies which can be attributed to the small dimensions of the specimens. Furthermore, the influence of the inhomogeneity of the material on the relative wave-velocity changes manifests itself through a discrepancy in the acoustoelasticity. Here, it is found that the ratio between the aggregate size, the specimen dimensions and the wavelength of the signal determines the sensitivity to the acoustoelastic effect. Therefore, before the data from the smart aggregates embedded in a real structure can be interpreted, the experiments need to be improved and expanded. It is important to investigate the acoustoelasticity of waves with non-orthogonal propagation and particle-oscillation direction, while applying various stress states to the medium. This is because the smart aggregates are arranged in a network, where the signals are emitted signals are propagating through the structure via arbitrary paths between various transducers.

Contents

Glossary

Abbreviations

CC	Cross-correlation
CWI	Coda Wave Interferometry
LVDT	Linear Variable Differential Transformer
FT	Fourier transform
IFT	Inverse Fourier transform
P-wave	Compressional wave
PS-wave	P-wave to S-wave conversion
S-wave	Shear wave
SH-wave	Shear wave with horizontal particle oscillation
SV-wave	Shear wave with vertical particle oscillation
SHM	Structural Health Monitoring
SNR	Signal-to-noise ratio
ToF	Time of Flight
UCS	Unconfined Compressive Strength

Latin Symbols

a, b, c	Initial coordinates
A_{ijkl}	Acoustoelastic constant
B	Configuration of a continuous body
B_{ijkl}	Elastic coefficients
c	Wave velocity
d	Specimen diameter
dm	Element of mass
ds	Scalar element of arc
dS	Scalar element of area
$\boldsymbol{dS}$	Matrix element of area
dV	Element of volume
e	Volumetric strain
e_{ij}	First-order strain component
E	Young's modulus
$\boldsymbol{E}$	Identity matrix
f	Linear frequency
f_s	Sampling frequency
h	Specimen height
$h(t)$	Continuous time signal
$h(n)$	Discretized time signal
I_1, I_2, I_3	Strain invariants
$\hat{\boldsymbol{\imath}}, \hat{\boldsymbol{\jmath}}, \hat{\boldsymbol{k}}$	Cartesian unit vectors
$\boldsymbol{J}$	Jacobian matrix
K	Bulk modulus
l, m, n	Murnaghan constants
$\boldsymbol{n}$	Outward normal vector
$\hat{\boldsymbol{n}}$	Unit outward normal vector
N	Sample size
p	Hydrostatic stress
s_{ij}	Incremental-stress
S_{ij}	Initial-stress
$\boldsymbol{t}$	Traction vector
t	Time / Arrival time
t'	Stretched time
T_{ij}	Cauchy stress tensor
u, v, w	Displacements
U	Strain energy
$\ddot{\boldsymbol{x}}$	Final acceleration vector
X, Y, Z	Mass forces
x, y, z	Final coordinates

Greek Symbols

α, β, γ	Independent variables
δ	Variation

δV	Virtual work
Δf	Frequency resolution
Δt	Time resolution
ϵ	Stretching factor
$\boldsymbol{\epsilon}$	Eulerian strain matrix
$\boldsymbol{\eta}$	Lagrangian strain matrix
λ, μ	Lamé parameters
λ	Wavelength
ν	Poisson's ratio
ρ	Mass density
σ_{ij}	Nominal stress tensor
τ	Time stretching
ϕ	Strain energy per initial volume
ψ	Strain-energy density
ω_{ij}	Rotation angle
ω	Angular frequency

Superscripts

(ref)	Denoting reference signal
(str)	Denoting stretched signal
$'$	Denoting the final position after dynamic deformation
0	Denoting the initial wave velocity
(0)	Denoting static displacement
(1)	Denoting dynamic displacement
-1	Inverse
S_{ij}	Denoting the wave velocity of a medium subjected to a stress - Biot
T	Transpose
σ_{kl}	Denoting the wave velocity of a medium subjected to a stress - Murnaghan
x, y, z	Denoting the direction of the outward normal to a coordinate plane
T	Transpose
σ_{kl}	Denoting the wave velocity of a medium subjected to a stress - Murnaghan
x, y, z	Denoting the direction of the outward normal to a coordinate plane

Subscripts

a	Initial configuration
$,a$	Short notation for a derivative with respect to the initial coordinates
A	Analytical representation of a signal
P	P-wave
S	S-wave
x	Final configuration
$,x$	Short notation for a derivative with respect to the final coordinates

Mathematical Operators

co	Cofactor matrix
$\det$	Determinant of a square matrix
$\in$	Element of a set
$\mathcal{F}$	Fourier transform
H	Hilbert transform
Tr	Trace of a matrix
δ_{ij}	Kronecker delta
$\frac{\partial}{\partial a}$	Partial derivative with respect to the initial coordinates
$\frac{\partial}{\partial x}$	Partial derivative with respect to the final coordinates
$\frac{\partial}{\partial t}$	Partial derivative with respect to time
$\times$	Cross product
$*$	Convolution
∇	Divergence
$\sum$	Summation
$\int$	Line integral
$\iint$	Surface integral
$\iiint$	Volume integral

1 Introduction

This chapter gives a general introduction to the subject of interest to provide a solid base for the reader. Limitations of the current assessment methods for structural health monitoring (SHM) and the desire to better understand the structural behaviour of existing structures, are detailed in the problem statement. Subsequently, a method is provided which could improve the conventional assessment for SHM as well as allow for an interpretation of the internal forces in existing structures. The scope and the objectives of this research are then captured by posing a number of research questions. Finally, the chosen research methodology is explained.

1.1. Problem statement

Due to the increase of traffic through the years, the structural safety of a large amount of existing infrastructure has to be assessed. Caused by a lack of information with respect to the design of aged concrete slab bridges, conventional assessment approaches cannot always provide an accurate evaluation of the current bearing capacity. Moreover, the absence of an appropriate measurement system makes that the stresses and strains within the concrete structure are unknown. These bridges are sometimes assessed through the application of a proof loading, depicted in Figure 1.1.

Figure 1.1: Proof loading on a bridge executed by Lantsoght et al. [16].

The proof loading is a force-controlled method in which a bridge is repeatedly loaded and unloaded at its midspan. This cyclic loading is realised by a truck which travels over a seesaw construction positioned on the bridge deck [14]. As the truck travels across the bridge while being charged piece-wise, the deflection of the bridge deck is measured with external sensors. To prevent unwanted damage to the structure, a set of stop criteria must be defined based on these measurements. The conventional assessment approaches to define the stop criteria are mainly focused on the deformation on the surface of the structure. The limitations of this method are the traffic hindrance on the bridge during the execution and the fact that proof loading cannot cover larger volumes.

The application of 'smart aggregates' is an interesting alternative to the conventional assessment approaches since it allows to also monitor the stresses and strains within the structure. Therefore, this application may help the monitoring the health condition of the structure in general. Smart aggregates are piezoelectric-based sensors that are embedded in the concrete structures and which can emit and receive wave signals. The implementation of these smart aggregates can be realised either through drill cores, in case of existing structures, or by casting them in concrete a priori, in case of new structures. Figure 1.2 (Yang 2021) displays the inclusion of smart aggregates within the formwork of a cast in-situ bridge under construction.

Figure 1.2: Positioning of smart aggregates in the formwork of a cast in-situ bridge under construction (Yang 2021).

The changes of the concrete medium in terms of either stresses or strains are reflected by the phase changes or decoherence of the wave signal, which travels between the smart aggregate source-receiver pairs. Based on the measurement of these changes it would be possible to create a digital twin of the structure, which would allow for a better understanding of the structural behaviour under normal traffic. Since the smart aggregates are embedded in the concrete structure, they are protected against potential damage from outside and provide a more accurate interpretation of the concrete medium, in comparison to external sensors. Smart aggregates could also be used to provide a more accurate stop criteria for the proof loading, based on the stresses. Therefore, a much better understanding of the structural response under high loads can be obtained. The installation of smart aggregates is also easier, which makes the proof loading method cheaper as well.

1.2. Acoustoelastic effect

To relate the relative change in the wave velocity, as waves propagate through the concrete medium, to a change in the initial-stress conditions it is important to understand the link between the two. This link, referred to as the acoustoelastic effect, has been a subject of research within other fields of application in the first half of the 20th century. The acoustoelastic effect states that the change in the wave velocity of a material as a function of stress is caused by the higher order terms in the constitutive relation. This effect has been theoretically established as early as 1925 in the article *"Sur les tensions de radiation"* by Brillouin [7]. In this article, the influence of a hydrostatic pressure p on the wave propagation in an elastic solid has been investigated. Brillouin has found that the longitudinal- and transverse-wave velocity of an elastic solid, subjected to an exterior hydrostatic pressure, can be described with [7, Eq. 43]:

$$c_P = \sqrt{\frac{\lambda + 2\mu - p}{\rho}}$$
$$c_S = \sqrt{\frac{\mu - p}{\rho}}, \tag{1.1}$$

respectively. This result implies that the waves would stop to propagate, i.e. the wave velocity would reduce to zero, if the pressure is sufficient. This contradiction in Brillouin's theory is caused by the incorrect assumption that the wave propagation is only influenced by a difference in the equation of motion, generated by the applied pressure. This led to the argument that the change in the wave velocity of a solid as a function of an applied pressure is due to the stress-dependency of the elastic coefficients as well as the difference in the equation of motion. Murnaghan [21] and Biot [4] have both introduced their theories which also take into account this stress-dependency of the elastic coefficients. In this thesis, these two theoretical models will be investigated and compared.

1.3. Coda Wave Interferometry

A wave signal, emitted by a source and recorded by a receiver, contains information of the medium through which it propagates. If it is assumed that the waves have undergone scattering through the medium, its time signature develops into a diffuse field, like depicted in Figure 1.3.

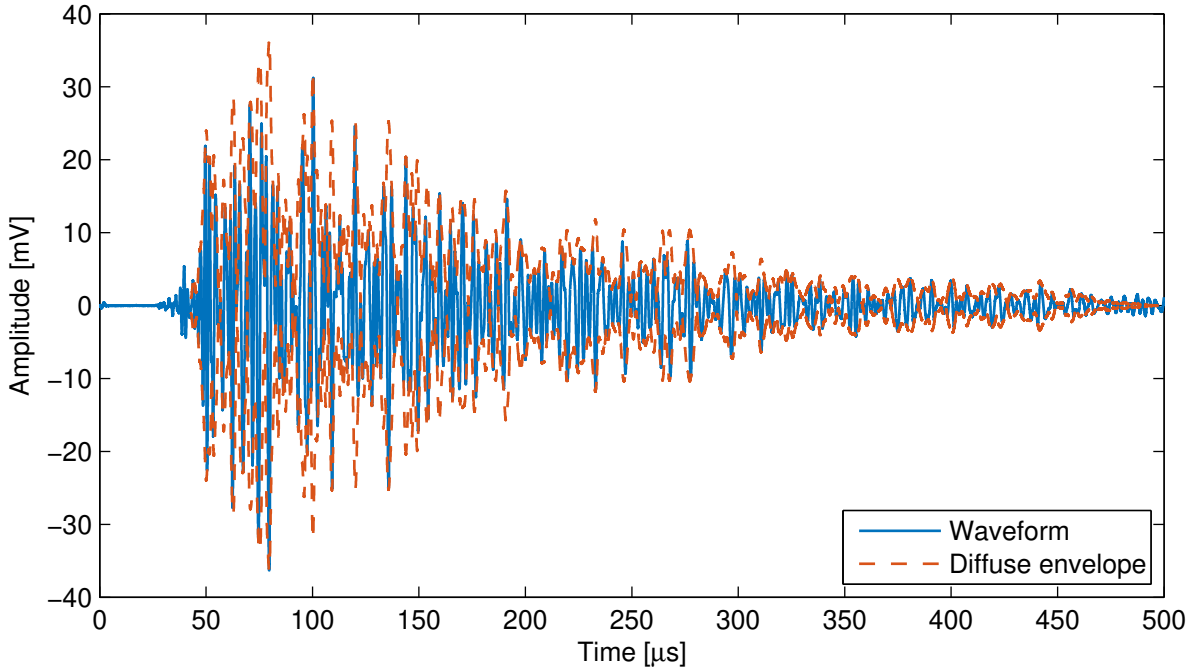

Figure 1.3: Time signature of a wave signal which has propagated through a concrete-like medium.

Within diffuse fields, a distinction can be made between the first arrival, consisting of direct waves that travel along the shortest path from source to receiver, and the diffuse part which includes the coda waves. The coda waves are the late part of the wave signal and are composed of waves which have travelled much longer paths than the source-receiver distance. Because of this larger travel distance, coda waves are much more sensitive to weak perturbations in the medium as opposed to direct or singly reflected waves.

The changes in the wave velocity of the medium can be monitored with two distinguished techniques, namely the Time of Flight (ToF) and Coda Wave Interferometry (CWI). The ToF is an old straightforward technique which focuses on the first arrival of the wave signal, whereas CWI is a recently developed technique which exploits the later part of the wave signal. Within CWI a distinction can be made between the Doublet Technique and the Stretching Technique. The latter has been applied in this thesis.

1.3.1. Time of Flight

The change of the wave velocity of the medium can be easily monitored with the ToF method. Through this monitoring technique the wave velocity of the medium can be extracted simply by dividing the source-receiver distance by the time of the first arrival. From this output, it possible to observe the increase or decrease of the wave velocity of the medium and to investigate the cause of these changes.

However, this monitoring technique comes with some limitations and uncertainties. The application of this method is limited to the first arrival of the wave signal, which contains far less information of the surrounding medium in comparison to the diffuse part. Therefore, the observations from this technique don't accurately represent the entire medium but rather a small portion of the medium. Furthermore, this technique is not applicable in strongly heterogeneous media. This is due to lack of direct waves, caused by the large amount of scattering. Therefore, the first arrival will have scattered within the medium before being recorded, making it impossible to identify the small variations in the wave velocity with the ToF. For these cases it is more convenient to utilise the CWI technique.

1.3.2. Stretching Technique

The small variations in the wave velocity of a medium result in a variation of the arrival time. Here, a shift towards earlier time implies an increase of the wave velocity, whereas a shift towards later time implies a decrease in the wave velocity. If a reference signal is assumed, then this time shift can also be reproduced by stretching said reference signal in time, like displayed in Figure 1.4.

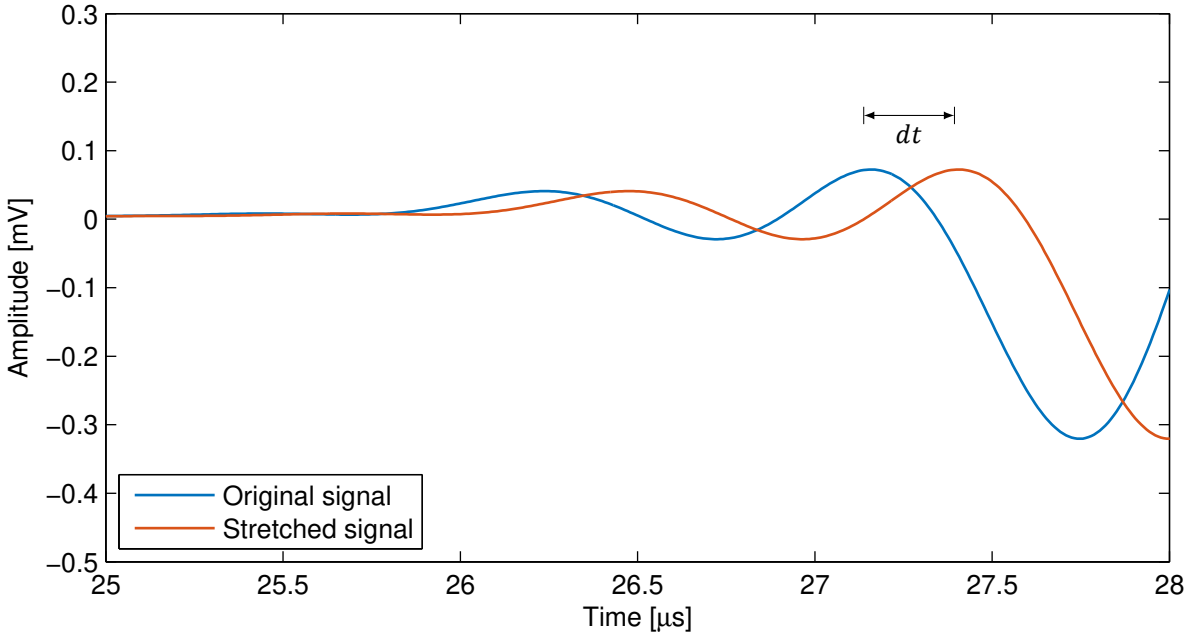

Figure 1.4: Visual representation of the Stretching Technique.

In order to realise this stretching, the original time axis t must be multiplied with a factor such that the stretched time axis

$$t' = t + dt = t(1 + \tau), \tag{1.2}$$

where τ denotes the amount of the stretching or compression of the original time axis:

$$\tau = \frac{dt}{t}. \tag{1.3}$$

It should be noted that a small stretch in time can be interpreted as a small decrease in the wave velocity, i.e. the wave signal takes longer to arrive. Since both the reference and the stretched signal have travelled the same distance within the medium, the following holds:

$$\frac{dt}{t} = -\frac{dc}{c}, \tag{1.4}$$

which yields:

$$t' = t(1 - \epsilon). \tag{1.5}$$

Here, ϵ denotes the relative wave-velocity change:

$$\epsilon = \frac{dc}{c}, \tag{1.6}$$

or simply the stretching factor. The relative wave-velocity change between the reference signal and the stretched signal can be determined by comparing both signals within a specified time window. This comparison is realised through the calculation of the cross-correlation as a function of the stretching factor [15, Eq. 1]:

$$CC(\epsilon) = \frac{\int_{t_1}^{t_2} \left\{ h^{(str)}\left[t(1-\epsilon)\right] h^{(ref)}(t) \right\} dt}{\sqrt{\int_{t_1}^{t_2} \left(h^{(str)}\right)^2 \left[t(1-\epsilon)\right] dt} \sqrt{\int_{t_1}^{t_2} \left(h^{(ref)}\right)^2 (t) dt}}, \tag{1.7}$$

where $h^{(ref)}$ and $h^{(str)}$ denote the reference and stretched signal, respectively. The intervals of the time window in which the cross-correlation is performed are denoted with t_1 and t_2. Figure 1.5 displays how the cross-correlation changes as a function of the stretching factor.

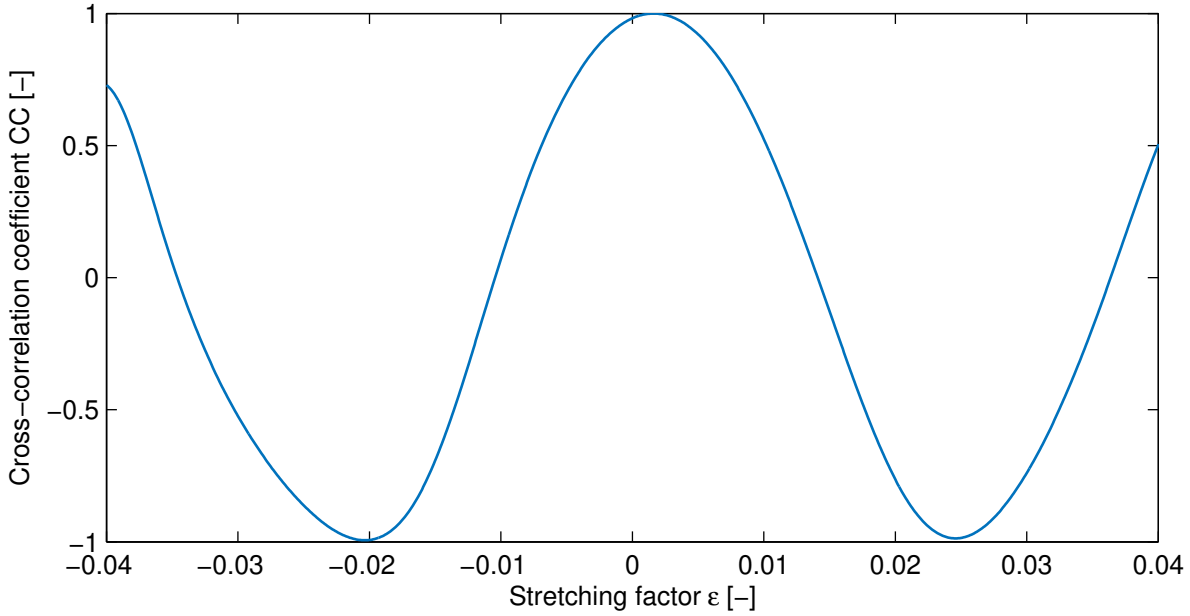

Figure 1.5: Typical $CC - \epsilon$ graph, maximum cross-correlation at $\epsilon = 0.0016$.

The cross-correlation coefficient CC represents the 'degree of similarity' between the reference signal and the stretched signal, where $CC = 1$ denotes a perfect correlation and $CC = -1$ – a perfect anti-correlation. The relative wave-velocity change is then obtained by searching the stretching factor for which a maximum CC-value is attained.

1.4. Research objective and scope

It is important to clearly define the objective and the scope of the research. Together, they determine the direction and breath of this research.

1.4.1. Objective and research questions

The research presented in this thesis encompasses the behaviour of elastic wave propagation, and the wave velocity in particular, in a concrete medium subjected to a stress field. The objective of this thesis is to establish a relation between the relative wave-velocity change within a concrete medium and the applied stress on said medium. This objective can be reached by finding the following research question:

"How are the stresses related to the relative wave-velocity change of a concrete-like medium?"

In order to formulate an answer to this research question the following sub-questions have been stated:

- How is the wave velocity related to the stresses and strains?
- What are the differences in the fundamental assumptions underlying Murnaghan's and Biot's theory, which lead to the changes of a wave velocity under a certain stress level?
- To what extent can the theoretic acoustoelastic effect be verified with the experimental results?
- What is the influence of the orientation of the stress with respect to the propagation and polarisation direction of the wave?
- What is the influence of the inclusion of aggregates in a concrete specimen on the wave velocity?

These sub-questions will be answered throughout the chapters of this report. Once the answers to these sub-questions and the research question have been formulated, the conclusions together with the recommendations regarding the continuation of this research will be summarised in the final chapter.

1.4.2. Scope of research

In order to accomplish the completion of the thesis within a realistic time frame it is of importance to set the scope for the research. This scope defines the boundaries and the depth within which the topic of interest will be investigated. Narrowing down the field of research allows for a in-depth study, focused on the important details which will result in a clear answer to the research question. The main focus of this thesis is on the study of the behaviour the velocity of body waves propagating within concrete subjected to applied stresses. Both the propagation and polarisation directions of the waves as well as the loading direction will be limited to orthogonal directions. That is, the propagation direction and the particle oscillation will be either in the x, y or z-direction, whereas the stresses will be uniaxial along either of these three directions. The acoustoelastic effect is only valid in the linear-elastic regime, therefore the range of the stress level is maintained small. Due to the complexity of interpreting the coda waves, the study of the time signatures of the wave signals will be focused on the first arrivals. However, taking into account the heterogeneity of the concrete medium, the ToF will not be applicable to monitor the wave velocity. Therefore, CWI will be applied in order to determine the relative wave-velocity change of the scattered arrivals.

1.5. Research methodology

The research starts with a theoretical study, during which previous research will be examined regarding the relation between the wave velocity and the stresses and strains. This phase is mainly focused on two theoretical models which are the result of the work of Murnaghan and Biot. Subsequently, the fundamental differences between these two distinctive formulations of the acoustoelastic effect will be discussed. The result of this theoretical study is the acoustoelastic effect, which will be verified through scaled laboratory experiments. Finally, the data acquired from the experiments will be interpreted through CWI and compared to the theoretical established link between the relative wave-velocity change and the stresses in the concrete. This research methodology can be summarised with the flowchart depicted in Figure 1.6.

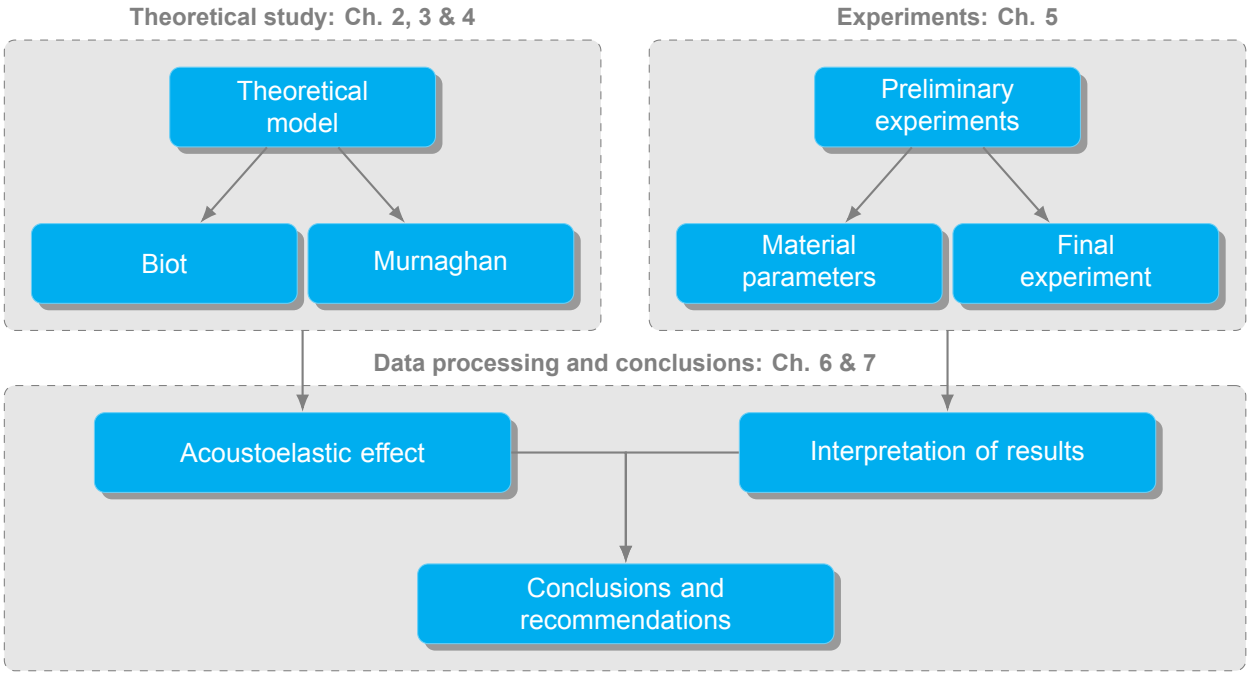

Figure 1.6: Flowchart describing the research presented in this thesis.

2

Theoretical study: F.D. Murnaghan

This chapter covers the first approach to the acoustoelastic effect. The paper *"Second-Order Elastic Deformation of Solids"* by Hughes and Kelly [13] describes how expressions for the velocities of elastic waves in stressed solids are derived. These expressions are based on Murnaghan's theory of finite deformations and third-order terms in the strain energy. This is covered in Murnaghan's paper and later on in his eponymous book *"Finite Deformation of an Elastic Solid"* [21] [22].

The aforementioned literature is used to rederive the relation between the stress and the strain in a consistent notation system. This rederivation is necessary because the original derivation and its corresponding notation can be regarded as unfit for modern standards. Intermediate steps, which have been left out by Murnaghan, are provided here as well. For the purpose of simplifying Murnaghan's expressions, the index notation as well as the alternative description of the strain energy from the thesis *"Measurement of non-linear acoustoelastic effect in steel using acoustic resonance"* [11, Eq. 2.50] have been adopted. With these simplified notations, expressions for wave velocities of a stressed medium [13, Eq. 12] have been derived.

2.1. Elastic deformation

This section describes the elastic deformation of a continuous solid, causing it to transform from its initial configuration to its final configuration. Surface forces, mass forces or temperature changes within this solid generate a stress field which may cause a deformation. This deformation can be represented as a relative displacement between the particles within the solid, otherwise referred to as the strain field. The connection between the applied stress field and the resulting strain field is established through the constitutive relations. It should be noted that isothermal conditions are assumed, meaning that the influences from temperature changes are neglected. A deformation is categorised as an elastic deformation if the deformation process is reversible, i.e. if the initial configuration can be restored by removing the stress field.

2.1.1. Deformation and strain

A three-dimensional, deformable medium is considered in its initial or unstrained state B_a. Within this medium, a variable point P_a, with initial coordinates (a, b, c), traces a curve C_a. A collection of particles within this medium is assumed to be situated on C_a. The final or strained state of the medium B_x is obtained by displacing point P_a to the variable point P_x with final coordinates (x, y, z). This can be realised by introducing the displacement vector,

$$\boldsymbol{u} = \begin{pmatrix} u \\ v \\ w \end{pmatrix} = \begin{pmatrix} x - a \\ y - b \\ z - c \end{pmatrix}, \tag{2.1}$$

or in vector notation,

$$\boldsymbol{u} = \boldsymbol{x} - \boldsymbol{a}. \tag{2.2}$$

The collection of particles is now situated on the curve C_x, traced by P_x. The relative displacement between the particles within the medium, i.e. the strain, is be defined as the difference in arc length between the initial curve C_a and final curve C_x. The medium is in compression if the particles have moved closer to each other, whereas if they've moved away from each other, the medium is in tension. Figure 2.1 displays the relative displacements of the particles.

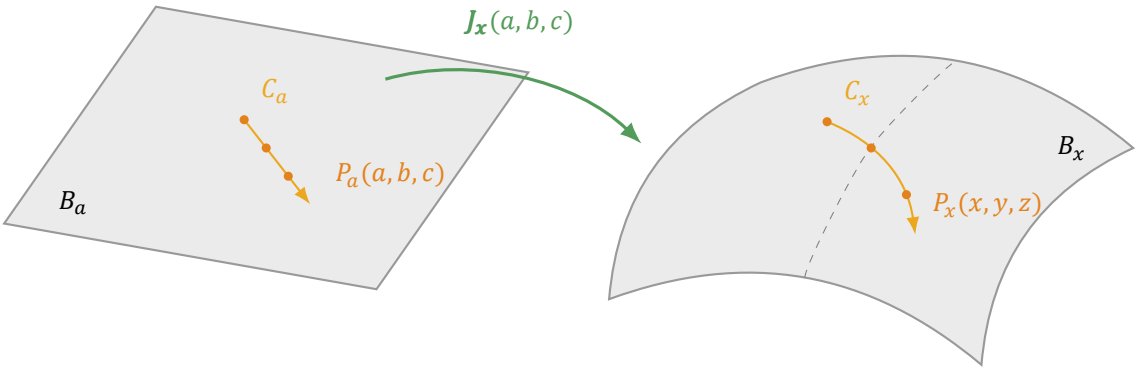

Figure 2.1: Visualisation of the relative displacement between the particles within the medium during a deformation.

The initial scalar element of arc ds_a and final scalar element of arc ds_x describe an infinitesimal portion of the arc length of C_a and C_x, respectively. They are defined as:

$$\begin{aligned} ds_a &= \sqrt{(\boldsymbol{da})^T(\boldsymbol{da})} \\ ds_x &= \sqrt{(\boldsymbol{dx})^T(\boldsymbol{dx})}, \end{aligned} \tag{2.3}$$

where $\boldsymbol{da}$ denotes the initial matrix element of arc,

$$\boldsymbol{da} = \begin{pmatrix} da \\ db \\ dc \end{pmatrix}, \tag{2.4}$$

and $\boldsymbol{dx}$ – the final matrix element of arc:

$$\boldsymbol{dx} = \begin{pmatrix} dx \\ dy \\ dz \end{pmatrix}. \tag{2.5}$$

The matrix elements of arc describe the distance between the begin and end point of an arc segment in the three orthogonal directions.

Upon introducing the definition of the Jacobian matrix, the initial and final matrix element of arc can be related to each other. The Jacobian matrix contains first-order partial derivatives and can be used to describe a linear transformation within the vicinity of a specified point. The transformation of the body within the vicinity of the initial coordinates is then described by the Jacobian matrix,

$$\boldsymbol{J_x}(a,b,c) \equiv \begin{pmatrix} x_a & x_b & x_c \\ y_a & y_b & y_c \\ z_a & z_b & z_c \end{pmatrix}, \tag{2.6}$$

whereas the transformation of the body within the proximity of the final coordinates is described by the Jacobian matrix,

$$\boldsymbol{J_a}(x,y,z) \equiv \begin{pmatrix} a_x & a_y & a_z \\ b_x & b_y & b_z \\ c_x & c_y & c_z \end{pmatrix}. \tag{2.7}$$

Here, x_a, y_a, z_a, etc. are short notations for derivatives of the final coordinates with respect to the initial coordinates,

$$x_a = \frac{\partial x}{\partial a}\,; \quad y_a = \frac{\partial y}{\partial a}\,; \quad z_a = \frac{\partial z}{\partial a}, \tag{2.8}$$

while a_x, a_y, a_z, etc. are short notations for derivatives of the initial coordinates with respect to the final coordinates:

$$a_x = \frac{\partial a}{\partial x}\,; \quad a_y = \frac{\partial a}{\partial y}\,; \quad a_z = \frac{\partial a}{\partial z}. \tag{2.9}$$

By elaborating the difference of the squared scalar elements of arc, two equivalent expressions are obtained[1]:

$$(ds_x)^2 - (ds_a)^2 = (\boldsymbol{da})^T 2\boldsymbol{\eta}\ (\boldsymbol{da}) = (\boldsymbol{dx})^T 2\boldsymbol{\epsilon}\ (\boldsymbol{dx}), \tag{2.10}$$

where $\boldsymbol{\eta}$ and $\boldsymbol{\epsilon}$ denote the Lagrangian and Eulerian description of the strain,

$$\begin{aligned} \boldsymbol{\eta} &\equiv \tfrac{1}{2}\Big(\boldsymbol{J_x}(a,b,c)^T\boldsymbol{J_x}(a,b,c) - \boldsymbol{E_3}\Big) \\ \boldsymbol{\epsilon} &\equiv \tfrac{1}{2}\Big(\boldsymbol{E_3} - \boldsymbol{J_a}(x,y,z)^T\boldsymbol{J_a}(x,y,z)\Big), \end{aligned} \tag{2.11}$$

respectively, and $\boldsymbol{E_3}$ – the 3 x 3 identity matrix. From relation (2.10) it can be concluded that equal squared elements of arc result in zero strain. This is the case for rigid displacements for which the Jacobian matrices are orthogonal[2]. If there is no displacement at all, i.e. the initial coordinates are equal to the final coordinates, the Jacobian matrices in definition (2.11) reduce to identity matrices, resulting in zero strain as well.

The Lagrangian description of the strain $\boldsymbol{\eta}$ is expressed in terms of the initial coordinates and describes the strain field over the body before the deformation has occurred, i.e. in its initial configuration B_a. The Eulerian description of the strain $\boldsymbol{\epsilon}$ is expressed in terms of the final coordinates and describes the strain field over the body after the deformation has occurred, i.e. in its final configuration B_x. Both sets of strain components can be assembled in the following matrices:

$$\boldsymbol{\eta}(a,b,c) = \begin{pmatrix} \eta_{aa} & \eta_{ab} & \eta_{ac} \\ \eta_{ba} & \eta_{bb} & \eta_{bc} \\ \eta_{ca} & \eta_{cb} & \eta_{cc} \end{pmatrix}\,; \quad \boldsymbol{\epsilon}(x,y,z) = \begin{pmatrix} \epsilon_{xx} & \epsilon_{xy} & \epsilon_{xz} \\ \epsilon_{yx} & \epsilon_{yy} & \epsilon_{yz} \\ \epsilon_{zx} & \epsilon_{zy} & \epsilon_{zz} \end{pmatrix}. \tag{2.12}$$

Through definition (2.11), the strain components can be elaborated[3]. The uniaxial strain components $\eta_{aa}, \eta_{bb}, \eta_{cc}$ and $\epsilon_{xx}, \epsilon_{yy}, \epsilon_{zz}$ are then of the form:

$$\begin{aligned} \eta_{aa} &= \frac{\partial u}{\partial a} + \frac{1}{2}\left[\left(\frac{\partial u}{\partial a}\right)^2 + \left(\frac{\partial v}{\partial a}\right)^2 + \left(\frac{\partial w}{\partial a}\right)^2\right] \\ \epsilon_{xx} &= \frac{\partial u}{\partial x} - \frac{1}{2}\left[\left(\frac{\partial u}{\partial x}\right)^2 + \left(\frac{\partial v}{\partial x}\right)^2 + \left(\frac{\partial w}{\partial x}\right)^2\right], \end{aligned} \tag{2.13}$$

whereas the symmetric shear strain components $\eta_{ab}, \eta_{ac}, \eta_{bc}$ and $\epsilon_{xy}, \epsilon_{xz}, \epsilon_{yz}$ are of the form:

$$\begin{aligned} \eta_{ab} &= \frac{1}{2}\left(\frac{\partial u}{\partial b} + \frac{\partial v}{\partial a}\right) + \frac{1}{2}\left(\frac{\partial u}{\partial a}\frac{\partial u}{\partial b} + \frac{\partial v}{\partial a}\frac{\partial v}{\partial b} + \frac{\partial w}{\partial a}\frac{\partial w}{\partial b}\right) \\ \epsilon_{xy} &= \frac{1}{2}\left(\frac{\partial u}{\partial y} + \frac{\partial v}{\partial x}\right) - \frac{1}{2}\left(\frac{\partial u}{\partial x}\frac{\partial u}{\partial y} + \frac{\partial v}{\partial x}\frac{\partial v}{\partial y} + \frac{\partial w}{\partial x}\frac{\partial w}{\partial y}\right). \end{aligned} \tag{2.14}$$

When the initial and final coordinates are approximately the same, the displacements become infinitesimal. In this theory of infinitesimal deformations, the higher-order terms can be neglected such that there is no distinction between the Lagrangian and Eulerian strain description.

[1] The detailed derivation of these two expressions is covered in App. A.3.1.
[2] That is, $\boldsymbol{J_x}(a,b,c)^T\boldsymbol{J_x}(a,b,c) = \boldsymbol{J_a}(x,y,z)^T\boldsymbol{J_a}(x,y,z) = \boldsymbol{E_3}$.
[3] The derivation of the strain components is elaborated in App. A.3.2.

2.1.2. Stress description

An arbitrary portion of the deformable medium is considered in its final configuration B_x. This portion has a final element of area dV_x and is subjected to two types of forces which have to be in equilibrium with each other. The first type are the mass forces $\boldsymbol{X_x}$ which act on the portion through its element of $dm = \rho_x dV_x$. Here, ρ_x denotes the final mass density. The second type are the traction forces $\boldsymbol{t_x}$ which act on the portion across its bounding surface, the final scalar element of area dS_x. The mass forces have the dimensions of a force per unit mass, i.e. of acceleration, whereas the traction forces have the dimensions of a force per unit area, i.e. of stress. The mass forces and traction forces are defined as:

$$\boldsymbol{X_x} = \begin{pmatrix} X_x \\ Y_x \\ Z_x \end{pmatrix}; \quad \boldsymbol{t_x} = \begin{pmatrix} t_x \\ t_y \\ t_z \end{pmatrix}, \tag{2.15}$$

respectively.

The traction acting on the final scalar element of area dS_x can be elaborated through the use of Cauchy's tetrahedron [2, Sec. 1.2]. This tetrahedron is obtained by cutting an infinitesimal cube in half. The final scalar element of area defines the base plane of the tetrahedron whereas its projections onto the coordinate planes, dS^x, dS^y and dS^z, define the other planes. Here, the superscripts x, y, z specify the direction of the outward normal vectors to these planes, $\boldsymbol{n^x}, \boldsymbol{n^y}, \boldsymbol{n^z}$, respectively. The outward normal to the base plane dS_x is denoted with $\boldsymbol{n_x}$. Figure 2.2 displays the planes of the tetrahedron with its traction vectors and outward normals.

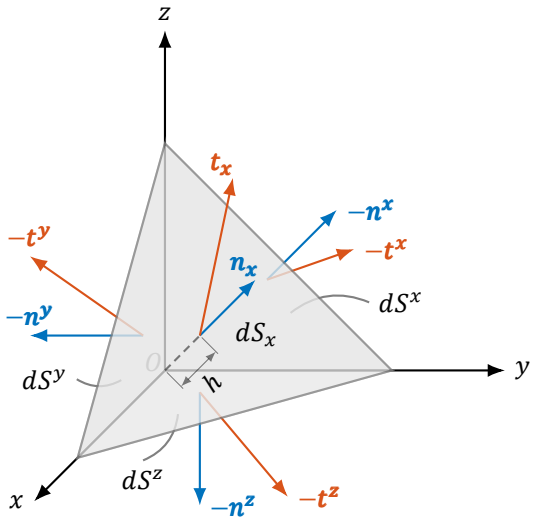

Figure 2.2: Visualisation of the traction acting on the planes of a tetrahedron with height h and base plane dS_x.

The traction forces acting on the planes of the tetrahedron must be in equilibrium with each other. Through Newton's second law of motion the traction vector $\boldsymbol{t_x}$ can be written as[4]:

$$\boldsymbol{t_x} = \begin{pmatrix} t_x \\ t_y \\ t_z \end{pmatrix} = \begin{pmatrix} T_{xx} & T_{yx} & T_{zx} \\ T_{xy} & T_{yy} & T_{zy} \\ T_{xz} & T_{yz} & T_{zz} \end{pmatrix} \begin{pmatrix} \hat{n}_x \\ \hat{n}_y \\ \hat{n}_z \end{pmatrix}, \tag{2.16}$$

where T_{ij} denotes a stress acting in the j-direction across a plane which has its outward normal in the i-direction.

[4]The derivation of the Cauchy stress equation is elaborated in App. A.4.1.

Relation (2.16) can be written in the vector notation such that the Cauchy stress equation reads:

$$\boldsymbol{t_x} = \boldsymbol{T}^T \hat{\boldsymbol{n}}_{\boldsymbol{x}}, \tag{2.17}$$

where $\boldsymbol{T}$ denotes the Cauchy stress tensor,

$$\boldsymbol{T} = \begin{pmatrix} T_{xx} & T_{xy} & T_{xz} \\ T_{yx} & T_{yy} & T_{yz} \\ T_{zx} & T_{zy} & T_{zz} \end{pmatrix}, \tag{2.18}$$

and $\hat{\boldsymbol{n}}_{\boldsymbol{x}}$ – the unit normal vector to the final scalar element of area. Figure 2.3 displays how the tractions and the stresses are acting on a cube.

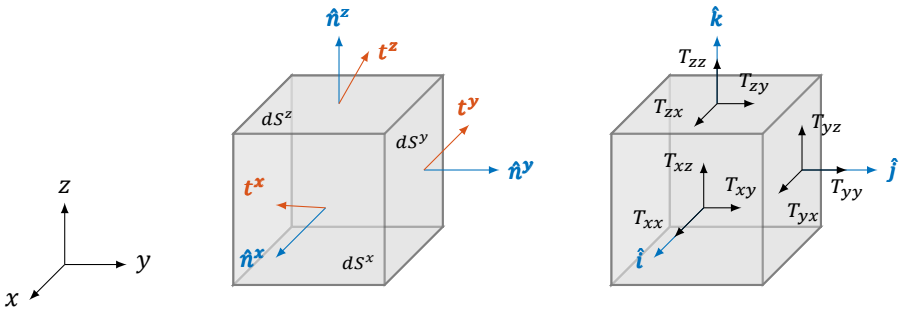

Figure 2.3: The positive definitions of the tractions and the Cauchy stresses acting on the coordinate planes of a cube.

2.1.3. Constitutive relation

The condition of equilibrium of the mass and traction forces can be formulated through the principle of virtual work. The concept of virtual work is defined as the energy needed to move a body with a virtual deformation. Unlike real deformations which require a finite time to develop, virtual deformations are considered to be instantaneous, imaginary deformations, causing an infinitesimal variation in the coordinates.

If it is assumed that the body in its final configuration undergoes an arbitrary virtual deformation,

$$\boldsymbol{\delta x} = \begin{pmatrix} \delta x \\ \delta y \\ \delta z \end{pmatrix}, \tag{2.19}$$

the total virtual work δV in any virtual deformation, exerted on the deformable body by the mass forces and the tractions, is defined as:

$$\delta V = \iiint_{V_x} \rho_x (\boldsymbol{\delta x})^T \boldsymbol{X_x} dV_x + \iint_{S_x} (\boldsymbol{\delta x})^T \boldsymbol{t_x} dS_x. \tag{2.20}$$

Upon further elaborating[5], the above can be written as a single volume integral:

$$\delta V = \iiint_{V_x} \left\{ (\boldsymbol{\delta x})^T \left[\rho_x \boldsymbol{X_x} + \left(\boldsymbol{\nabla_x T} \right)^T \right] + \mathrm{Tr}\left(\boldsymbol{T} (\boldsymbol{\delta x})_{\boldsymbol{x}} \right) \right\} dV_x, \tag{2.21}$$

where $\left(\boldsymbol{\nabla_x T} \right)^T$ denotes the divergence of the stress tensor with respect to the final coordinates,

$$\left(\boldsymbol{\nabla_x T} \right)^T = \begin{pmatrix} \frac{\partial T_{xx}}{\partial x} + \frac{\partial T_{yx}}{\partial y} + \frac{\partial T_{zx}}{\partial z} \\ \frac{\partial T_{xy}}{\partial x} + \frac{\partial T_{yy}}{\partial y} + \frac{\partial T_{zy}}{\partial z} \\ \frac{\partial T_{xz}}{\partial x} + \frac{\partial T_{yz}}{\partial y} + \frac{\partial T_{zz}}{\partial z} \end{pmatrix}, \tag{2.22}$$

[5]The extensive derivation of the expression for the virtual work are elaborated in App. A.4.2.

and $\mathrm{Tr}\left(\boldsymbol{T}(\boldsymbol{\delta x})_{\boldsymbol{x}}\right)$ – the trace of the matrix product of the stress tensor and the Jacobian matrix of the virtual deformations with respect to the final coordinates:

$$\mathrm{Tr}\left(\boldsymbol{T}(\boldsymbol{\delta x})_{\boldsymbol{x}}\right) = \mathrm{Tr}\left[\begin{pmatrix} T_{xx} & T_{xy} & T_{xz} \\ T_{yx} & T_{yy} & T_{yz} \\ T_{zx} & T_{zy} & T_{zz} \end{pmatrix}\begin{pmatrix} (\delta x)_x & (\delta x)_y & (\delta x)_z \\ (\delta y)_x & (\delta y)_y & (\delta y)_z \\ (\delta z)_x & (\delta z)_y & (\delta z)_z \end{pmatrix}\right]. \tag{2.23}$$

From now on the Jacobian matrix of the final coordinates with respect to the initial coordinates will be written in the compact form:

$$\boldsymbol{J} = \boldsymbol{J}_{\boldsymbol{x}}(a, b, c). \tag{2.24}$$

If the left-multiplication with its transpose is denoted with $\boldsymbol{M} = \boldsymbol{J}^T\boldsymbol{J}$, then from relation (2.11) follows:

$$\boldsymbol{M} = 2\boldsymbol{\eta} + \boldsymbol{E_3}. \tag{2.25}$$

The variation $\boldsymbol{\delta M}$ can then be written in two equivalent expressions as (see App. A.4.2 for details):

$$\boldsymbol{\delta M} = 2\boldsymbol{J}^T\boldsymbol{D}\boldsymbol{J} = 2\boldsymbol{\delta\eta}, \tag{2.26}$$

where $\boldsymbol{D}$ denotes the symmetric matrix:

$$\boldsymbol{D} = \frac{1}{2}\left\{\left[(\boldsymbol{\delta x})_{\boldsymbol{x}}\right]^T + (\boldsymbol{\delta x})_{\boldsymbol{x}}\right\}, \tag{2.27}$$

and $\boldsymbol{\delta\eta}$ – the variation of the Lagrangian strain matrix. By combining these two expressions, the variation $\boldsymbol{\delta\eta}$ can be expressed as:

$$\boldsymbol{\delta\eta} = \boldsymbol{J}^T\boldsymbol{D}\boldsymbol{J}. \tag{2.28}$$

The virtual deformation causes an infinitesimal variation in the squared final scalar element of arc,

$$\delta(ds_x)^2 = 2(\boldsymbol{dx})^T\boldsymbol{D}\ (\boldsymbol{dx}), \tag{2.29}$$

According to the virtual work principle, the total virtual work of all the forces on the body is zero if the virtual deformation is a virtual rigid displacement. The term virtual rigid displacement can refer to both a virtual translation and a virtual rotation. For these virtual deformations the 3 x 1 vector $\boldsymbol{\delta x}$ is such that the variation $\delta(ds_x)^2 = 0$, i.e. $\boldsymbol{D}$ is a zero matrix. For a constant virtual translation of the form,

$$\boldsymbol{\delta x} = \begin{pmatrix} \delta x \\ \delta y \\ \delta z \end{pmatrix} = \begin{pmatrix} f \\ g \\ h \end{pmatrix}, \tag{2.30}$$

it holds that the Jacobian matrix $(\boldsymbol{\delta x})_{\boldsymbol{x}}$ is a zero matrix. For this type of virtual deformation, the following volume integral must be zero:

$$\delta V = \iiint_{V_x}\left\{(\boldsymbol{\delta x})^T\left[\rho_x\boldsymbol{X}_{\boldsymbol{x}} + \left(\boldsymbol{\nabla}_{\boldsymbol{x}}\,\boldsymbol{T}\right)^T\right]\right\}dV_x = 0. \tag{2.31}$$

Granted that $\boldsymbol{\delta x}$ is non-zero, the above yields a system of equations of equilibrium:

$$\rho_x\boldsymbol{X}_{\boldsymbol{x}} + \left(\boldsymbol{\nabla}_{\boldsymbol{x}}\,\boldsymbol{T}\right)^T = \boldsymbol{0}. \tag{2.32}$$

Therefore, the virtual work for any arbitrary virtual deformation is obtained by reducing relation (2.21) to:

$$\delta V = \iiint_{V_x}\mathrm{Tr}\left(\boldsymbol{T}(\boldsymbol{\delta x})_{\boldsymbol{x}}\right)dV_x. \tag{2.33}$$

From relation (2.27) follows, by definition, that $\mathrm{Tr}\left((\boldsymbol{\delta x})_{\boldsymbol{x}}\right) = \mathrm{Tr}\left(\boldsymbol{D}\right)$, resulting in:

$$\delta V = \iiint_{V_x}\mathrm{Tr}\left(\boldsymbol{T}\boldsymbol{D}\right)dV_x. \tag{2.34}$$

The symmetric matrix $\boldsymbol{D}$ can be isolated in relation (2.28) such that

$$\boldsymbol{D} = \left(\boldsymbol{J}^T\right)^{-1} \boldsymbol{\delta\eta}\, \boldsymbol{J}^{-1}. \tag{2.35}$$

By substituting the above in relation (2.34), the virtual work can be expressed in terms of the stress tensor and the variation of the strain. Since the order of the trace is not of importance, i.e. $\mathrm{Tr}(\boldsymbol{AB}) = \mathrm{Tr}(\boldsymbol{BA})$, the following holds:

$$\delta V = \iiint_{V_x} \mathrm{Tr}\left(\boldsymbol{J}^{-1}\boldsymbol{T}(\boldsymbol{J}^T)^{-1}\boldsymbol{\delta\eta}\right) dV_x. \tag{2.36}$$

The total work exerted by all the forces on the volume of the deformable body in any deformation is assumed to be stored in the volume as strain energy. This strain energy is distributed throughout V_x with a mass density:

$$U = \iiint_{V_x} \rho_x \psi dV_x, \tag{2.37}$$

where $\psi(\boldsymbol{\eta})$ denotes the strain-energy density per unit mass. The constitutive relations are obtained by implementing the law of conservation of energy. In compliance with this law, the exerted virtual work on any portion of the volume of the deformable body in any virtual deformation should be equal to the variation of the strain energy δU. By elaborating this equality, the Cauchy stress tensor can eventually be expressed in terms of the Lagrangian strain matrix (see App. A.4.3 for details):

$$\boldsymbol{T} = \frac{1}{\det(\boldsymbol{J})} \boldsymbol{J} \frac{\partial \phi}{\partial \boldsymbol{\eta}} \boldsymbol{J}^T, \tag{2.38}$$

where $\det(\boldsymbol{J})$ denotes the determinant of the Jacobian matrix (see App. A.2.3 for details),

$$\det(\boldsymbol{J}) = \left(\frac{\rho_a}{\rho_x}\right) = \begin{vmatrix} x_a & x_b & x_c \\ y_a & y_b & y_c \\ z_a & z_b & z_c \end{vmatrix} > 0, \tag{2.39}$$

and ϕ – the strain-energy density per unit initial element of volume. The absolute value of the Jacobian determinant at a specified point defines the factor by which the volume of the body has been scaled after the deformation.

For an isotropic material, the strain-energy density $\phi(\boldsymbol{\eta})$ only depends on the three strain invariants I_1, I_2 and I_3 [22, Ch. 4.1][8, Eq. 1.46]. These strain invariants are defined as $\mathrm{Tr}(\boldsymbol{\eta})$, $\mathrm{Tr}(\mathrm{co}\ \boldsymbol{\eta})$ and $\det(\boldsymbol{\eta})$, respectively[6]. The representation of the strain-energy density ϕ as a power series in these strain invariants is written as:

$$\phi = \phi_0 + \phi_1 + \phi_2 + \phi_3 + \dots \tag{2.40}$$

where the terms are defined as[7]:

$$\begin{aligned} \phi_1 &= pI_1 \\ \phi_2 &= \frac{\lambda + 2\mu}{2} I_1^2 - 2\mu I_2 \\ \phi_3 &= \frac{l + 2m}{3} I_1^3 - 2mI_1 I_2 + nI_3. \end{aligned} \tag{2.41}$$

Here, p is an arbitrary constant and the second-order coefficients, λ and μ, are defined as the first and second Lamé parameter, respectively. The third-order coefficients l, m, n are the Murnaghan constants.

[6]The derivation of the strain invariants is elaborated in App. A.3.3.
[7]The derivation of the expression for the strain energy is given in App. A.4.3.

The stress matrix $\boldsymbol{T}$ can be expressed in terms of the Lamé parameters and the Murnaghan constants by substituting relation (2.40) into (2.38):

$$\boldsymbol{T} = \frac{1}{\det(\boldsymbol{J})}\boldsymbol{J}\Big(p\boldsymbol{E_3} + (\lambda I_1\boldsymbol{E_3} + 2\mu\boldsymbol{\eta}) + \big(lI_1^2 - 2mI_2\big)\boldsymbol{E_3} + 2mI_1\boldsymbol{\eta} + n\ \mathrm{co}\,\boldsymbol{\eta}\Big)\boldsymbol{J}^T. \tag{2.42}$$

If the strain is set to zero, the above reduces to:

$$\boldsymbol{T_0} = p\boldsymbol{E_3} = \begin{pmatrix} p & 0 & 0 \\ 0 & p & 0 \\ 0 & 0 & p \end{pmatrix}, \tag{2.43}$$

where $\boldsymbol{T_0}$ denotes a initial-stress matrix and p – the strain-independent hydrostatic stress.

2.2. Dynamic deformation

This section covers the derivation of the wave equation and serves as a bridge between Murnaghan's theory and the formulations of the wave velocities of a stressed solid [13, Eq. 12]. After being subjected to the large elastic deformation, the medium subsequently undergoes a superposed small dynamic deformation, resulting in the new position with coordinates (x', y', z'). The wave equation is then obtained through the Lagrangian form of Cauchy's first law of motion in this new position.

2.2.1. Cauchy's first law of motion

From the principle of virtual work, the system of equations of equilibrium is obtained:

$$\big(\boldsymbol{\nabla_x}\,\boldsymbol{T}\big)^T + \rho_x\boldsymbol{X_x} = \boldsymbol{0}, \tag{2.32}$$

which, upon introducing an inertia term, yields Cauchy's first law of motion [1, Eq. 2.13]:

$$\big(\boldsymbol{\nabla_x}\,\boldsymbol{T}\big)^T + \rho_x\boldsymbol{X_x} = \rho_x\ddot{\boldsymbol{x}}. \tag{2.44}$$

Here, $\ddot{\boldsymbol{x}}$ denotes the 3 x 1 vector containing the accelerations of the final coordinates.

It should be noted that the Cauchy stress tensor, and by extension also Cauchy's first law of motion, is an Eulerian description. Therefore, the matrix $\boldsymbol{T}$ describes the stress field over the body in its final configuration B_x. However, for the purpose of deriving the formulations of the wave velocity, it is more convenient to use a Lagrangian description of the stress. This stress description describes the stress field in the initial configuration B_a for which the element definitions are assumed to be known. By comparing a portion of a force $\boldsymbol{df}$ acting on both the initial and final scalar element of area, it is possible to relate both stress descriptions to each other. Figure 2.4 displays the transformation of the scalar element of area and its traction vector.

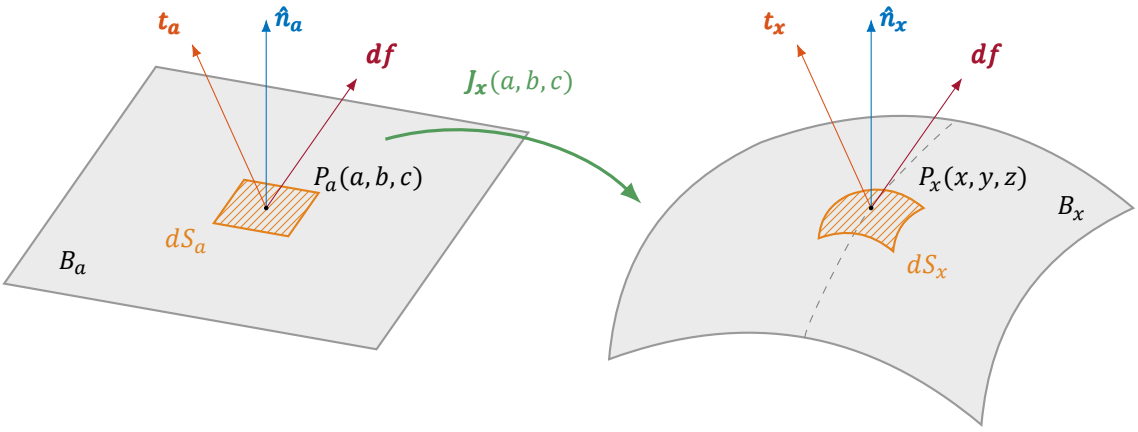

Figure 2.4: Visualisation of the initial and final scalar elements of area and their respective force vectors.

The portion of the force can be written as two equivalent expressions:

$$\boldsymbol{t_a} dS_a = \boldsymbol{df} = \boldsymbol{t_x} dS_x, \tag{2.45}$$

where $\boldsymbol{t_a}$ denotes the traction vector acting on the initial scalar element of area dS_a. A Lagrangian stress description can be introduced through the first Piola-Kirchoff stress tensor, $\boldsymbol{P} = \boldsymbol{\sigma}^T$. By using the Cauchy stress equation (2.16) and its Lagrangian counterpart, it is possible to rewrite the above to:

$$\boldsymbol{\sigma}^T \hat{\boldsymbol{n}}_{\boldsymbol{a}} dS_a = \boldsymbol{df} = \boldsymbol{T}^T \hat{\boldsymbol{n}}_{\boldsymbol{x}} dS_x. \tag{2.46}$$

After elaborating further, the nominal stress tensor $\boldsymbol{\sigma}$ can be expressed in terms of the strain-energy density with[8]:

$$\boldsymbol{\sigma} = \frac{\partial \phi}{\partial \boldsymbol{\eta}} \boldsymbol{J}^T. \tag{2.47}$$

Contrary to the Cauchy stress tensor, both the nominal stress tensor and the first Piola-Kirchoff stress tensor are asymmetric in general, i.e. $\boldsymbol{P} \neq \boldsymbol{\sigma}$. They are symmetric only and only if the Jacobian matrix $\boldsymbol{J}$ is symmetric as well.

The Lagrangian form of Cauchy's first law of motion (2.44) is then defined as:

$$\left(\boldsymbol{\nabla_a}\, \boldsymbol{\sigma}\right)^T + \rho_a \boldsymbol{X_a} = \rho_a \ddot{\boldsymbol{x}}, \tag{2.48}$$

where $\left(\boldsymbol{\nabla_a}\, \boldsymbol{\sigma}\right)^T$ denotes the divergence of the nominal stress tensor with respect to the initial coordinates and $\boldsymbol{X_a}$ – the initial mass forces.

2.2.2. Wave equation

For the purpose of deriving the wave equation, it is convenient to introduce the index notation. In accordance with this index notation, the indices are denoted with arbitrary letters which are part of the set $\{1, 2, 3\}$. The nominal stress tensor (2.47) can then be written as:

$$\sigma_{\beta q} = \frac{\partial \phi}{\partial \eta_{\alpha\beta}} J_{\alpha q}, \tag{2.49}$$

where ϕ denotes the strain-energy density[9]:

$$\phi = \tfrac{1}{2!} C_{ijkl} \eta_{ij} \eta_{kl} + \tfrac{1}{3!} C_{ijklmn} \eta_{ij} \eta_{kl} \eta_{mn} + \ldots, \tag{2.50}$$

The above represents the strain-energy density as a power series of strain components (see App. A.5.2) with the fourth-order tensor,

$$C_{ijkl} = \lambda \delta_{ij} \delta_{kl} + 2\mu I_{ijkl}, \tag{2.51}$$

and the sixth-order tensor,

$$\begin{aligned} C_{ijklmn} = {} & 2\left(l - m + \tfrac{1}{2}n\right)\delta_{ij}\delta_{kl}\delta_{mn} + 2\left(m - \tfrac{1}{2}n\right)\left(\delta_{ij} I_{klmn} + \delta_{kl} I_{mnij} + \delta_{mn} I_{ijkl}\right) \\ & + \tfrac{1}{2} n \left(\delta_{ik} I_{jlmn} + \delta_{il} I_{jkmn} + \delta_{jk} I_{ilmn} + \delta_{jl} I_{ikmn}\right). \end{aligned} \tag{2.52}$$

In these expressions, λ and μ denote the first and second Lamé parameter, respectively, and l, m, n – the Murnaghan constants. The fourth order tensor I_{ijkl} is defined as:

$$I_{ijkl} = \tfrac{1}{2}\left(\delta_{ik}\delta_{jl} + \delta_{il}\delta_{jk}\right), \tag{2.53}$$

where δ_{ij} denotes the Kronecker delta:

$$\delta_{ij} = \begin{cases} 1 & ; \quad \text{for} \quad i = j \\ 0 & ; \quad \text{else} \end{cases}. \tag{2.54}$$

[8]The derivation of the nominal stress tensor is covered in App. A.5.1.

[9]Upon assuming that the strain energy is minimal when there's zero strain, the linear term can be neglected.

By generalising relations (2.13) and (2.14), the Lagrangian strain tensor is obtained:

$$\eta_{kl} = \frac{1}{2}\left(\frac{\partial u_l}{\partial a_k} + \frac{\partial u_k}{\partial a_l} + \frac{\partial u_i}{\partial a_k}\frac{\partial u_i}{\partial a_l}\right), \tag{2.55}$$

whereas rewriting relation (2.6) yields the gradient tensor

$$J_{i\alpha} = \frac{\partial u_i}{\partial a_\alpha} + \delta_{i\alpha}. \tag{2.56}$$

With these new index notations, the nominal stress tensor (2.49) can be expanded with:

$$\begin{aligned}\sigma_{\beta q} \approx &\left(\frac{\partial u_\alpha}{\partial a_q} + \delta_{\alpha q}\right)\left[\frac{1}{2}\left(C_{ijkl}\frac{\partial \eta_{ij}}{\eta_{\alpha\beta}}\eta_{kl} + C_{ijkl}\eta_{ij}\frac{\partial \eta_{kl}}{\eta_{\alpha\beta}}\right)\right.\\ &\left.+\frac{1}{3!}\left(C_{ijklmn}\frac{\partial \eta_{ij}}{\eta_{\alpha\beta}}\eta_{kl}\eta_{mn} + C_{ijklmn}\eta_{ij}\frac{\partial \eta_{kl}}{\eta_{\alpha\beta}}\eta_{mn} + C_{ijklmn}\eta_{ij}\eta_{kl}\frac{\partial \eta_{mn}}{\eta_{\alpha\beta}}\right)\right]\\ = &\left(\frac{\partial u_\alpha}{\partial a_q} + \delta_{\alpha q}\right)\left[\frac{1}{2}\left(C_{\alpha\beta kl}\eta_{kl} + C_{ij\alpha\beta}\eta_{ij}\right)\right.\\ &\left.+\frac{1}{3!}\left(C_{\alpha\beta klmn}\eta_{kl}\eta_{mn} + C_{ij\alpha\beta mn}\eta_{ij}\eta_{mn} + C_{ijkl\alpha\beta}\eta_{ij}\eta_{kl}\right)\right].\end{aligned} \tag{2.57}$$

After further elaborating (see App. A.5.3 for details), the above becomes:

$$\sigma_{ji} = C_{ijkl}\frac{\partial u_k}{\partial a_l} + \frac{1}{2}M_{ijklmn}\frac{\partial u_k}{\partial a_l}\frac{\partial u_m}{\partial a_n} + \ldots, \tag{2.58}$$

with the sixth-order tensor

$$M_{ijklmn} = C_{ijklmn} + C_{ijln}\delta_{km} + C_{jnkl}\delta_{im} + C_{jlmn}\delta_{ik}. \tag{2.59}$$

This expression of the nominal stress tensor can be linearised by using the theory of infinitesimal deformations. In accordance with this theory, terms of an order higher than the first in the strains are neglected, resulting in the linearised nominal stress tensor

$$\sigma_{ji} \approx C_{ijkl}\frac{\partial u_k}{\partial x_l}. \tag{2.60}$$

Upon neglecting the mass forces in relation (2.48), the index notation of the Lagrangian form of Cauchy's first law of motion becomes:

$$\frac{\partial \sigma_{ji}}{\partial a_j} = \rho_a \frac{\partial x_i}{\partial t^2}. \tag{2.61}$$

which now solely consists of a space-dependent part and a time-dependent part.

If it is assumed that a small dynamic deformation $\boldsymbol{u}^{(1)}$ is superposed on the large static deformation $\boldsymbol{u}^{(0)}$ such that $\left|\boldsymbol{u}^{(1)}\right| \lll \left|\boldsymbol{u}^{(0)}\right|$, then the total deformation is defined as:

$$\boldsymbol{u} = \boldsymbol{u}^{(0)} + \boldsymbol{u}^{(1)} = \boldsymbol{x}' - \boldsymbol{a}. \tag{2.62}$$

Here, $\boldsymbol{x}'$ denotes the new position after this dynamic deformation has occurred:

$$\boldsymbol{x}' = \begin{pmatrix} x' \\ y' \\ z' \end{pmatrix} = \begin{pmatrix} u^{(1)} + x \\ v^{(1)} + y \\ w^{(1)} + z \end{pmatrix}, \tag{2.63}$$

or, equivalently, in index notation:

$$x_i' = u_i^{(1)} + x_i. \tag{2.64}$$

The Lagrangian form of Cauchy's first law of motion in this new position then reads:

$$\frac{\partial \sigma_{ji}}{\partial a_j} = \rho_a \frac{\partial x_i'}{\partial t^2}, \tag{2.65}$$

which, after substituting relation (2.64) and elaborating the time-dependent part, yields (see App. A.5.4 for details):

$$\rho_a \frac{\partial u_i^{(1)}}{\partial t^2} - \frac{\partial \sigma_{ji}}{\partial a_j} = 0. \tag{2.66}$$

The space-dependent part can be expressed in terms of the final coordinates by rewriting the partial derivative with respect to the initial coordinates:

$$\frac{\partial}{\partial a_j} = \frac{\partial}{\partial x_j} + u_{k,j}^{(0)} \frac{\partial}{\partial x_k} + \dots \tag{2.67}$$

Here, $u_{k,j}^{(0)}$ is a compact notation for the spatial derivative of the static deformation $u_k^{(0)}$ with respect to the final coordinate x_j:

$$u_{k,j}^{(0)} = \frac{\partial u_k^{(0)}}{\partial x_j} = \begin{cases} e_{jk} & ; \quad \text{for} \quad j = k \\ 0 & ; \quad \text{else} \end{cases}, \tag{2.68}$$

where e_{jk} denotes the first-order approximation of the strain. The spatial derivative of the nominal stress tensor then becomes:

$$\begin{aligned} \frac{\partial \sigma_{ji}}{\partial a_j} &\approx \frac{\partial \sigma_{ji}}{\partial x_j} + u_{p,j}^{(0)} \frac{\partial \sigma_{ji}}{\partial x_p} \\ &\approx C_{ijkl} \frac{\partial}{\partial x_j} \left(\frac{\partial u_k}{\partial x_l} + u_{q,l}^{(0)} \frac{\partial u_k}{\partial x_q} \right) + u_{p,j}^{(0)} C_{ijkl} \frac{\partial}{\partial x_j} \left(\frac{\partial u_k}{\partial x_l} + u_{q,l}^{(0)} \frac{\partial u_k}{\partial x_q} \right) \\ &\quad + \frac{1}{2} M_{ijklmn} \frac{\partial}{\partial x_j} \left[\left(\frac{\partial u_k}{\partial x_l} + u_{q,l}^{(0)} \frac{\partial u_k}{\partial x_q} \right) \left(\frac{\partial u_m}{\partial x_n} + u_{r,n}^{(0)} \frac{\partial u_m}{\partial x_r} \right) \right] + u_{p,j}^{(0)} \frac{1}{2} M_{ijklmn} \frac{\partial}{\partial x_j} \left[\dots \right] \\ &\quad + \dots \end{aligned} \tag{2.69}$$

which, after elaborating further[10], eventually yields:

$$\frac{\partial \sigma_{ji}}{\partial a_j} \approx \left(C_{ijkl} + C_{ijkq} u_{l,q}^{(0)} + C_{ipkl} u_{j,p}^{(0)} + C_{ijklmn} u_{m,n}^{(0)} + C_{ijln} u_{k,n}^{(0)} + C_{jnkl} u_{i,n}^{(0)} + C_{jlmn} \delta_{ik} u_{m,n}^{(0)} \right) \frac{\partial^2 u_k^{(1)}}{\partial x_j \partial x_l}. \tag{2.70}$$

By substituting the above in (2.66), the wave equation is obtained:

$$\rho_a \frac{\partial^2 u_i^{(1)}}{\partial t^2} - B_{ijkl} \frac{\partial^2 u_k^{(1)}}{\partial x_j \partial x_l} = 0, \tag{2.71}$$

where the fourth-order tensor

$$B_{ijkl} = C_{ijkl} + \delta_{ik} C_{jlqr} u_{q,r}^{(0)} + C_{rjkl} u_{i,r}^{(0)} + C_{irkl} u_{j,r}^{(0)} + C_{ijrl} u_{k,r}^{(0)} + C_{ijkr} u_{l,r}^{(0)} + C_{ijklmn} u_{m,n}^{(0)}, \tag{2.72}$$

denotes the effective elastic moduli.

[10] The expansion of the spatial derivative of the nominal stress tensor is covered in App. A.5.4.

2.2.3. Wave velocity

The formulation of the wave velocity is obtained upon division of both sides of the wave equation (2.71) by the initial mass density ρ_a:

$$\frac{\partial^2 u_i^{(1)}}{\partial t^2} - c_{ji}^2 \frac{\partial^2 u_k^{(1)}}{\partial x_j \partial x_l} = 0, \tag{2.73}$$

where the second-order tensor

$$c_{ji} = \sqrt{\frac{B_{ijkl}}{\rho_a}}, \tag{2.74}$$

describes the velocity of a wave which polarises in the i-direction while propagating in the j-direction.

For a longitudinal wave, which propagates along the x-direction, relation (2.73) becomes:

$$\frac{\partial^2 u^{(1)}}{\partial t^2} - c_{xx}^2 \frac{\partial^2 u^{(1)}}{\partial x^2} = 0. \tag{2.75}$$

The wave velocity c_{xx} is then defined as[11]:

$$c_{xx} = \sqrt{\frac{\lambda + 2\mu + (2l + \lambda)e + (4\lambda + 4m + 10\mu)e_{xx}}{\rho_a}}, \tag{2.76}$$

where e denotes volumetric strain:

$$e = e_{xx} + e_{yy} + e_{zz}. \tag{2.77}$$

This relation expresses the wave velocity in terms of the Murnaghans constants and the uniaxial strains. By using the definition of the linearised nominal stress (2.60), the uniaxial strains can be written in terms of the uniaxial stress (see App. A.5.5 for details):

$$\sigma_{ii} = (3\lambda + 2\mu)e. \tag{2.78}$$

By using the above, the description of the longitudinal-wave velocity of a medium which is stressed parallel to its propagation direction is obtained:

$$c_{xx}{}^{\sigma_{xx}} = \sqrt{\frac{\lambda + 2\mu \pm \frac{\sigma_{xx}}{3K}\left[2l + \lambda + \frac{\lambda + \mu}{\mu}(4\lambda + 4m + 10\mu)\right]}{\rho_a}}, \tag{2.79}$$

where K denotes the bulk modulus:

$$K = \lambda + \frac{2}{3}\mu, \tag{2.80}$$

whereas $+\sigma_{xx}$ and $-\sigma_{xx}$ – a tensile stress and a compressive stress, respectively. Through a similar approach, the description of the longitudinal-wave velocity of a medium which is stressed perpendicular to its propagation direction can be found:

$$\begin{aligned} c_{xx}{}^{\sigma_{yy}} &= \sqrt{\frac{\lambda + 2\mu \pm \frac{\sigma_{yy}}{3K}\left[2l + \lambda - \frac{\lambda}{2\mu}(4\lambda + 4m + 10\mu)\right]}{\rho_a}} \\ c_{xx}{}^{\sigma_{zz}} &= \sqrt{\frac{\lambda + 2\mu \pm \frac{\sigma_{zz}}{3K}\left[2l + \lambda - \frac{\lambda}{2\mu}(4\lambda + 4m + 10\mu)\right]}{\rho_a}}. \end{aligned} \tag{2.81}$$

[11] The expansion of the wave velocities is elaborated in App. A.5.5.

For transverse waves, which propagate along the x-direction and polarise in the y-direction or z-direction, relation (2.73) becomes:

$$\begin{aligned} \frac{\partial^2 v^{(1)}}{\partial t^2} - c_{xy}^2 \frac{\partial^2 v^{(1)}}{\partial x^2} &= 0 \\ \frac{\partial^2 w^{(1)}}{\partial t^2} - c_{xz}^2 \frac{\partial^2 w^{(1)}}{\partial x^2} &= 0, \end{aligned} \tag{2.82}$$

respectively. The transverse-wave velocity of a medium which is subjected to a stress parallel to the propagation direction is then defined as:

$$c_{xy}{}^{\sigma_{xx}} = c_{xz}{}^{\sigma_{xx}} = \sqrt{\frac{\mu \pm \frac{\sigma_{xx}}{3K}\left(m + \frac{\lambda n}{4\mu} + 4\lambda + 4\mu\right)}{\rho_a}}, \tag{2.83}$$

whereas the transverse-wave velocity of a medium which is subjected to a stress parallel to the polarisation direction is defined as:

$$\begin{aligned} c_{xy}{}^{\sigma_{yy}} &= \sqrt{\frac{\mu \pm \frac{\sigma_{yy}}{3K}\left(m + \frac{\lambda n}{4\mu} + \lambda + 2\mu\right)}{\rho_a}} \\ c_{xz}{}^{\sigma_{zz}} &= \sqrt{\frac{\mu \pm \frac{\sigma_{zz}}{3K}\left(m + \frac{\lambda n}{4\mu} + \lambda + 2\mu\right)}{\rho_a}}. \end{aligned} \tag{2.84}$$

When loading the medium with a stress perpendicular to both the propagation direction and polarisation direction, the transverse-wave velocity becomes:

$$\begin{aligned} c_{xy}{}^{\sigma_{zz}} &= \sqrt{\frac{\mu \pm \frac{\sigma_{zz}}{3K}\left[\lambda + m - \frac{\lambda+\mu}{\mu}\left(\frac{3\mu\lambda}{\lambda+\mu} + \frac{1}{2}n\right)\right]}{\rho_a}} \\ c_{xz}{}^{\sigma_{yy}} &= \sqrt{\frac{\mu \pm \frac{\sigma_{yy}}{3K}\left[\lambda + m - \frac{\lambda+\mu}{\mu}\left(\frac{3\mu\lambda}{\lambda+\mu} + \frac{1}{2}n\right)\right]}{\rho_a}}. \end{aligned} \tag{2.85}$$

From the several expressions of the wave velocities it can be observed that the wave velocity is dependent on the orientation of the stress with respect to both the propagation and the polarisation direction. It should be noted that the uniaxial stress σ_{ii} depends on the strain, which results in a second-order term. When the infinitesimal theory is taken into account, the contribution of the stress can be neglected, resulting in:

$$c_{ij}{}^{0} = \begin{cases} \sqrt{\dfrac{\lambda + 2\mu}{\rho_a}} & ; \quad \text{for} \quad i = j \\ \sqrt{\dfrac{\mu}{\rho_a}} & ; \quad \text{else} \end{cases}, \tag{2.86}$$

which is defined as the initial wave velocity.

In this chapter, Murnaghan's formulation of the wave velocities of a medium subjected to a stress has been derived. It has been shown that influence of the stress differs according to the orientation of the stress with respect to the propagation and polarisation directions of the wave. This influence is regulated by the Murnaghan constants, which still need to be determined.

3

Theoretical study: M.A. Biot

The second approach to the acoustoelastic effect is covered in this chapter. In his paper *"The Influence of Initial Stress on Elastic Waves"* Biot [4] describes how a relation between the initial stress and the wave velocity of a medium can be established. Later on, he wrote the book *"Mechanics of incremental deformations"* [5], in which he expanded upon this theory. This chapter contains Biot's theory in the way it has been presented in his aforementioned paper, as well as additional derivations and intermediate steps which are necessary to obtain certain expressions. Afterwards, the index notation from Biot's book has been adopted for the purpose of extending the theory to the third dimension.

3.1. Two-dimensional medium

This section deals with the derivation of both the static and dynamic-equilibrium equations of a two-dimensional medium as it is transformed from its initial to its final configuration. This transformation is the result of a displacement which is accordance with the theory infinitesimal deformations. The medium is assumed to be deformable and is, in its initial configuration, subjected to both initial-stress components and mass forces. After the medium has deformed, it is subjected to strain-dependent incremental-stress components as well.

3.1.1. Initial-stress field

A point P_a with initial coordinates (a, b) is situated within an infinitesimal medium which is assumed to be subjected to initial-stress components S_{11}, S_{22}, S_{12}, and mass forces, displayed in Figure 3.1.

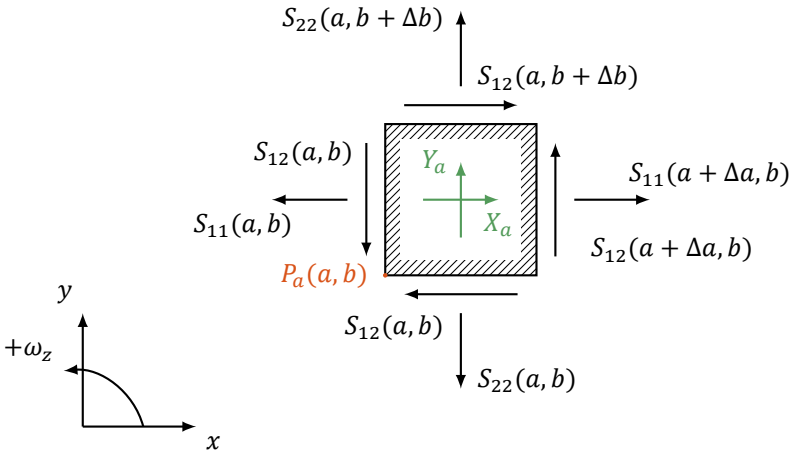

Figure 3.1: Initial-stresses acting on a square with dimensions $\Delta a, \Delta b$.

Based on Figure 3.1, the following equilibrium conditions hold[1]:

$$\begin{aligned} \frac{\partial S_{11}}{\partial a} + \frac{\partial S_{12}}{\partial b} + \rho_a X_a = 0 \\ \frac{\partial S_{12}}{\partial a} + \frac{\partial S_{22}}{\partial b} + \rho_a Y_a = 0, \end{aligned} \tag{3.1}$$

where ρ_a denotes initial mass density and X_a, Y_a – the components of the mass force which have the unit of acceleration.

3.1.2. Transformation of the medium

Through infinitesimal deformations u and v, the medium is displaced to the point P_x with final coordinates (x, y),

$$\begin{aligned} x = a + u \\ y = b + v, \end{aligned} \tag{3.2}$$

and subsequently undergoes a pure homogeneous deformation and a rotation:

$$\omega_z = \frac{1}{2}\left(\frac{\partial v}{\partial a} - \frac{\partial u}{\partial b}\right). \tag{3.3}$$

As a result of this deformation, incremental-stress components s_{ij} are generated which depend on the strain. This deformation and the resulting stress state of the medium is displayed in Figure 3.2.

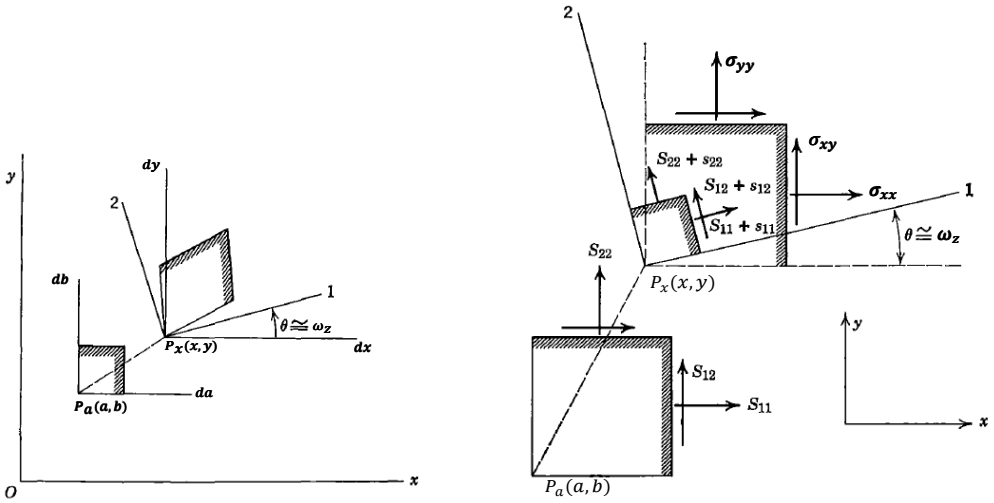

Figure 3.2: Representation of the deformation and the stresses of the medium within the vicinity of point $P_x(x, y)$ [5] (edited). (a) Deformation and rotation of the medium. (b) Initial-stresses and the incremental-stresses.

The stress components at this point $P_x(x, y)$, referred to the rotated axes, are defined as:

$$\begin{aligned} \sigma_{11} = S_{11} + s_{11} \\ \sigma_{22} = S_{22} + s_{22} \\ \sigma_{12} = S_{12} + s_{12}. \end{aligned} \tag{3.4}$$

[1]The derivation of these equilibrium conditions are derived in App. B.1.1.

The stress components σ_{xx}, σ_{yy} and σ_{xy}, displayed in Figure 3.2b, refer to the unrotated axes, x and y, and can be obtained by means of the tensor transformation relation[2]:

$$\begin{aligned}\sigma_{xx} &= S_{11} + s_{11} - 2S_{12}\omega_z \\ \sigma_{yy} &= S_{22} + s_{22} + 2S_{12}\omega_z \\ \sigma_{xy} &= S_{12} + s_{12} + (S_{11} - S_{22})\omega_z.\end{aligned} \tag{3.5}$$

3.1.3. Dynamic equilibrium after deformation

The dynamic equilibrium of the stresses at the point $P_x(x, y)$ is defined as:

$$\begin{aligned}\frac{\partial \sigma_{xx}}{\partial x} + \frac{\partial \sigma_{xy}}{\partial y} + \rho_x X_x &= \rho_x \frac{\partial^2 u}{\partial t^2} \\ \frac{\partial \sigma_{xy}}{\partial x} + \frac{\partial \sigma_{yy}}{\partial y} + \rho_x Y_x &= \rho_x \frac{\partial^2 v}{\partial t^2},\end{aligned} \tag{3.6}$$

where ρ_x denotes the final mass density and X_x, Y_x – the components of the final mass force.

By making use of the chain rule of differentiation, it is possible to express the dynamic equilibrium in terms of the initial coordinates:

$$\begin{aligned}\frac{\partial \sigma_{xx}}{\partial a}\frac{\partial a}{\partial x} + \frac{\partial \sigma_{xx}}{\partial b}\frac{\partial b}{\partial x} + \frac{\partial \sigma_{xy}}{\partial a}\frac{\partial a}{\partial y} + \frac{\partial \sigma_{xy}}{\partial b}\frac{\partial b}{\partial y} + \rho_x X_x &= \rho_x \frac{\partial^2 u}{\partial t^2} \\ \frac{\partial \sigma_{xy}}{\partial a}\frac{\partial a}{\partial x} + \frac{\partial \sigma_{xy}}{\partial b}\frac{\partial b}{\partial x} + \frac{\partial \sigma_{yy}}{\partial a}\frac{\partial a}{\partial y} + \frac{\partial \sigma_{yy}}{\partial b}\frac{\partial b}{\partial y} + \rho_x Y_x &= \rho_x \frac{\partial^2 v}{\partial t^2},\end{aligned} \tag{3.7}$$

where the partial derivatives of initial coordinates with respect to the final coordinates are defined as[3]:

$$\begin{aligned}\frac{\partial a}{\partial x} &= \frac{1}{\det(\boldsymbol{J})}\left(1 + \frac{\partial v}{\partial b}\right) \quad ; \quad \frac{\partial a}{\partial y} = -\frac{1}{\det(\boldsymbol{J})}\frac{\partial u}{\partial b} \\ \frac{\partial b}{\partial x} &= -\frac{1}{\det(\boldsymbol{J})}\frac{\partial v}{\partial a} \quad ; \quad \frac{\partial b}{\partial y} = \frac{1}{\det(\boldsymbol{J})}\left(1 + \frac{\partial u}{\partial a}\right).\end{aligned} \tag{3.8}$$

Here, $\boldsymbol{J}$ denotes the 2 x 2 Jacobian matrix:

$$\boldsymbol{J} = \begin{pmatrix} \frac{\partial x}{\partial a} & \frac{\partial x}{\partial b} \\ \frac{\partial y}{\partial a} & \frac{\partial y}{\partial b} \end{pmatrix}. \tag{3.9}$$

After substituting expressions (3.8) into relation (3.7) and using the definition of the Jacobian determinant (2.39), the dynamic equilibrium becomes :

$$\begin{aligned}\frac{\partial \sigma_{xx}}{\partial a} + \frac{\partial \sigma_{xy}}{\partial b} + e_{yy}\frac{\partial \sigma_{xx}}{\partial a} + e_{xx}\frac{\partial \sigma_{xy}}{\partial b} - (e_{xy} - \omega_z)\frac{\partial \sigma_{xy}}{\partial a} - (e_{xy} + \omega_z)\frac{\partial \sigma_{xx}}{\partial b} + \rho_a X_x &= \rho_a \frac{\partial^2 u}{\partial t^2} \\ \frac{\partial \sigma_{xy}}{\partial a} + \frac{\partial \sigma_{yy}}{\partial b} + e_{yy}\frac{\partial \sigma_{xy}}{\partial a} + e_{xx}\frac{\partial \sigma_{yy}}{\partial b} - (e_{xy} - \omega_z)\frac{\partial \sigma_{yy}}{\partial a} - (e_{xy} + \omega_z)\frac{\partial \sigma_{xy}}{\partial b} + \rho_a Y_x &= \rho_a \frac{\partial^2 v}{\partial t^2},\end{aligned} \tag{3.10}$$

where the first-order approximations of the strain components are denoted with:

$$\begin{aligned}e_{xx} &= \frac{\partial u}{\partial a} \\ e_{yy} &= \frac{\partial v}{\partial b} \\ e_{xy} &= \frac{1}{2}\left(\frac{\partial v}{\partial a} + \frac{\partial u}{\partial b}\right).\end{aligned} \tag{3.11}$$

[2]This tensor transformation relation is elaborated in App. B.1.2

[3]The partial derivatives are elaborated in App. B.1.3.

Substituting the stress components (3.5) into relations (3.10), eventually results in[4]:

$$\begin{aligned}
&\frac{\partial s_{11}}{\partial a}+\frac{\partial s_{12}}{\partial b}+\rho_a u\frac{\partial X_x}{\partial a}+\rho_a v\frac{\partial X_x}{\partial b}+\rho_a\omega_z Y_a-2S_{12}\frac{\partial \omega_z}{\partial a}\\
&\quad+\left(S_{11}-S_{22}\right)\frac{\partial \omega_z}{\partial b}+e_{yy}\frac{\partial S_{11}}{\partial a}+e_{xx}\frac{\partial S_{12}}{\partial b}-e_{xy}\left(\frac{\partial S_{12}}{\partial a}+\frac{\partial S_{11}}{\partial b}\right)=\rho_a\frac{\partial^2 u}{\partial t^2}\\
&\frac{\partial s_{12}}{\partial a}+\frac{\partial s_{22}}{\partial b}+\rho_a u\frac{\partial Y_x}{\partial a}+\rho_a v\frac{\partial Y_x}{\partial b}-\rho_a\omega_z X_a+2S_{12}\frac{\partial \omega_z}{\partial b}\\
&\quad+\left(S_{11}-S_{22}\right)\frac{\partial \omega_z}{\partial a}+e_{yy}\frac{\partial S_{12}}{\partial a}+e_{xx}\frac{\partial S_{22}}{\partial b}-e_{xy}\left(\frac{\partial S_{22}}{\partial a}+\frac{\partial S_{12}}{\partial b}\right)=\rho_a\frac{\partial^2 v}{\partial t^2}.
\end{aligned}\tag{3.12}$$

Since it is known that the incremental-stress components only depend on the strain, they may be written as linear functions of the strain components:

$$\begin{aligned}
s_{11}&=B_{1111}e_{xx}+B_{1122}e_{yy}+2B_{1112}e_{xy}\\
s_{22}&=B_{2211}e_{xx}+B_{2222}e_{yy}+2B_{2212}e_{xy}\\
s_{12}&=B_{1211}e_{xx}+B_{1222}e_{yy}+2B_{1212}e_{xy}.
\end{aligned}\tag{3.13}$$

In Biot's book *"Mechanics of incremental deformation"* [5, Ch. 2.3], it is explained how relations between the elastic coefficients B_{ijkl} and the initial-stress components S_{ij} can be established through the principle of virtual work[5] :

$$\begin{aligned}
B_{1122}+S_{11}&=B_{2211}+S_{22}\\
B_{1112}-\tfrac{1}{2}S_{12}&=B_{1211}+\tfrac{1}{2}S_{12}\\
B_{2212}-\tfrac{1}{2}S_{12}&=B_{1222}+\tfrac{1}{2}S_{12}.
\end{aligned}\tag{3.14}$$

3.2. Three-dimensional medium

This section covers the derivation of the wave equation and, with it, the expressions of the wave velocities, expressed in terms of the initial-stress components. By extending the two-dimensional stress field of Figure 3.1 to a three-dimensional case, it is possible to observe the influence of the orientation of the stress direction with the respect to the propagation and polarisation direction of a wave.

3.2.1. Index notation

For the purpose of expanding the two-dimensional dynamic equilibrium (3.12) to the third dimension, it is convenient to adopt the index notation. In this notation system the indices have to abide to the following:

$$i,j,k,l\in\{1,2,3\}.\tag{3.15}$$

The three dynamic-equilibrium conditions can now be written in the compact form [5, Eq. 7.42]:

$$\frac{\partial s_{ij}}{\partial a_j}+\rho_a\Delta X_i-\rho_a\omega_{ik}X_k(x_l)-\rho_a eX_i(x_l)+S_{jk}\frac{\partial \omega_{ik}}{\partial a_j}+S_{ik}\frac{\partial \omega_{jk}}{\partial a_j}-e_{jk}\frac{\partial S_{ik}}{\partial a_j}=\rho_a\frac{\partial^2 u_i}{\partial t^2},\tag{3.16}$$

where $e=e_{xx}+e_{yy}+e_{zz}$ denotes the volumetric strain and the indices i,j,k range over the set {1,2,3}. The strain components and the rotations are defined as:

$$\begin{aligned}
e_{ij}&=\frac{1}{2}\left(\frac{\partial u_i}{\partial a_j}+\frac{\partial u_j}{\partial a_i}\right)\\
\omega_{ij}&=\frac{1}{2}\left(\frac{\partial u_i}{\partial a_j}-\frac{\partial u_j}{\partial a_i}\right),
\end{aligned}\tag{3.17}$$

respectively.

[4] The derivation of the final expression of the dynamic equilibrium is covered in App. B.1.4.
[5] The proof of these relations is derived in App. B.2.1.

The initial coordinates and the displacements are denoted with:

$$\begin{aligned} a_i &= (a_1, a_2, a_3) = (a, b, c) \\ u_i &= (u_1, u_2, u_3) = (u, v, w), \end{aligned} \tag{3.18}$$

respectively. The notation for the rotation angles can be simplified by specifying the orthogonal axis of rotation. It should be noted that the rotation angles are ant-symmetric, resulting in the following definitions:

$$\begin{aligned} \omega_{11} &= 1 & \omega_{12} &= -\omega_z & \omega_{13} &= \omega_y \\ \omega_{21} &= \omega_z & \omega_{22} &= 1 & \omega_{23} &= -\omega_x \\ \omega_{31} &= -\omega_y & \omega_{32} &= \omega_x & \omega_{33} &= 1. \end{aligned} \tag{3.19}$$

The quantity ΔX_i denotes the increment in mass force from the initial location to the displaced location and is defined as

$$\Delta X_i = u_j \frac{\partial X_i(a_l)}{\partial a_j}, \tag{3.20}$$

where the $X_i(a_l)$ are the initial mass forces. The incremental-stress components s_{ij} can be written as:

$$s_{ij} = Z_{ijkl} e_{kl} - S_{ij} e. \tag{3.21}$$

The fourth-order tensor Z_{ijkl} is defined as:

$$Z_{ijkl} = B_{ijkl} + S_{ij}\delta_{kl}, \tag{3.22}$$

where δ_{kl} denotes the Kronecker delta. The relations between the initial-stress components and the elastic coefficients, (3.14), then become:

$$B_{ijkl} + S_{ij}\delta_{kl} = B_{klij} + S_{kl}\delta_{ij}. \tag{3.23}$$

3.2.2. Wave equation

By setting the conditions for the initial-stress components, it is possible to examine the corresponding behaviour of elastic waves. This can be done by elaborating the dynamic-equilibrium relations (3.16). In order to study the influence of the initial-stress components on the wave velocity, a stressed cube is considered. A uniform initial-stress state in the principal directions along the x, y, z axes is assumed . This results in the stress components depicted in Figure 3.3.

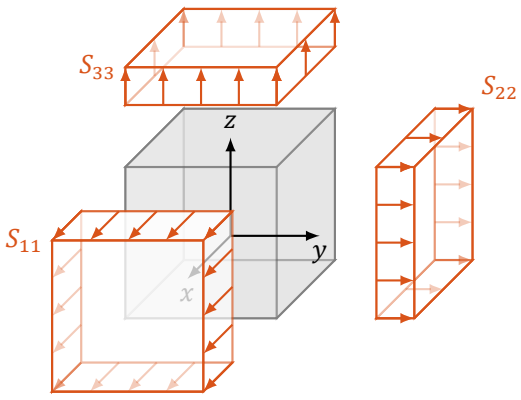

Figure 3.3: Initial tensile stresses acting on a cube, including the assumed sign conventions.

Following from the theory infinitesimal deformations, the initial and final coordinates are approximately the same. Therefore, the spatial derivatives with respect to the initial coordinates can be written in terms of the final coordinates.

Relation (3.16) then yields the following three dynamic-equilibrium conditions[6]:

$$\begin{aligned}
\frac{\partial s_{11}}{\partial x} + \frac{\partial s_{12}}{\partial y} + \frac{\partial s_{13}}{\partial z} + \left(S_{11} - S_{22}\right)\frac{\partial \omega_z}{\partial y} + \left(S_{33} - S_{11}\right)\frac{\partial \omega_y}{\partial z} &= \rho_a \frac{\partial^2 u}{\partial t^2} \\
\frac{\partial s_{12}}{\partial x} + \frac{\partial s_{22}}{\partial y} + \frac{\partial s_{23}}{\partial z} + \left(S_{11} - S_{22}\right)\frac{\partial \omega_z}{\partial x} + \left(S_{22} - S_{33}\right)\frac{\partial \omega_x}{\partial z} &= \rho_a \frac{\partial^2 v}{\partial t^2} \\
\frac{\partial s_{13}}{\partial x} + \frac{\partial s_{23}}{\partial y} + \frac{\partial s_{33}}{\partial z} + \left(S_{33} - S_{11}\right)\frac{\partial \omega_y}{\partial x} + \left(S_{22} - S_{33}\right)\frac{\partial \omega_x}{\partial y} &= \rho_a \frac{\partial^2 w}{\partial t^2}.
\end{aligned} \tag{3.24}$$

The wave equations are obtained by substituting relation (3.21) and using the definition of the rotation angles ω_{ij}. For each wave equation only one type of solution is assumed, as displayed in Figure 3.4.

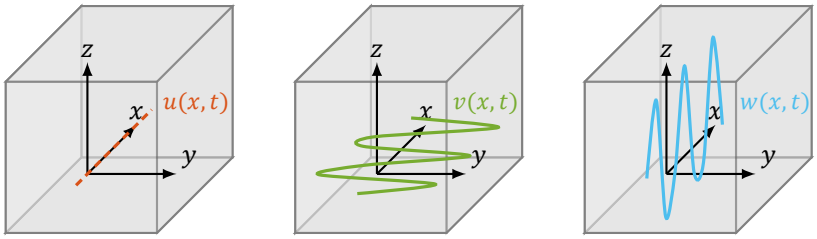

Figure 3.4: Graphical representation of the assumed waveforms for each wave equation.

For these waveforms, the set of wave equations becomes:

$$\begin{aligned}
\rho_a \frac{\partial^2 u}{\partial t^2} - \left(Z_{1111} - S_{11}\right)\frac{\partial^2 u}{\partial x^2} &= 0 \\
\rho_a \frac{\partial^2 v}{\partial t^2} - \left(Z_{1212} + \tfrac{1}{2}S_{11} - \tfrac{1}{2}S_{22}\right)\frac{\partial^2 v}{\partial x^2} &= 0 \\
\rho_a \frac{\partial^2 w}{\partial t^2} - \left(Z_{1313} + \tfrac{1}{2}S_{11} - \tfrac{1}{2}S_{33}\right)\frac{\partial^2 w}{\partial x^2} &= 0.
\end{aligned} \tag{3.25}$$

3.2.3. Wave velocity

Upon division by the mass density ρ_a, relation (3.25) can be simplified to:

$$\begin{aligned}
\frac{\partial^2 u}{\partial t^2} - {c_{xx}}^2 \frac{\partial^2 u}{\partial x^2} &= 0 \\
\frac{\partial^2 v}{\partial t^2} - {c_{xy}}^2 \frac{\partial^2 v}{\partial x^2} &= 0 \\
\frac{\partial^2 w}{\partial t^2} - {c_{xz}}^2 \frac{\partial^2 w}{\partial x^2} &= 0,
\end{aligned} \tag{3.26}$$

where c_{xx}, c_{xy} and c_{xz} denote the wave velocities of waves propagating in the x-direction while polarising in the x, y and z-direction, respectively. By using relation (3.22), these wave velocities of the stressed medium can be defined as[7]:

$$\begin{aligned}
{c_{xx}}^{S_{11}} &= \sqrt{\frac{\lambda + 2\mu}{\rho_a}} \\
{c_{xy}}^{S_{11};S_{22}} &= \sqrt{\frac{\mu + \frac{1}{2}S_{11} - \frac{1}{2}S_{22}}{\rho_a}} \\
{c_{xz}}^{S_{11};S_{33}} &= \sqrt{\frac{\mu + \frac{1}{2}S_{11} - \frac{1}{2}S_{33}}{\rho_a}}.
\end{aligned} \tag{3.27}$$

[6]The derivation is covered in App. B.2.2
[7]The intermediate steps are elaborated in App. B.2.3

These relations show that only the expressions for transverse-wave velocities are directly influenced by the initial-stress components. For a longitudinal wave, the expression of the wave velocity remains equal to that of an unstressed medium. Due to the absence of initial-stress components in the formulation of the longitudinal-wave velocity, it seems as if there is no influence from the initial-stress at first sight. However, the expression is indirectly influenced through relation (3.23). Note that the definition of the initial wave velocity, ${c_{ij}}^0$, is obtained once the initial-stress components are identical or both equal to zero:

$$ {c_{ij}}^0 = \begin{cases} \sqrt{\dfrac{\lambda + 2\mu}{\rho_a}} & ; \quad \text{for} \quad i = j \\ \sqrt{\dfrac{\mu}{\rho_a}} & ; \quad \text{else} \end{cases} , \tag{2.86} $$

where λ and μ denote the first and second Lamé parameter, respectively.

The elaboration of Biot's theoretical model has been covered in this chapter. It has been demonstrated how the initial-stress component influences the wave velocities of the medium, according to Biot. The next chapter contains a discussion of both Biot's and Murnaghan's model. Through a comparison, their similarities as well as the differences in their fundamental assumptions are detailed.

4

Discussion: Murnaghan and Biot

In Chapters 2 and 3, theoretical review studies have been conducted on the behaviour of elastic waves, propagating through a stressed medium. This chapter serves as a discussion in which a comparison will be made between the two approaches with respect to the elastic wave propagation and the wave velocity in particular. The similarities between Murnaghan's and Biot's theory as well as their fundamental differences, are elaborated here.

4.1. Fundamental assumptions

From the theoretical studies, it shows that both models are accompanied with different analytical observations with respect to the change of the wave velocity under certain stress conditions. These differences stem from the fundamental assumptions made by the two authors, upon which their theories are based. Therefore, the foundations of both models will be revised in this section.

4.1.1. F.D. Murnaghan

In his theory, Murnaghan describes how a three-dimensional deformable medium transforms under an elastic deformation. He made the assumption that this deformation is of a sufficient magnitude such that its second-order terms are of importance for the dynamic response of the medium. Therefore, a distinction can be made between the initial and final configuration of the medium, expressed in the coordinates (a, b, c) and (x, y, z), respectively. As a result, the strains, and consequently the stresses, can be either presented with the Eulerian description, i.e. expressed in terms of the final coordinates:

$$\epsilon_{kl} = \frac{1}{2}\left(\frac{\partial u_l}{\partial x_k} + \frac{\partial u_k}{\partial x_l} - \frac{\partial u_i}{\partial x_k}\frac{\partial u_i}{\partial x_l}\right), \tag{4.1}$$

or with the Lagrangian description, i.e. expressed in terms of the initial coordinates:

$$\eta_{kl} = \frac{1}{2}\left(\frac{\partial u_l}{\partial a_k} + \frac{\partial u_k}{\partial a_l} + \frac{\partial u_i}{\partial a_k}\frac{\partial u_i}{\partial a_l}\right). \tag{2.55}$$

Another assumption Murnaghan makes is that the medium is an isotropic material. Accordingly, the strain-energy density only depends on the three strain invariants:

$$\phi(\boldsymbol{\eta}) = pI_1 + \frac{\lambda + 2\mu}{2}I_1^2 - 2\mu I_2 + \frac{l + 2m}{3}I_1^3 - 2mI_1I_2 + nI_3, \tag{4.2}$$

where the introduction of the Murnaghan constants l, m, n is a direct result of the inclusion of the second-order terms with respect to the deformation. The constitutive relation links the strains to the stresses through this formulation of the strain-energy density:

$$\boldsymbol{T} = \frac{1}{\det(\boldsymbol{J})}\boldsymbol{J}\Big(p\boldsymbol{E_3} + (\lambda I_1\boldsymbol{E_3} + 2\mu\boldsymbol{\eta}) + \left(lI_1^2 - 2mI_2\right)\boldsymbol{E_3} + 2mI_1\boldsymbol{\eta} + n\ \mathrm{co}\,\boldsymbol{\eta}\Big)\boldsymbol{J}^T. \tag{2.42}$$

Here, the arbitrary constant p denotes the initial-stress state of the medium, which, in line with the assumption that the material is isotropic, has to be a hydrostatic stress [22, Ch. 4.2].

The downside of this ideal assumption is that the applicability of Murnaghan's theory is limited to isotropic materials. Since it is the link between the stresses and strains in the constitutive relation, the formulation of the strain-energy density is a core element of Murnaghan's theory. For anisotropic materials there is a large variety of formulations for the strain-energy density. Implementing these formulations in Murnaghan's theory could therefore yield results which differ from the current outcome.

4.1.2. M.A. Biot

Biot's theory describes the transformation of a deformable medium caused by an elastic deformation as well. Contrary to Murnaghan's assumption, Biot implements the theory of infinitesimal deformations. According this theory, the deformation is assumed to be sufficiently small such that its second-order terms can be discarded. As a result of this infinitesimal deformation, there is no distinction between the initial and final configuration of the medium. Therefore, the strain components can be approximated such that both the Eulerian and Lagrangian description yield:

$$e_{ij} = \frac{1}{2}\left(\frac{\partial u_i}{\partial a_j} + \frac{\partial u_j}{\partial a_i}\right) = \frac{1}{2}\left(\frac{\partial u_i}{\partial x_j} + \frac{\partial u_j}{\partial x_i}\right). \tag{4.3}$$

Biot states that an initial-stress state acting on the deformable medium must influence its elastic wave propagation. He assumes that this influence largely depends on the magnitude of the strain-independent stress. Biot describes that the initial-stress components only satisfy the conditions of internal equilibrium,

$$\begin{aligned} \frac{\partial S_{11}}{\partial a} + \frac{\partial S_{12}}{\partial b} + \rho_a X_a &= 0 \\ \frac{\partial S_{12}}{\partial a} + \frac{\partial S_{22}}{\partial b} + \rho_a Y_a &= 0, \end{aligned} \tag{3.1}$$

where the positive stresses are denoted as tensile stresses. However, Biot has made no assumption on how these stresses are generated.

Moreover, he attempts to demonstrate the influence of the initial stress on the elastic wave propagation by considering the well-known equation of motion of a bending rod subjected to an axial compression P [4, Eq. 1]:

$$EI\frac{d^4W(x)}{dx^4} + P\frac{d^2W(x)}{dx^2} - \rho\omega^2 W(x) = 0, \tag{4.4}$$

where W denotes the deflection of the rod and EI – its bending stiffness. The rod has a length l and a mass per unit length ρ. The elementary theory of wave propagation in simple structural elements such as a rod approximates the real behaviour of a solid, based on assumptions on how this solid deforms [26][25, Sec. 3.3]. Biot presumes that the phenomena following from this example are a particular instance of a more general case of elastic wave propagation in three dimensions in a solid subjected to initial stresses. Therefore, he generalised a limited model for his theory of three-dimensional wave propagation in a solid. This troublesome assumption could be the reason why Biot's final results seem to be counter-intuitive with respect to the physics.

4.2. Influence of the stress on the equation of motion

The first aspect of the acoustoelastic effect manifests itself through the change in the equation of motion, caused by the applied stress. This change results in formulations of the wave equation, and with it the wave velocity, which are influenced by the stress.

4.2.1. Wave equation

Each approach results in a different derivation of the wave equation. Murnaghan's derivation of the wave equation is based on the principles of virtual work and conservation of energy. These two principles yield the Lagrangian form of Cauchy's first law of motion after a small dynamic deformation,

$$\rho_a \frac{\partial u_i^{(1)}}{\partial t^2} - \frac{\partial \sigma_{ji}}{\partial a_j} = 0, \tag{2.66}$$

and the formulation of the nominal stress tensor, expressed in terms of the Lamé parameters and the Murnaghan constants,

$$\sigma_{ji} = C_{ijkl}\frac{\partial u_k}{\partial a_l} + \frac{1}{2}M_{ijklmn}\frac{\partial u_k}{\partial a_l}\frac{\partial u_m}{\partial a_n} + \ldots, \tag{2.58}$$

respectively. Here, the fourth-order tensor C_{ijkl} is expressed in terms of the Lamé parameters:

$$C_{ijkl} = \lambda\delta_{ij}\delta_{kl} + 2\mu I_{ijkl}. \tag{2.51}$$

The sixth-order tensor M_{ijklmn} is defined as:

$$M_{ijklmn} = C_{ijklmn} + C_{ijln}\delta_{km} + C_{jnkl}\delta_{im} + C_{jlmn}\delta_{ik}, \tag{2.59}$$

where the inclusion of the Murnaghan constants is established through the sixth-order tensor

$$C_{ijklmn} = 2\left(l - m + \tfrac{1}{2}n\right)\delta_{ij}\delta_{kl}\delta_{mn} + 2\left(m - \tfrac{1}{2}n\right)\left(\delta_{ij}I_{klmn} + \delta_{kl}I_{mnij} + \delta_{mn}I_{ijkl}\right) + \tfrac{1}{2}n\left(\delta_{ik}I_{jlmn} + \delta_{il}I_{jkmn} + \delta_{jk}I_{ilmn} + \delta_{jl}I_{ikmn}\right). \tag{2.52}$$

By observing relations (2.58) and (2.52) it can be concluded that the Murnaghan constants are only present when the terms of the second order in the deformations are maintained.

Upon elaborating the space-dependent part of relation (2.66), Murnaghan's formulation of the wave equation is obtained:

$$\rho_a \frac{\partial^2 u_i^{(1)}}{\partial t^2} - B_{ijkl}\frac{\partial^2 u_k^{(1)}}{\partial x_j \partial x_l} = 0, \tag{2.71}$$

with

$$B_{ijkl} = C_{ijkl} + \delta_{ik}C_{jlqr}u_{q,r}^{(0)} + C_{rjkl}u_{i,r}^{(0)} + C_{irkl}u_{j,r}^{(0)} + C_{ijrl}u_{k,r}^{(0)} + C_{ijkr}u_{l,r}^{(0)} + C_{ijklmn}u_{m,n}^{(0)}. \tag{2.72}$$

At first sight, there seems to be no influence from the stress on the wave equation. However, the fourth-order tensor B_{ijkl} does contain the uniaxial strains,

$$u_{k,j}^{(0)} = \frac{\partial u_k^{(0)}}{\partial x_j} = \begin{cases} e_{jk} & ; \quad \text{for} \quad j = k \\ 0 & ; \quad \text{else} \end{cases}, \tag{2.68}$$

which can be rewritten to any of the three uniaxial stresses through Poisson's ratio and the formulation of the linearised nominal stress:

$$\sigma_{ji} \approx C_{ijkl}\frac{\partial u_k}{\partial x_l}. \tag{2.60}$$

Note that if the second-order deformations are discarded, the uniaxial stress will be discarded as well since it then holds, by definition, that $B_{ijkl} = C_{ijkl}$. Thus, it can be concluded that the influence of the stress on the wave equation is generated by the deformations of the second order.

The derivation of the wave equation according to Biot's theory is based on the dynamic equilibrium of both the initial-stress components S_{ij} and the incremental-stress components s_{ij} acting on the medium after it has been deformed:

$$\frac{\partial s_{ij}}{\partial a_j} + \rho_a \Delta X_i - \rho_a \omega_{ik}X_k(x_l) - \rho_a e X_i(x_l) + S_{jk}\frac{\partial \omega_{ik}}{\partial a_j} + S_{ik}\frac{\partial \omega_{jk}}{\partial a_j} - e_{jk}\frac{\partial S_{ik}}{\partial a_j} = \rho_a \frac{\partial^2 u_i}{\partial t^2}. \tag{3.16}$$

Upon assuming that the medium is subjected to an initial-stress field acting in the principal directions, the above reduces to:

$$\begin{aligned}
\frac{\partial s_{11}}{\partial x} + \frac{\partial s_{12}}{\partial y} + \frac{\partial s_{13}}{\partial z} + \left(S_{11} - S_{22}\right)\frac{\partial \omega_z}{\partial y} + \left(S_{33} - S_{11}\right)\frac{\partial \omega_y}{\partial z} &= \rho_a \frac{\partial^2 u}{\partial t^2} \\
\frac{\partial s_{12}}{\partial x} + \frac{\partial s_{22}}{\partial y} + \frac{\partial s_{23}}{\partial z} + \left(S_{11} - S_{22}\right)\frac{\partial \omega_z}{\partial x} + \left(S_{22} - S_{33}\right)\frac{\partial \omega_x}{\partial z} &= \rho_a \frac{\partial^2 v}{\partial t^2} \\
\frac{\partial s_{13}}{\partial x} + \frac{\partial s_{23}}{\partial y} + \frac{\partial s_{33}}{\partial z} + \left(S_{33} - S_{11}\right)\frac{\partial \omega_y}{\partial x} + \left(S_{22} - S_{33}\right)\frac{\partial \omega_x}{\partial y} &= \rho_a \frac{\partial^2 w}{\partial t^2}.
\end{aligned} \tag{3.24}$$

From the above it can be seen that the initial-stress components are already introduced. Upon looking closer, it can be observed that the initial-stress components are arranged in a particular manner. They are always present in a set of two with opposing signs and are multiplied with the derivatives of the rotations of the plane across which they are acting. After elaborating these dynamic-equilibrium equations, the following three wave equations are obtained:

$$\begin{aligned}
\rho_a \frac{\partial^2 u}{\partial t^2} - \left(Z_{1111} - S_{11}\right)\frac{\partial^2 u}{\partial x^2} &= 0 \\
\rho_a \frac{\partial^2 v}{\partial t^2} - \left(Z_{1212} + \tfrac{1}{2}S_{11} - \tfrac{1}{2}S_{22}\right)\frac{\partial^2 v}{\partial x^2} &= 0 \\
\rho_a \frac{\partial^2 w}{\partial t^2} - \left(Z_{1313} + \tfrac{1}{2}S_{11} - \tfrac{1}{2}S_{33}\right)\frac{\partial^2 w}{\partial x^2} &= 0.
\end{aligned} \tag{3.25}$$

From these three wave equations it is observed how a stress is denoted positive, i.e. a tensile stress, when acting in the direction of the wave propagation and negative, i.e. a compressive stress, when acting in the direction of the particle oscillation. Furthermore, it can be concluded that there are some limitations in Biot's theory with regard to the orientation of the initial-stress components. Here, it is witnessed how the initial-stress components are orientated in the directions defined by the propagation and particle-oscillation directions of the wave. This particular arrangement is a result of the dynamic-equilibrium equations which dictate the multipliers of the initial-stress components. This constraint makes it impossible to investigate a change in the wave velocity caused by an initial-stress component which is not present in the wave equation. For instance, the influence of a stress acting in the z-direction, i.e. S_{33}, on a transverse wave propagating in the x-direction while polarising in the y-direction, is not accounted for by Biot's model.

4.2.2. Wave velocity

The expressions for the wave velocities are obtained upon dividing both sides of the wave equation by the initial mass density ρ_a. Based on Murnaghan's theory, Hughes and Kelly [13, Eq. 12] introduced expressions for wave velocities of a medium subjected to both a hydrostatic stress and uniaxial stresses. From these expressions it is shown that the longitudinal-wave velocity of a medium subjected to a stress parallel to the propagation direction is of the form:

$$c_{xx}{}^{\sigma_{xx}} = \sqrt{\frac{\lambda + 2\mu \pm \frac{\sigma_{xx}}{3K}\left[2l + \lambda + \frac{\lambda + \mu}{\mu}(4\lambda + 4m + 10\mu)\right]}{\rho_a}}, \tag{2.79}$$

whereas Biot's equivalent formulation reads:

$$c_{xx}{}^{S_{11}} = \sqrt{\frac{\lambda + 2\mu}{\rho_a}}. \tag{4.5}$$

From the above, another limitation of Biot's theory is presented. It can be observed that Biot's formulation of the longitudinal-wave velocity of a medium stressed parallel to the propagation direction is not different from the initial wave velocity. This is a shortcoming he admits as he states that only the behaviour of transverse waves are affected by the principal stress.

Murnaghan's formulation for a transverse-wave velocity of a medium stressed in the propagation direction reads

$$c_{xy}{}^{\sigma_{xx}} = \sqrt{\frac{\mu \pm \frac{\sigma_{xx}}{3K}\left(m + \frac{\lambda n}{4\mu} + 4\lambda + 4\mu\right)}{\rho_a}}, \tag{2.83}$$

whereas the transverse-wave velocity of a medium stressed parallel to the particle oscillation becomes

$$c_{xy}{}^{\sigma_{yy}} = \sqrt{\frac{\mu \pm \frac{\sigma_{yy}}{3K}\left(m + \frac{\lambda n}{4\mu} + \lambda + 2\mu\right)}{\rho_a}}. \tag{4.6}$$

Meanwhile, Biot's theory yields an expression of a transverse-wave velocity of a medium subjected to a stress parallel to the propagation direction as well as a stress parallel to the polarisation direction:

$$c_{xy}{}^{S_{11};S_{22}} = \sqrt{\frac{\mu + \frac{1}{2}S_{11} - \frac{1}{2}S_{22}}{\rho_a}}. \tag{4.7}$$

By comparing these formulations it can be observed that Murnaghan's theory only allows for the influence of one stress component on the wave velocity at a time whereas with Biot's theory the influence of two stress components on the wave velocity can be investigated. As concluded from Biot's wave equation, the orientation and the sign of the initial-stress components are constraint by the plane defined by the propagation and polarisation directions of the wave. This restriction with respect to the stress orientation makes it impossible to observe the influence of a stress acting perpendicular to both the propagation and polarisation direction of the wave. Murnaghan's theory does not show any of these restrictions as the orientation of the uniaxial stress can be chosen freely through the implementation of Poison's ratio of an isotropic medium. This can be shown by formulating the transverse-wave velocity of a medium stressed perpendicular to both the propagation direction and the polarisation direction:

$$c_{xy}{}^{\sigma_{zz}} = \sqrt{\frac{\mu \pm \frac{\sigma_{zz}}{3K}\left[\lambda + m - \frac{\lambda + \mu}{\mu}\left(\frac{3\mu\lambda}{\lambda + \mu} + \frac{1}{2}n\right)\right]}{\rho_a}}. \tag{4.8}$$

By observing relation (4.7) some conclusions can be made with respect to Biot's interpretation of the influence of stress on the wave velocity. Supposedly, the wave velocity increases when the medium is subjected to a tensile stress in the propagation direction and a compressive stress in the polarisation direction of the wave. Conversely, the wave velocity decreases when the medium is subjected to a compressive stress in the propagation direction and a tensile stress in the polarisation direction of the wave. When both stress components are equal in magnitude and are either tensile or compressive stresses, there is no influence of the initial-stress components on the wave velocity.

These results are incoherent with the observations made from laboratory tests. Both Larose and Hall [17] and Lillamand et al. [18] conducted experiments through which the relative wave-velocity change of a concrete specimen has been monitored while being subjected to a uniaxial compression. Their findings demonstrate that the relative wave-velocity change increases when the medium is compressed along the propagation direction. Therefore, Biot's conclusions with respect to the influence of stress on the wave velocity is incorrect.

The observations made by Biot are reminiscent of the wave propagation within a bending rod under an axial load (see App. C.1 for details). Upon substituting the first mode shape,

$$W(x) = A \sin\left(\frac{\pi x}{l}\right), \tag{4.9}$$

the influence of the compression on the frequency, and thus the wave velocity, can be observed [4, Eq. 4]:

$$\frac{\omega}{2\pi} = \frac{c}{\lambda} = \frac{\pi}{2l^2}\sqrt{\frac{EI}{\rho}\left(1 - \frac{P}{P_c}\right)}, \tag{4.10}$$

where λ denotes the wavelength and P_c – the buckling load:

$$P_c = \frac{EI\pi^2}{l^2}. \tag{4.11}$$

As the axial compression increases, the frequency and wave velocity decrease. When the axial compression reaches the buckling load P_c, the frequency and wave velocity reduce to zero. If the axial force is a tensile force T, the wave velocity will increase. Moreover, from this model it is possible to obtain the expression for the frequency of a string under tension, by neglecting the bending stiffness of the rod [4, Eq. 5][19, Sec. 1.2]:

$$\frac{\omega}{2\pi} = \frac{c}{\lambda} = \frac{1}{2l}\sqrt{\frac{T}{\rho}}. \tag{4.12}$$

It is likely that Biot's conclusions are a result of his assumptions with respect to the initial-stress components and the elastic wave propagation in a medium. Similar to the axial force in the bending-rod model, the initial-stress components are introduced in the wave equation solely through force equilibrium. Since Biot generalised the bending-rod model, it is not surprising his theory yields similar results with respect to the increase and decrease of the wave velocity.

When examining Murnaghan's formulations of the wave velocities it is clear that no concrete conclusions can be made with respect to the influence of the stress on the wave velocity. This is due to the Murnaghan constants which still need to be determined. If it is assumed that the Murnaghan constants are positive, it could appear as if the wave velocity increases with tensile stresses in the propagation direction and decreases with compressive stresses in the propagation direction. However, Hughes and Kelly [13, Tab. II] have shown through experiments that the Murnaghan constants appear to be in general negative and an order of magnitude larger than the Lamé parameters. This would imply that compressive stresses along the propagation direction of a wave increase its velocity.

4.3. Influence of the stress on the elastic coefficients

The second aspect of the acoustoelastic effect is expressed through the stress-dependency of the elastic coefficients of the medium. In order to prevent Brillouin's paradoxical result (1.1), the stress must influence the formulation of the wave velocity while also generating small changes to the second-order elastic coefficients. Based on Murnaghan's theory and through experiments, Hughes and Kelly [13] have shown that a linear change in the second-order elastic coefficients, λ and μ, caused by an applied hydrostatic pressure can be expressed by the Murnaghan constants. Similarly, a linear change in the second-order elastic coefficients due to an applied uniaxial compressive stress σ_{xx} can be demonstrated by rewriting relations (2.79) and (2.83) to the equivalent expressions,

$$\begin{aligned} {c_{xx}}^{\sigma_{xx}} &= \sqrt{\frac{\Lambda(\sigma_{xx}) + 2\mathrm{M}(\sigma_{xx})}{\rho_a}} \\ {c_{xy}}^{\sigma_{xx}} &= \sqrt{\frac{\mathrm{M}(\sigma_{xx})}{\rho_a}}, \end{aligned} \tag{4.13}$$

respectively. Here, the stress-dependent elastic coefficients Λ and M are defined as:

$$\begin{aligned} \Lambda(\sigma_{xx}) &= \lambda - \frac{\lambda + 2\mu + 2l + 2m + \frac{\lambda}{\mu}\left(4\lambda + 4m + 6\mu - \frac{1}{2}n\right)}{3K}\sigma_{xx} \\ \mathrm{M}(\sigma_{xx}) &= \mu - \frac{m + \frac{\lambda n}{4\mu} + 4\lambda + 4mu}{3K}\sigma_{xx}, \end{aligned} \tag{4.14}$$

respectively. From the above, it is clear that the expressions for the initial wave velocities are obtained if σ_{xx} reduces to zero.

In Biot's theory, a relation is established between the initial-stress components and the material coefficients through the principle of virtual work:

$$B_{ijkl} + S_{ij}\delta_{kl} = B_{klij} + S_{kl}\delta_{ij}, \tag{3.23}$$

which can be rewritten to:

$$B_{ijkl} - B_{klij} = S_{kl}\delta_{ij} - S_{ij}\delta_{kl}. \tag{4.15}$$

This relation shows that the isotropy of a material, i.e. $B_{ijkl} = B_{klij}$, is only maintained through a state of zero stress or a hydrostatic stress state. Analogous to relation (4.7), an increase in tensile stresses increases the material coefficients whereas an increase in compressive stresses decreases the material coefficients. Moreover, for the material coefficients of the form B_{1111} and B_{1212}, i.e. for longitudinal waves and transverse waves, relation (3.23) becomes:

$$\begin{aligned} B_{1111} + S_{11}\delta_{11} &= B_{1111} + S_{11}\delta_{11} \\ B_{1212} + S_{12}\delta_{12} &= B_{1212} + S_{12}\delta_{12}, \end{aligned} \tag{4.16}$$

respectively. These redundant expressions do not add to the influence of the stress on the elastic coefficients. Only for waves propagating along non-orthogonal directions, relation (3.23) becomes non-trivial. These wave types, however, are not considered within the research scope of this thesis.

4.4. Acoustoelastic effect

The acoustoelastic effect serves as a linear relation between the relative wave-velocity change and the applied stress on a medium. The paper *"Acoustoelastic effect in concrete material under uni-axial compressive loading"* by Lillamand et al. [18] contains a study on the acoustoelasticity of a concrete material. In this study, Murnaghan's theory has been used as a foundation to interpret the relative wave-velocity change of a concrete medium subjected to a uniaxial stress. Through the linearisation of the first order[1] of the formulations of the wave velocities [13, Eq. 12] the following is obtained [18, Eq. 2]:

$${c_{ij}}^{\sigma_{kl}} = {c_{ij}}^{0}(1 + A_{ijkl}\sigma_{kl}), \tag{4.17}$$

where the acoustoelastic constant is denoted by the fourth-order tensor A_{ijkl}. This acoustoelastic constant depends on the directions of the wave propagation, the particle oscillation and the uniaxial stress. Relation (4.17) can be further elaborated such that a linear relation between the relative wave-velocity change and the uniaxial stress is obtained:

$$\Delta c_{ij}\,(\sigma_{kl}) = A_{ijkl}\sigma_{kl}, \tag{4.18}$$

where Δc_{ij} denotes the relative wave-velocity change:

$$\Delta c_{ij} = \frac{{c_{ij}}^{\sigma_{kl}} - {c_{ij}}^{0}}{{c_{ij}}^{0}}. \tag{4.19}$$

As mentioned above, the acoustoelastic constants differ according to the reciprocal orientation of the wave and the uniaxial stress. All the different values for the acoustoelastic constants, following from all possible combinations of wave orientation with respect to stress orientation can be assembled in the matrix

[1] The derivation of this formulation is covered in App. C.2.2.

$$\boldsymbol{A} = \begin{pmatrix} A_{xxxx} & A_{xxyy} & A_{xxzz} & A_{xxxy} & A_{xxxz} & A_{xxyx} & A_{xxyz} & A_{xxzx} & A_{xxzy} \\ A_{yyxx} & A_{yyyy} & A_{yyzz} & A_{yyxy} & A_{yyxz} & A_{yyyx} & A_{yyyz} & A_{yyzx} & A_{yyzy} \\ A_{zzxx} & A_{zzyy} & A_{zzzz} & A_{zzxy} & A_{zzxz} & A_{zzyx} & A_{zzyz} & A_{zzzx} & A_{zzzy} \\ A_{xyxx} & A_{xyyy} & A_{xyzz} & A_{xyxy} & A_{xyxz} & A_{xyyx} & A_{xyyz} & A_{xyzx} & A_{xyzy} \\ A_{xzxx} & A_{xzyy} & A_{xzzz} & A_{xzxy} & A_{xzxz} & A_{xzyx} & A_{xzyz} & A_{xzzx} & A_{xzzy} \\ A_{yxxx} & A_{yxyy} & A_{yxzz} & A_{yxxy} & A_{yxxz} & A_{yxyx} & A_{yxyz} & A_{yxzx} & A_{yxzy} \\ A_{yzxx} & A_{yzyy} & A_{yzzz} & A_{yzxy} & A_{yzxz} & A_{yzyx} & A_{yzyz} & A_{yzzx} & A_{yzzy} \\ A_{zxxx} & A_{zxyy} & A_{zxzz} & A_{zxxy} & A_{zxxz} & A_{zxyx} & A_{zxyz} & A_{zxzx} & A_{zxzy} \\ A_{zyxx} & A_{zyyy} & A_{zyzz} & A_{zyxy} & A_{zyxz} & A_{zyyx} & A_{zyyz} & A_{zyzx} & A_{zyzy} \end{pmatrix}. \tag{4.20}$$

Since relation (4.18) has not been evaluated for shear stresses, only the entries on the first three columns of the matrix $\boldsymbol{A}$ have been defined. If for the sake of argument, the same relation is established based on Biot's theory, it is possible to have two different interpretations of the acoustoelastic constants. For Murnaghan's theory, the matrix $\boldsymbol{A}$ then becomes:

$$\boldsymbol{A_{Murnaghan}} = \begin{pmatrix} \Upsilon & \Phi & \Phi \\ \Phi & \Upsilon & \Phi \\ \Phi & \Phi & \Upsilon \\ \mathrm{X} & \Psi & \Omega \\ \mathrm{X} & \Omega & \Psi \\ \Psi & \mathrm{X} & \Omega \\ \Omega & \mathrm{X} & \Psi \\ \Psi & \Psi & \mathrm{X} \\ \Omega & \Psi & \mathrm{X} \end{pmatrix}, \tag{4.21}$$

where the entries, expressed in terms of the Lamé parameters and the Murnaghan constants, are defined as:

$$\begin{aligned} \Upsilon &= \frac{2l + \lambda + \dfrac{\lambda + \mu}{\mu}(4\lambda + 4m + 10\mu)}{6K(\lambda + 2\mu)} \\ \Phi &= \frac{2l + \lambda - \dfrac{\lambda}{2\mu}(4\lambda + 4m + 10\mu)}{6K(\lambda + 2\mu)} \\ \mathrm{X} &= \frac{m + \dfrac{\lambda n}{4\mu} + 4\lambda + 4\mu}{6K\mu} \\ \Psi &= \frac{m + \dfrac{\lambda n}{4\mu} + \lambda + 2\mu}{6K\mu} \\ \Omega &= \frac{\lambda + m - \dfrac{\lambda + \mu}{\mu}\left(\dfrac{3\mu\lambda}{\lambda + 2\mu} + \dfrac{1}{2}n\right)}{6K\mu}. \end{aligned} \tag{4.22}$$

From the above it can be concluded that the magnitude of the acoustoelastic effect depends on the orientation of the stress with respect to the propagation and polarisation directions of the wave. This phenomenon has been observed by Lillamand et al. [18, Ch. 5] who described that waves that polarise in the loading direction are the most sensitive to the stress level. As has been shown in their study, the values of these acoustoelastic constants, and with them the Murnaghan constants, can be determined through scaled laboratory experiments.

For Biot's theory, the matrix is defined as:

$$\boldsymbol{A_{Biot}} = \frac{1}{4\mu}\begin{pmatrix} 0 & 0 & 0 \\ 0 & 0 & 0 \\ 0 & 0 & 0 \\ 1 & -1 & 0 \\ 1 & 0 & -1 \\ -1 & 1 & 0 \\ 0 & 1 & -1 \\ -1 & -1 & 1 \\ 0 & -1 & 1 \end{pmatrix}. \tag{4.23}$$

The additional zero entries of this matrix reflect the limitation of Biot's theory with respect to the influence of the initial stress on the longitudinal-wave velocity and the influence of the out-of-plane initial stress on the transverse-wave velocity. Furthermore, it can be observed that the magnitude of the acoustoelastic constants are all equal. This implies that the orientation of the stress with respect to the direction of the wave propagation and particle oscillation has no influence on the acoustoelastic constants, which opposes the conclusions made by Lillamand et al. [18, Ch. 5], proving once more that Biot's theory is not applicable for the purpose of this research.

4.5. Murnaghan constants

According to Murnaghan's model, the influence of the orientation of the stress with respect to the propagation and particle-oscillation directions of the wave are dictated by the Murnaghan constants. Since they are non-conventional material parameters, the Murnaghan constants are less renowned within the field of Engineering. From the linearised acoustoelastic constants (4.22) it can be observed that the three Murnaghan constants are distributed among the different waveforms in pairs of two. The parameter m influences all wave velocities whereas l and n only affect the longitudinal- and transverse-wave velocity, respectively.

Hughes and Kelly [13] have demonstrated how the Murnaghan constants can be found through experiments. By monitoring the wave signals at increasing compressive stress levels, it is possible to determine the relative wave-velocity changes (4.18). The Murnaghan constants are then obtained by fitting the data with linear regressions and equating their slopes to the corresponding linearised acoustoelastic constants. Assuming a uniaxial compression σ_{xx}, the following relative wave-velocity changes can be measured:

$$\begin{aligned} \Delta c_{xx} &= A_{xxxx}\sigma_{xx} \Longrightarrow \Upsilon \\ \Delta c_{yy} &= A_{yyxx}\sigma_{xx} \Longrightarrow \Phi \\ \Delta c_{xy} &= A_{xyxx}\sigma_{xx} \Longrightarrow \mathrm{X} \\ \Delta c_{yx} &= A_{yxxx}\sigma_{xx} \Longrightarrow \Psi \\ \Delta c_{yz} &= A_{yzxx}\sigma_{xx} \Longrightarrow \Omega. \end{aligned} \tag{4.24}$$

Since the Murnaghan constants involve three parameters, three equation are needed in order to solve the unknowns. Therefore, only three of the five linearised acoustoelastic constants are necessary for the determination of l, m and n. By measuring all five waveforms it is possible to select a set of three linearised acoustoelastic constants to determine the Murnaghan constants. The found parameters can then be validated by using the remnant linearised acoustoelastic constants.

4.6. Conclusions

In this chapter, the differences in the fundamental assumptions between Murnaghan's and Biot's theory regarding the acoustoelastic effect have been presented. It has been demonstrated that the core differences in the description of the influence of the stress stems from the inclusion of the second-order deformations, or lack thereof.

Murnaghan's description of the stress is generated by these second-order deformations and is linked to the Murnaghan constants through the constitutive relation. Therefore, this stress description not only abides to the condition of internal equilibrium but is also related to the strains. On the other hand, the

origin of Biot's stress description is not specified and solely abides to the internal equilibrium, much like the axial compression or tension acting on a bending rod. Due to the constraint of the directions of the initial-stress components and the inability to express the initial-stress component in terms each other, Biot's model does not allow for the investigation of the influence of the stress on the longitudinal-wave velocity. In addition, it is also not possible to study the influence of all possible orientations of the uniaxial stresses on the wave velocity with Biot's model.

No solid conclusions can be drawn with respect to the influence of the stress on the wave propagation in a medium according to Murnaghan's theory. In order to elaborate on this influence, the Murnaghan constants need to be determined. Despite the unknown Murnaghan constants, it has been found through experiments [13][18] that they are negative in general, eluding to the fact that compression along the propagation direction increases the wave velocity. These findings are directly opposed to Biot's description of the influence of the stress on the wave velocity, which states that tension along the propagation direction increases the wave velocity. His results can be attributed to the erroneous generalisation of the bending-rod model.

The differences in the magnitude of Murnaghan's formulation of the acoustoelastic constants implies that the orientation of the stress with respect to the wave influences the acoustoelastic effect. This observation is confirmed by the experiments conducted by Lillamand et al. [18] which concluded that the acoustoelasticity in concrete is the highest for waves that polarise along the loading direction. Biot's formulation, however, shows no difference in the magnitude of the acoustoelastic constants, implying that the stress orientation is of no influence on the acoustoelasticity.

From the comparison in this chapter can be concluded that Biot's theory is not fit to describe the influence of the stress on the wave velocity in a concrete medium. Therefore, only Murnaghan's theory will be verified with scaled laboratory experiments. The main purpose of these experiments will be to determine the acoustoelastic constants and with them, the Murnaghan constants for a concrete-like medium. This will be realised by equating Murnaghan's linearised theory with the linearised data.

5

Experimental setup

The theoretic formulation of the acoustoelastic effect has been established in the previous chapters. In order to study the influence of stress changes on the relative wave-velocity change within the concrete medium, several experiments have been performed. The objectives of these experiments are to verify the occurrence of acoustoelasticity in concrete-like materials and subsequently to determine the unknown Murnaghan constants. This chapter covers the description of the experimental procedure and the test specimens as well as the quantities used for the measurements. The data acquired from these experiments is processed and analysed as described in Chapter 6.

5.1. Instrumentation and specimens

Within the experimental setup, a distinction can be made between two types of instrumentation. The first type is related to the uniaxial compression, applied by the triaxial stress vessel. The second type deals with the wave signals, which are emitted and measured by the ultrasonic monitoring system. Multiple cylindrical specimens have been tested by using these instruments. The specification of both the instrumentation and the test specimens are described in this section.

5.1.1. Triaxial stress vessel

During the experiment, a triaxial stress vessel is used to perform a Unconfined Compressive Strength (UCS) test on the cylindrical specimens. This UCS test enables a displacement-controlled uniaxial compression of cylindrical specimens, making it suitable to observe the stress dependency of the wave velocity of a specimen.

The measurement of the displacements within the triaxial stress vessel is performed through the use of Linear Variable Differential Transformers (LVDT). A distinction between two types of LVDT is made. The first type is orientated along the vertical direction and measures the axial displacement. The second type is mounted around the circumference of the specimen with a chain and measures the transverse contraction/expansion. The setup of the triaxial stress vessel can be altered such that it is most fitting for the intended experiment. For instance, the bottom plate can be equipped with a range of pedestals with a varying height which accommodates for specimens of different lengths. It is also possible to adjust the positioning of the vertical LVDT, so different locations can be investigated. For this experiment, the bottom plate (A) is equipped with a pedestal (E) which houses a set of two vertical LVDT (G), such that they are positioned in between the top and bottom plate. An incremental displacement is generated through the bottom plate, which translates vertically with respect to the top plate (H). The set of vertical LVDT then measures the relative displacement between the two plates. The specimen (B) is placed between the top and bottom plate and is equipped with the chain around its circumference (F), which measures the radial strain. The force that is present under the applied displacement is measured by a loading cell (D). The spherical bearing (C) connects the top plate to the loading cell and corrects any imperfections in the flat sides of the specimen, ensuring a uniform load application. Figure 5.1 displays the various components which make up the triaxial stress vessel.

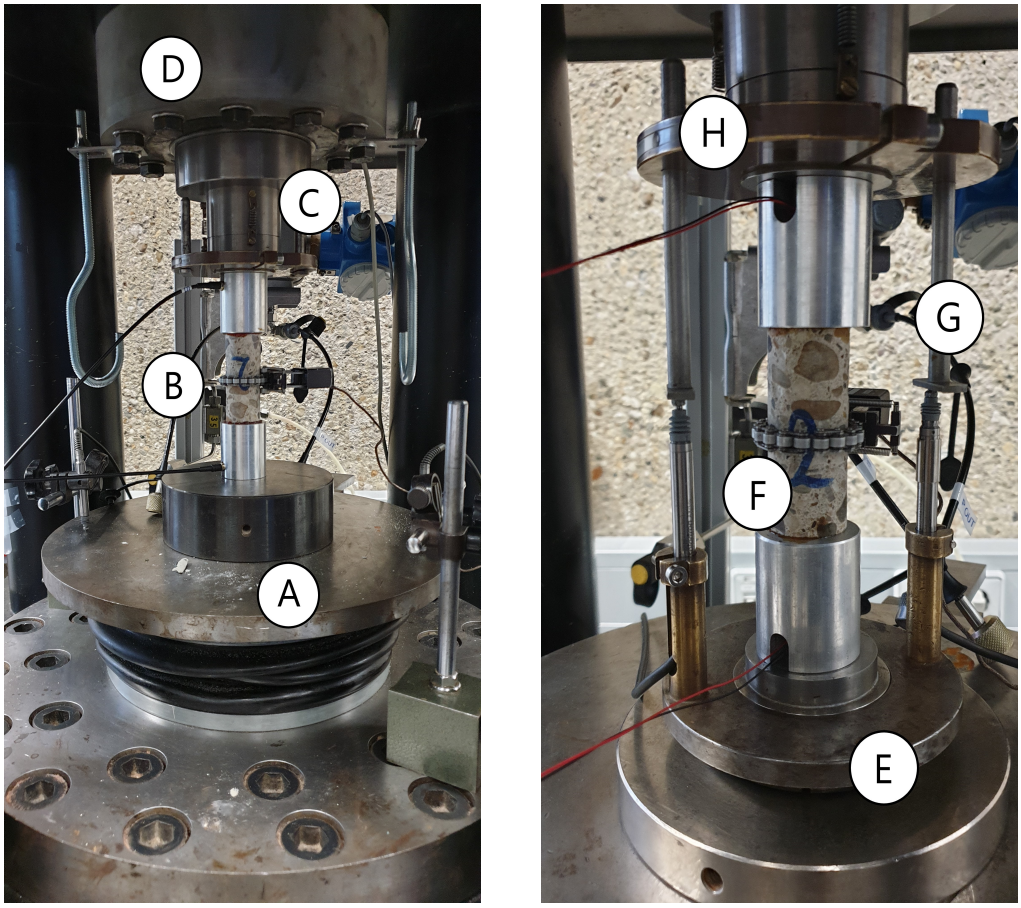

(a) (b)

Figure 5.1: Photos taken of the triaxial stress vessel setup. (a) Overview; (A) bottom plate, (B) specimen, (C) spherical bearing, (D) loading cell. (b) Close-up; (E) pedestal, (F) circumferential LVDT, (G) vertical LVDT, (H) top plate.

5.1.2. Ultrasonic monitoring system

The emission and recording of wave signals propagating through a medium is realised with a four-channel ultrasonic monitoring system. This system consists of a generator, an amplifier, ultrasonic transducers and an oscilloscope, displayed in Figure 5.2.

The generator enables the regulation of an input (wave) signal by specifying the shape, the amplitude, the duration and the frequency of the signal. Once the electric signal has been generated, its amplitude is increased by the amplifier, upon which it relays the signal to a transducer. This piezoelectric-based transducer acts as a source which converts the electric signal into a mechanical deformation. By attaching this source to a specimen with a highly viscous polymer gel, the converted signal is transferred to and then propagates through the medium as a seismic wave. Another piezoelectric-based transducer is then attached to the other side of the specimen, acting as a receiver which converts the deformation back to an electric signal. Upon conversion, the receiver relays the signal to the oscilloscope where it is recorded on one of the available channels. The recorded signal is then stored by a PC as binary data, which can be read with a MATLAB script. The specifications of the recording parameters such as the sampling frequency, the recording time and the vertical and horizontal stepsizes are enabled by the oscilloscope. The recorded data may contain a certain amount of unwanted noise, which is quantified by the signal-to-noise ratio (SNR). The reduction of the noise content in the data can be achieved through the method of ‘stacking’. This technique refers to the repeated emission of the same signal by the transducer source. Consequently, the receiver collects an amount of similar signals, with a different noise content. By averaging these signals, the SNR is increased. This process of stacking occurs in the oscilloscope, in which the stacking amount is configured. This amount should not be too large as the averaging could distort the original signal.

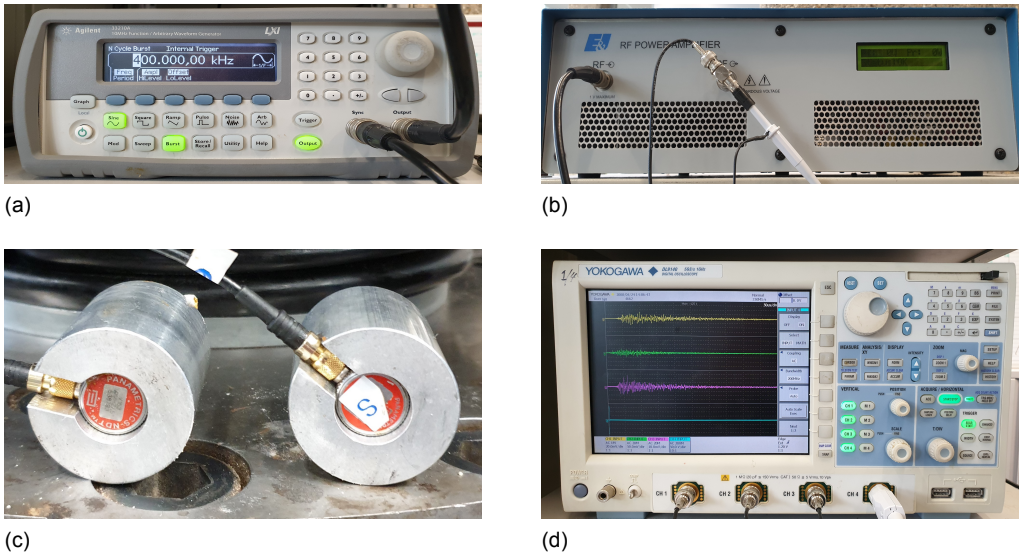

(a) (b)

(c) (d)

Figure 5.2: Components of the ultrasonic monitoring system; (a) Generator, (b) Amplifier, (c) Ultrasonic transducer in aluminum piston, (d) Oscilloscope with four channels.

The wave signals emitted by the transducer source can be categorised by the direction of the particle oscillation of the wave with respect to the propagation direction. A particle oscillation along the propagation direction results in waves which compress/elongate the medium, i.e. longitudinal waves, also called compressional or primary (P-)waves. When the particle-oscillation direction is perpendicular to the propagation direction, the wave shears the medium. These waves are called transverse waves, also known as shear or secondary (S-)waves. P-waves arrive earlier than S-waves, since their wave velocity is higher. Hence their names primary waves and secondary waves, respectively. Within the latter, a distinction is made with respect to a horizontally propagating P-wave. One could use a pair of S-wave transducers aligned perpendicularly to the loading direction and either polarised along the loading direction, i.e. SV-waves, or perpendicular to the loading direction, i.e. SH-waves. Through the measurement of these waveforms it is possible to observe how the wave velocity is influenced by the orientation of the loading with respect to the particle-oscillation direction. The direction of the particle oscillation is determined by the piezoelectric crystal within the transducer. By subjecting this crystal to an electric field, caused by the electric signal, the crystal undergoes a mechanical deformation resulting in an elastic wave. Inversely, when the crystal is subjected to a deformation, it generates an electric field. The piezoelectric effect is visually displayed in Figure 5.3.

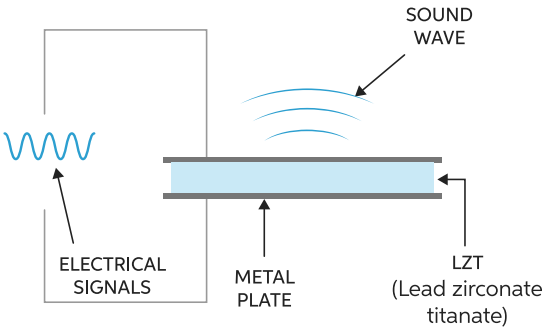

Figure 5.3: Visual representation of the piezoelectric effect of the piezoelectric crystal LZT [9].

In theory, the orientation of the piezoelectric crystal defines whether a transducer generates P-waves or S-waves. The transducers used for the experiments house crystals that expand/contract transversely, i.e. S-wave transducers. Due to the round shaped housing of these transducers, boundary effects occur. Consequently, in addition to the intended S-wave energy, low P-wave energy is generated as well. This effect of coupled P- and S-wave content increases the complexity of interpret-

ing the time signature, especially within the diffuse part.

5.1.3. Specimens

During the experiment, four concrete-like cylindrical specimens have been used for measurements with the triaxial stress vessel. The dimensions of these specimens are constraint by the chosen configuration of the triaxial stress vessel. Considering the size of the aluminum pistons, it follows that the specimens need to have a height and diameter of approximately 70 mm and 30 mm, respectively.

In order to investigate the influence of the inhomogeneity of the material on the changes in the wave velocity, two different material compositions have been investigated. The first type of specimen consists of a homogeneous cement paste made of Cugla HSM mortar which is cast in a PVC tube. The shrinkage of this cement paste has been limited by adding 50% fine sand (diameter smaller than 0.25 mm) to the mixture. The second type of specimen represents heterogeneous concrete including aggregates. Due to the constraint of the diameter of the specimen it is not possible to cast a mixture with aggregates in a mold. Therefore, a C55/67 concrete cube was cast from which cores of the specified diameter were drilled. Afterwards, these cores were cut to the required length. Figure 5.4 displays the different types of specimen and a drawing displaying the dimensions.

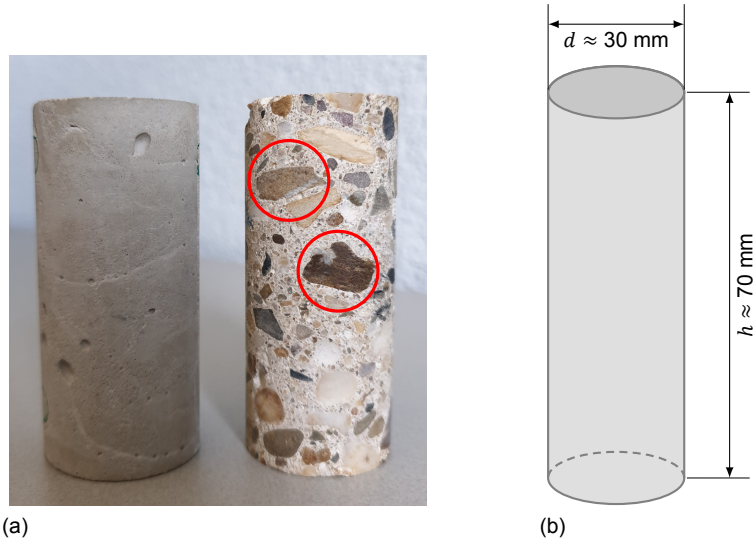

Figure 5.4: Display of the different types of specimen and the dimensions. (a) Cement-paste specimen (left) and concrete core specimen (right). (b) Drawing of the dimensions of the specimen.

For the purpose of providing more reliable results, two specimens of each type have been tested. The exact dimensions of the specimens have been measured and are summarized in Table 5.1.

Table 5.1: Measured dimensions of the test specimens.

Specimen	Type	Height h [mm]	Diameter d [mm]	Mass m [g]
CP-1	Cement paste	71.78	32.66	123.05
CC-2	Concrete	70.53	29.82	111.92
CP-3	Cement paste	70.02	32.20	116.17
CC-4	Concrete	64.48	29.79	101.80

5.2. Experimental procedure

As a means to observe the changes in the wave velocity of the test specimen at various stress levels, the triaxial stress vessel and the ultrasonic monitoring system have been used simultaneously. The preparation of the specimens for the experiment as well as the description of the used experimental setup together with the chosen procedure of the experiment is covered in this section.

5.2.1. Preliminary experiments

To ensure that the specimens are representative and provide reliable results, some preliminary experiments have been performed. These experiments are initiated with elementary measurements and are piecewise increased in complexity. The first objective of these preliminary experiments is to inspect whether the transducers are working properly. This has been carried out by looking for the centre frequency of the transducer and by altering the amplitude of the signal such that a clear time signature is obtained. The second objective is to validate the specimens by comparing the identified initial wave velocities with the expected values for a concrete-like material. The third objective is to observe any stress-dependent changes within the time signature of the recorded signal. This has been accomplished by using the ultrasonic monitoring system in tandem with the triaxial stress vessel.

During the first step, the initial wave velocities of the specimens are identified. This has been realised by placing the transducers directly on the flat sides of a specimen, emitting a wave signal along its height. The initial wave velocities are then estimated by using the ToF method on the time signature of the wave signal (see App. D.1 for details). The identification of the arrival times is visually represented in Figure 5.5.

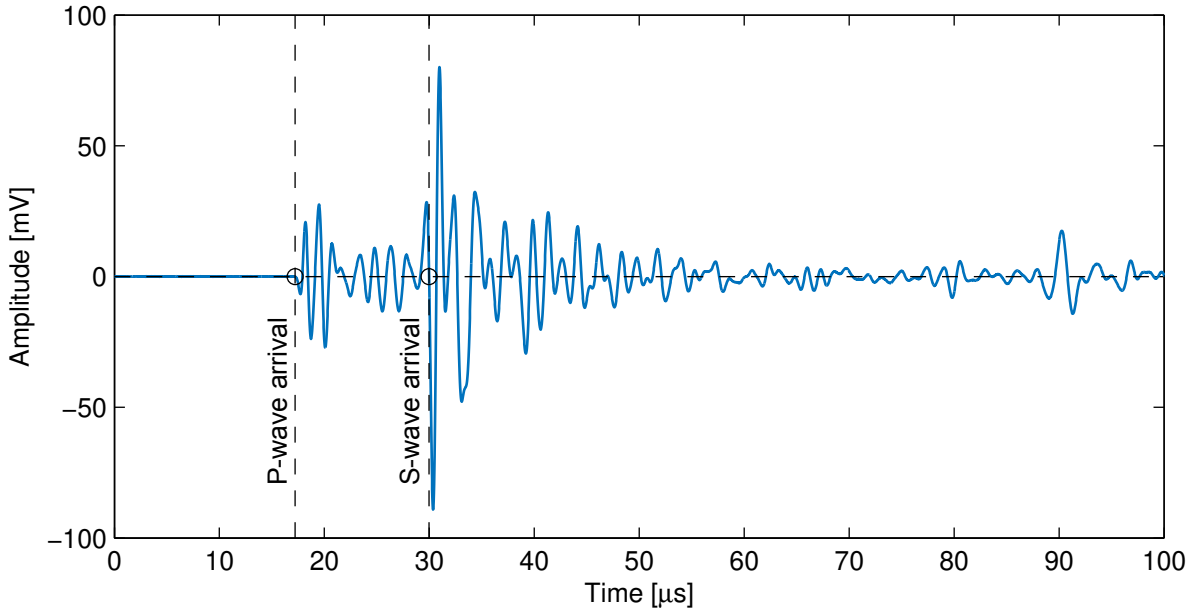

Figure 5.5: Identification of the arrival times for specimen CP-3 along the axial direction through handpicking with the ToF method.

Table 5.2 displays both the identified arrival times and the wave velocities of the specimens as well as the theoretically estimated values (see App. D.1.1 for details).

Table 5.2: Identified arrival times and initial wave velocities of the specimens along the axial direction.

Specimen	Arrival t_P [µs]	Arrival t_S [µs]	P-wave velocity c_P [m/s]	S-wave velocity c_S [m/s]
CP-1	17.50	29.60	4102	2425
CC-2	15.70	26.40	4492	2672
CP-3	17.20	30.00	4071	2334
CC-4	14.00	24.90	4606	2590
Theoretically estimated values			4000	2500

From this summary, it can be observed that the values of the wave velocities are within the proximity of the theoretically estimated values for a concrete-like material. Therefore, it can be concluded that all specimens are deemed representative. Another observation that can be made is that the wave velocities of the concrete specimens are higher than those of the cement-paste specimens. These differences can be attributed to the inclusion of the aggregates, which contribute to the stiffness, and thus to the wave velocity, of the concrete specimens.

Due to the large size of the transducer (Figure 5.6a) with respect to the dimensions of the specimen, it is impossible to use them in the radial direction. Therefore, a second type of ultrasonic transducer with a smaller size has been used, displayed in Figure 5.6b.

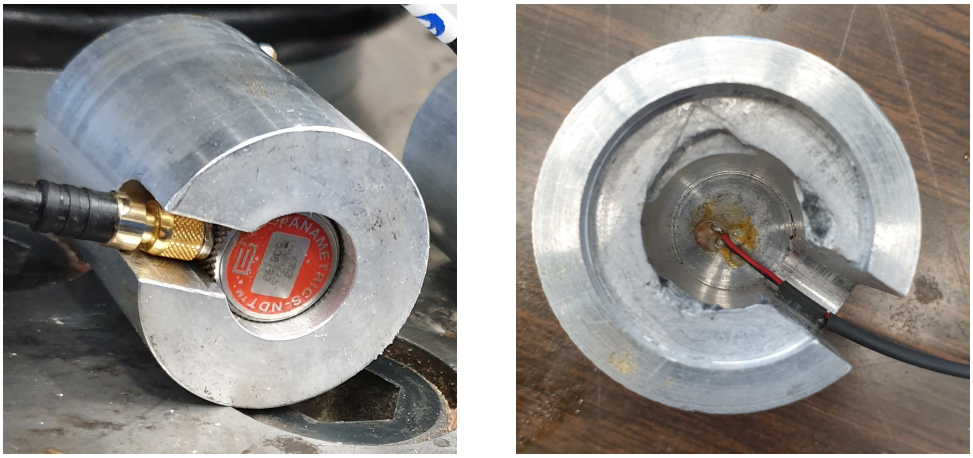

(a) (b)

Figure 5.6: Side-by-side comparison of the transducers within the aluminum piston; (a) Large transducer, diameter = 15 mm, (b) Small transducer, diameter = 5 mm.

These smaller transducers are mountable in both the axial and radial direction of the specimen. However, the amplitude of the signal they generate is significantly lower than that of the larger transducer. Therefore, the usability of these smaller transducers with respect to the signal strength must be verified (see App. D.1.2 for details). Besides the verification of their amplitude, the centre frequency of the smaller transducers must be found as well. This has been achieved by repeatedly emitting signals through the specimen while changing the amplitude and frequency of the signal. From these measurements it is found that a frequency of 400 kHz results in a recorded time signature which still has a significant amplitude, displayed in Figure 5.7.

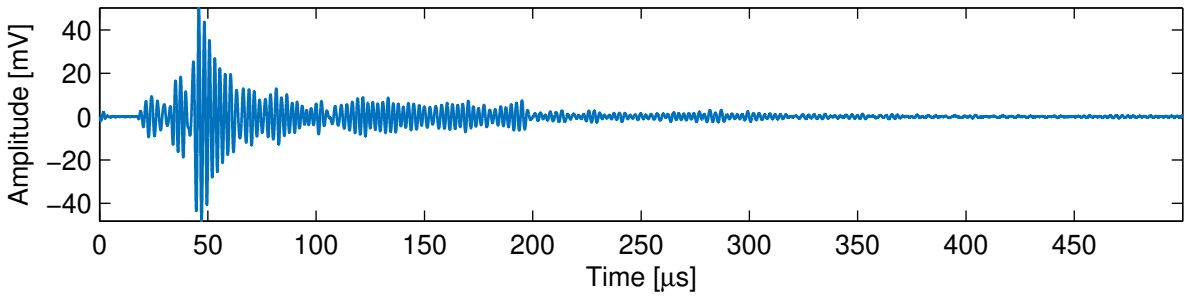

(a)

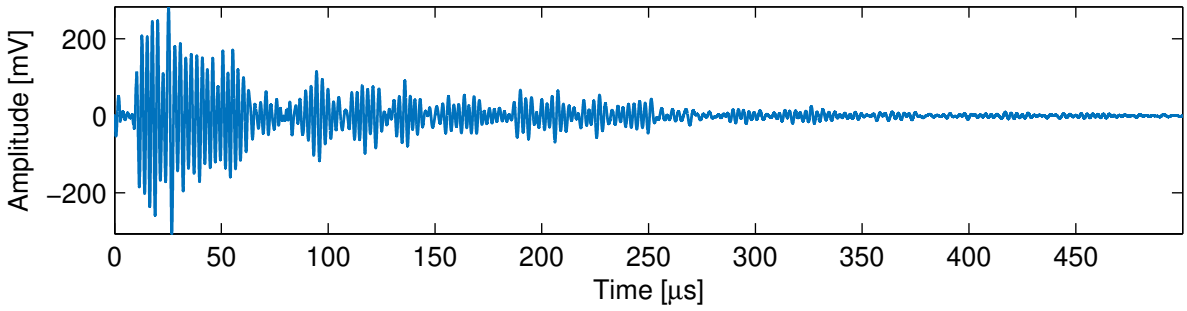

(b)

Figure 5.7: Time signature of signals emitted through CP-1 by the small transducers at a frequency of 400 kHz. (a) Signal along the axial direction of the specimen. (b) Signal along the radial direction of the specimen.

By comparing the amplitudes from Figures 5.7a and 5.7b it can be concluded that the signal along the axial direction has undergone more damping than the signal along the radial direction. This discrepancy is a result of the difference of the source-receiver distance of the two signals which is also reflected by their respective first arrivals. The signal along the radial direction has a much smaller travel path and thus experiences less damping. Based on these results, it can be concluded that the small transducers are suitable for the monitoring of the signal propagation through the specimens.

The relation of the wavelength of a signal with respect to size of the medium through which it propagates determines the behaviour of the waves. In order to ensure that the measured vibrations still behave as propagating waves, instead of normal modes, the wavelength should be small compared to the size of the medium. A requirement with regard to the wavelength has been set up through a rule of thumb which states that the wavelength should be at least three times smaller than the dimensions of a specimen. Upon assuming a frequency of $f = 400$ kHz and by using the theoretically estimated wave velocities, the wavelengths for the P- and S-waves become

$$\begin{aligned} \lambda_P \approx \frac{c_P}{f} &= \frac{4000 \text{ m/s}}{400 \text{ kHz}} = 10.00 \text{ mm} \\ \lambda_S \approx \frac{c_S}{f} &= \frac{2500 \text{ m/s}}{400 \text{ kHz}} = 6.25 \text{ mm}, \end{aligned} \tag{5.1}$$

respectively. Since both values are at least three times smaller than both the height and diameter of the specimens, the requirement is met. Therefore, during the main experiment the wave signals have been emitted at a frequency of 400 kHz.

Next, these measurements are repeated several times while the specimen is being subjected to a cyclic axial compression ranging from 0 to 20 MPa. Since the compression is applied on the flat sides of the specimen, the transducers need to be embedded in aluminum pistons. The inclusion of these aluminum pistons prevents the transducers from being damaged while also ensuring a uniform pressure on the flat sides of the specimen. As a result, the wave signal emitted by the source has to propagate twice through an aluminum medium before being recorded, causing additional scattering and reflections which generates a more complex time signature. Therefore, the focus has been on the stress-induced changes on a larger part of the time signature instead of the first arrivals. Figure 5.8 displays how a part of the signal is shifting towards the left as the stress level increases, indicating an increase in the wave velocity.

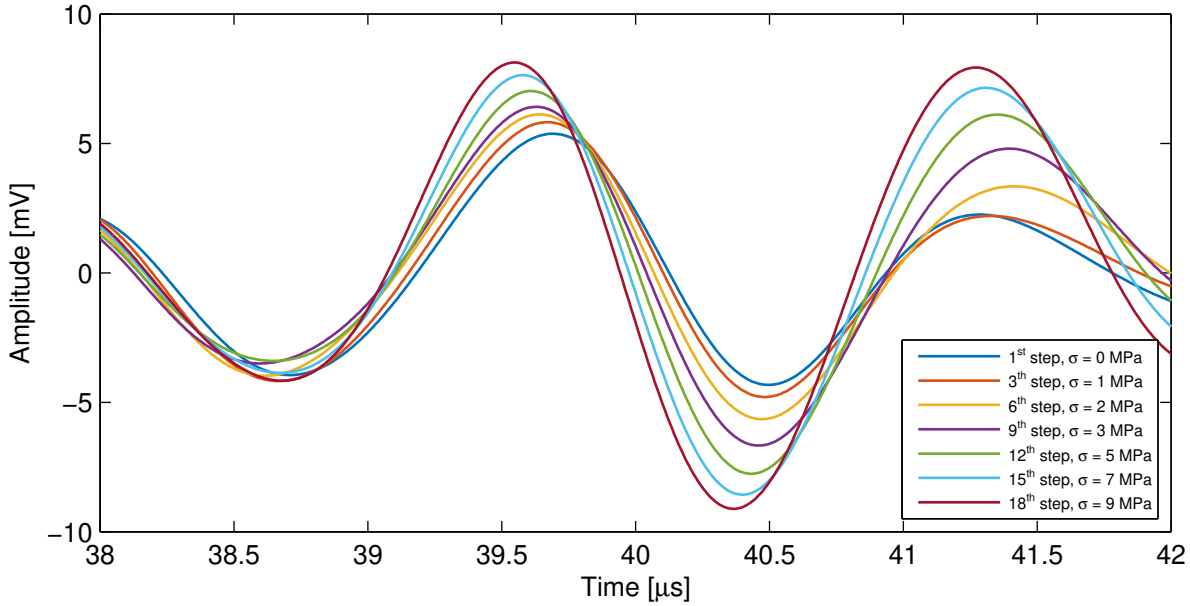

Figure 5.8: Zoom-in on a collection of time signatures that are recorded along the axial direction of CP-1 at various stress levels.

Based on these observations, it can be concluded that the stress has an observable influence on the wave velocity of the specimen, proving the proper functionality of the transducers.

It should be noted that specimens CC-2 and CC-4 have been slightly damaged during the cyclic uniaxial compression. In these specimens, the weakest link is the bond between the cement matrix and the aggregates. This is especially the case at the edges of the cylinders which show signs of damage caused by aggregate spalling, displayed in Figure 5.9.

(a) (b)

Figure 5.9: (a) Damaged concrete core specimens CC-2 and CC-4. (b) Concrete cube from which the concrete cores are drilled.

Considering this damage and the inconsistent dimensions of specimens CC-2 and CC-4, new cores have been drilled from the same concrete cube, displayed in Figure 5.10.

(a) (b)

Figure 5.10: (a) Close-up of the new concrete core specimens. (b) New concrete core specimens with consistent dimensions.

The damaged specimens are replaced by specimens CC-2B and CC-4B. Since these specimens are extracted from the same concrete cube, they are assumed to be valid as well. Therefore, they have not been subjected to the aforementioned preliminary experiments. Instead, they have been used in the main experiment, during which wave signals with various orientations are emitted through the specimens. Table 5.3 displays the dimensions of these new specimens.

Table 5.3: Measured dimensions of the new concrete specimens.

Specimen	Type	Height h [mm]	Diameter d [mm]	Mass m [g]
CC-2B	Concrete	69.86	31.66	124.02
CC-4B	Concrete	69.96	31.72	125.71

5.2.2. Experimental configuration and measurements

During the main experiment, waveforms of different orientations are emitted by the source transducers which propagate through the specimen subjected to a compressive stress level and recorded by the receiver transducers. The objective of this experiment is to observe how the propagation time is influenced by the increasing stress. Due to symmetry, the amount of different combinations of the loading direction with respect to the propagation and polarisation directions of the wave can be narrowed down to five different combinations. As a result of the coupling effect of the transducers, the application of three transducer pairs is sufficient for this experiment. One pair has been aligned in the axial direction of the specimen, whereas the other two pairs has been mounted along the radial direction, orientated perpendicular with respect to each other. Figure 5.11 displays the numbered transducers and the waveforms they are emitting.

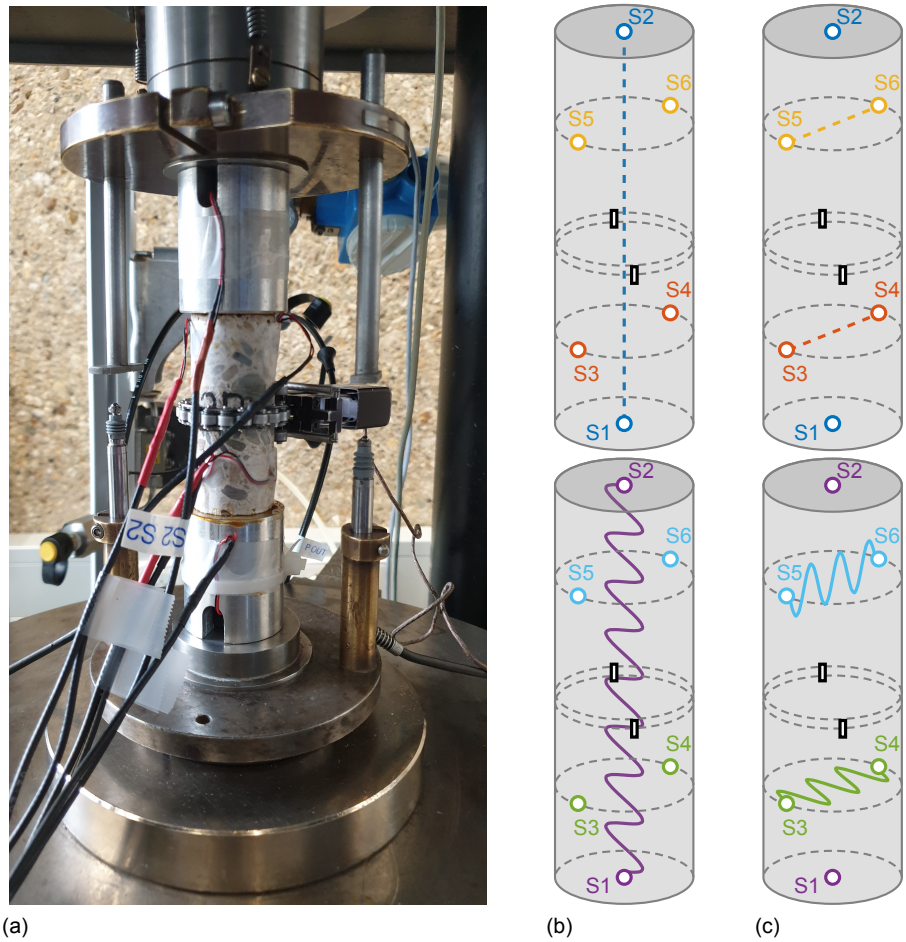

Figure 5.11: Visualisation of how the transducer pairs are arranged on the specimen during the experiment. (a) Photo taken of the experimental configuration of specimen CC-2B. (b) Wave propagation between the axial transducer pair S1-S2, P-wave content (top) and S-wave content (bottom). (c) Wave propagation between the radial transducer pairs, P-wave content (top) and S-wave content (bottom); SH-wave between pair S3-S4 and SV-wave between pair S5-S6.

The axial transducers are placed within the aluminum pistons. Due to their smaller size and the lack of a built-in acoustic insulation, a piece of rubber has been used to seal off the open end of the piston

which keeps the transducer in place. The specimen and the aluminum pistons are coupled through a small layer of shear gel, ensuring that the setup remains aligned throughout the uniaxial compression. The radial transducers are attached to the circumference of the specimens with shear gel and kept in place with tape. Due to the chain around the middle of the specimen, the radial transducers have been positioned at approximately 10 mm away from the flat sides.

Each specimen has been subjected to a cyclic loading which is repeated three times. The loading and unloading rate are based on a displacement rate of 0.0005 mm/s and 0.0015 mm/s, respectively. Figure 5.12 displays a graph of one typical load cycle.

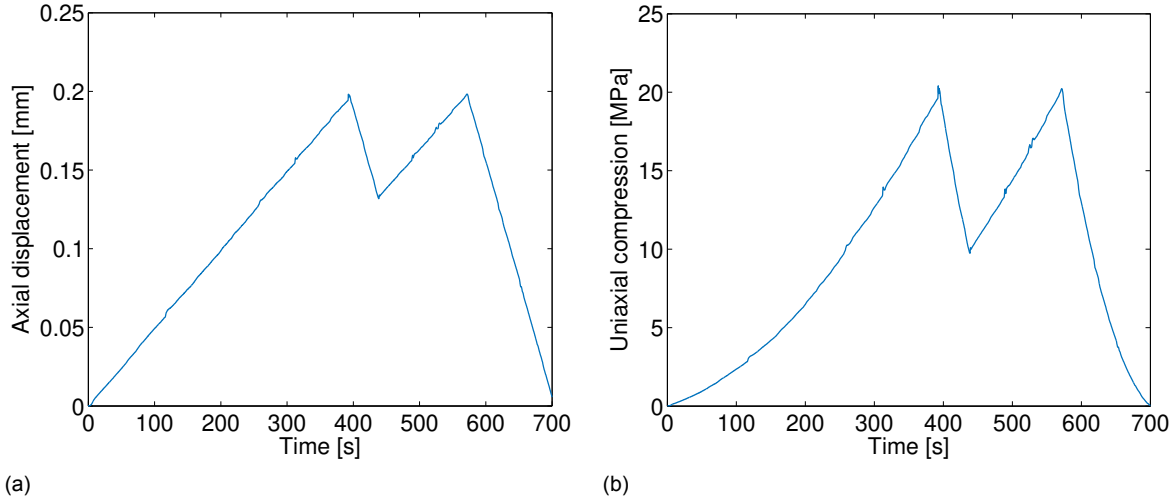

Figure 5.12: (a) Axial displacement over time, measured by the vertical LVDT. (b) Uniaxial compression from 0 to 20 MPa, including a partial unloading for the purpose of condensing the specimens. The non-linear behaviour at low stress levels is caused by the shear gel.

During each of these load cycles only one transducer is acting as a source whereas all the other transducers are acting as receivers. A sinusoidal signal is emitted repeatedly over an interval of 20 seconds during each load cycle. Each of these signals is emitted at frequency of 400 kHz and is subsequently recorded for a duration of 500 µs. The signals have been discretized with a sampling frequency of $f_s = 250$ MHz and each time signature is obtained by stacking 1024 waveforms before being recorded. Once a load cycle has been completed, the source is changed. This process is repeated for all specimens until all the possible waveforms have been emitted. Table 5.4 shows the schedule which has been used for every specimen during the experiment.

Table 5.4: Order of signal emission during the cyclic loading of the specimens.

Load cycle	Waveform	Source	Receiver CH1	Receiver CH2	Receiver CH3
1	S-wave	S1	S2	S3	S5
2	SH-wave	S3	S4	S1	S5
3	SV-wave	S5	S6	S1	S4

By using three channels to record the waveforms, a total of three traces per measurement are obtained, like depicted on Figure 5.13. Among these traces are the waveforms which have been emitted by a source of one transducer pair while being recorded by the receiver of another transducer pair. Therefore, some of these traces contain waveforms with non-orthogonal propagation and polarisation directions. From Figures 5.13a - 5.13c it is witnessed how the source-receiver distance influences the time signature of the signals. It is observed that the further the source is from the receiver, the lower the amplitude of the signal and the later its first arrival. The signal with the lowest amplitude and the latest first arrival is displayed in Figure 5.13a. This wave has propagated from S1 to S2, which is the largest source-receiver distance within the specimen. Therefore, the wave signal undergoes significant damping, which is reflected by its low amplitude. On the other hand, the highest amplitude

and the earliest first arrival are witnessed in the wave that has propagated through the specimen from S1 to S3 (Figure 5.13c). This wave signal has the smallest source-receiver distance, and therefore experiences less damping.

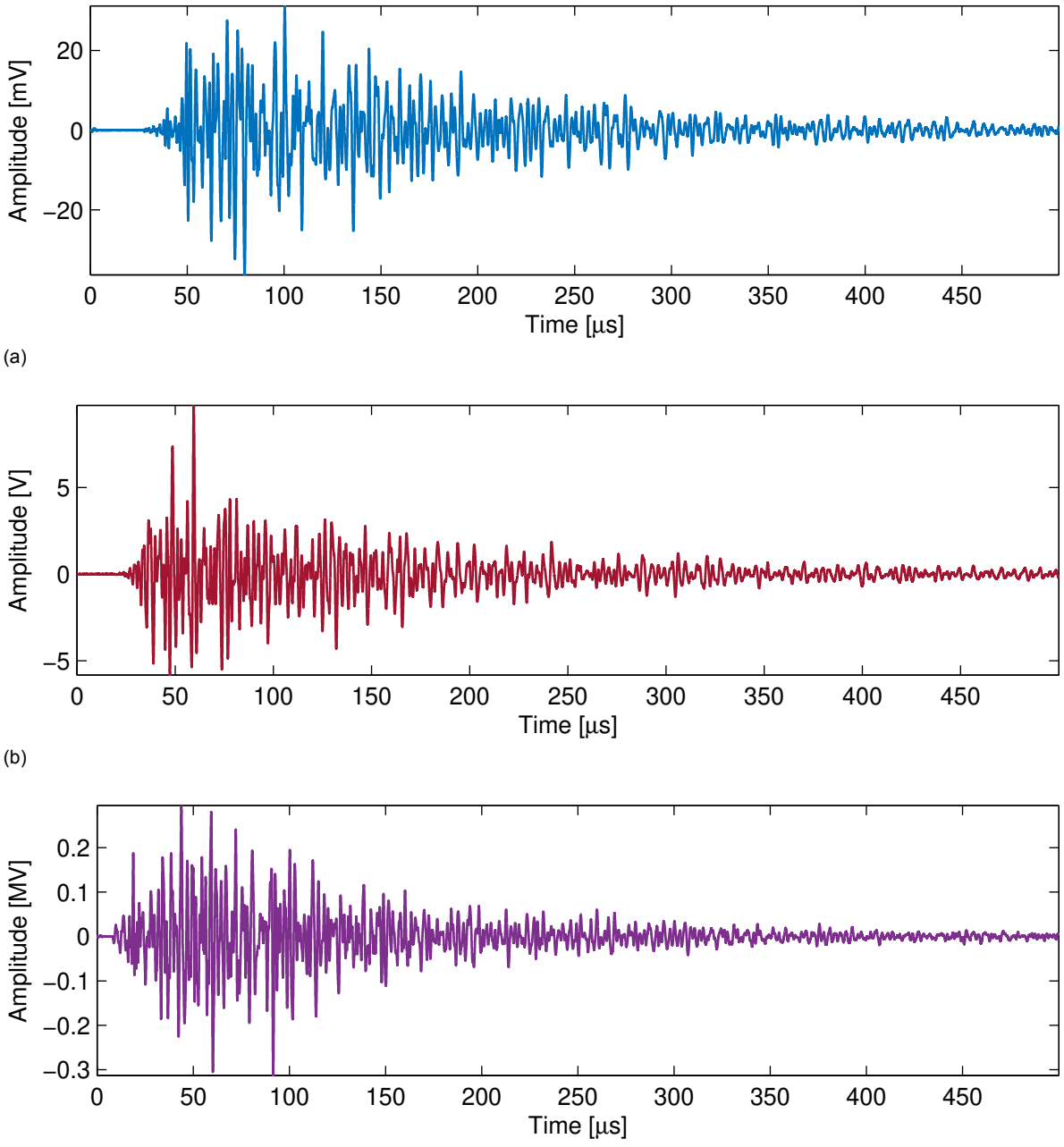

Figure 5.13: Time signature of signals emitted through CP-1 by source S1. (a) Signal recorded on channel 1 by receiver S2. (b) Signal recorded on channel 3 by receiver S5. (c) Signal recorded on channel 2 by receiver S3.

As has been stated earlier, these waveforms are not within the scope of this research. Consequently, the receivers have been connected to the oscilloscope in such a manner that channel 1 always yields the trace of a waveform which has been transmitted and recorded within the same transducer pair. So, of all the data acquired through the main experiment, only those yielded by channel 1 are considered. The data from channels 2 and 3 could potentially be used in future work that investigates the behaviour of these waveforms.

Adding to the acquired data are the stress-strain diagrams which allow for the determination of both the Young's modulus and Poisson's ratio of the specimens (see App. D.2 for details). Through these

two parameters, it is possible to determine the Lamé parameters λ and μ:

$$\lambda = \frac{E\nu}{(1+\nu)(1-2\nu)}$$
$$\mu = \frac{E}{2(1+\nu)}. \tag{5.2}$$

The second-order elastic parameters of the specimens are of importance for the determination of the third-order Murnaghan constants of the specimens. Table 5.5 displays a summary of the final test specimens and their respective elastic parameters.

Table 5.5: Overview of the final test specimens and their second-order elastic parameters.

Specimen	Young's modulus E [GPa]	Poisson's ratio ν $[-]$	λ [GPa]	μ [GPa]
CP-1	20.30	0.20	5.64	8.46
CC-2B	37.25	0.35	32.19	13.80
CP-3	25.80	0.21	7.72	10.66
CC-4B	51.10	0.28	25.40	19.96
Expected values	20-40	0.20		

From the values in Table 5.5, it can be concluded that the Young's modulus and Poisson's ratio of the cement-paste specimens are within the range of the expected values and consistent. However, the concrete core specimens display some inconsistencies with respect to these values. The outlier of Poisson's ratio of specimen CC-2B may be attributed to an inaccuracy of the measurements of the radial strain. The large difference in the Young's modulus, however, does not seem to be the result of a faulty device. Instead, this difference can be linked to the heterogeneity of the concrete core specimens. Figure 5.14 shows a side-by-side comparison of specimens CC-2B and CC-4B. From this comparison, it can be observed that specimen CC-4B contains larger aggregates. This results in a stiffer mixture, which explains the higher Young's modulus.

(a) (b)

Figure 5.14: (a) Front view of specimens CC-2B (left) and CC-4B (right). (b) Back view of specimens CC-2B (left) and CC-4B (right).

In this chapter, the procedure of the experiments has been described in detail. The results from these experiments are stored as discretized data signals of a sample size $N = 125000$ each. The next chapter covers the processing and analysis of this data.

6

Results and data processing

In Chapter 5, the configuration and the procedure of the main experiment have been elaborated upon in detail. The results of this experiment are expressed in binary data-files. The processing of this data has been performed through the use of various scripts written in MATLAB. For the purpose of removing any undesired content such as noise, the data has been filtered in this chapter. The data was then post-processed through the implementation of CWI [20, Ch. 2][24]. The outcome of these analyses and the ensuing observations with respect to the acoustoelasticity of the test specimens (from Table 5.5) are covered in this chapter as well. Finally, these findings have been validated through the determination of the Murnaghan constants and their comparison with the literature.

6.1. Data filtering

The raw data obtained from the experiment can be either interpreted in the time domain or the frequency domain. The time domain contains the information of the excitations of the wave as a function of the time. The frequency domain displays at what frequencies the wave is excited. The combination of both allows for a thorough analysis of the wave signal and is necessary for the data filtering. The first objective of the filtering is to suppress the noise in the signal of both high and low frequencies. The second objective is to attempt to decouple the P-wave and S-wave content such that the stress-induced changes for each waveform can be examined separately.

6.1.1. Time domain and frequency domain

Within the field of signal processing, the analysis of data is performed in both the time domain and the frequency domain. The time domain of a signal, which is excited at various frequencies, displays the development of its amplitudes as time passes. The same data can also be observed in the frequency domain which displays at which frequencies these amplitudes are excited. Figure 6.1 depicts a visual representation of a signal in both the time domain and the frequency domain.

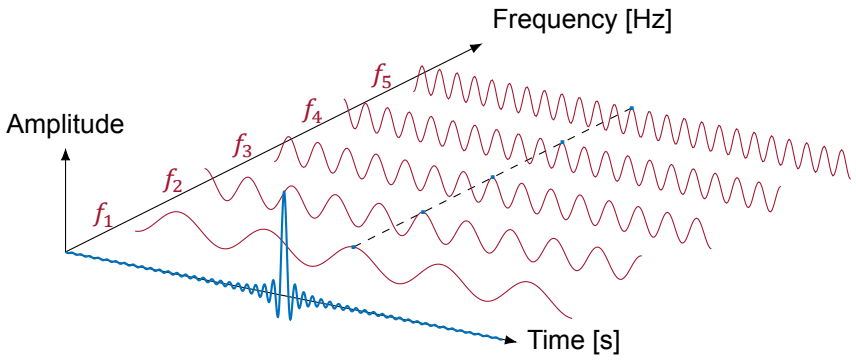

Figure 6.1: Graphical representation of the time domain and frequency domain. The total time signature is obtained through the summation of the several signals, excited at different frequencies.

For continuous signals, the Fourier transform (FT) and the Inverse Fourier transform (IFT) are used to alternate between the time domain and the frequency domain. If a continuous function of time $h(t)$ is considered, then a continuous function of frequency $H(f)$ is obtained through the FT [6, Sec. 2.7]:

$$H(f) = \mathcal{F}\{h(t)\} = \int_{-\infty}^{+\infty} h(t) e^{-i2\pi f t} dt. \tag{6.1}$$

The original time signature is then again retrieved through the IFT of the frequency-dependent function:

$$h(t) = \mathcal{F}^{-1}\{H(f)\} = \int_{-\infty}^{+\infty} H(f) e^{i2\pi f t} df. \tag{6.2}$$

For example, the FT of a rectangular pulse becomes a cardinal sine function:

$$\Pi(t) \overset{\mathcal{F}}{\Rightarrow} \operatorname{sinc}(f) = \frac{\sin(\pi f)}{\pi f}, \tag{6.3}$$

where $\Pi(t)$ denotes a rectangular pulse function and $\operatorname{sinc}(f)$ – the cardinal sine function in the frequency domain. The rectangular pulse is an important function for its use in 'windowing' of the data, which is frequently required in digital signal processing. Figure 6.2 displays the graphs of both of these functions.

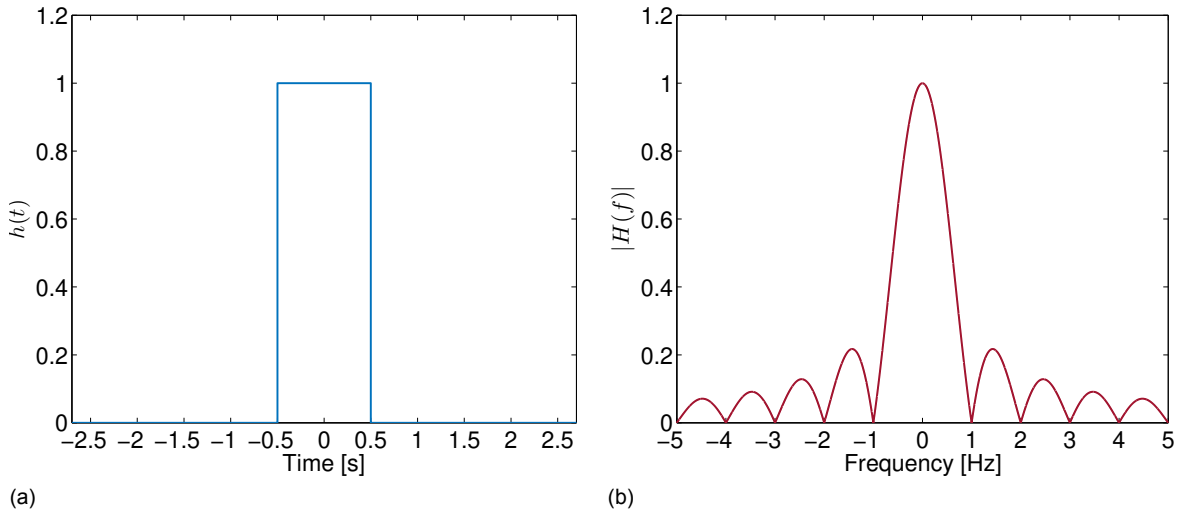

Figure 6.2: Example of a Fourier transform pair. (a) Rectangular pulse function in the time domain. (b) Double-sided amplitude spectrum of a rectangular pulse function.

The discretization of the continuous data has been performed through the use of a sampling frequency $f_s = 250$ MHz, resulting in a discrete signal of $N = 125000$ samples [6, Sec. 3.1]. The stepsize between the samples in the time domain is defined as the time resolution

$$\Delta t = \frac{1}{f_s} = \frac{1}{250\ \text{MHz}} = 0.004\ \mu\text{s}, \tag{6.4}$$

whereas the stepsize between the samples in the frequency domain is defined as the frequency resolution

$$\Delta f = \frac{f_s}{N} = \frac{250\ \text{MHz}}{125000} = 2\ \text{kHz}. \tag{6.5}$$

For discrete signals, altering between the time and frequency domain is achieved through the Discrete Fourier transform (DFT) and the Inverse Discrete Fourier transform (IDFT) [6, Sec. 9.3]. A discretized signal in the time domain $h(n)$ is then transformed to the frequency domain with

$$h(n) \overset{DFT}{\Longrightarrow} H(k) = \sum_{n=0}^{N-1} h(n) e^{-\frac{i2\pi kn}{N}} \qquad \text{for} \quad k = 0, 1, 2..., N-1, \tag{6.6}$$

and is retrieved again with the IDFT of the discretized frequency signal:

$$H(k) \overset{IDFT}{\Longrightarrow} h(n) = \frac{1}{N} \sum_{k=0}^{N-1} H(k) e^{\frac{i2\pi kn}{N}} \qquad \text{for} \quad n = 0, 1, 2..., N-1. \tag{6.7}$$

MATLAB handles these transformations numerically through the Fast Fourier transform (FFT) and Inverse Fast Fourier transform (IFFT), respectively. These two algorithms have been used in order to analyse the acquired data. Figure 6.3 displays the frequency spectrum of the time data which has been obtained trough the FFT in MATLAB.

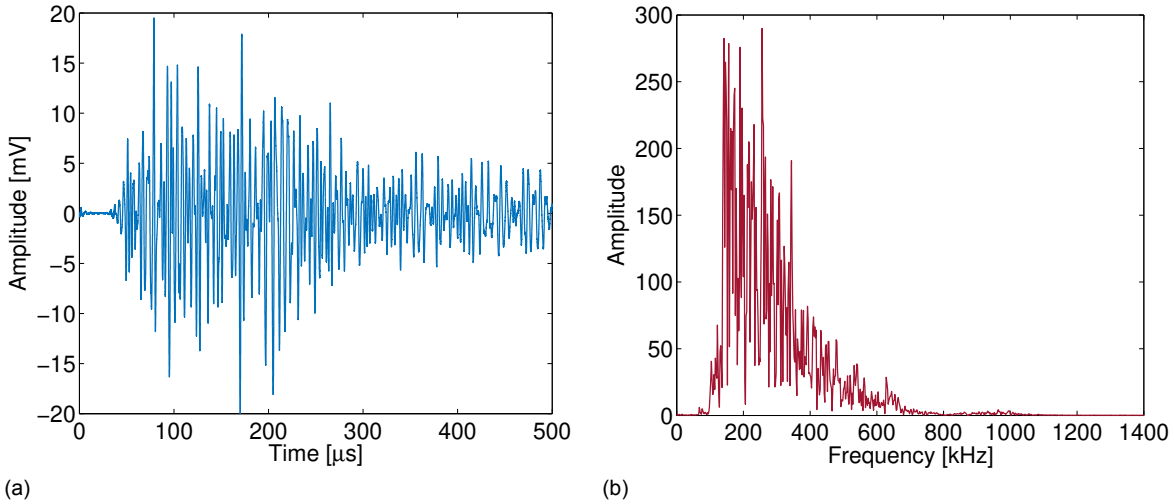

Figure 6.3: Representation of the discretized data signal, emitted along the axial direction of specimen CC-2B. (a) Discretized time signature. (b) Single-sided amplitude spectrum, obtained through the FFT of the discrete time data. The significant energy manifests itself within the range of 0-800 kHz.

Figure 6.3b displays how the implementation of the FFT reveals the range of frequencies at which the total time signature is excited. In order to differentiate between the different types of frequency content that make up the total spectrum, both the time and frequency data need to be analysed. This has been done by means of a time-frequency analysis as well as a frequency filter analysis.

6.1.2. Time-frequency analysis

For the purpose of filtering the unwanted portions of the data, it is necessary to identify the different frequency contents. This can be achieved through the windowing of data. Windowing refers to the isolation of portions of the data in either the time domain or the frequency domain. These portions or windows are then transformed with the (I)FFT such that they can be analysed in both domains. The desired data is isolated by multiplying the total data with a specified window, which tapers data which are outside of its boundaries. One typical example of such a window is a rectangular window (Figure 6.2a). Since this window discards all data outside its boundaries without a gradient, it is ideal for isolating the desired data. However, a disadvantage of this window is the distortion of the signal which is obtained after the FT. This phenomenon is caused by the multiplication and convolution properties of the FT [6, Sec. 2.7]:

$$\begin{aligned} h(t)w(t) &\overset{\mathcal{F}}{\Leftrightarrow} H(f) * W(f) \\ h(t) * w(t) &\overset{\mathcal{F}}{\Leftrightarrow} H(f)W(f), \end{aligned} \tag{6.8}$$

respectively. These properties state that the multiplication of two functions in the time domain result in a convolution in the frequency domain and vice versa. Depending on the type of window, this convolution can distort the signal such that it is beyond recognition. This is especially the case for a rectangular window, for which the FT is a cardinal sine (Figure 6.2b). The convolution of a signal with this cardinal sine function is referred to as the Gibbs phenomenon or 'ringing' and is to be avoided when the preservation of the signal is desired [10, Sec. 6.9]. This can be accomplished by ensuring that the window gradually tapers the unwanted data. The downside of this taper is that a portion of the unwanted data is included within the window. When choosing the window type, a trade-off has to be made between the data preservation and the data isolation.

The time-frequency analysis provides an insight in the frequency spectrum and serves as a preliminary observation to the data filtering. With the time-frequency analysis, multiple windows are taken from different parts of the time signature and are subsequently transformed to the frequency domain with the FFT. The frequency spectrum of each of these windows is then analysed. During this analysis, the frequencies are observed at which the different parts of time signature are excited. These frequencies are indicated by the peaks in the amplitude spectrum. Here, the effect of ringing is inconsequential since only the amplitudes of the peaks are of importance. Therefore, the portions of the time signature are isolated by using rectangular windows. The frequency content can be divided in four groups; low-frequency noise, high-frequency noise, P-wave content and S-wave content. The noise content is found before the first arrival, indicated by the mix of slow and fast oscillations in the time domain. Figure 6.4 displays the windowing of this noise content its frequency spectrum.

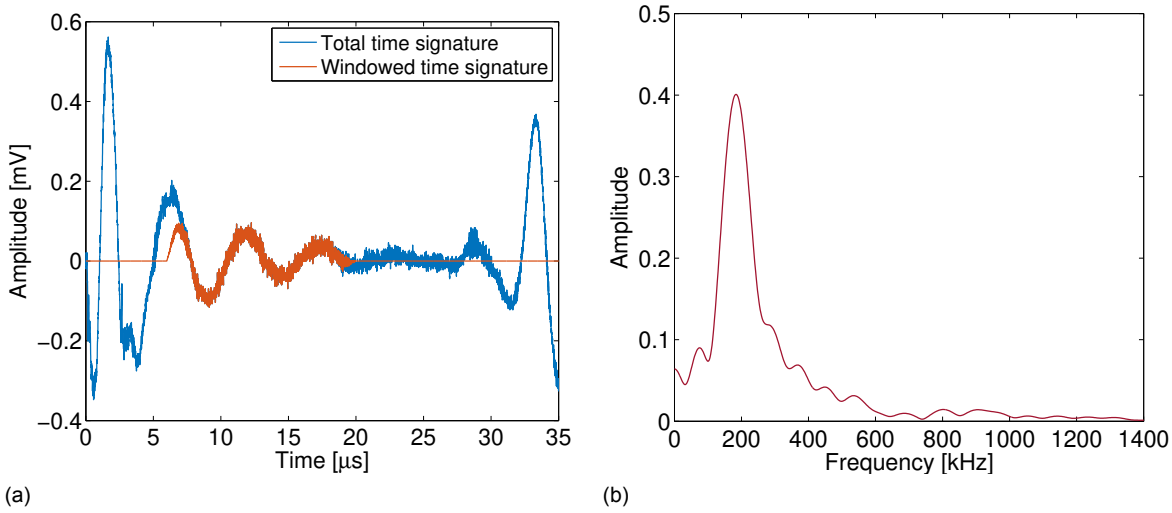

Figure 6.4: Time-frequency analysis of the noise in the discretized data signal, emitted along the axial direction of specimen CC-2B. (a) Windowing of the time signature before the first arrival. (b) Single-sided amplitude spectrum: large peak around 200 kHz and small peaks above 700 kHz possibly indicating the low-frequency and high-frequency noise, respectively. The wobbly spectrum is caused by the ringing effect.

From these graphs, it can be argued that the larger periods are a result of the low-frequency noise which is most likely within the range of 0-200 kHz, whereas the shorter periods indicate the high-frequency noise which is excited at frequencies above 700 kHz. Based on these findings, both the low- and high-frequency content have been identified. Table 6.1 displays a summary of the frequency range of the noise content for both the axial and radial recordings.

Table 6.1: Summary of the noise content for all specimens.

Propagation direction	Low-frequency noise content [kHz]	High-frequency noise content [kHz]
Axial	0-200	>700
Radial	0-200	>800

After the frequencies of the noise content have been identified, it is possible to locate the P- and S-wave frequency content. This is accomplished by centering the time windows around their arrival times and subsequently analysing their amplitude spectra. The analysis is performed in a chronological order, i.e. the frequency content of the P-wave arrival are analysed first. By doing this, it is possible to monitor how the amplitude spectrum changes piece-wise as time advances. The occurrence of new peaks in the amplitude spectrum then indicates the frequencies at which the content within the adjacent window is excited. Figure 6.5 displays the windowing of the time signature, focused around the two arrivals, and the corresponding frequency spectrum.

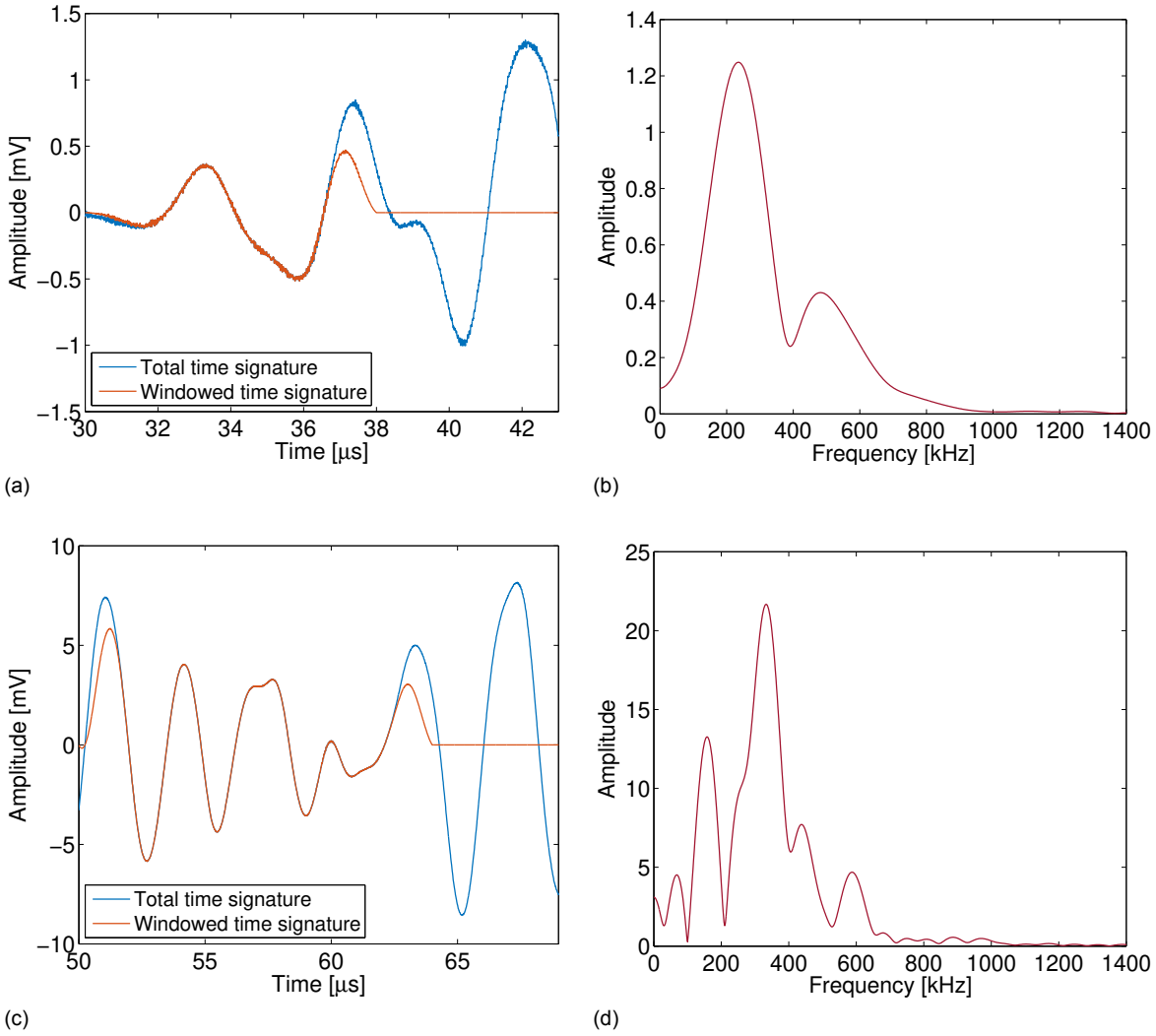

Figure 6.5: Time-frequency analysis of the discretized data signal, emitted along the axial direction of specimen CC-2B. (a) Windowing of the time signature centered around the P-wave arrival. (b) Single-sided amplitude spectrum: peak around 500-700 kHz indicating the P-wave content. (c) Windowing of the time signature centered around the S-wave arrival. (d) Single-sided amplitude spectrum: large peak around 300-400 kHz indicating the S-wave content.

Figures 6.5a and 6.5b display the time window centered around the P-wave arrival and its amplitude spectrum. From the amplitude spectrum, two significant peaks are observed. In addition to the peak centered around 200 kHz, a second peak is observed within the range of 500-700 kHz, indicating the frequencies at which the P-wave content is excited. The windowing of part of the time signature after the S-wave arrival and its amplitude spectrum are displayed in Figures 6.5c and 6.5d. Roughly three significant peaks can be distinguished in the amplitude spectrum. It can be observed that the two previous peaks are almost overshadowed by the third peak, which is focused around 300-400 kHz. This peak is most likely related to the S-wave content within the time window, indicated by the typical larger amplitude with respect to the P-wave content.

This procedure has been repeated for all the recordings of the four specimens. Through this time-frequency analysis, the frequency content of all the data has been analysed. A summary of the P- and S-wave content and the range of frequency at which they are excited is displayed in Table 6.2.

Table 6.2: Summary of the frequency content for each measurement.

Propagation direction	Waveform	P-wave content [kHz]	S-wave content [kHz]
Specimen CP-1			
Axial	S-wave	500-700	300-500
Radial	SH-wave	400-500	500-700
Radial	SV-wave	400-500	500-700
Specimen CC-2B			
Axial	S-wave	500-700	300-400
Radial	SH-wave	500-700	300-500
Radial	SV-wave	200-400	500-700
Specimen CP-3			
Axial	S-wave	300-400	400-600
Radial	SH-wave	600-800	400-600
Radial	SV-wave	600-800	300-500
Specimen CC-4B			
Axial	S-wave	400-600	300-400
Radial	SH-wave	500-700	300-400
Radial	SV-wave	300-400	500-700

These observations indicate that the P- and S-wave content are close to each other, which is reflected by their overlapping bandwidths. It can also be observed that in most cases the content is excited at frequencies which are close to the centre frequency of 400 kHz. This especially the case for the S-wave content. This can be attributed to the fact that S-wave transducers have been used for all sources and receivers. The accuracy of the indications of these frequency bandwidths are to be checked through the application of a frequency filter.

6.1.3. Frequency filter analysis

Following from the time-frequency analysis, the frequency content of the measurements has been identified. These indications form the basis for the frequency filtering. By filtering particular content in the frequency domain it is possible to observe the influences in the time domain. During this process, the frequency spectrum of a signal is filtered through the application of a window. Subsequently, the isolated frequency data is transformed to the time domain with the IFFT. From the obtained time signature it is possible to observe the changes caused by the filtering.

Unlike with the time-frequency analysis, the preservation of the data is of importance. Therefore, band-pass filters with sinusoidal tapers have been constructed. In order to prevent the effect of ringing, the bandwidth of these tapers has been set at one octave [6, Sec. 3.3]. This means that the high end of each taper is at least twice the frequency of the low end of the taper. The downside of these band-pass filters is that it becomes nearly impossible to completely decouple the P-wave content from the S-wave content. From the time-frequency analysis it has been estimated that the P- and S-wave content are close-ranged, demonstrated by their identified frequency bandwidths in Table 6.2. The separation of P- and S-wave content has an important role in the analysis of the stress-dependency of their respective velocities. Since the focus of the analysis is on the arrival times, the coupled content is no issue for the P-wave velocity. This is because the unwanted coupling effect only occurs after the S-wave arrival. Therefore, the mixed signal only arises when observing the stress-dependence of the S-wave velocity.

The noise content, however, is present throughout the entire time signature. Therefore, the noise must be filtered first. In Figure 6.6 it is shown how the application of a noise filter influences the time signature of a signal.

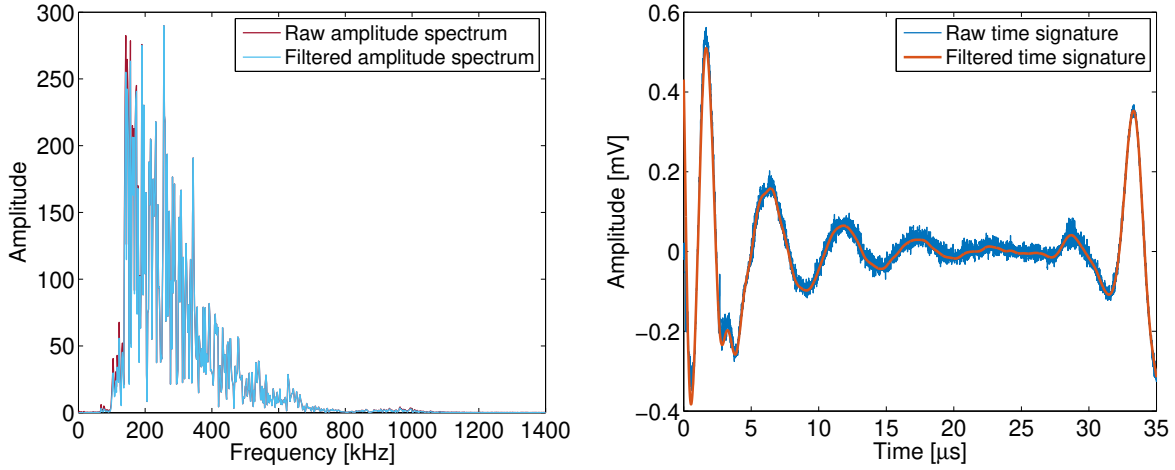

Figure 6.6: Noise filtering of the discretized data signal, emitted along the axial direction of specimen CC-2B. (a) Filtering of the amplitude spectrum, realised by a band-pass of 200-700 kHz with sinusoidal tapers. (b) Time signature, reflecting the results of the frequency filtering.

The impact of the noise filter can be observed by comparing the time signature from Figure 6.4a with the one displayed in Figure 6.6b. From this comparison it is witnessed how the low-amplitude spikes are no longer present after the filtering. This indicates that the filtering of the high-frequency noise has been successful. The large-amplitude oscillations at the start of the recording, however, still remain. Therefore, it is likely that these large periods are not a result of the low-frequency noise. Instead, it's probable that they are a result of crosstalk, caused by the electromagnetic interference of the amplifier. These oscillations decay rapidly and are completely diminished before the first arrival. Therefore, the influence of the crosstalk does not affect the wave content.

In an attempt to decouple the P- and S-wave content, another band-pass filter has been constructed. This filter aims to suppress the P-wave content of the time signature. During the construction of the band-pass filter, the S-wave content has been monitored carefully. This ensures that the S-wave content itself is not influenced by the band-pass filter. Figure 6.7 displays the outcome of the P-wave content filter on the time signature.

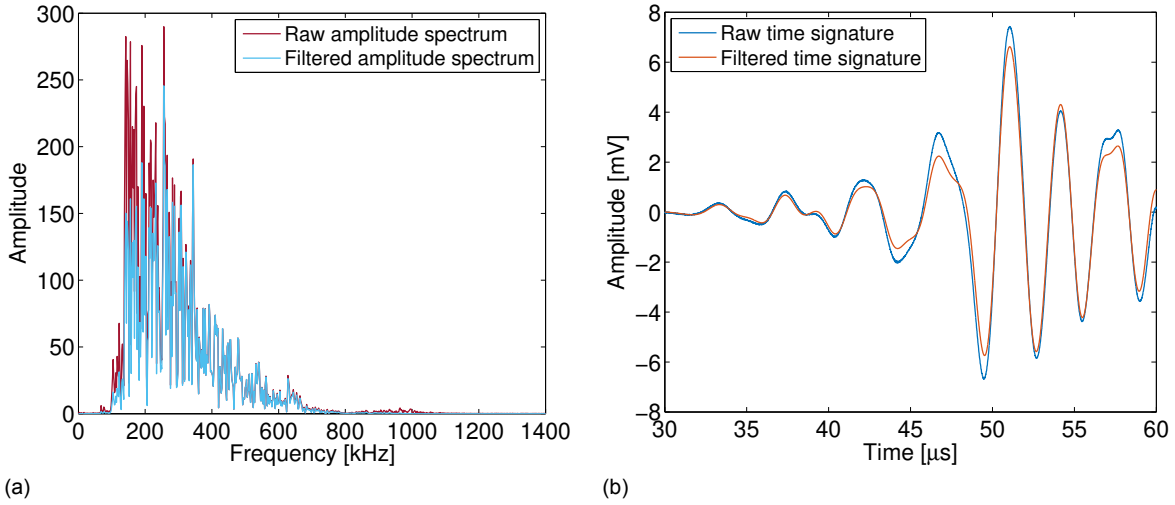

Figure 6.7: P-wave filtering of the discretized data signal, emitted along the axial direction of specimen CC-2B. (a) Filtering of the amplitude spectrum, realised by a band-pass of 400-500 kHz with sinusoidal tapers. (b) Time signature centered around the arrival times, reflecting the results of the frequency filtering.

From Figure 6.7b it is observed that the oscillations around the first arrival are distorted, whereas the large S-wave amplitudes remain unchanged. The procedure of constructing both type of band-pass filters has been repeated for all measurements. The frequency boundaries of the applied band-pass filters are summarised in Table 6.3.

Table 6.3: Summary of the applied band-pass filters for each measurement.

Propagation direction	Waveform	Low taper [kHz]	Band-pass [kHz]	High taper [kHz]
		Specimen CP-1		
Axial	S-wave	0-300	300-500	500-1000
Radial	SH-wave	0-500	500-700	700-1400
Radial	SV-wave	0-500	500-700	700-1400
		Specimen CC-2B		
Axial	S-wave	0-400	400-500	500-1000
Radial	SH-wave	0-300	300-500	500-1000
Radial	SV-wave	0-300	300-500	500-1000
		Specimen CP-3		
Axial	S-wave	0-300	300-400	500-800
Radial	SH-wave	0-500	500-700	700-1400
Radial	SV-wave	0-600	600-800	800-1600
		Specimen CC-4B		
Axial	S-wave	0-250	250-350	350-700
Radial	SH-wave	0-300	300-500	500-1000
Radial	SV-wave	0-500	500-700	700-1400

Based on this frequency filter analysis, the original data set has been partitioned in two groups. The first group is focused on the P-wave content and is only subjected to the noise filters. The second group is centered around the S-wave content and is filtered from both noise and P-wave content.

6.2. Post-processing: Stretching Technique algorithm

As has been determined in the introductory chapter, the relative wave-velocity changes within the concrete medium have been monitored with CWI. For this post-processing of the data, an algorithm in MATLAB has been used, which emulates the Stretching Technique (see App. E for details). By means of a cross-correlation, this algorithm compares a reference signal with a stretched signal within a time window. The acquired data is arranged in a sets of time signatures per measurement. Each time signature has been recorded at a different stress level. The first time signature of a set has been chosen as the reference signal for the other time signatures. In the algorithm, the cross-correlation is interpreted so that the reference signal is stretched or compressed in such a way that it matches the other signals within the set. This match is quantified with the maximum cross-correlation coefficient, which indicates the stretching factor ϵ or the relative wave-velocity change Δc. This section elaborates on the various parameters of the algorithm, as well as the protocol used for determining the relative wave-velocity changes.

6.2.1. Peak amplitude threshold

The cross-correlation is centered around the first P- and S-wave arrivals. This has been achieved through the implementation of a time window which starts at their respective first breaks. Within the boundaries of this time window, the cross-correlation is performed. Due to the large amount of data as well as the interference from reflections, it is not efficient to determine the arrival times with the ToF method. Instead, the arrival times have been determined through the Peak amplitude threshold method.

This method uses the exceedance of an amplitude threshold to identify the arrival time of a signal. This amplitude threshold is based on the analytical representation of the signal, which comprises of the

original signal and its Hilbert transform:

$$h_A(t) = h(t) + i\mathrm{H}\{h(t)\}, \tag{6.9}$$

where $h_A(t)$ denotes the analytical signal and $\mathrm{H}\{h(t)\}$ – the Hilbert transform of the original signal. The Hilbert transform of a signal is a linear operator which convolutes the signal with the Cauchy Kernel [6, Sec. 16.2]:

$$\mathrm{H}\{h(t)\} = h(t) * \frac{1}{\pi t}. \tag{6.10}$$

In doing so, the Hilbert transform conveys a phase shift of $\pm\frac{\pi}{2}$ in the frequency domain.

By taking the absolute value of the analytical representation of the signal, the Hilbert envelope is obtained. The threshold is expressed as a percentage of the maximum peak amplitude of the Hilbert envelope. The position on the time axis at which this threshold is exceeded indicates the arrival time of the wavelet. The partition caused by the inclusion of a P-wave content filter, makes this method suitable for the P-wave arrival as well as the S-wave arrival. The graph in Figure 6.8 displays a visual representation of the identification of the arrival time.

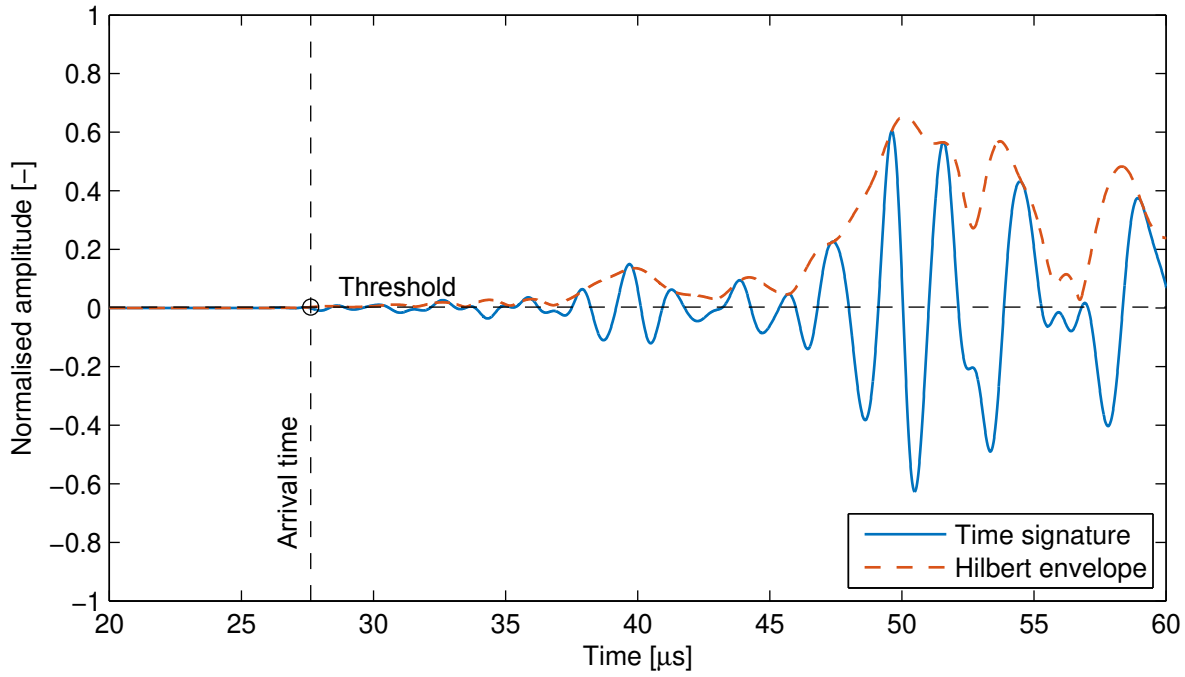

Figure 6.8: Graphical representation of the Peak amplitude threshold method: threshold chosen to identify the P-wave arrival.

6.2.2. Cross-correlation: Protocol

Even though the algorithm is efficient, it does have its flaws. The algorithm does not feature the ability to track a specific wavelet as it translates along the time axis. Its main objective is to find a wavelet for which the cross-correlation is maximum. Due to the stress-induced changes, it frequently occurs that the target wavelet changes in such a manner that it resembles the reference wavelet less. Consequently, the algorithm chooses a completely different wavelet which displays a higher resemblance with the reference. Therefore, it might occur that the corresponding stretching factor does not display a correct representation of the relative wave-velocity change.

In order to prevent this from happening, the input parameters of the algorithm need to be regulated through a protocol. The two most prominent input parameters are the boundaries of time window and the range of stretching. The boundaries of the time window dictate what wavelets are included in the cross-correlation, whereas the range of stretching determines the boundaries between which the reference signal can be stretched. The time window is the most sensitive parameter and must be

regulated such that at least one full period of the pulse is included. As has been determined earlier, the time window starts at the first break of the wavelet. The end of the time window has been decided through iterations. During these iterations, the time window has been tweaked slightly for the purpose of ensuring that only the targeted wavelet is present within its boundaries. If the range is too large, the algorithm might find a distant period which yields a better match than the targeted pulse. This phenomenon has been displayed in Figure 6.9.

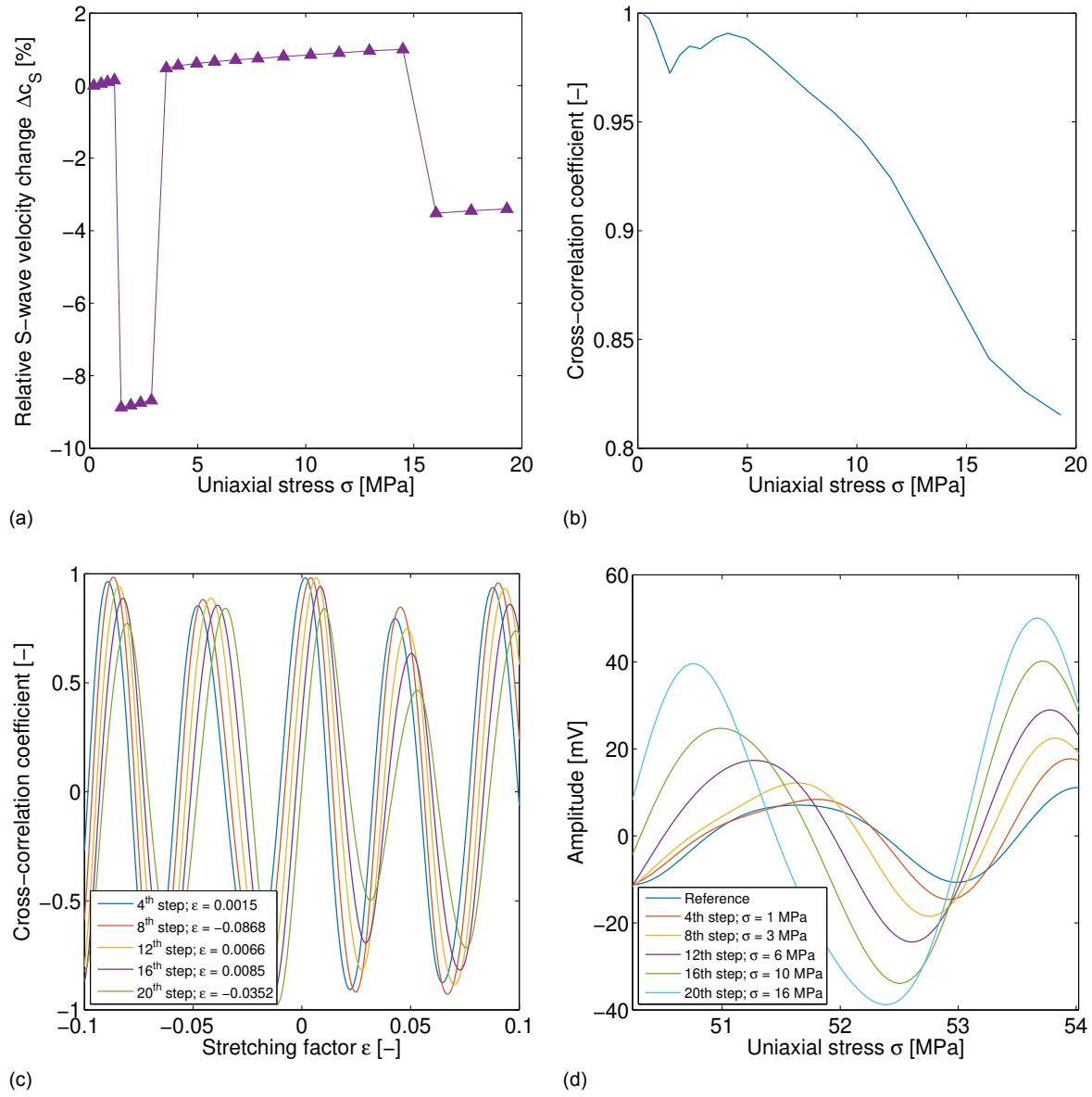

Figure 6.9: Initial cross-correlation of the S-wave content along the axial direction of CP-3. (a) The relative S-wave velocity change at various stress levels; displays a distorted trend. (b) The maximum cross-correlation coefficient at various stress levels. (c) The cross-correlation coefficient for a stretching from -10% to 10%. (d) The time window centered around the S-wave arrival; includes approximately one and a half period.

Figures 6.9a and 6.9b display the course of the relative S-wave velocity change and the maximum cross-correlation coefficient, respectively, as the stress ranges from 0 to 20 MPa. From these graphs, it is observed how the relative wave-velocity change develops in a discontinued manner, whereas the maximum cross-correlation coefficient demonstrates a continuous decline. This confirms that the algorithm's sole objective is to find the highest possible cross-correlation coefficient it can find within the set range of stretch and the boundaries of the time window. This manifestation can be witnessed in

Figures 6.9c and 6.9d which display the most prominent input parameters of the algorithm. Here, it can be observed that the two distortions in Figure 6.9a are caused by the wide range of both the stretching factor and the time window. At stress levels around 3 MPa and 16 MPa, the algorithm finds the largest cross-correlation coefficient if the reference signal is compressed. That is, the reference wavelet matches best with the first oscillation of the adjacent period. Therefore, the cross-correlation can be fine-tuned by narrowing the range of these input parameters through various iterations. Throughout these iterations, the cross-correlation coefficient has been monitored such that it does not fall below 60%. The results of this fine-tuning are displayed in Figure 6.10.

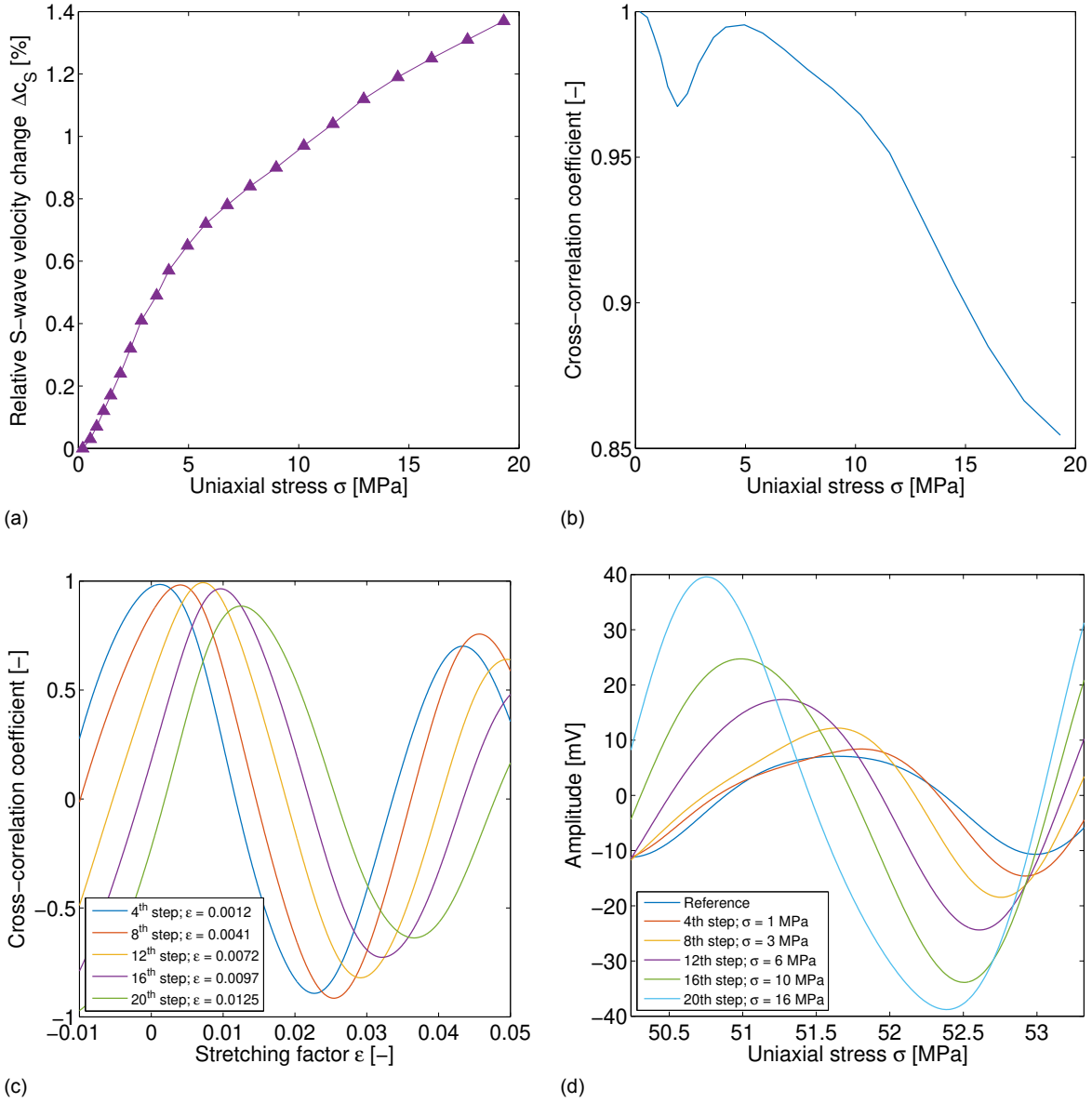

Figure 6.10: Fine-tuning of the cross-correlation of the S-wave content along the axial direction of CP-3. (a) The relative S-wave velocity change at various stress levels; displays a continuous trend. (b) The maximum cross-correlation coefficient at various stress levels. (c) The cross-correlation coefficient for a stretching from -1% to 5%. (d) The time window centered around the S-wave arrival; includes approximately one period.

The narrowing of both the range of stretching and the time window is demonstrated in Figures 6.10c and 6.10d. Here, it is witnessed that the stretching factor is centered around 0% and slightly increases as the stress increases, which is reflected by the continuous increase of the relative S-wave velocity change (Figure 6.10a). Furthermore, the fine-tuning has had no negative impact on the maximum

cross-correlation coefficient. This protocol has been applied to all the other measurements.

6.3. Relative wave-velocity change

Resulting from the Stretching Technique are the various graphs, displaying the acoustoelasticity of the four test specimens. The relation between the relative wave-velocity changes and the applied uniaxial compression for all waveforms are presented in this section. In order to relate the results to Murnaghan's theory, a hypothesis with regard to the expected behaviour of the relative wave velocity has been formed. Subsequently, the observations following from the measurements are discussed and compared to the hypothesis.

6.3.1. Hypotheses

In Chapter 4 it has been stated that the influence of the stress on the wave velocity according to Murnaghan's theory strongly depends on the unknown third-order coefficients l, m and n. However, a hypothesis can be formed if some assumptions are made with regard to these Murnaghan constants. Based on the results of their experiments, Hughes and Kelly [13] found that the Murnaghan constants are generally negative and of an order higher than the second-order coefficients. The hypotheses concerning the influence of the stress on the wave velocity follow from these findings. The P-wave velocities of a medium subjected to compression are described by the following expressions:

$$
\begin{aligned}
{c_{xx}}^{\sigma_{xx}} &= \sqrt{\frac{\lambda + 2\mu - \frac{\sigma_{xx}}{3K}\left[2l + \lambda + \frac{\lambda + \mu}{\mu}(4\lambda + 4m + 10\mu)\right]}{\rho_a}} \\
{c_{yy}}^{\sigma_{xx}} &= \sqrt{\frac{\lambda + 2\mu - \frac{\sigma_{xx}}{3K}\left[2l + \lambda - \frac{\lambda}{2\mu}(4\lambda + 4m + 10\mu)\right]}{\rho_a}}.
\end{aligned}
\tag{6.11}
$$

Here, ${c_{xx}}^{\sigma_{xx}}$ denotes the velocity of a P-wave propagating along the loading direction and ${c_{yy}}^{\sigma_{xx}}$ – the velocity of a P-wave propagating perpendicular to the loading direction. Their relative wave-velocity changes are then denoted with Δc_{xx} and Δc_{yy}, respectively. Based on the assumptions made with regard to the Murnaghan constants and the expressions (6.11), it can be deducted that the relative P-wave velocity change Δc_{xx} increases as the compression increases. The influence of the compression on the relative P-wave velocity Δc_{yy} is less in comparison to Δc_{xx}. Whether Δc_{yy} increases or decreases as the compression increases, depends on the magnitude of the Murnaghan constants with m having a significant influence.

For the S-wave velocities, the following expressions hold:

$$
\begin{aligned}
{c_{xy}}^{\sigma_{xx}} &= \sqrt{\frac{\mu - \frac{\sigma_{xx}}{3K}\left(m + \frac{\lambda n}{4\mu} + 4\lambda + 4\mu\right)}{\rho_a}} \\
{c_{yx}}^{\sigma_{xx}} &= \sqrt{\frac{\mu - \frac{\sigma_{xx}}{3K}\left(m + \frac{\lambda n}{4\mu} + \lambda + 2\mu\right)}{\rho_a}} \\
{c_{yz}}^{\sigma_{xx}} &= \sqrt{\frac{\mu - \frac{\sigma_{xx}}{3K}\left[\lambda + m - \frac{\lambda + \mu}{\mu}\left(\frac{3\mu\lambda}{\lambda + \mu} + \frac{1}{2}n\right)\right]}{\rho_a}},
\end{aligned}
\tag{6.12}
$$

Here, ${c_{xy}}^{\sigma_{xx}}$ denotes the velocity of a S-wave propagating along the loading direction. Its relative wave-velocity change is then denoted with Δc_{xy}. The S-waves propagating perpendicular to the loading direction while polarising along to and perpendicular to the loading direction are represented with ${c_{yx}}^{\sigma_{xx}}$ and ${c_{yz}}^{\sigma_{xx}}$, respectively. Their respective relative wave-velocity changes are denoted with Δc_{yx} and Δc_{yz}. By using the same argumentation as before, it can be deducted that the relative S-wave velocity changes Δc_{xy} and Δc_{yx} should increase the most under the compression, with the latter being slightly

more sensitive to the acoustoelastic effect. On the other hand, $c_{yz}{}^{\sigma_{xx}}$ should increase the least or even decrease as compression increases, mainly depending on the magnitude of n. Figure 6.11 displays a visual representation of the predicted behaviour of the relative wave-velocity changes for different sets of Murnaghan constants.

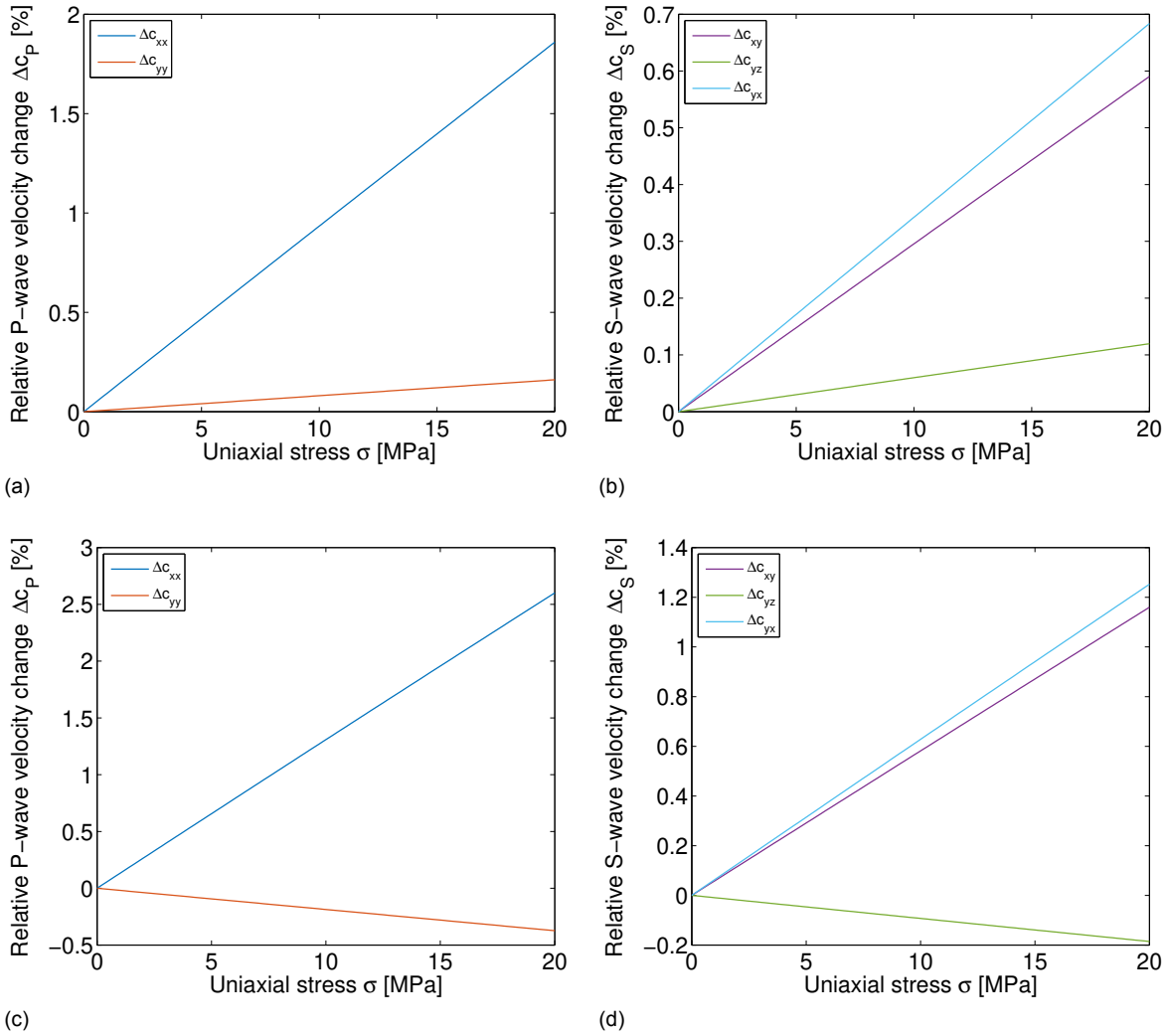

Figure 6.11: Prediction of the relative wave-velocity changes for different sets of Murnaghan constants: (a and b) $l = m = n$ = -300 GPa; (c and d) l = -100 GPa, m = -500 GPa, n = -700 GPa. (a and c) Relative P-wave velocity changes. (b and d) Relative S-wave velocity changes.

6.3.2. Cement-paste specimens

Following from the experiment and the data processing, three relative P-wave velocity changes and three relative S-wave velocity changes have been obtained. Corresponding to Figures 5.11b and 5.11c, Table 6.4 displays a summary of the transducer pairs and the measured relative wave-velocity changes.

Table 6.4: Summary of the measured relative wave-velocity changes.

Transducer pair	Relative P-wave velocity change Δc_P	Relative S-wave velocity change Δc_S
S1-S2	Δc_{xx}	Δc_{xy}
S3-S4	Δc_{yy}	Δc_{yz}
S5-S6	Δc_{yy}	Δc_{yx}

The relative wave-velocity changes of the cement-paste specimens are displayed in Figure 6.12.

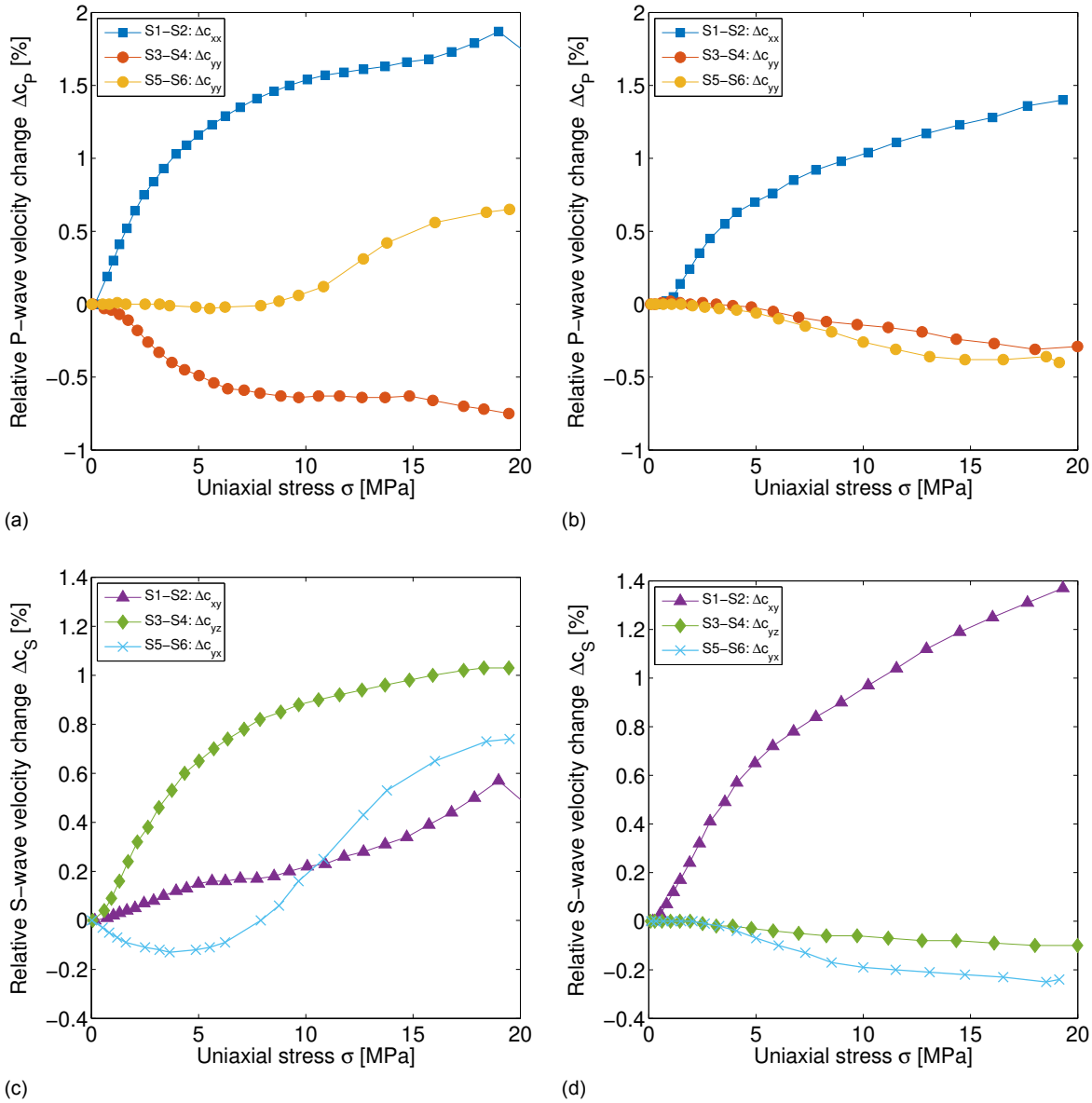

Figure 6.12: Relative wave-velocity changes of the cement-paste specimens. (a) Relative P-wave velocity change of specimen CP-1. (b) Relative P-wave velocity change of specimen CP-3. (c) Relative S-wave velocity change of specimen CP-1. (d) Relative S-wave velocity change of specimen CP-3.

From the comparison of Figures 6.12a and 6.12b it can be observed that the relative P-wave velocity change Δc_{xx} is quite consistent for both specimens. As the uniaxial compression increases, Δc_{xx} increases as well, within the range of approximately 0 to 2%. The trend of both graphs displays an increase of Δc_{xx} at the low stress levels which drops gradually as the compression increases. This curved trend could be a result of the flawed cross-correlation. Due to a possible attenuation of the target wavelet, it is likely that the stretching algorithm picks another wavelet for the cross-correlation. This new wavelet is then monitored as the compression increases, until a better wavelet has been detected by the algorithm. This procedure would manifest itself in the relative wave-velocity change consisting of multiple linear parts. Each of these linear parts would then denote another wavelet which has been cross-correlated with the reference wavelet. This phenomenon is witnessed more clearly in Figure 6.12b, displaying an almost bi-linear trend which suggests the monitoring of two different wavelets in the cross-correlation.

The differences between the results of the specimens is noticed when observing the behaviour of Δc_{yy}. Since two transducer pairs have been applied along the circumference of the specimens, two radial P-waves have been measured. According to Murnaghan's theory, these P-waves should yield the same results. This is the case for specimen CP-3, which displays that Δc_{yy} is almost identical for both measurements, like depicted in Figure 6.12b. However, this phenomenon is not observed in the results for specimen CP-1. This inconsistency could be attributed to the waves being emitted at two different locations. Another reason could be that the radial transducers do not make full contact on the rounded surface of the cylinder, resulting in inconsistent measurements. Overall, it is witnessed that Δc_{yy} slightly decreases as the uniaxial compression increases. Therefore, it can be concluded that the observations of the relative P-wave velocity changes of the cement-paste specimens are quite coherent with the hypothesis in Figure 6.11c.

From the graphs in Figures 6.12c and 6.12d it can be observed that the measurements of the S-waves propagating along the loading direction yield conflicting results. This is manifested through the inconsistency in the range of the magnitude of Δc_{xy} as well as the difference in the shape of its trend. It is found that the magnitude of Δc_{xy} for specimen CP-3 is twice as large as for specimen CP-1. Also, for CP-1 the relation between Δc_{xy} and σ_{xx} seems to be linear whereas for CP-3 this is more bi-linear. This could indicate that the cross-correlation for this waveform has been performed more accurately for CP-1. Furthermore, all the relative S-wave velocity changes of specimen CP-3 (Figure 6.12d) show great resemblances to their P-wave counterparts from Figure 6.12b. This could elude to the possibility that the attempt to decouple the P- and S-wave content has not been successful. Another reason for the incoherence of the relative S-wave velocity changes could be the potential interference from a P-wave which has been converted to an S-wave after reflecting of a boundary, i.e. a PS-wave. In terms of acoustoelasticity, Δc_{yz} yields the highest magnitude for CP-1, while the largest magnitude for CP-3 is witnessed with Δc_{xy}. This manifestation is contradicting the hypothesis displayed in Figures 6.11b and 6.11d. Moreover, it is observed in Figure 6.12c that, after 10 MPa, Δc_{yx} surpasses Δc_{xy} in terms of magnitude. This particular behaviour seems to be in accordance with the hypothesis (Figures 6.11b and 6.11d). However, considering the non-monotonic trend of Δc_{yx}, this behaviour could also be caused by the inaccurate measurement of the radial transducers.

Due to the large curvature of the specimens, the radially applied transducers have a small contact surface. This could result in some limitations with respect to the transmission of the transverse motion of the transducers, depicted in Figure 6.13.

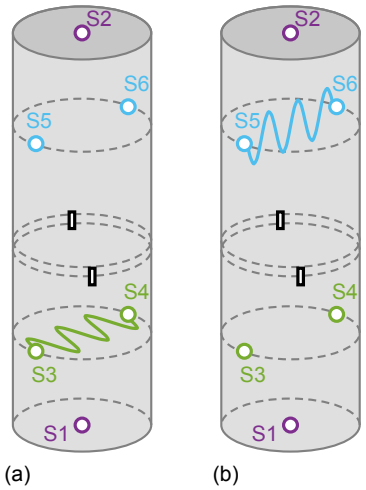

Figure 6.13: Particle-oscillation direction of the radially applied transducer pairs. (a) Transducer pair S3-S4: SH-wave. (b) Transducer pair S5-S6: SV-wave.

From Figure 6.13, it can be argued that the radially applied transducers only make contact with the specimen in a single point. From this, it could be possible that, due to the large curvature, the transverse motion of transducer pair S3-S4, i.e. of the SH-wave, is not transferred properly. As a result, only the additional P-wave motion would have propagated through the specimen. This does not hold for transducer pair S5-S6 which has its particle-oscillation direction along the single point of

contact. Therefore, the non-monotonic trend of Δc_{yx} from CP-1 (Figure 6.12c) could have been a result of some PS-wave interference.

6.3.3. Concrete core specimens

The relative wave-velocity changes of the concrete core specimens are presented in Figure 6.14.

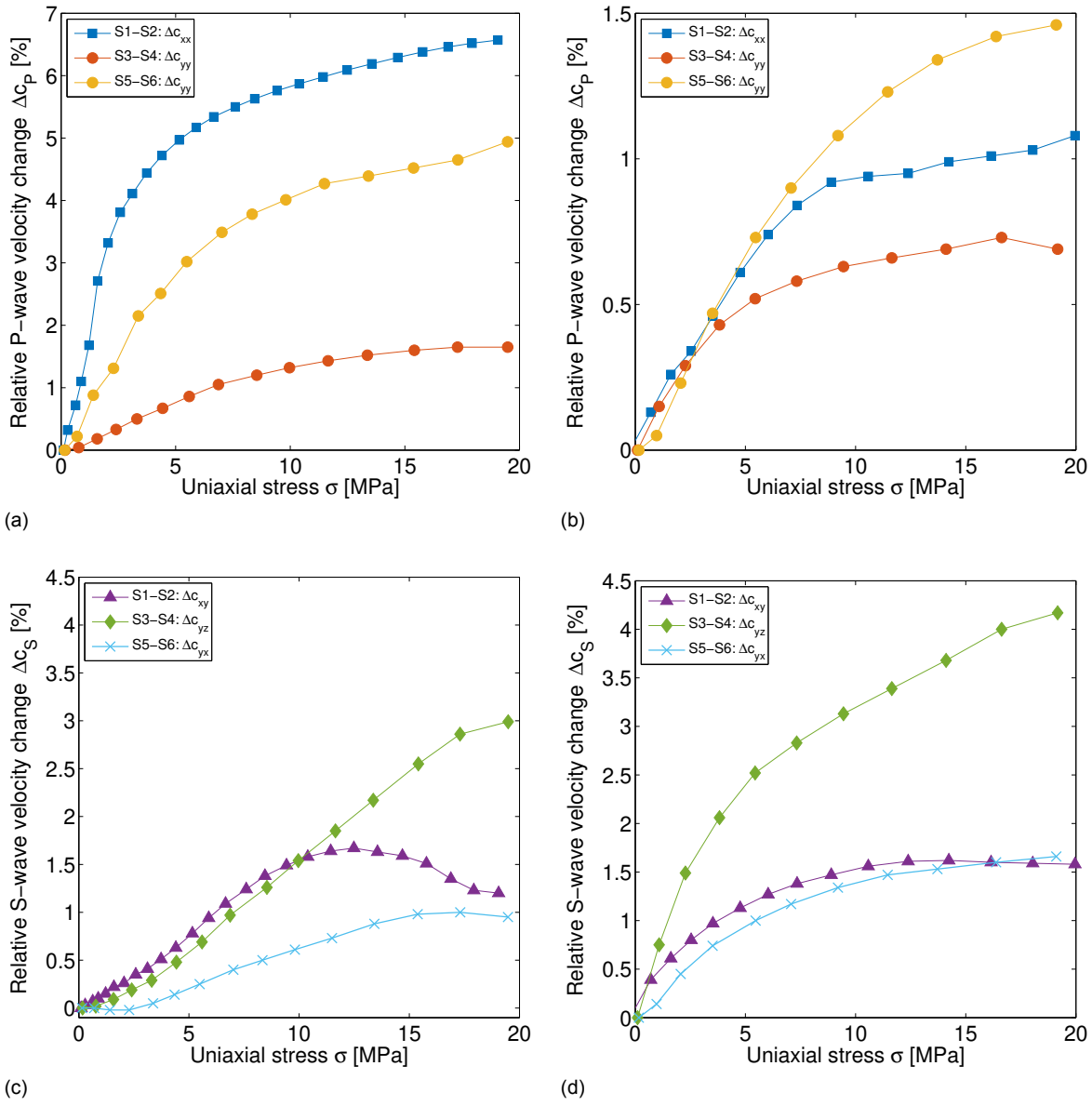

Figure 6.14: Relative wave-velocity changes of the concrete core specimens. (a) Relative P-wave velocity change of specimen CC-2B. (b) Relative P-wave velocity change of specimen CC-4B. (c) Relative S-wave velocity change of specimen CC-2B. (d) Relative S-wave velocity change of specimen CC-4B.

From Figures 6.14a and 6.14b it is observed that for the concrete core specimens all relative P-wave velocity changes increases as compression increases. Like with Δc_{xx} from the cement-paste specimens, the increase of these relative P-wave velocities is the highest at low stress levels and drops gradually at higher compressive stress levels. Another similarity with the results from the cement-paste specimens is the discrepancy in the measurements of Δc_{yy}. However, when comparing the results from CC-2B with CC-4B, some inconsistencies are witnessed. Beginning with the relative P-wave velocity change in the axial direction, it can be observed that the magnitude of Δc_{xx} for CC-2B is approximately seven times larger than for CC-4B. In addition, no consistent ranking between the Δc_{xx} and Δc_{yy} in

terms of magnitude has been observed. This especially the case for specimen CC-4B where it is witnessed that the magnitude of Δc_{xx} lies in between those of the two measurements of Δc_{yy}, which is contradicting the hypotheses (Figures 6.11a and 6.11c).

Unlike with the relative P-wave velocity changes, the graphs from Figures 6.14c and 6.14d display moderately consistent results between the two concrete core specimens. The range of the magnitude for these relative S-wave velocity changes is much closer for both specimens than for their P-wave counterparts. It is also striking that for both specimens the largest changes with respect to the wave velocity are observed in Δc_{yz}, whereas the smallest changes are found in Δc_{yx}. These findings are contradicting the hypotheses from Figures 6.11b and 6.11d. Furthermore, it is observed that the magnitude of Δc_{yx} stops increasing after approximately 10 MPa. This phenomenon is even more prominent with specimen CC-2B, where Δc_{xy} even decreases.

The influence of the inclusion of aggregates in the concrete medium has been observed from the results for specimens CC-2B and CC-4B. Contrary to the cement-paste specimens, the concrete core specimens display less coherence with each other in terms of the relative wave-velocity changes. This is especially prominent with the relative P-wave velocity changes. These inconsistencies are manifested through both the large differences in magnitude of the relative wave-velocity changes as well as their random sensitivity to the acoustoelastic effect. The discrepancy in the aggregate size is highly associated with the frequency of the emitted signals. According to Planès and Larose [24], the ultrasonic monitoring of signals can be categorised based on the frequency band. The behaviour of the signal in terms of interaction with the aggregates depends on the wavelength with respect to both the aggregate size and the specimen size. If the wavelength is of the same order as the specimen size, the signal is within the stationary-wave regime. Since the wavelength is also much larger than the aggregate size, the interaction between aggregates and the waves is insignificant. Therefore, the sensitivity to the acoustoelastic effect is limited. A wave signal is within the simple-scattering regime when the wavelength is larger than the aggregates but smaller than the specimen size. Here, there is a weak interaction between the wave signal and the aggregates, manifested through scattering. When the wavelength is shorter than the aggregate size, the wave signal is in the multiple-scattering regime. The wave signal in this regime is strongly affected by the aggregates, making the signal more sensitive to the acoustoelastic effect. However, in this regime the wave signal is also strongly attenuated [12].

The used centre frequency of 400 kHz has resulted in a wavelength of $\lambda_P \approx 10.00$ mm for the P-wave and $\lambda_S \approx 6.25$ mm for the S-wave. From Figure 5.14 it can be estimated that the average aggregate size is approximately 10 mm. Following from this, it can be argued that the P-waves in specimen CC-2B are within the simple-scattering regime. This can be elaborated by comparing the magnitudes in Figure 6.14a with those of the relative P-wave velocity changes of the cement-past specimens, which do not include aggregates. By taking into account the larger aggregate size in CC-4B it can be deducted that the P-waves in this specimen could be within the multiple-scattering regime. This argument might explain the lower magnitudes of Δc_P, which could be a result of the strong attenuation. With the same reasoning, it can be argued that the S-waves in both concrete core specimens are most likely within the multiple-scattering regime as well.

6.4. Validation

The last step of the data processing is the validation of the results. This validation has been carried out in twofold. The first part concerns the determination of the Murnaghan constants of the specimens. The veracity of these parameters are then verified according to the expectations with regard to their characteristics. The second part involves a comparison with the findings in the paper *"Acoustoelastic Response of Concrete under Uniaxial Compression"* by Nogueira and Rens [23], following from a similar experiment. This has been accomplished by using the Murnaghan constants from this paper in order to match the relative wave-velocity changes.

6.4.1. Murnaghan constants

Based on the findings of the relative wave-velocity changes, it has been concluded that the concrete cores specimens do not yield consistent results. Therefore, the validation has been centered around the cement-paste specimens. The Murnaghan constants of these specimens have been determined by creating linear fits to the data and subsequently equating them with the expressions for the linearised acoustoelastic constants (4.22). Since the Murnaghan constants consist of three parameters, three

equations are sufficient to determine them. Therefore, only three of the six measurements are considered when solving this system of equations. For the purpose of yielding reliable results, the three most consistent measurements have been chosen and subsequently fitted with a linear regression. These are the relative wave-velocity changes Δc_{xx}, Δc_{xy} and Δc_{yy} (from transducer pair S3-S4), which have been equated with their theoretical counterparts,

$$\begin{aligned} A_{xxxx} \Longrightarrow \Upsilon &= \frac{2l + \lambda + \frac{\lambda + \mu}{\mu}(4\lambda + 4m + 10\mu)}{6K(\lambda + 2\mu)} \\ A_{xyxx} \Longrightarrow \mathrm{X} &= \frac{m + \frac{\lambda n}{4\mu} + 4\lambda + 4\mu}{6K\mu} \\ A_{yyxx} \Longrightarrow \Phi &= \frac{2l + \lambda - \frac{\lambda}{2\mu}(4\lambda + 4m + 10\mu)}{6K(\lambda + 2\mu)}, \end{aligned} \tag{6.13}$$

respectively. Figure 6.15 displays the chosen measurements and their acoustoelastic constants.

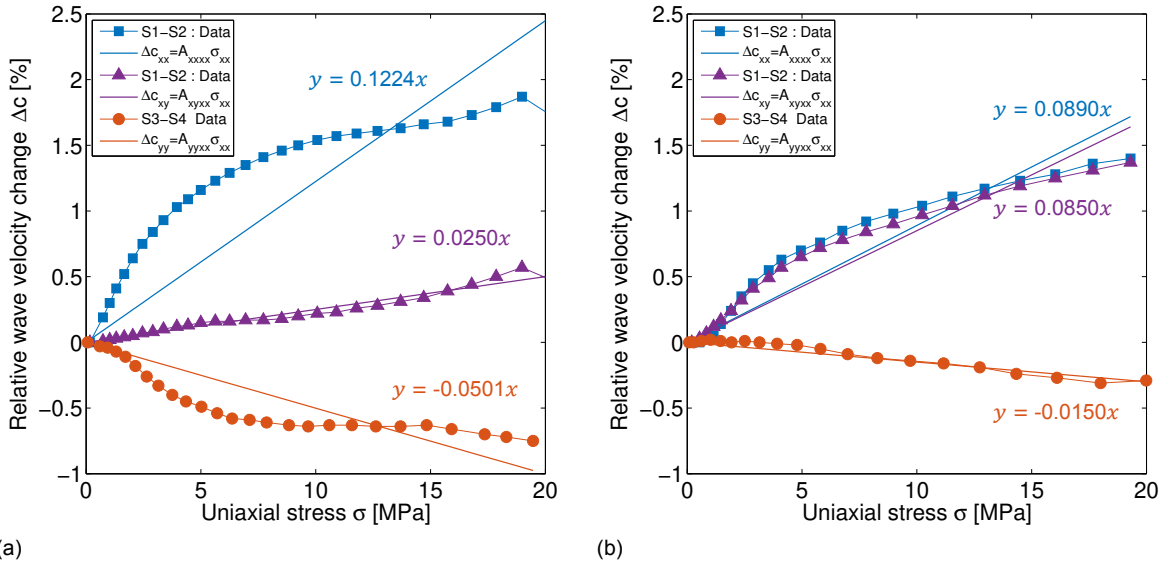

Figure 6.15: The linearised acoustoelastic constants of the cement-paste specimens. (a) Specimen CP-1: A_{xxxx} = -1.22 GPa^{-1}, A_{xyxx} = -0.25 GPa^{-1}, A_{yyxx} = 0.50 GPa^{-1}. (b) Specimen CP-3: A_{xxxx} = -0.89 GPa^{-1}, A_{xyxx} = -0.85 GPa^{-1}, A_{yyxx} = 0.15 GPa^{-1}.

The Murnaghan constants have been determined by equating the acoustoelastic constants (Figure6.15) to the expressions (6.13) and solving this system. Table 6.5 displays both the Murnaghan constants and the Lamé parameters of the cement-paste specimens. For comparison, Table 6.5 displays the Murnaghan constants of a mortar specimen [23] as well.

Table 6.5: Summary of the second- and third-order material parameters of the cement-paste specimens.

Specimen	Lamé parameters [GPa]		Murnaghan constants [GPa]		
	λ	μ	l	m	n
CP-1	5.64	8.46	160.10	−355.98	938.51
CP-3	7.72	10.66	−43.40	−356.33	−2890.00
Mortar specimen [23]			−170.70	−235.80	−280.00

The hypotheses regarding the Murnaghan constants involved that they should be negative and of a

larger order of magnitude than the Lamé parameters. From the found parameters in Table 6.5 it can be observed that the Murnaghan constants of both specimens are indeed much larger than the second-order coefficients. Besides, it is observed that for both specimens n has a magnitude of an order higher than l and m. This parameter is only present in the expression for the linearised S-wave velocity, which is the least consistent of the three measurements. Therefore, the remarkable difference in magnitude of n with respect to the other Murnaghan constants could be attributed to the inaccurate measurement of Δc_{xy}. Furthermore, for specimen CP-1 holds that only one of the three constants is negative. This phenomenon is not witnessed in specimen CP-3, which meets both of the set expectations. From the observation of the Murnaghan constants, it can be concluded that CP-3 is the only specimen which can be deemed representative. Therefore, the Murnaghan constants from CP-3 have been used in order to validate the data from CP-1, like depicted in Figure 6.16.

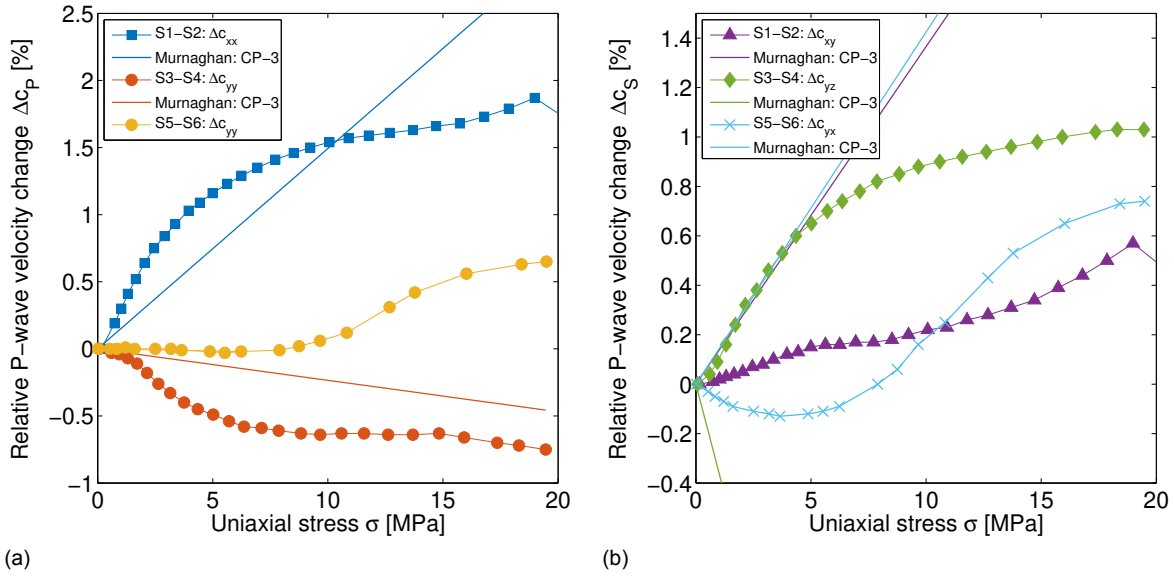

Figure 6.16: Validation of the results from CP-1 with the Murnaghan constants of CP-3: l = -43.40 GPa, m = -356.33 GPa, n = -2890.00 GPa. (a) Relative P-wave velocity change Δc_P. (b) Relative S-wave velocity change Δc_S.

From this validation in Figure 6.16a it can be observed that the linear fits, formed by the Murnaghan constants of CP-3, are in accordance with the trend of the relative P-wave velocity changes. This is especially the case at low stress levels. It is also witnessed that the linear fit of Δc_{yy} lies within the boundaries set by the two measurements. This indicates that the inconsistency between the two measurements of Δc_{yy} are caused by the inaccuracy of the radial recordings. When investigating the relative S-wave velocity changes, no accordance between the linear fits and the data from CP-1 is found. Again, this can be attributed to the inaccuracy of the radial recordings as well as the coupled P- and S-wave content.

6.4.2. Comparison with literature

In the paper by Nogueira and Rens [23], it is described how experiments have been conducted during which wave signals have been emitted through various specimens subjected to a uniaxial compression. Resulting from these experiments are the Murnaghan constants of the tested specimens, among which a mortar specimen. The Murnaghan constants of these specimens have been determined in a similar way as explained in the previous section. Following from the results is that the relation between the applied stress and the relative wave-velocity is indeed linear, confirming the hypotheses from Figure 6.11. The measurements of the relative wave-velocity changes of both CP-1 and CP-3 have been validated by using the Murnaghan constants of the mortar specimen [23], displayed in Table 6.5. This has been realised by substituting the Murnaghan constants from mortar specimens in the expressions (6.13). Figure 6.17 displays the relative wave-velocity changes of the cement-paste specimens together with the linear fit from the mortar specimen.

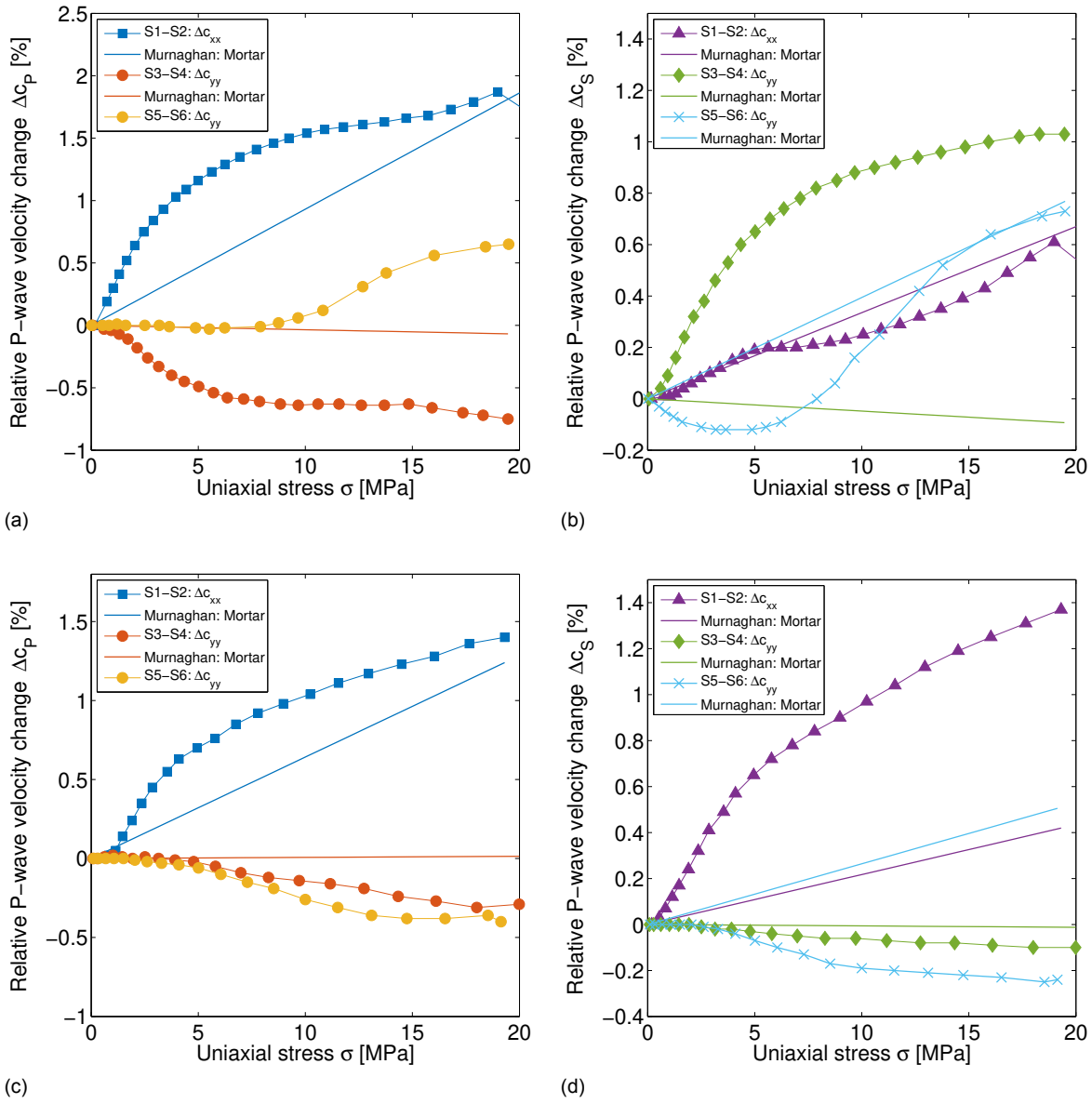

Figure 6.17: Validation of the results from CP-1 with the Murnaghan constants of the mortar specimen: l = -170.70 GPa, m = -235.80 GPa, n = -280.00 GPa. (a) Relative P-wave velocity change Δc_P. (b) Relative S-wave velocity change Δc_S.

The graphs in Figures 6.17a and 6.17c show that for the relative P-wave velocity change Δc_{xx}, the mortar specimen accurately approximates the data of specimen CP-1 and CP-3. This consistency is not observed in Δc_{yy}, where it is unclear whether the data from the mortar specimen increases or decreases. When investigating the relative S-wave velocity changes it is witnessed that the data of the mortar specimen precisely matches Δc_{xy} from CP-1, especially for the first 5 MPa (Figure 6.17b). In addition, the mortar specimen approximates the last 10 MPa of Δc_{yx} as well. The relative S-wave velocity Δc_{yz} from CP-1 does not coincide with the fit from the mortar specimen. Again, this can be attributed to the inaccurate measurement of the radial transducers. Overall, no clear relations can be observed from the comparison between the relative S-wave velocity changes of CP-3 and the mortar specimen (Figure 6.17d).

6.5. Conclusions

From the results of the data processing, it has been found that the acoustoelastic effect has been confirmed for all four specimens. That is, it has been concluded that the increase of the uniaxial com-

pression results in an increase or decrease of the relative wave-velocity change. For the cement-paste specimens, and CP-3 in particular, the relative P-wave velocity changes seem to yield consistent results. This has been validated quantitatively by comparing the specimens with each other as well as with the mortar specimen from the literature [23]. From these findings, it can be concluded that the P-waves propagating along the loading direction display higher sensitivity to the acoustoelasticity than P-waves propagating perpendicular to the loading direction. Furthermore, it is found that the velocity of a P-wave propagating along the loading direction increases if the compression is increased. These findings confirm again that Biot's model does not work for the analysis of elastic wave propagation in a solid. For P-waves propagating perpendicular to the loading direction, it has been observed that the wave velocity slightly decreases under an increasing uniaxial compression. The results in [18][23] show that the velocity of these P-waves increases moderately under an increasing uniaxial compression. Both of these trends have been predicted in the hypothesis, which concludes that the magnitude of the Murnaghan constants determines whether the wave velocity of P-waves propagating perpendicular to the loading direction increases or decreases. On the other hand, no consistent results have been found for the relative S-wave velocity changes. This observation can be attributed to a combination of the discussed issues concerning both the coupled wave content and the radial recordings.

Throughout the data processing several difficulties have arisen. The first issue which has been experienced involves the characteristics of the ultrasonic transducers. The coupling and close range of the P- and S-wave content is most likely the reason why the relative S-wave velocity changes are inaccurate. It seems that even after applying a P-wave filter, there is still some interference present from remnant P-wave content. Another issue is met when observing the relative wave velocities of the radial wave recordings. The inconsistencies within these measurements seem to stem from the small diameter of the specimens. This causes inconveniences on both a practical level and an analytic level. Due to the larger curvature of the cylindrical specimens, it is harder to ensure that the transducers make full contact with the curved surface of the specimens. Therefore, this could result in inaccurate data being recorded. Another issue is related to the constraint on the time window caused by the close arrival times of the first P- and S-waves. This leaves almost no margin to vary the boundaries of the time window in order to fine-tune the results of the stretching algorithm.

The discrepancies in the results of the relative P-wave velocity changes of the concrete core specimens can be attributed to the difference in aggregate size. The sensitivity of the P-waves to the acoustoelastic effect are determined by the amount of interaction with the aggregates through scattering. The ratio between the wavelength and the size of both the specimen and the aggregate dictate the wave regime, for which the amount of scattering and attenuation is specified. Therefore, it has been concluded that the aggregates influence the wave regime and thus the acoustoelasticity. Here, it has been found that the P-waves of the concrete core specimens are most likely within different wave regimes. With the same reasoning, it has been argued that the S-waves are probably within the same wave regime.

7

Conclusions and recommendations

The final chapter of this thesis is centered around the conclusions that can be drawn from the research. The sub-questions which have been stated in the introductory chapter are treated here. Subsequently, an answer to the research question is formulated. Finally, some recommendations with regard to future works are elaborated as well.

7.1. Conclusions

The structure of the thesis can be divided in two segments. The first segment encompasses the theoretical part of the research, during which the acoustoelastic effect is investigated theoretically. The second segment is centered around the conduction of experiments and processing of the acquired data for the purpose of determining the relative wave-velocity changes. The conclusions following from these segments, as well as an answer to the research question, are covered in this section.

7.1.1. Theoretical conclusions

In Chapters 2 and 3, both Murnaghan and Biot's theoretical models regarding the elastic wave propagation under a stress state have been elaborated and critically reviewed. As a result, two distinct formulations of the relation between the wave velocity and the stress have been discussed. In Chapter 2, expressions for the wave velocities of a medium subjected to a stress have been elaborated, based on Murnaghan's theory. From this, it is concluded that the influence of the stress in the expression for the wave velocity stems from the second-order deformation terms in the constitutive relations. Chapter 3 has covered Biot's theory with regard to the stress influence on the wave velocity. Here, it is found that he assumed an initial strain-independent stress, which enters the expression for the wave velocity through the dynamic-equilibrium equation.

The comparison between the fundamental assumptions, made by both Murnaghan and Biot, has been discussed in Chapter 4. The most significant difference between the two models is the way they consider the higher-order deformation terms. Murnaghan established the constitutive relations through the introduction of a deformation energy function including the second-order deformation terms. The form of this deformation energy function is based on his assumption that the material is isotropic. Therefore, Murnaghan's theory is not suitable when studying anisotropic materials. Through the constitutive relation, the second-order stress terms enter the wave equation, resulting in stress-dependent expressions of the wave velocity. In these expressions, the increase/decrease of the wave velocities is regulated by the unknown Murnaghan constants which have to be determined. Biot assumed the infinitesimal theory and therefore discards all deformation terms of an order higher than the first. As a result, he assumes that the initial-stress components enter the wave equation, and thus the expression for the wave velocity, through force equilibrium. This phenomenon is reminiscent of the equation of motion of a bending rod subjected to an axial force. Biot also assumes that the elastic wave propagation in a three-dimensional medium, subjected to initial stresses, is a general case of the bending-rod model. However, the implications with respect to the increase/decrease of the wave velocity following from these assumptions clearly contradict the results which are attained through experiments. Therefore, it

has been concluded that Biot's model is not an accurate depiction of the elastic wave propagation in a solid. Consequently, the thesis has progressed by focussing on Murnaghan's theory only. In order to determine the Murnaghan constants, an experiment has been designed during which the influence of the stress on the velocity of different waveforms is monitored.

7.1.2. Experimental conclusions

The second part of the research has been dedicated to experiments and the data processing of the acquired data. In an attempt to verify the acoustoelastic effect in a concrete-like material, experiments have been designed and performed. During these tests, various wave signals have been emitted through four specimens, which have been subjected to a uniaxial compression. The specifications of the emitted wave signals and the uniaxial loading have been elaborated in Chapter 5. The data acquired from these experiments has been evaluated in Chapter 6.

The verification of the theoretic acoustoelastic effect has been considered in two steps. The first step concerns a qualification of the acoustoelastic effect. During this step, it has been investigated whether the applied stress has an influence on the wave velocity. The second step involves a quantification of the acoustoelastic effect. Here, it has been attempted to examine the specific characteristics of the relation between the applied uniaxial compressive stress and the relative wave-velocity change. The results of the data processing show that all of the specimens display some degree of acoustoelasticity. The data from the homogeneous cement-paste specimens display quite consistent results. This is especially the case for the waves propagating along the loading direction. Here, it is found that the measurements of the relative P-wave velocity Δc_{xx} are coherent. Both specimens display a proportionate relation between Δc_{xx} and the applied compression, where the range of the magnitude of Δc_{xx} is almost identical. Furthermore, the increase of Δc_{xx} is the highest at low stress levels and drops gradually as compression increases. The coherence in results is not observed for the relative S-wave velocity Δc_{xy}, which yields inconsistencies between the specimens with regard to the magnitude and the shape of the function. This is most likely caused by the unsuccessful attempt to decouple the close-ranged P- and S-wave content. Apart from the P-waves, the recordings following from the radially applied transducers are incoherent between the specimens. The inaccuracy of these measurements could be attributed to a combination of the coupled frequency content and the small specimen size.

The challenges caused by the small diameter of the cylindrical specimens are in twofold. The first challenge is related to the contact between the transducers and the curved surface of the specimen. Due to the large curvature, it is possible that the transducers only make contact with the specimen in a single point. As a result, the intended transverse motion might not be transferred properly to the specimen. The second challenge is with regard to the data processing. Due to the small diameter, the P- and S-arrivals are close in time. Consequently, this constraints the time window in which the cross-correlation in the radial direction is performed. Therefore, it is nearly impossible to improve the cross-correlation by fine-tuning the boundaries of the time window.

For the purpose of assessing the veracity of the results, a validation of the data has been performed. This has been done by using the Murnaghan constants to recreate the data. The Murnaghan constants of one specimen have been determined and used to fit the data of the other specimen. From this, it has been concluded that the relative P-wave velocity changes are consistent among the specimens. From the literature [23], another set of Murnaghan constants has been used to validate both cement-paste specimens. Here, it has been found that these Murnaghan constants match the data of Δc_{xx} for both specimens and the data of Δc_{xy} for only one of the two specimens.

When observing the waves propagating perpendicular to the loading direction, it is found that only the P-waves display consistent results. Since two P-waves have been emitted perpendicular to the loading direction, it has been possible to validate the results from these waves with each other. From this it is found that the relative P-wave velocity Δc_{yy} is much less sensitive to the acoustoelasticity in comparison with Δc_{xx}. This particular behaviour is in accordance with the formed hypothesis and the literature [18][23], from which follows that the acoustoelastic effect is the strongest for waves with a particle-oscillation direction which is parallel to the loading direction. However, due to the inconsistent results from the relative S-wave velocity changes, it has not been possible to draw the same conclusions.

In addition to the cement-paste specimens, two concrete core specimens have been examined as well. From these results, it has been possible to observe the influence of the aggregates on the wave velocity. Even though stress-induced changes have been observed, the measurements of the concrete core specimens do not seem to be consistent. This is especially the case for the relative P-wave velocity changes which display incoherent results with regard to the sensitivity of different waveforms to the acoustoelastic effect. These inconsistencies in the measurements of the concrete core specimen can be attributed to a discrepancy in the heterogeneity of the material. This difference is a result of the varying ratio between the aggregate and specimen size, caused by the random distribution and dimensions of the aggregates. Therefore, based on these measurements, it has not been possible to establish the shape of the relation between the applied compression and the wave velocities of the concrete core specimens.

7.1.3. Final conclusion

From the research conducted in this thesis, it has been concluded that Murnaghan's theory yields the most accurate representation of the stress-induced changes in the wave velocity. In his theory, it is displayed how the wave velocity of a solid is influenced by the stress through the inclusion of the second-order deformations. The performed experiments and the subsequent data processing have displayed that the concrete-like medium demonstrates acoustoelastic behaviour. From the measurements, it has been possible to conclude that the relative P-wave velocity changes exhibit consistent results between the cement-paste specimens. From this, it is witnessed that the P-waves propagating along the loading direction increase in velocity with an increasing compression. On the other hand, P-waves propagating perpendicular to the loading direction decrease in velocity with an increasing compression. Besides, the data shows that the relative wave-velocity change is linked to the applied stress following an approximate linear relation. Furthermore, it has been found that P-waves with a particle oscillation along the loading direction are more sensitive to the acoustoelastic effect, which is also in accordance with Murnaghan's theory.

The inclusion of the aggregates in the specimens has been shown to cause incoherent results with respect to the acoustoelastic behaviour between the specimens. These inconsistencies are a result of the random size and distribution of the aggregates within the concrete cores. The sensitivity to the acoustoelastic effect is heavily dependent on the relation between the wavelength, the aggregate size and the specimen size. The magnitude of the wavelength of a signal with respect to both the aggregate size and the specimen size regulates the occurrence of scattering and attenuation, or lack thereof. Therefore, due to the discrepancies within the aggregate size of the concrete core specimens, different acoustoelastic behaviour has been witnessed. This has been mainly the case for the relative P-wave velocity changes. A wave with a wavelength of a magnitude in between the specimen size and the aggregate size scatters between the aggregates. This yields a higher sensitivity to the acoustoelastic effect in comparison to a wave which does not interact with the aggregates, like the cement-paste specimens. When the wavelength is shorter than the aggregate size, the amount of scattering is even larger which would increase the acoustoelasticity. However, the additional strong attenuation negatively impacts the acoustoelasticity which could outweigh the influence of the scattering. Due to these varieties between the concrete core samples, it has not been possible to quantify the acoustoelastic effect for the concrete core specimens.

7.2. Recommendations for future works

Throughout the research of the thesis, various lessons have been learnt. This section covers the recommendations following directly from the difficulties which have been experienced during the thesis work. The challenges are mainly related to the practical aspect of the experiments. In general, there are two major difficulties which have been experienced. The first one is related to the inability to separate the P- and S-wave pulses. This originates from the used ultrasonic transducers which emit wave signals with coupled P- and S-wave content. For the experiments solely S-wave transducers have been used to emit and record both P- and S-waves. Therefore, it is advised to use P-wave transducers to monitor P-waves and S-wave transducers to monitor S-waves. Doing this could yield more accurate results.

The second difficulty regards the inconsistencies of the radial measurements. The uncertain attachment of the transducers and the small difference between the arrival times are all results from the small diameter of the specimens. This issue of the small dimensions of the specimens also leads to the

large density of the aggregates within the concrete cores, causing inconsistent results as well. Considering these inconveniences and the specimen dimensions used in the literature, it would be advised to test larger specimens. By doing this, it would be possible to achieve a better attachment of the radial transducers as well as to vary more within the boundaries of the time windows. Another benefit could be that the distribution of the aggregates in the concrete core specimens would be more constant. This would result in both specimens being in the same wave regime within the same frequency band.

In order to use wave signals to monitor the stress changes of a concrete structure, the following research steps are advised. First, it is of essence to analyse and quantify the acoustoelasticity of all waveforms considered in this thesis. The outcome should be a theoretical model which predicts the relative wave-velocity changes in a concrete-like material, based on the Murnaghan constants. These experiments should be conducted multiple times while up-scaling the dimensions of the specimens. The next step would be to investigate the acoustoelasticity of waves with non-orthogonal propagation and particle-oscillation direction, while applying various stress states. This step is of great importance and could be the first step towards stress measurement through smart aggregates in concrete structures.

A

Side notes F.D. Murnaghan

The expressions and derivations which Murnaghan made in his theory are elaborated here with additional intermediate steps. Based on Murnaghan's theory, Hughes and Kelly introduced their own expressions for wave velocities of a solid subjected to various stress states. The derivation of these expressions will be elaborated here as well.

A.1. Vectors and matrices

The implementations of vectors and matrices is a convenient method to present the theory of finite deformations of an elastic solid. The description of the strain and the stress as well as their relation can be derived by using the element definitions of an elastic solid.

A.1.1. Matrix element of arc

Assume a variable point $P(x, y, z)$ in a plane of which the coordinates are functions of a single independent parameter α. As α varies, the point P traces a curve C_x. If the coordinates are constant functions of α, then this curve reduces to a single point. The matrix element of arc of the curve that is traced by P is then be defined as:

$$\boldsymbol{dx} = \begin{pmatrix} dx \\ dy \\ dz \end{pmatrix} = \begin{pmatrix} x_\alpha d\alpha \\ y_\alpha d\alpha \\ z_\alpha d\alpha \end{pmatrix}, \tag{A.1}$$

where x_α, y_α and z_α are short notations for the derivatives of x, y and z with respect to the variable α:

$$\begin{aligned} x_\alpha &= \frac{\partial x}{\partial \alpha} \\ y_\alpha &= \frac{\partial y}{\partial \alpha}. \\ z_\alpha &= \frac{\partial z}{\partial \alpha} \end{aligned} \tag{A.2}$$

The scalar element of arc ds_x of the curve C_x is then defined as:

$$ds_x = \sqrt{(\boldsymbol{dx})^T(\boldsymbol{dx})} = \sqrt{(dx)^2 + (dy)^2 + (dz)^2}. \tag{A.3}$$

A.1.2. Element of area

Now assume a point $P(x, y, z)$ of which the coordinates are functions of two independent variables α and β. This results in two matrix elements of arc $\boldsymbol{d_\alpha x}$ and $\boldsymbol{d_\beta x}$:

$$\boldsymbol{d_\alpha x} = \begin{pmatrix} x_\alpha d\alpha \\ y_\alpha d\alpha \\ z_\alpha d\alpha \end{pmatrix}; \quad \boldsymbol{d_\beta x} = \begin{pmatrix} x_\beta d\beta \\ y_\beta d\beta \\ z_\beta d\beta \end{pmatrix}, \tag{A.4}$$

which can be used to define the column vectors of the 3 x 2 matrix:

$$\begin{pmatrix} x_\alpha d\alpha & x_\beta d\beta \\ y_\alpha d\alpha & y_\beta d\beta \\ z_\alpha d\alpha & z_\beta d\beta \end{pmatrix}. \tag{A.5}$$

If it is assumed that this 3 x 2 matrix is obtained by removing the first column of a 3 x 3 matrix, the first column of the cofactor matrix of this original 3 x 3 matrix denotes the matrix element of area $\boldsymbol{dS^x}$ of the surface traced out by the point P:

$$\boldsymbol{dS^x} = \begin{pmatrix} dS^x \\ dS^y \\ dS^z \end{pmatrix} = \begin{pmatrix} \begin{vmatrix} y_\alpha & y_\beta \\ z_\alpha & z_\beta \end{vmatrix} d\alpha d\beta \\ \begin{vmatrix} z_\alpha & z_\beta \\ x_\alpha & x_\beta \end{vmatrix} d\alpha d\beta \\ \begin{vmatrix} x_\alpha & x_\beta \\ y_\alpha & y_\beta \end{vmatrix} d\alpha d\beta \end{pmatrix}, \tag{A.6}$$

where dS^x, dS^y and dS^z denote surface areas which have their outward normals in the x, y and z-direction, respectively.

According to the definitions of linear algebra, the same expression can be obtained through the calculation of the normal vector to the plane defined by the two matrix elements of arc, $\boldsymbol{d_\alpha x}$ and $\boldsymbol{d_\beta x}$, in P. This normal vector $\boldsymbol{n_x}$ is defined as:

$$\boldsymbol{n_x} = \begin{pmatrix} dS^x \\ dS^y \\ dS^z \end{pmatrix} = \begin{pmatrix} x_\alpha d\alpha \\ y_\alpha d\alpha \\ z_\alpha d\alpha \end{pmatrix} \times \begin{pmatrix} x_\beta d\beta \\ y_\beta d\beta \\ z_\beta d\beta \end{pmatrix} = \begin{pmatrix} y_\alpha z_\beta d\alpha d\beta - z_\alpha y_\beta d\alpha d\beta \\ z_\alpha x_\beta d\alpha d\beta - x_\alpha z_\beta d\alpha d\beta \\ x_\alpha y_\beta d\alpha d\beta - y_\alpha x_\beta d\alpha d\beta \end{pmatrix} = \begin{pmatrix} \begin{vmatrix} y_\alpha & y_\beta \\ z_\alpha & z_\beta \end{vmatrix} d\alpha d\beta \\ \begin{vmatrix} z_\alpha & z_\beta \\ x_\alpha & x_\beta \end{vmatrix} d\alpha d\beta \\ \begin{vmatrix} x_\alpha & x_\beta \\ y_\alpha & y_\beta \end{vmatrix} d\alpha d\beta \end{pmatrix}. \tag{A.7}$$

This confirms that the matrix element of area $\boldsymbol{dS^x}$ has the direction of the normal to the surface. By using the definition of the differentials, the entries of the matrix element of area can be written in a compact form:

$$\begin{aligned} dx &= x_\alpha d\alpha + x_\beta d\beta \\ dy &= y_\alpha d\alpha + y_\beta d\beta \\ dz &= z_\alpha d\alpha + z_\beta d\beta. \end{aligned} \tag{A.8}$$

The surface areas are obtained upon multiplication of two differentials which define a plane. For example, the area dS^x is defined by the plane which is constructed by the differentials dy and dz and has its outward normal in the direction of the x-axis. Therefore, the following holds:

$$dydz = (y_\alpha d\alpha + y_\beta d\beta)(z_\alpha d\alpha + z_\beta d\beta) = y_\alpha z_\alpha d\alpha d\alpha + y_\alpha z_\beta d\alpha d\beta + y_\beta z_\alpha d\beta d\alpha + y_\beta z_\beta d\beta d\beta. \tag{A.9}$$

Here, the order of multiplication of the differentials determines the direction of the surface area, i.e. of its outward normal. The permutations of the differentials are defined as: $d\beta d\alpha = -d\alpha d\beta$, $d\alpha d\alpha = 0$, $d\beta d\beta = 0$. By obeying this order of multiplication, the area $dydz$ becomes:

$$dydz = (y_\alpha z_\beta - y_\beta z_\alpha) d\alpha d\beta = \begin{vmatrix} y_\alpha & y_\beta \\ z_\alpha & z_\beta \end{vmatrix} d\alpha d\beta = dS^x. \tag{A.10}$$

It can be shown that the outward normal to dS_x is indeed orientated in the x-direction with:

$$\boldsymbol{n^x} = \begin{pmatrix} 0 \\ dy \\ 0 \end{pmatrix} \times \begin{pmatrix} 0 \\ 0 \\ dz \end{pmatrix} = \begin{pmatrix} dydz \\ 0 \\ 0 \end{pmatrix} = \begin{pmatrix} dS^x \\ 0 \\ 0 \end{pmatrix}. \tag{A.11}$$

If the order of the cross-product is changed the following is obtained:

$$-\boldsymbol{n^x} = \begin{pmatrix} 0 \\ 0 \\ dz \end{pmatrix} \times \begin{pmatrix} 0 \\ dy \\ 0 \end{pmatrix} = \begin{pmatrix} -dydz \\ 0 \\ 0 \end{pmatrix} = \begin{pmatrix} -dS^x \\ 0 \\ 0 \end{pmatrix}, \tag{A.12}$$

confirming that the order of multiplication changes the direction of the surface area. By using the same approach for the other surface areas, $\boldsymbol{dS^x}$ can be written in a more compact form:

$$\boldsymbol{dS^x} = \begin{pmatrix} dydz \\ dzdx \\ dxdy \end{pmatrix}. \tag{A.13}$$

The scalar element of area dS_x is obtained by taking the norm of its normal vector $\boldsymbol{n_x}$:

$$dS_x = \|\boldsymbol{n_x}\| = \sqrt{(dS^x)^2 + (dS^y)^2 + (dS^z)^2}. \tag{A.14}$$

Through the definition of the unit outward normal to dS_x, it is possible to express the matrix element of area in terms of the scalar element of area:

$$\boldsymbol{dS^x} = dS_x \hat{\boldsymbol{n}}_{\boldsymbol{x}}, \tag{A.15}$$

where $\hat{\boldsymbol{n}}_{\boldsymbol{x}}$ denotes the normalised outward normal to dS_x:

$$\hat{\boldsymbol{n}}_{\boldsymbol{x}} = \begin{pmatrix} \hat{n}_x \\ \hat{n}_y \\ \hat{n}_z \end{pmatrix} = \frac{\boldsymbol{n_x}}{\|\boldsymbol{n_x}\|}. \tag{A.16}$$

The above can be further elaborated by substituting relation (A.7) and (A.14):

$$\hat{\boldsymbol{n}}_{\boldsymbol{x}} = \frac{1}{dS_x} \begin{pmatrix} dS^x \\ dS^y \\ dS^z \end{pmatrix}. \tag{A.17}$$

Figure A.1 displays the scalar element of area dS_x with its positive outward normal, as well the projections on the coordinate planes and their respective negative outward normals.

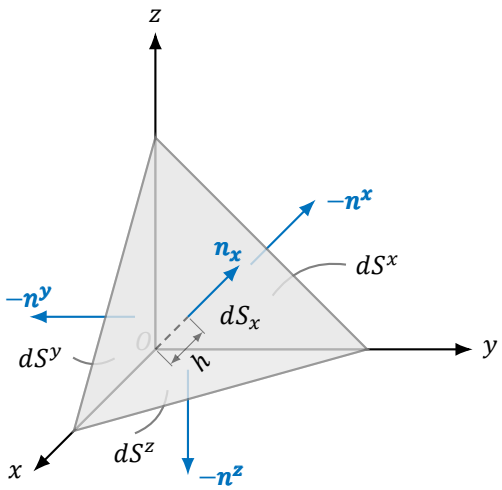

Figure A.1: Visualisation of the scalar element of area dS_x and its projections on the coordinate planes.

A.1.3. Element of volume

If now is assumed that the coordinates of point $P(x, y, z)$ are functions of three independent variables α, β and γ, three matrix elements of arc are obtained:

$$\boldsymbol{d_\alpha x} = \begin{pmatrix} x_\alpha d\alpha \\ y_\alpha d\alpha \\ z_\alpha d\alpha \end{pmatrix}; \quad \boldsymbol{d_\beta x} = \begin{pmatrix} x_\beta d\beta \\ y_\beta d\beta \\ z_\beta d\beta \end{pmatrix}; \quad \boldsymbol{d_\gamma x} = \begin{pmatrix} x_\gamma d\gamma \\ y_\gamma d\gamma \\ z_\gamma d\gamma \end{pmatrix}, \tag{A.18}$$

which can be used to define the column vectors of the 3 x 3 matrix:

$$\begin{pmatrix} x_\alpha d\alpha & x_\beta d\beta & x_\gamma d\gamma \\ y_\alpha d\alpha & y_\beta d\beta & y_\gamma d\gamma \\ z_\alpha d\alpha & z_\beta d\beta & z_\gamma d\gamma \end{pmatrix}. \tag{A.19}$$

The absolute value of the determinant of this matrix, granted that the matrix is non-singular, is defined as the element of volume in space dV_x. The cofactor expansion of the first column of this 3 x 3 matrix yields:

$$dV_x = x_\alpha d\alpha \begin{vmatrix} y_\beta d\beta & y_\gamma d\gamma \\ z_\beta d\beta & z_\gamma d\gamma \end{vmatrix} - y_\alpha d\alpha \begin{vmatrix} x_\beta d\beta & x_\gamma d\gamma \\ z_\beta d\beta & z_\gamma d\gamma \end{vmatrix} + z_\alpha d\alpha \begin{vmatrix} x_\beta d\beta & x_\gamma d\gamma \\ y_\beta d\beta & y_\gamma d\gamma \end{vmatrix}. \tag{A.20}$$

This expression can be elaborated to:

$$dV_x = \left(x_\alpha \begin{vmatrix} y_\beta & y_\gamma \\ z_\beta & z_\gamma \end{vmatrix} - y_\alpha \begin{vmatrix} x_\beta & x_\gamma \\ z_\beta & z_\gamma \end{vmatrix} + z_\alpha \begin{vmatrix} x_\beta & x_\gamma \\ y_\beta & y_\gamma \end{vmatrix} \right) d\alpha d\beta d\gamma, \tag{A.21}$$

in which the cofactor expansion of the first column of the 3 x 3 matrix,

$$\boldsymbol{J_x}(\alpha, \beta, \gamma) = \begin{pmatrix} x_\alpha & x_\beta & x_\gamma \\ y_\alpha & y_\beta & y_\gamma \\ z_\alpha & z_\beta & z_\gamma \end{pmatrix}, \tag{A.22}$$

can be recognised. This 3 x 3 matrix is defined as a Jacobian matrix, containing the derivatives of the coordinates (x, y, z) with respect to the variables α, β and γ. Therefore, the following holds:

$$dV_x = \det\big(\boldsymbol{J_x}(\alpha, \beta, \gamma)\big) d\alpha d\beta d\gamma. \tag{A.23}$$

The same expression can be found by making use of the definitions of the differentials:

$$dxdydz = (x_\alpha d\alpha + x_\beta d\beta + x_\gamma d\gamma)(y_\alpha d\alpha + y_\beta d\beta + y_\gamma d\gamma)(z_\alpha d\alpha + z_\beta d\beta + z_\gamma d\gamma). \tag{A.24}$$

The permutations of the differentials $d\alpha$, $d\beta$ and $d\gamma$ are defined as:

$$\begin{aligned} d\gamma d\alpha d\beta = d\beta d\gamma d\alpha = d\alpha d\beta d\gamma = +d\alpha d\beta d\gamma \\ d\gamma d\beta d\alpha = d\beta d\alpha d\gamma = d\alpha d\gamma d\beta = -d\alpha d\beta d\gamma, \end{aligned} \tag{A.25}$$

whereas all the other combinations of the differentials are zero. By respecting the order of multiplication of the differentials in relation (A.24), expression (A.21) is obtained:

$$dxdydz = \left(x_\alpha \begin{vmatrix} y_\beta & y_\gamma \\ z_\beta & z_\gamma \end{vmatrix} - y_\alpha \begin{vmatrix} x_\beta & x_\gamma \\ z_\beta & z_\gamma \end{vmatrix} + z_\alpha \begin{vmatrix} x_\beta & x_\gamma \\ y_\beta & y_\gamma \end{vmatrix} \right) d\alpha d\beta d\gamma. \tag{A.26}$$

Therefore, the element of volume dV_x can be rewritten in the short notation:

$$dV_x = dxdydz. \tag{A.27}$$

A.2. Initial and final configurations

In the definition of the matrix elements of arc, $\boldsymbol{d_\alpha x}$, $\boldsymbol{d_\beta x}$ and $\boldsymbol{d_\gamma x}$, the coordinates (x, y, z) are assumed to be direct functions of variables α, β and γ. However, it is more common that these coordinates are functions of another set of coordinates (a, b, c), which in turn are functions of α, β and γ. This is the case for a point P_a with initial coordinates (a, b, c) which is transformed to point P_x with final coordinates (x, y, z) due to a displacement (u, v, w):

$$\boldsymbol{x} = \begin{pmatrix} x \\ y \\ z \end{pmatrix} = \begin{pmatrix} a \\ b \\ c \end{pmatrix} + \begin{pmatrix} u \\ v \\ w \end{pmatrix}. \tag{A.28}$$

Now a distinction can be made between the initial and final configuration of the previously established elements (A.3), (A.14) and (A.27). By using the definition of the differentials, the initial and final configurations can be expressed into each other.

A.2.1. Matrix element of arc

A variable point $P_a(a, b, c)$ traces a curve C_a as the parameter α varies. After a displacement, $P_a(a, b, c)$ and C_a are transformed to $P_x(x, y, z)$ and C_x, respectively. The final matrix element of arc is then defined as:

$$\boldsymbol{dx} = \begin{pmatrix} dx \\ dy \\ dz \end{pmatrix} = \begin{pmatrix} x_a da + x_b db + x_c dc \\ y_a da + y_b db + y_c dc \\ z_a da + z_b db + z_c dc \end{pmatrix}. \tag{A.29}$$

The above can be expressed in terms of the initial element of arc with:

$$\boldsymbol{dx} = \boldsymbol{J_x}(a, b, c)\ \boldsymbol{da}, \tag{A.30}$$

where $\boldsymbol{J_x}(a, b, c)$ denotes the Jacobian matrix containing the partial derivatives of the final coordinates with respect to the initial coordinates,

$$\boldsymbol{J_x}(a, b, c) \equiv \begin{pmatrix} x_a & x_b & x_c \\ y_a & y_b & y_c \\ z_a & z_b & z_c \end{pmatrix}, \tag{2.6}$$

and $\boldsymbol{da}$ – the initial matrix element of arc. Similarly, the initial matrix element of arc can be expressed in terms of the final element of arc:

$$\boldsymbol{da} = \boldsymbol{J_a}(x, y, z)\ \boldsymbol{dx}, \tag{A.31}$$

where $\boldsymbol{J_a}(x, y, z)$ denotes the Jacobian matrix containing the partial derivatives of the initial coordinates with respect to the final coordinates,

$$\boldsymbol{J_a}(x, y, z) \equiv \begin{pmatrix} a_x & a_y & a_z \\ b_x & b_y & b_z \\ c_x & c_y & c_z \end{pmatrix}. \tag{2.7}$$

Therefore, the initial and final scalar element of arc can be written as:

$$\begin{aligned} ds_a &= \sqrt{(\boldsymbol{da})^T(\boldsymbol{da})} = \sqrt{(\boldsymbol{dx})^T \boldsymbol{J_a}(x, y, z)^T \boldsymbol{J_a}(x, y, z)\ (\boldsymbol{dx})} \\ ds_x &= \sqrt{(\boldsymbol{dx})^T(\boldsymbol{dx})} = \sqrt{(\boldsymbol{da})^T \boldsymbol{J_x}(a, b, c)^T \boldsymbol{J_x}(a, b, c)\ (\boldsymbol{da})}, \end{aligned} \tag{A.32}$$

respectively.

A.2.2. Matrix element of area

The initial matrix element of area $\boldsymbol{dS^a}$, defined by the the initial matrix elements of arc $\boldsymbol{d_\alpha a}$ and $\boldsymbol{d_\beta a}$, is described as:

$$\boldsymbol{dS^a} = \begin{pmatrix} dS^a \\ dS^b \\ dS^c \end{pmatrix} = \begin{pmatrix} \begin{vmatrix} b_\alpha & b_\beta \\ c_\alpha & c_\beta \end{vmatrix} d\alpha d\beta \\ \begin{vmatrix} c_\alpha & c_\beta \\ a_\alpha & a_\beta \end{vmatrix} d\alpha d\beta \\ \begin{vmatrix} a_\alpha & a_\beta \\ b_\alpha & b_\beta \end{vmatrix} d\alpha d\beta \end{pmatrix} = \begin{pmatrix} dbdc \\ dcda \\ dadb \end{pmatrix}, \tag{A.33}$$

whereas the final matrix element of area $\boldsymbol{dS^x}$, defined by the the final matrix elements of arc $\boldsymbol{d_\alpha x}$ and $\boldsymbol{d_\beta x}$, is described as:

$$\boldsymbol{dS^x} = \begin{pmatrix} dS^x \\ dS^y \\ dS^z \end{pmatrix} = \begin{pmatrix} \begin{vmatrix} y_\alpha & y_\beta \\ z_\alpha & z_\beta \end{vmatrix} d\alpha d\beta \\ \begin{vmatrix} z_\alpha & z_\beta \\ x_\alpha & x_\beta \end{vmatrix} d\alpha d\beta \\ \begin{vmatrix} x_\alpha & x_\beta \\ y_\alpha & y_\beta \end{vmatrix} d\alpha d\beta \end{pmatrix} = \begin{pmatrix} dydz \\ dzdx \\ dxdy \end{pmatrix}. \tag{A.34}$$

The 2 x 2 determinants of these two expressions can be related to each other through the chain rule of differentiation: $y_\alpha = y_a a_\alpha + y_b b_\alpha + y_c c_\alpha$, $y_\beta = y_a a_\beta + y_b b_\beta + y_c c_\beta$, etc. Therefore, the following holds:

$$\begin{vmatrix} y_\alpha & y_\beta \\ z_\alpha & z_\beta \end{vmatrix} = (y_a a_\alpha + y_b b_\alpha + y_c c_\alpha)(z_a a_\beta + z_b b_\beta + z_c c_\beta) - (z_a a_\alpha + z_b b_\alpha + z_c c_\alpha)(y_a a_\beta + y_b b_\beta + y_c c_\beta), \tag{A.35}$$

which, upon elaborating and rearranging, can be written as:

$$\begin{vmatrix} y_\alpha & y_\beta \\ z_\alpha & z_\beta \end{vmatrix} = \begin{vmatrix} y_b & y_c \\ z_b & z_c \end{vmatrix} \begin{vmatrix} b_\alpha & b_\beta \\ c_\alpha & c_\beta \end{vmatrix} + \begin{vmatrix} y_c & y_a \\ z_c & z_a \end{vmatrix} \begin{vmatrix} c_\alpha & c_\beta \\ a_\alpha & a_\beta \end{vmatrix} + \begin{vmatrix} y_a & y_b \\ z_a & z_b \end{vmatrix} \begin{vmatrix} a_\alpha & a_\beta \\ b_\alpha & b_\beta \end{vmatrix}. \tag{A.36}$$

By using this chain rule of differentiation for determinants, the final matrix element of area can be rewritten to:

$$\boldsymbol{dS^x} = \begin{pmatrix} dS^x \\ dS^y \\ dS^z \end{pmatrix} = \begin{pmatrix} \begin{vmatrix} y_b & y_c \\ z_b & z_c \end{vmatrix} \begin{vmatrix} b_\alpha & b_\beta \\ c_\alpha & c_\beta \end{vmatrix} + \begin{vmatrix} y_c & y_a \\ z_c & z_a \end{vmatrix} \begin{vmatrix} c_\alpha & c_\beta \\ a_\alpha & a_\beta \end{vmatrix} + \begin{vmatrix} y_a & y_b \\ z_a & z_b \end{vmatrix} \begin{vmatrix} a_\alpha & a_\beta \\ b_\alpha & b_\beta \end{vmatrix} \\ \begin{vmatrix} z_b & z_c \\ x_b & x_c \end{vmatrix} \begin{vmatrix} b_\alpha & b_\beta \\ c_\alpha & c_\beta \end{vmatrix} + \begin{vmatrix} z_c & z_a \\ x_c & x_a \end{vmatrix} \begin{vmatrix} c_\alpha & c_\beta \\ a_\alpha & a_\beta \end{vmatrix} + \begin{vmatrix} z_a & z_b \\ x_a & x_b \end{vmatrix} \begin{vmatrix} a_\alpha & a_\beta \\ b_\alpha & b_\beta \end{vmatrix} \\ \begin{vmatrix} x_b & x_c \\ y_b & y_c \end{vmatrix} \begin{vmatrix} b_\alpha & b_\beta \\ c_\alpha & c_\beta \end{vmatrix} + \begin{vmatrix} x_c & x_a \\ y_c & y_a \end{vmatrix} \begin{vmatrix} c_\alpha & c_\beta \\ a_\alpha & a_\beta \end{vmatrix} + \begin{vmatrix} x_a & x_b \\ y_a & y_b \end{vmatrix} \begin{vmatrix} a_\alpha & a_\beta \\ b_\alpha & b_\beta \end{vmatrix} \end{pmatrix} d\alpha d\beta, \tag{A.37}$$

which, upon substitution of relation (A.33), can be elaborated to:

$$\boldsymbol{dS^x} = \begin{pmatrix} dS^x \\ dS^y \\ dS^z \end{pmatrix} = \begin{pmatrix} \begin{vmatrix} y_b & y_c \\ z_b & z_c \end{vmatrix} dS^a + \begin{vmatrix} y_c & y_a \\ z_c & z_a \end{vmatrix} dS^b + \begin{vmatrix} y_a & y_b \\ z_a & z_b \end{vmatrix} dS^c \\ \begin{vmatrix} z_b & z_c \\ x_b & x_c \end{vmatrix} dS^a + \begin{vmatrix} z_c & z_a \\ x_c & x_a \end{vmatrix} dS^b + \begin{vmatrix} z_a & z_b \\ x_a & x_b \end{vmatrix} dS^c \\ \begin{vmatrix} x_b & x_c \\ y_b & y_c \end{vmatrix} dS^a + \begin{vmatrix} x_c & x_a \\ y_c & y_a \end{vmatrix} dS^b + \begin{vmatrix} x_a & x_b \\ y_a & y_b \end{vmatrix} dS^c \end{pmatrix}. \tag{A.38}$$

From this it can be found that the final matrix element of area $\boldsymbol{dS^x}$ can be expressed in terms of the initial matrix element of area $\boldsymbol{dS^a}$ with:

$$\boldsymbol{dS^x} = \left(\operatorname{co} \boldsymbol{J_x}(a,b,c)\right) \boldsymbol{dS^a}, \tag{A.39}$$

where $\operatorname{co} \boldsymbol{J_x}(a,b,c)$ denotes the 3 x 3 cofactor matrix of the Jacobian matrix $\boldsymbol{J_x}(a,b,c)$:

$$\operatorname{co} \boldsymbol{J_x}(a,b,c) = \begin{pmatrix} \begin{vmatrix} y_b & y_c \\ z_b & z_c \end{vmatrix} & \begin{vmatrix} z_a & z_c \\ y_a & y_c \end{vmatrix} & \begin{vmatrix} y_a & y_b \\ z_a & z_b \end{vmatrix} \\ \begin{vmatrix} z_b & z_c \\ x_b & x_c \end{vmatrix} & \begin{vmatrix} x_a & x_c \\ z_a & z_c \end{vmatrix} & \begin{vmatrix} z_a & z_b \\ x_a & x_b \end{vmatrix} \\ \begin{vmatrix} x_b & x_c \\ y_b & y_c \end{vmatrix} & \begin{vmatrix} y_a & y_c \\ x_a & x_c \end{vmatrix} & \begin{vmatrix} x_a & x_b \\ y_a & y_b \end{vmatrix} \end{pmatrix}. \tag{A.40}$$

Through the definition of the inverse of a non-singular matrix $\boldsymbol{A}$,

$$\boldsymbol{A}^{-1} = \frac{1}{\det(\boldsymbol{A})} \operatorname{co} \boldsymbol{A}^T, \tag{A.41}$$

the cofactor matrix of its transpose is defined as:

$$\operatorname{co} \boldsymbol{A}^T = \det(\boldsymbol{A}) \boldsymbol{A}^{-1}. \tag{A.42}$$

By using this definition and $\det \boldsymbol{A}^T = \det \boldsymbol{A}$ in relation (A.39), Nanson's formula is obtained:

$$\boldsymbol{dS^x} = \det\left(\boldsymbol{J_x}(a,b,c)\right) \boldsymbol{J_x}(a,b,c)^{-T} \boldsymbol{dS^a}. \tag{A.43}$$

A.2.3. Element of volume

The initial element of volume dV_a is defined as:

$$dV_a = \det\left(\boldsymbol{J_a}(\alpha,\beta,\gamma)\right) d\alpha d\beta d\gamma = da db dc, \tag{A.44}$$

whereas the final element of volume dV_x is defined as:

$$dV_x = \det\left(\boldsymbol{J_x}(\alpha,\beta,\gamma)\right) d\alpha d\beta d\gamma = dx dy dz. \tag{A.45}$$

The final element of volume can be expressed in terms of the initial element of volume by making use of the chain rule of differentiation for determinants (A.36):

$$\begin{aligned} dV_x = \Bigg[& x_\alpha \left(\begin{vmatrix} y_b & y_c \\ z_b & z_c \end{vmatrix} \begin{vmatrix} b_\beta & b_\gamma \\ c_\beta & c_\gamma \end{vmatrix} + \begin{vmatrix} y_c & y_a \\ z_c & z_a \end{vmatrix} \begin{vmatrix} c_\beta & c_\gamma \\ a_\beta & a_\gamma \end{vmatrix} + \begin{vmatrix} y_a & y_b \\ z_a & z_b \end{vmatrix} \begin{vmatrix} a_\beta & a_\gamma \\ b_\beta & b_\gamma \end{vmatrix} \right) \\ & - y_\alpha \left(\begin{vmatrix} x_b & x_c \\ z_b & z_c \end{vmatrix} \begin{vmatrix} b_\beta & b_\gamma \\ c_\beta & c_\gamma \end{vmatrix} + \begin{vmatrix} x_c & x_a \\ z_c & z_a \end{vmatrix} \begin{vmatrix} c_\beta & c_\gamma \\ a_\beta & a_\gamma \end{vmatrix} + \begin{vmatrix} x_a & x_b \\ z_a & z_b \end{vmatrix} \begin{vmatrix} a_\beta & a_\gamma \\ b_\beta & b_\gamma \end{vmatrix} \right) \\ & + z_\alpha \left(\begin{vmatrix} x_b & x_c \\ y_b & y_c \end{vmatrix} \begin{vmatrix} b_\beta & b_\gamma \\ c_\beta & c_\gamma \end{vmatrix} + \begin{vmatrix} x_c & x_a \\ y_c & y_a \end{vmatrix} \begin{vmatrix} c_\beta & c_\gamma \\ a_\beta & a_\gamma \end{vmatrix} + \begin{vmatrix} x_a & x_b \\ y_a & y_b \end{vmatrix} \begin{vmatrix} a_\beta & a_\gamma \\ b_\beta & b_\gamma \end{vmatrix} \right) \Bigg] d\alpha d\beta d\gamma. \end{aligned} \tag{A.46}$$

After applying the chain rule of differentiation: $x_\alpha = x_a a_\alpha + x_b b_\alpha + x_c c_\alpha$, $y_\alpha = y_a a_\alpha + y_b b_\alpha + y_c c_\alpha$, etc. and elaborating further, the following terms remain:

$$\begin{aligned} dV_x = \Bigg[& \left(x_a \begin{vmatrix} y_b & y_c \\ z_b & z_c \end{vmatrix} - y_a \begin{vmatrix} x_b & x_c \\ z_b & z_c \end{vmatrix} + z_a \begin{vmatrix} x_b & x_c \\ y_b & y_c \end{vmatrix} \right) a_\alpha \begin{vmatrix} b_\beta & b_\gamma \\ c_\beta & c_\gamma \end{vmatrix} \\ & - \left(- x_b \begin{vmatrix} z_c & z_a \\ y_c & y_a \end{vmatrix} + y_b \begin{vmatrix} z_c & z_a \\ x_c & x_a \end{vmatrix} - z_b \begin{vmatrix} y_c & y_a \\ x_c & x_a \end{vmatrix} \right) b_\alpha \begin{vmatrix} a_\beta & a_\gamma \\ c_\beta & c_\gamma \end{vmatrix} \\ & + \left(x_c \begin{vmatrix} y_a & y_b \\ z_a & z_b \end{vmatrix} - y_c \begin{vmatrix} x_a & x_b \\ z_a & z_b \end{vmatrix} + z_c \begin{vmatrix} x_a & x_b \\ y_a & y_b \end{vmatrix} \right) c_\alpha \begin{vmatrix} a_\beta & a_\gamma \\ b_\beta & b_\gamma \end{vmatrix} \Bigg] d\alpha d\beta d\gamma, \end{aligned} \tag{A.47}$$

from which the cofactor expansion of the first, second and third column of the Jacobian matrix $\boldsymbol{J_x}(a,b,c)$ can be recognised. Therefore, the above can be simplified to:

$$dV_x = \det\big(\boldsymbol{J_x}(a,b,c)\big)\left(a_\alpha \begin{vmatrix} b_\beta & b_\gamma \\ c_\beta & c_\gamma \end{vmatrix} - b_\alpha \begin{vmatrix} a_\beta & a_\gamma \\ c_\beta & c_\gamma \end{vmatrix} + c_\alpha \begin{vmatrix} a_\beta & a_\gamma \\ b_\beta & b_\gamma \end{vmatrix}\right) d\alpha d\beta d\gamma, \tag{A.48}$$

from which the cofactor expansion of the first column of the Jacobian matrix $\boldsymbol{J_a}(\alpha,\beta,\gamma)$ can be identified:

$$dV_x = \det\big(\boldsymbol{J_x}(a,b,c)\big)\,\det\big(\boldsymbol{J_a}(\alpha,\beta,\gamma)\big)\,d\alpha d\beta d\gamma. \tag{A.49}$$

Upon substitution of relation (initial element of volume), the final element of volume can be expressed in terms of the initial element of volume:

$$dV_x = \det\big(\boldsymbol{J_x}(a,b,c)\big)\,dV_a. \tag{A.50}$$

According to the law of conservation of mass, the mass dm must remain the same after the deformation has occurred:

$$\rho_a dV_a = dm = \rho_x dV_x, \tag{A.51}$$

where ρ_a and ρ_x denote the initial and final mass densities, respectively. After substituting relation (A.50), the determinant of the Jacobian matrix $\boldsymbol{J_x}(a,b,c)$ can be expressed as a ratio of mass densities:

$$\det\big(\boldsymbol{J_x}(a,b,c)\big) = \left(\frac{\rho_a}{\rho_x}\right). \tag{A.52}$$

A.3. Specification of the strain

A deformable three-dimensional medium is considered. Particles in the initial or unstrained state of this medium are denoted by the coordinates (a,b,c). After the medium has been subjected to a deformation (u,v,w), the particles are set in their final or strained state, denoted by the coordinates (x,y,z).

A.3.1. Squared scalar element of arc

A collection of particles of a deformable medium is assumed to be initially situated on the curve C_a. After a deformation these particles lie on the final curve C_x. Figure A.2 displays the relative displacement between the particles after the deformation has occurred.

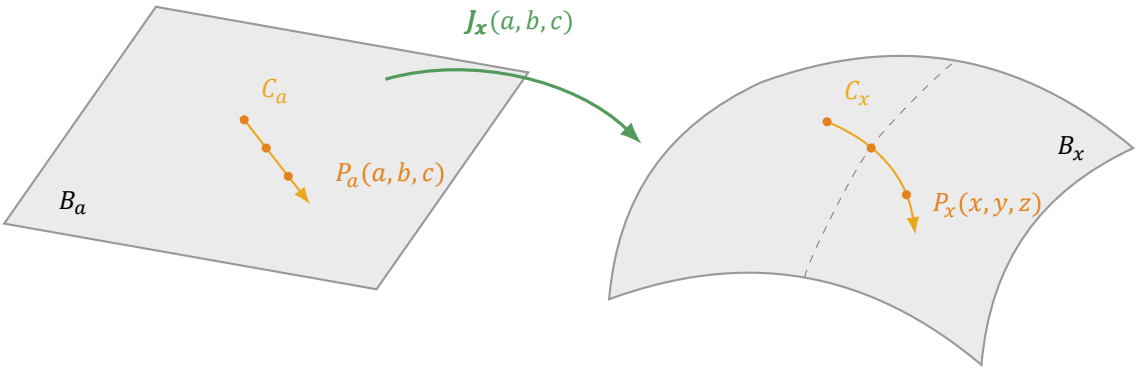

Figure A.2: Visualisation of the relative displacement between the particles within the medium during a deformation.

The initial and final squared scalar elements of arc of these particles within the deformable medium are then defined as:

$$\begin{aligned}(ds_a)^2 &= (\boldsymbol{da})^T(\boldsymbol{da}) = (\boldsymbol{dx})^T\boldsymbol{J_a}(x,y,z)^T\boldsymbol{J_a}(x,y,z)\ (\boldsymbol{dx}) \\ (ds_x)^2 &= (\boldsymbol{dx})^T(\boldsymbol{dx}) = (\boldsymbol{da})^T\boldsymbol{J_x}(a,b,c)^T\boldsymbol{J_x}(a,b,c)\ (\boldsymbol{da}),\end{aligned} \tag{A.53}$$

respectively. Their difference can be expressed in either of the two matrix elements of arc. For the initial matrix element of arc the difference reads:

$$\begin{aligned}(ds_x)^2 - (ds_a)^2 &= (\boldsymbol{dx})^T(\boldsymbol{dx}) - (\boldsymbol{da})^T(\boldsymbol{da}) \\ &= (\boldsymbol{da})^T\boldsymbol{J_x}(a,b,c)^T\boldsymbol{J_x}(a,b,c)\ (\boldsymbol{da}) - (\boldsymbol{da})^T(\boldsymbol{da}) \\ &= (\boldsymbol{da})^T\Big(\boldsymbol{J_x}(a,b,c)^T\boldsymbol{J_x}(a,b,c) - \boldsymbol{E_3}\Big)(\boldsymbol{da}) \\ &= (\boldsymbol{da})^T 2\boldsymbol{\eta}\ (\boldsymbol{da}).\end{aligned} \tag{A.54}$$

Upon writing the squared scalar elements of arc in terms of the final matrix element of arc, two equivalent expressions are obtained:

$$(ds_x)^2 - (ds_a)^2 = (\boldsymbol{da})^T 2\boldsymbol{\eta}\ (\boldsymbol{da}) = (\boldsymbol{dx})^T 2\boldsymbol{\epsilon}\ (\boldsymbol{dx}), \tag{2.10}$$

where $\boldsymbol{\eta}$ and $\boldsymbol{\epsilon}$ denote the Lagrangian and Eulerian description of the strain,

$$\begin{aligned}\boldsymbol{\eta} &\equiv \tfrac{1}{2}\Big(\boldsymbol{J_x}(a,b,c)^T\boldsymbol{J_x}(a,b,c) - \boldsymbol{E_3}\Big) \\ \boldsymbol{\epsilon} &\equiv \tfrac{1}{2}\Big(\boldsymbol{E_3} - \boldsymbol{J_a}(x,y,z)^T\boldsymbol{J_a}(x,y,z)\Big),\end{aligned} \tag{2.11}$$

respectively, and $\boldsymbol{E_3}$ – the 3 x 3 identity matrix. These expressions describe the strain of a medium after being displaced from its initial to its final coordinates. Note that if the initial and final coordinates are equal, the Jacobian matrices reduce to identity matrices, resulting in zero strain. From definition (2.10) it follows that a zero difference of the squared elements of arc also results in zero strain, which is the case for rigid displacements.

A.3.2. Lagrangian and Eulerian strain description

The Lagrangian strain components η_{ij} are expressed in the initial coordinates (a,b,c) and describe the strain field over the undeformed medium, i.e. before the deformation. The Eulerian strain components ϵ_{ij} are expressed in the final coordinates (x,y,z) and describe the strain field over the deformed medium, i.e. after the deformation. Both sets of strain components can be assembled in the following matrices:

$$\boldsymbol{\eta}(a,b,c) = \begin{pmatrix}\eta_{aa} & \eta_{ab} & \eta_{ac} \\ \eta_{ba} & \eta_{bb} & \eta_{bc} \\ \eta_{ca} & \eta_{cb} & \eta_{cc}\end{pmatrix}; \quad \boldsymbol{\epsilon}(x,y,z) = \begin{pmatrix}\epsilon_{xx} & \epsilon_{xy} & \epsilon_{xz} \\ \epsilon_{yx} & \epsilon_{yy} & \epsilon_{yz} \\ \epsilon_{zx} & \epsilon_{zy} & \epsilon_{zz}\end{pmatrix}, \tag{2.12}$$

where the quantities η_{ij} and ϵ_{ij} can be derived by introducing the displacement vector,

$$\boldsymbol{u} = \begin{pmatrix}u \\ v \\ w\end{pmatrix} = \begin{pmatrix}x-a \\ y-b \\ z-c\end{pmatrix}, \tag{2.1}$$

or more compact:

$$\boldsymbol{u} = \boldsymbol{x} - \boldsymbol{a}. \tag{2.2}$$

For a Cartesian coordinate system, the Jacobian matrix $\boldsymbol{J_u}(a,b,c)$ containing the derivatives of the displacements with respect to the initial coordinates is defined as:

$$\boldsymbol{J_u}(a,b,c) = \begin{pmatrix}u_a & u_b & u_c \\ v_a & v_b & v_c \\ w_a & w_b & w_c\end{pmatrix} = \begin{pmatrix}x_a - 1 & x_b & x_c \\ y_a & y_b - 1 & y_c \\ z_a & z_b & z_c - 1\end{pmatrix}. \tag{A.55}$$

This definition can be used to rewrite the Jacobian matrix $\boldsymbol{J_x}(a,b,c)$ to:

$$\boldsymbol{J_x}(a,b,c) = \boldsymbol{J_u}(a,b,c) + \boldsymbol{E_3}. \tag{A.56}$$

The left-multiplication with its transpose then becomes:

$$\begin{aligned}\boldsymbol{J_x}(a,b,c)^T\boldsymbol{J_x}(a,b,c) &= \big(\boldsymbol{J_u}(a,b,c) + \boldsymbol{E_3}\big)^T\big(\boldsymbol{J_u}(a,b,c) + \boldsymbol{E_3}\big) \\ &= \boldsymbol{J_u}(a,b,c) + \boldsymbol{J_u}(a,b,c)^T + \boldsymbol{E_3} + \boldsymbol{J_u}(a,b,c)^T\boldsymbol{J_u}(a,b,c),\end{aligned} \tag{A.57}$$

which can then be substituted in $\boldsymbol{\eta}$ from expression (2.11):

$$\begin{aligned}\boldsymbol{\eta} &= \tfrac{1}{2}\big(\boldsymbol{J_u}(a,b,c) + \boldsymbol{J_u}(a,b,c)^T + \boldsymbol{E_3} + \boldsymbol{J_u}(a,b,c)^T\boldsymbol{J_u}(a,b,c) - \boldsymbol{E_3}\big)\\ &= \tfrac{1}{2}\big(\boldsymbol{J_u}(a,b,c) + \boldsymbol{J_u}(a,b,c)^T\big) + \tfrac{1}{2}\,\boldsymbol{J_u}(a,b,c)^T\boldsymbol{J_u}(a,b,c).\end{aligned} \tag{A.58}$$

With a similar approach, $\boldsymbol{\epsilon}$ can be rewritten to:

$$\boldsymbol{\epsilon} = \tfrac{1}{2}\big(\boldsymbol{J_u}(x,y,z) + \boldsymbol{J_u}(x,y,z)^T\big) - \tfrac{1}{2}\,\boldsymbol{J_u}(x,y,z)^T\boldsymbol{J_u}(x,y,z), \tag{A.59}$$

where $\boldsymbol{J_u}(x,y,z)$ is the Jacobian matrix containing the derivatives of the displacements with respect to the final coordinates:

$$\boldsymbol{J_u}(x,y,z) = \begin{pmatrix} u_x & u_y & u_z \\ v_x & v_y & v_z \\ w_x & w_y & w_z \end{pmatrix} = \begin{pmatrix} 1-x_a & x_b & x_c \\ y_a & 1-y_b & y_c \\ z_a & z_b & 1-z_c \end{pmatrix}. \tag{A.60}$$

The Lagrangian strain components can be derived by substituting relation (A.55) in expression (A.58). The terms η_{aa}, η_{bb} and η_{cc} are defined as uniaxial strains and are of the form:

$$\eta_{aa} = \frac{\partial u}{\partial a} + \frac{1}{2}\left[\left(\frac{\partial u}{\partial a}\right)^2 + \left(\frac{\partial v}{\partial a}\right)^2 + \left(\frac{\partial w}{\partial a}\right)^2\right], \tag{A.61}$$

whereas the off-diagonal terms, defined as shear strains, are of the form:

$$\begin{aligned}\eta_{ab} &= \frac{1}{2}\left(\frac{\partial u}{\partial b} + \frac{\partial v}{\partial a}\right) + \frac{1}{2}\left(\frac{\partial u}{\partial a}\frac{\partial u}{\partial b} + \frac{\partial v}{\partial a}\frac{\partial v}{\partial b} + \frac{\partial w}{\partial a}\frac{\partial w}{\partial b}\right)\\ \eta_{ba} &= \frac{1}{2}\left(\frac{\partial v}{\partial a} + \frac{\partial u}{\partial b}\right) + \frac{1}{2}\left(\frac{\partial u}{\partial b}\frac{\partial u}{\partial a} + \frac{\partial v}{\partial b}\frac{\partial v}{\partial a} + \frac{\partial w}{\partial b}\frac{\partial w}{\partial a}\right),\end{aligned} \tag{A.62}$$

proving that $\boldsymbol{\eta}(a,b,c)$ is a symmetric matrix. The same holds for the Eulerian strain components, which are derived by substituting relation (A.60) in expression (A.59). The uniaxial strains and shear strains of the Eulerian strain description are of the form:

$$\begin{aligned}\epsilon_{xx} &= \frac{\partial u}{\partial x} - \frac{1}{2}\left[\left(\frac{\partial u}{\partial x}\right)^2 + \left(\frac{\partial v}{\partial x}\right)^2 + \left(\frac{\partial w}{\partial x}\right)^2\right]\\ \epsilon_{xy} &= \frac{1}{2}\left(\frac{\partial u}{\partial y} + \frac{\partial v}{\partial x}\right) - \frac{1}{2}\left(\frac{\partial u}{\partial x}\frac{\partial u}{\partial y} + \frac{\partial v}{\partial x}\frac{\partial v}{\partial y} + \frac{\partial w}{\partial x}\frac{\partial w}{\partial y}\right),\end{aligned} \tag{A.63}$$

respectively. According to the theory of infinitesimal deformations, the higher order terms in the displacements can be neglected. From the expressions above it can be observed that for this theory the Lagrangian strain components and Eulerian strain components are equal to each other.

A.3.3. Strain invariants

The strain invariants can be derived by determining the eigenvalues of the strain matrix $\boldsymbol{\eta}$. This can be done by setting the determinant of the matrix $\boldsymbol{\eta} - \lambda\boldsymbol{E_3}$ to zero:

$$\det\big(\boldsymbol{\eta} - \lambda\boldsymbol{E_3}\big) = \begin{vmatrix} \eta_{aa}-\lambda & \eta_{ab} & \eta_{ac} \\ \eta_{ba} & \eta_{bb}-\lambda & \eta_{bc} \\ \eta_{ca} & \eta_{cb} & \eta_{cc}-\lambda \end{vmatrix} = 0. \tag{A.64}$$

By applying the cofactor expansion of the first row of the matrix, the determinant becomes:

$$\det\big(\boldsymbol{\eta} - \lambda\boldsymbol{E_3}\big) = (\eta_{aa}-\lambda)\begin{vmatrix} \eta_{bb}-\lambda & \eta_{bc} \\ \eta_{cb} & \eta_{cc}-\lambda \end{vmatrix} - \eta_{ab}\begin{vmatrix} \eta_{ba} & \eta_{bc} \\ \eta_{ca} & \eta_{cc}-\lambda \end{vmatrix} + \eta_{ac}\begin{vmatrix} \eta_{ba} & \eta_{bb}-\lambda \\ \eta_{ca} & \eta_{cb} \end{vmatrix}, \tag{A.65}$$

which, after writing out, can be formulated as a polynomial of λ:

$$\det\big(\boldsymbol{\eta} - \lambda\boldsymbol{E_3}\big) = -\lambda^3 + I_1\lambda^2 - I_2\lambda + I_3. \tag{A.66}$$

The first strain invariant I_1 is equal to the trace of the strain matrix $\boldsymbol{\eta}$:

$$I_1 = \mathrm{Tr}(\boldsymbol{\eta}) = \eta_{aa} + \eta_{bb} + \eta_{cc}. \tag{A.67}$$

The second strain invariant I_2 consists of the following terms:

$$I_2 = (\eta_{bb}\eta_{cc} - \eta_{bc}\eta_{cb}) + (\eta_{aa}\eta_{cc} - \eta_{ac}\eta_{ca}) + (\eta_{aa}\eta_{bb} - \eta_{ab}\eta_{ba}), \tag{A.68}$$

which can be recognised as a summation of 2 x 2 determinants. By using the definition of the cofactor matrix of the strain matrix $\boldsymbol{\eta}$,

$$\mathrm{co}\,\boldsymbol{\eta} = \begin{pmatrix} \begin{vmatrix} \eta_{bb} & \eta_{bc} \\ \eta_{cb} & \eta_{cc} \end{vmatrix} & \begin{vmatrix} \eta_{ca} & \eta_{cc} \\ \eta_{ba} & \eta_{bc} \end{vmatrix} & \begin{vmatrix} \eta_{ba} & \eta_{bb} \\ \eta_{ca} & \eta_{cb} \end{vmatrix} \\ \begin{vmatrix} \eta_{cb} & \eta_{cc} \\ \eta_{ab} & \eta_{ac} \end{vmatrix} & \begin{vmatrix} \eta_{aa} & \eta_{ac} \\ \eta_{ca} & \eta_{cc} \end{vmatrix} & \begin{vmatrix} \eta_{ca} & \eta_{cb} \\ \eta_{aa} & \eta_{ab} \end{vmatrix} \\ \begin{vmatrix} \eta_{ab} & \eta_{ac} \\ \eta_{bb} & \eta_{bc} \end{vmatrix} & \begin{vmatrix} \eta_{ba} & \eta_{bc} \\ \eta_{aa} & \eta_{ac} \end{vmatrix} & \begin{vmatrix} \eta_{aa} & \eta_{ab} \\ \eta_{ba} & \eta_{bb} \end{vmatrix} \end{pmatrix}, \tag{A.69}$$

it is clear that the second strain invariant I_2 is equal to the trace of the cofactor matrix $\mathrm{co}\,\boldsymbol{\eta}$:

$$I_2 = \mathrm{Tr}(\mathrm{co}\,\boldsymbol{\eta}) = \begin{vmatrix} \eta_{bb} & \eta_{bc} \\ \eta_{cb} & \eta_{cc} \end{vmatrix} + \begin{vmatrix} \eta_{aa} & \eta_{ac} \\ \eta_{ca} & \eta_{cc} \end{vmatrix} + \begin{vmatrix} \eta_{aa} & \eta_{ab} \\ \eta_{ba} & \eta_{bb} \end{vmatrix}. \tag{A.70}$$

The third strain invariant I_3 contains the terms:

$$I_3 = \eta_{aa}\eta_{bb}\eta_{cc} - \eta_{aa}\eta_{cb}\eta_{bc} - \eta_{ab}\eta_{ba}\eta_{cc} + \eta_{ab}\eta_{ca}\eta_{bc} + \eta_{ac}\eta_{ba}\eta_{cb} - \eta_{ac}\eta_{ca}\eta_{bb}. \tag{A.71}$$

Factorising the common terms results in:

$$I_3 = \eta_{aa}(\eta_{bb}\eta_{cc} - \eta_{cb}\eta_{bc}) - \eta_{ab}(\eta_{ba}\eta_{cc} - \eta_{ca}\eta_{bc}) + \eta_{ac}(\eta_{ba}\eta_{cb} - \eta_{ca}\eta_{bb}), \tag{A.72}$$

which can be recognised as the cofactor expansion of the first row of the strain matrix $\boldsymbol{\eta}$. From this it follows that the third strain invariant I_3 is equal to the determinant of $\boldsymbol{\eta}$:

$$I_3 = \det(\boldsymbol{\eta}) = \eta_{aa}\begin{vmatrix} \eta_{bb} & \eta_{bc} \\ \eta_{cb} & \eta_{cc} \end{vmatrix} - \eta_{ab}\begin{vmatrix} \eta_{ba} & \eta_{bc} \\ \eta_{ca} & \eta_{cc} \end{vmatrix} + \eta_{ac}\begin{vmatrix} \eta_{ba} & \eta_{bb} \\ \eta_{ca} & \eta_{cb} \end{vmatrix}. \tag{A.73}$$

A.4. Connection between stress and strain

The three-dimensional deformable medium is considered in its final or deformed state. It is supposed that, while in this deformed state, the deformable medium is in equilibrium when subjected to various forces. A distinction can be made between two types of forces. The first type are the mass forces $\boldsymbol{X_x}$ acting on the element of mass dm. The second type are the traction forces $\boldsymbol{t_x}$ acting on dV_x across its bounding surface dS_x. The mass forces and the traction forces are defined as:

$$\boldsymbol{X_x} = \begin{pmatrix} X_x \\ Y_x \\ Z_x \end{pmatrix}; \quad \boldsymbol{t_x} = \begin{pmatrix} t_x \\ t_y \\ t_z \end{pmatrix}, \tag{2.15}$$

respectively.

A.4.1. Cauchy stress tensor

The traction describes the forces acting in the x,y and z-direction across a surface area. By presenting the deformable medium as a tetrahedron, the traction forces acting on their respective planes can be visualised like depicted in Figure A.3.

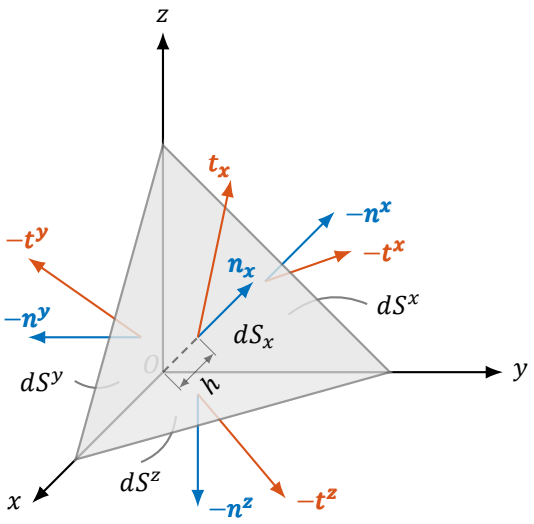

Figure A.3: Visualisation of the traction acting on the planes of a tetrahedron with height h and base plane dS_x.

This tetrahedron must be in equilibrium, therefore Newton's second law of motion yields:

$$\boldsymbol{t_x} dS_x - \boldsymbol{t^x} dS^x - \boldsymbol{t^y} dS^y - \boldsymbol{t^z} dS^z = dm\ddot{\boldsymbol{x}}, \tag{A.74}$$

where $dm = \rho_x dV_x$ denotes the element of mass of the tetrahedron and $\ddot{\boldsymbol{x}}$ – its acceleration vector. The vectors $\boldsymbol{t^z}, \boldsymbol{t^y}$ and $\boldsymbol{t^z}$ denote the traction forces acting on dS^x, S^y and S^z, respectively. Through the definition of the unit vectors in the direction of the x, y and z axes of a Cartesian coordinate system,

$$\hat{\boldsymbol{i}} = \begin{pmatrix} 1 \\ 0 \\ 0 \end{pmatrix}; \quad \hat{\boldsymbol{j}} = \begin{pmatrix} 0 \\ 1 \\ 0 \end{pmatrix}; \quad \hat{\boldsymbol{k}} = \begin{pmatrix} 0 \\ 0 \\ 1 \end{pmatrix}, \tag{A.75}$$

these traction forces can be expressed as:

$$\begin{aligned} \boldsymbol{t^x} &= T_{xx}\hat{\boldsymbol{i}} + T_{xy}\hat{\boldsymbol{j}} + T_{xz}\hat{\boldsymbol{k}} \\ \boldsymbol{t^y} &= T_{yx}\hat{\boldsymbol{i}} + T_{yy}\hat{\boldsymbol{j}} + T_{yz}\hat{\boldsymbol{k}} \\ \boldsymbol{t^z} &= T_{zx}\hat{\boldsymbol{i}} + T_{zy}\hat{\boldsymbol{j}} + T_{zz}\hat{\boldsymbol{k}}. \end{aligned} \tag{A.76}$$

Here, T_{ij} denotes a stress acting in the j-direction across a plane which has its outward normal in the i-direction.

The element of mass dm can be rewritten in terms of the base plane of the tetrahedron dS_x with:

$$dm = \rho_x dV_x = \rho_x \left(\frac{h}{3} dS_x \right). \tag{A.77}$$

Upon substitution of this expression into Newton's second law of motion and using relation (A.17) the following is obtained:

$$\boldsymbol{t_x} dS_x - \boldsymbol{t^x} dS_x \hat{n}_x - \boldsymbol{t^y} dS_x \hat{n}_y - \boldsymbol{t^z} dS_x \hat{n}_z = \rho_x \left(\frac{h}{3} dS_x \right) \ddot{\boldsymbol{x}}, \tag{A.78}$$

which can be simplified to:

$$\boldsymbol{t_x} - \boldsymbol{t^x} \hat{n}_x - \boldsymbol{t^y} \hat{n}_y - \boldsymbol{t^z} \hat{n}_z = \rho_x \left(\frac{h}{3} \right) \ddot{\boldsymbol{x}}. \tag{A.79}$$

If it is assumed that the tetrahedron is infinitesimal, then the following holds for the limit case $\lim_{h \to 0}$:

$$\boldsymbol{t_x} = \boldsymbol{t^x} \hat{n}_x + \boldsymbol{t^y} \hat{n}_y + \boldsymbol{t^z} \hat{n}_z. \tag{A.80}$$

Note that all the traction vectors in this expression are, by default, column vectors. However, it is more convenient to write them as row vectors. By transposing both sides of the equation, relation (A.80) becomes:

$$\boldsymbol{t_x}^T = \begin{pmatrix} t_x & t_y & t_z \end{pmatrix} = \begin{pmatrix} \hat{n}_x & \hat{n}_y & \hat{n}_z \end{pmatrix} \begin{pmatrix} \boldsymbol{t^x}^T \\ \boldsymbol{t^y}^T \\ \boldsymbol{t^z}^T \end{pmatrix}, \tag{A.81}$$

which after substituting relation (A.76), yields:

$$\boldsymbol{t_x}^T = \begin{pmatrix} t_x & t_y & t_z \end{pmatrix} = \begin{pmatrix} \hat{n}_x & \hat{n}_y & \hat{n}_z \end{pmatrix} \begin{pmatrix} T_{xx} & T_{xy} & T_{xz} \\ T_{yx} & T_{yy} & T_{yz} \\ T_{zx} & T_{zy} & T_{zz} \end{pmatrix}. \tag{A.82}$$

Here, t_i denotes the i-components of the stresses acting on the surfaces areas dS^x, S^y and S^z. By transposing both sides of the equation again, the Cauchy stress equation is obtained:

$$\boldsymbol{t_x} = \boldsymbol{T}^T \hat{\boldsymbol{n}}_{\boldsymbol{x}}, \tag{2.17}$$

where $\boldsymbol{T}$ denotes the Cauchy stress tensor:

$$\boldsymbol{T} = \begin{pmatrix} T_{xx} & T_{xy} & T_{xz} \\ T_{yx} & T_{yy} & T_{yz} \\ T_{zx} & T_{zy} & T_{zz} \end{pmatrix}. \tag{2.18}$$

The tractions and the stresses, working on their respective planes, are graphically displayed in Figure A.4.

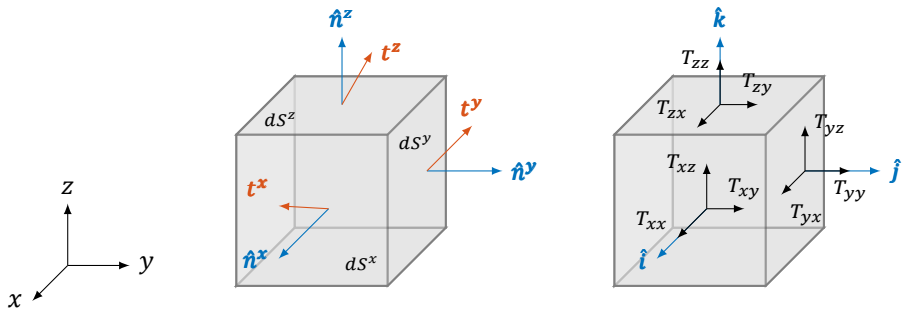

Figure A.4: The positive definitions of the tractions and the Cauchy stresses acting on the coordinate planes of a cube.

A.4.2. Virtual work principle

The principle of virtual work states that the virtual work, exerted by all forces acting on a body in equilibrium, in any virtual rigid displacement is zero. The term 'virtual rigid displacement' is a specific type of virtual deformation. The latter can be defined by assuming that the final coordinates (x, y, z) are not only functions of the initial coordinates (a, b, c) but also of an additional parameter θ. The variables a, b, c and θ are considered to be independent of each other. If there exists a continuous function f of these four variables, then its differential can be written in the form $df + \delta f$ with

$$df = f_a da + f_b db + f_c dc \; ; \quad \delta f = f_\theta d\theta. \tag{A.83}$$

The term df is obtained by taking the differential of f while assuming that θ is kept constant whereas the term δf is obtained by taking the differential of f while assuming that the initial coordinates (a, b, c) are kept constant.

A virtual deformation is established by the 3 x 1 vector,

$$\boldsymbol{\delta x} = \begin{pmatrix} \delta x \\ \delta y \\ \delta z \end{pmatrix}, \tag{2.19}$$

which is a function of the final coordinates. A virtual rigid displacement implies that no deformation occurs, i.e., the variation of the squared final scalar element of arc in θ is zero:

$$\delta(ds_x)^2 = 0. \tag{A.84}$$

By assuming that the variables a, b, c and θ are independent of each other and that the second-order derivatives with respect to these variables are continuous, it follows that the order in which these derivatives are determined is irrelevant:

$$x_{a\theta} = x_{\theta a}, \tag{A.85}$$

where $x_{a\theta}$ denotes the derivative of x_a with respect to θ and $x_{\theta a}$ – the derivative of x_θ with respect to a. Multiplying both sides of this equation with $d\theta$ results in a property of the variation:

$$\delta(x_a) = (\delta x)_a. \tag{A.86}$$

From now on the Jacobian matrix of the final coordinates with respect to initial coordinates will be written in a shorter notation:

$$\boldsymbol{J} = \boldsymbol{J_x}(a, b, c). \tag{2.24}$$

The variation of this Jacobian matrix, $\boldsymbol{\delta J}$, is then defined as:

$$\boldsymbol{\delta J} = \begin{pmatrix} \delta(x_a) & \delta(x_b) & \delta(x_c) \\ \delta(y_a) & \delta(y_b) & \delta(y_c) \\ \delta(z_a) & \delta(z_b) & \delta(z_c) \end{pmatrix}. \tag{A.87}$$

By using the property (A.86) and the chain rule of differentiation:

$$(\delta x)_a = (\delta x)_x x_a + (\delta x)_y y_a + (\delta x)_z z_a, \tag{A.88}$$

expression (A.87) can be written as:

$$\boldsymbol{\delta J} = (\boldsymbol{\delta x})_{\boldsymbol{x}}\, \boldsymbol{J}, \tag{A.89}$$

where $(\boldsymbol{\delta x})_{\boldsymbol{x}}$ denotes the Jacobian matrix of the virtual deformations with the respect to the final coordinates:

$$(\boldsymbol{\delta x})_{\boldsymbol{x}} = \begin{pmatrix} (\delta x)_x & (\delta x)_y & (\delta x)_z \\ (\delta y)_x & (\delta y)_y & (\delta y)_z \\ (\delta z)_x & (\delta z)_y & (\delta z)_z \end{pmatrix}. \tag{A.90}$$

The variation of the transposed Jacobian matrix $\boldsymbol{J}$, $\boldsymbol{\delta J}^T = \left(\boldsymbol{\delta J}\right)^T$, then becomes

$$\boldsymbol{\delta J}^T = \boldsymbol{J}^T \left[(\boldsymbol{\delta x})_{\boldsymbol{x}}\right]^T. \tag{A.91}$$

If a matrix $\boldsymbol{M} = \boldsymbol{J}^T\boldsymbol{J}$ is introduced, then its variation is defined as:

$$\begin{aligned} \boldsymbol{\delta M} &= \boldsymbol{\delta}\left(\boldsymbol{J}^T\boldsymbol{J}\right) \\ &= \left(\boldsymbol{\delta J}^T\right)\boldsymbol{J} + \boldsymbol{J}^T\,\boldsymbol{\delta J} \\ &= \boldsymbol{J}^T\left[(\boldsymbol{\delta x})_{\boldsymbol{x}}\right]^T\boldsymbol{J} + \boldsymbol{J}^T(\boldsymbol{\delta x})_{\boldsymbol{x}}\,\boldsymbol{J} \\ &= \boldsymbol{J}^T\left\{\left[(\boldsymbol{\delta x})_{\boldsymbol{x}}\right]^T + (\boldsymbol{\delta x})_{\boldsymbol{x}}\right\}\boldsymbol{J}. \end{aligned} \tag{A.92}$$

The variation $\boldsymbol{\delta M}$ can be written more compact by introducing a symmetric matrix,

$$\boldsymbol{D} = \tfrac{1}{2}\left\{\left[(\boldsymbol{\delta x})_{\boldsymbol{x}}\right]^T + (\boldsymbol{\delta x})_{\boldsymbol{x}}\right\}, \tag{A.93}$$

which, upon substitution in expression (A.92) yields:

$$\boldsymbol{\delta M} = 2\boldsymbol{J}^T\boldsymbol{D}\boldsymbol{J}. \tag{A.94}$$

From the Lagrangian strain description (2.11) it holds that $\boldsymbol{M} = 2\boldsymbol{\eta} + \boldsymbol{E_3}$ and therefore, expression (A.92) can also be written in terms of the strain:

$$\begin{aligned} \boldsymbol{\delta M} &= \delta\left(2\boldsymbol{\eta} + \boldsymbol{E_3}\right) \\ &= 2\boldsymbol{\delta\eta} + \boldsymbol{\delta E_3} \\ &= 2\boldsymbol{\delta\eta}. \end{aligned} \tag{A.95}$$

By combining expressions (A.94) and (A.95), the variation of the strain becomes:

$$\boldsymbol{\delta\eta} = \boldsymbol{J}^T\boldsymbol{D}\boldsymbol{J}. \tag{2.28}$$

The variation of the squared final scalar element of arc can be elaborated by using definition (A.53):

$$\begin{aligned} \delta(ds_x)^2 &= \delta\left((\boldsymbol{da})^T\boldsymbol{M}\ (\boldsymbol{da})\right) \\ &= \delta(\boldsymbol{da})^T\boldsymbol{M}\ (\boldsymbol{da}) + (\boldsymbol{da})^T\boldsymbol{\delta M}\ (\boldsymbol{da}) + (\boldsymbol{da})^T\boldsymbol{M}\ \delta(\boldsymbol{da}). \end{aligned} \tag{A.96}$$

Since the initial coordinates (a, b, c) are independent of θ, it holds by definition that $\delta(\boldsymbol{da})^T = \delta(\boldsymbol{da}) = 0$. The above can then be further elaborated by substituting expressions (A.94) and (A.30):

$$\delta(ds_x)^2 = 2(\boldsymbol{dx})^T\boldsymbol{D}\ (\boldsymbol{dx}). \tag{A.97}$$

If the virtual deformation is a virtual rigid displacement, then this expression has to be zero for any arbitrary $\boldsymbol{dx}$. Therefore, a virtual deformation $\boldsymbol{\delta x}$ is defined as a virtual rigid displacement if, and only if, $\boldsymbol{D}$ is a zero matrix.

The total virtual work δV exerted by the mass forces, acting on the element of mass $dm = \rho_x dV_x$, and the traction forces, acting on the final scalar element of area dS_x, is defined as:

$$\delta V = \iiint_{V_x} \rho_x(\boldsymbol{\delta x})^T\boldsymbol{X_x}dV_x + \iint_{S_x}(\boldsymbol{\delta x})^T\boldsymbol{t_x}dS_x, \tag{2.20}$$

which, upon substitution of the Cauchy stress equation (2.17) and definition (A.15), yields:

$$\delta V = \iiint_{V_x} \rho_x(\boldsymbol{\delta x})^T\boldsymbol{X_x}dV_x + \iint_{S_x}(\boldsymbol{\delta x})^T\boldsymbol{T}^T\boldsymbol{dS^x}. \tag{A.98}$$

By using the divergence theorem it is possible to express the virtual work as one single volume integral. Assume an arbitrary 1 x 3 vector $\boldsymbol{\xi} = (\xi, \eta, \zeta)$ such that its surface integral is defined as:

$$\iint_{S_x}\boldsymbol{\xi dS^x} = \iint_{S_x}\left(\xi dS^x + \eta dS^y + \zeta dS^z\right) = \iint_{S_x}\left(\xi dydz + \eta dzdx + \zeta dxdy\right). \tag{A.99}$$

This surface integral can be further elaborated by introducing a third integral

$$\iint_{S_x}\boldsymbol{\xi dS^x} = \iint_{S_x}\left[\left(\int\frac{\partial\xi}{\partial x}dx\right)dydz + \left(\int\frac{\partial\eta}{\partial y}dy\right)dzdx + \left(\int\frac{\partial\zeta}{\partial z}dz\right)dxdy\right], \tag{A.100}$$

which, upon factorising the final element of volume, $dV_x = dxdydz$, yields the volume integral

$$\iiint_{V_x}\left(\xi_x + \eta_y + \zeta_z\right)dV_x = \iiint_{V_x}\left(\boldsymbol{\nabla_x}\ \boldsymbol{\xi}^T\right)dV_x, \tag{A.101}$$

where the divergence of any 3 x m matrix is obtained by taking the gradient of each of its columns with respect to the final coordinates:

$$\boldsymbol{\nabla_x}\ \boldsymbol{\xi}^T = \begin{pmatrix}\frac{\partial}{\partial x} & \frac{\partial}{\partial y} & \frac{\partial}{\partial z}\end{pmatrix}\begin{pmatrix}\xi\\ \eta\\ \zeta\end{pmatrix} = \xi_x + \eta_y + \zeta_z. \tag{A.102}$$

Using the same approach for relation (A.98) yields

$$\delta V = \iiint_{V_x}\left[\rho_x(\boldsymbol{\delta x})^T\boldsymbol{X_x} + \boldsymbol{\nabla_x}\ (\boldsymbol{T\delta x})\right]dV_x. \tag{A.103}$$

The divergence $\boldsymbol{\nabla_x}\,(\boldsymbol{T\delta x})$ is defined as:

$$\boldsymbol{\nabla_x}\,(\boldsymbol{T\delta x}) = \begin{pmatrix} \frac{\partial}{\partial x} & \frac{\partial}{\partial y} & \frac{\partial}{\partial z} \end{pmatrix} \left[\begin{pmatrix} T_{xx} & T_{xy} & T_{xz} \\ T_{yx} & T_{yy} & T_{yz} \\ T_{zx} & T_{zy} & T_{zz} \end{pmatrix} \begin{pmatrix} \delta x \\ \delta y \\ \delta z \end{pmatrix} \right], \tag{A.104}$$

which after using the chain rule of differentiation,

$$\frac{\partial}{\partial x}\left(T_{xx}\delta x\right) = \frac{\partial T_{xx}}{\partial x}\delta x + \frac{\partial \delta x}{\partial x}T_{xx}, \;\; \frac{\partial}{\partial x}\left(T_{xy}\delta y\right) = \frac{\partial T_{xy}}{\partial x}\delta y + \frac{\partial \delta y}{\partial x}T_{xy}, \text{ etc.}, \tag{A.105}$$

can be written as:

$$\begin{aligned} \boldsymbol{\nabla_x}\,(\boldsymbol{T\delta x}) = {} & \frac{\partial T_{xx}}{\partial x}\delta x + \frac{\partial T_{xy}}{\partial x}\delta y + \frac{\partial T_{xz}}{\partial x}\delta z + \frac{\partial T_{yx}}{\partial y}\delta x + \frac{\partial T_{yy}}{\partial y}\delta y + \frac{\partial T_{yz}}{\partial y}\delta z \\ & + \frac{\partial T_{zx}}{\partial z}\delta x + \frac{\partial T_{zy}}{\partial z}\delta y + \frac{\partial T_{zz}}{\partial z}\delta z \\ & + \frac{\partial \delta x}{\partial x}T_{xx} + \frac{\partial \delta y}{\partial x}T_{xy} + \frac{\partial \delta z}{\partial x}T_{xz} + \frac{\partial \delta x}{\partial y}T_{yx} + \frac{\partial \delta y}{\partial y}T_{yy} + \frac{\partial \delta z}{\partial y}T_{yz} \\ & + \frac{\partial \delta x}{\partial z}T_{zx} + \frac{\partial \delta y}{\partial z}T_{zy} + \frac{\partial \delta z}{\partial z}T_{zz}. \end{aligned} \tag{A.106}$$

In the expression above, the divergence,

$$(\boldsymbol{\nabla_x}\,\boldsymbol{T})\boldsymbol{\delta x} = \begin{pmatrix} \frac{\partial T_{xx}}{\partial x} + \frac{\partial T_{yx}}{\partial y} + \frac{\partial T_{zx}}{\partial z} & \frac{\partial T_{xy}}{\partial x} + \frac{\partial T_{yy}}{\partial y} + \frac{\partial T_{zy}}{\partial z} & \frac{\partial T_{xz}}{\partial x} + \frac{\partial T_{yz}}{\partial y} + \frac{\partial T_{zz}}{\partial z} \end{pmatrix} \begin{pmatrix} \delta x \\ \delta y \\ \delta z \end{pmatrix}, \tag{A.107}$$

and the trace,

$$\mathrm{Tr}\big(\boldsymbol{T}(\boldsymbol{\delta x})_{\boldsymbol{x}}\big) = \mathrm{Tr}\left[\begin{pmatrix} T_{xx} & T_{xy} & T_{xz} \\ T_{yx} & T_{yy} & T_{yz} \\ T_{zx} & T_{zy} & T_{zz} \end{pmatrix} \begin{pmatrix} (\delta x)_x & (\delta x)_y & (\delta x)_z \\ (\delta y)_x & (\delta y)_y & (\delta y)_z \\ (\delta z)_x & (\delta z)_y & (\delta z)_z \end{pmatrix} \right], \tag{2.23}$$

can be recognised. Therefore, relation (A.104) can be written as:

$$\boldsymbol{\nabla_x}\,(\boldsymbol{T\delta x}) = (\boldsymbol{\nabla_x}\,\boldsymbol{T})\boldsymbol{\delta x} + \mathrm{Tr}\big(\boldsymbol{T}(\boldsymbol{\delta x})_{\boldsymbol{x}}\big). \tag{A.108}$$

Note that the term $(\boldsymbol{\nabla_x}\,\boldsymbol{T})\boldsymbol{\delta x}$ is a 1 x 1 matrix, i.e. a scalar, which makes it equal to its transpose $(\boldsymbol{\delta x})^T(\boldsymbol{\nabla_x}\,\boldsymbol{T})^T$. Therefore, expression (A.103) can be rewritten to:

$$\delta V = \iiint_{V_x} \left\{ (\boldsymbol{\delta x})^T \left[\rho_x \boldsymbol{X_x} + (\boldsymbol{\nabla_x}\,\boldsymbol{T})^T \right] + \mathrm{Tr}\big(\boldsymbol{T}(\boldsymbol{\delta x})_{\boldsymbol{x}}\big) \right\} dV_x. \tag{2.21}$$

The virtual work must be zero if the virtual deformation is a virtual rigid displacement, or more specific: a virtual translation. For such virtual deformations $\boldsymbol{\delta x}$ is an arbitrary constant 3 x 1 vector:

$$\boldsymbol{\delta x} = \begin{pmatrix} \delta x \\ \delta y \\ \delta z \end{pmatrix} = \begin{pmatrix} f \\ g \\ h \end{pmatrix}, \tag{2.30}$$

where f, g and h denote translations in the x, y and z-direction, respectively. For this type of virtual deformation, the Jacobian matrix $(\boldsymbol{\delta x})_{\boldsymbol{x}}$ is a zero matrix. Therefore, the following volume integral must be equal to zero for all virtual translations:

$$\delta V = \iiint_{V_x} \left\{ (\boldsymbol{\delta x})^T \left[\rho_x \boldsymbol{X_x} + (\boldsymbol{\nabla_x}\,\boldsymbol{T})^T \right] \right\} dV_x = 0, \tag{2.31}$$

which leads to a system of equations of equilibrium

$$\rho_x \boldsymbol{X_x} + \left(\boldsymbol{\nabla_x}\, \boldsymbol{T}\right)^T = \boldsymbol{0}. \tag{2.32}$$

This implies that the virtual work in any arbitrary virtual deformation (2.21) reduces to:

$$\delta V = \iiint_{V_x} \mathrm{Tr}\left(\boldsymbol{T}(\boldsymbol{\delta x})_{\boldsymbol{x}}\right) dV_x. \tag{2.33}$$

This integral must be zero for all virtual rigid displacements. This is the case for all virtual deformations which are of the form:

$$\boldsymbol{\delta x} = \begin{pmatrix} \delta x \\ \delta y \\ \delta z \end{pmatrix} = \begin{pmatrix} f - ry + qz \\ g + rx - pz \\ h - qx + py \end{pmatrix}, \tag{A.109}$$

where p, q and r denote rotations around the x, y and z-axis, respectively. For these virtual deformations the Jacobian matrix $(\boldsymbol{\delta x})_{\boldsymbol{x}}$ is of the form:

$$(\boldsymbol{\delta x})_{\boldsymbol{x}} = \begin{pmatrix} 0 & -r & q \\ r & 0 & -p \\ -q & p & 0 \end{pmatrix}. \tag{A.110}$$

Note that for these virtual rigid displacements, expression (A.93) becomes:

$$\boldsymbol{D} = \frac{1}{2}\left[\begin{pmatrix} 0 & -r & q \\ r & 0 & -p \\ -q & p & 0 \end{pmatrix} + \begin{pmatrix} 0 & r & -q \\ -r & 0 & p \\ q & -p & 0 \end{pmatrix}\right] = \boldsymbol{0}, \tag{A.111}$$

which confirms that $\boldsymbol{D}$ must be a zero matrix for virtual rigid displacements. By stating that the virtual work for these type of virtual deformations must be zero, it follows from expression (2.33) that the trace $\mathrm{Tr}\left(\boldsymbol{T}(\boldsymbol{\delta x})_{\boldsymbol{x}}\right)$ must be equal to zero:

$$\mathrm{Tr}\left(\boldsymbol{T}(\boldsymbol{\delta x})_{\boldsymbol{x}}\right) = \mathrm{Tr}\begin{pmatrix} T_{xy}r - T_{xz}q & -T_{xx}r + T_{xz}p & T_{xx}q - T_{xy}p \\ T_{yy}r - T_{yz}q & -T_{yx}r + T_{yz}p & T_{yx}q - T_{yy}p \\ T_{zy}r - T_{zz}q & -T_{zx}r + T_{zz}p & T_{zx}q - T_{zy}p \end{pmatrix} = 0. \tag{A.112}$$

By factorising the common terms, expression (A.112) becomes:

$$\mathrm{Tr}\left(\boldsymbol{T}(\boldsymbol{\delta x})_{\boldsymbol{x}}\right) = \left(T_{yz} - T_{zy}\right)p + \left(T_{zx} - T_{xz}\right)q + \left(T_{xy} - T_{yx}\right)r = 0. \tag{A.113}$$

Since the above must hold for any arbitrary choice of the parameters p, q, r, the off-diagonal terms of the matrix $\boldsymbol{T}$ have to be equal. Therefore, the Cauchy stress matrix $\boldsymbol{T}$ must be symmetric, which makes it equal to its transpose $\boldsymbol{T}^T$.

According to definition (A.93), it holds, by definition, that $\mathrm{Tr}\left((\boldsymbol{\delta x})_{\boldsymbol{x}}\right) = \mathrm{Tr}\left(\boldsymbol{D}\right)$. Therefore, expression (2.33) can be rewritten in the form:

$$\delta V = \iiint_{V_x} \mathrm{Tr}\left(\boldsymbol{TD}\right) dV_x. \tag{2.34}$$

The relation between the stress matrix $\boldsymbol{T}$ and the strain matrix $\boldsymbol{\eta}$ can be established by isolating the symmetric matrix $\boldsymbol{D}$ in relation (2.28):

$$\boldsymbol{D} = \left(\boldsymbol{J}^T\right)^{-1} \boldsymbol{\delta\eta}\, \boldsymbol{J}^{-1}. \tag{2.35}$$

Since the order of the quantities of the trace is not of importance, $\mathrm{Tr}\left(\boldsymbol{AB}\right) = \mathrm{Tr}\left(\boldsymbol{BA}\right)$, the following is found after substituting the above in definition (2.34):

$$\delta V = \iiint_{V_x} \mathrm{Tr}\left(\boldsymbol{J}^{-1}\boldsymbol{T}\left(\boldsymbol{J}^T\right)^{-1}\boldsymbol{\delta\eta}\right) dV_x. \tag{2.36}$$

A.4.3. Strain energy

It is assumed that the work exerted by all the forces acting on V_x of the deformable medium in any deformation is stored up in V_x as strain energy. This strain energy is distributed throughout V_x with a mass density:

$$U = \iiint_{V_x} \rho_x \psi dV_x, \tag{2.37}$$

where ψ denotes the strain energy per unit mass which is assumed to be a function of the strain matrix:

$$\psi = \psi(\boldsymbol{\eta}). \tag{A.114}$$

According to the law of conservation of energy, the exerted virtual work on any portion of the volume V_x of the deformable medium in any virtual deformation should be equal to the variation of the strain energy δU:

$$\iiint_{V_x} \mathrm{Tr}\big(\boldsymbol{J}^{-1}\boldsymbol{T}\big(\boldsymbol{J}^T\big)^{-1}\boldsymbol{\delta\eta}\big)dV_x = \iiint_{V_x} \rho_x \delta\psi dV_x, \tag{A.115}$$

from which follows that the integrands should be equal:

$$\mathrm{Tr}\big(\boldsymbol{J}^{-1}\boldsymbol{T}\big(\boldsymbol{J}^T\big)^{-1}\boldsymbol{\delta\eta}\big) = \rho_x \delta\psi. \tag{A.116}$$

The variation of the strain-energy density $\delta\psi$ can be elaborated by using relation (A.83):

$$\delta\psi = \psi_\theta d\theta, \tag{A.117}$$

which, upon using the chain rule of differentiation, becomes:

$$\delta\psi = \frac{\partial\psi}{\partial\boldsymbol{\eta}}\frac{\partial\boldsymbol{\eta}}{\partial\theta}d\theta = \frac{\partial\psi}{\partial\boldsymbol{\eta}}\boldsymbol{\delta\eta}. \tag{A.118}$$

By using the fact that the strain matrix $\boldsymbol{\eta}$ is symmetric, the above can be expanded to:

$$\begin{aligned}\delta\psi = \Bigg(&\frac{\partial\psi}{\partial\eta_{aa}}\frac{\partial\eta_{aa}}{\partial\theta} + \frac{\partial\psi}{\partial\eta_{ab}}\frac{\partial\eta_{ba}}{\partial\theta} + \frac{\partial\psi}{\partial\eta_{ac}}\frac{\partial\eta_{ca}}{\partial\theta} + \frac{\partial\psi}{\partial\eta_{ba}}\frac{\partial\eta_{ab}}{\partial\theta} + \frac{\partial\psi}{\partial\eta_{bb}}\frac{\partial\eta_{bb}}{\partial\theta} + \frac{\partial\psi}{\partial\eta_{bc}}\frac{\partial\eta_{cb}}{\partial\theta} \\ &+ \frac{\partial\psi}{\partial\eta_{ca}}\frac{\partial\eta_{ac}}{\partial\theta} + \frac{\partial\psi}{\partial\eta_{cb}}\frac{\partial\eta_{bc}}{\partial\theta} + \frac{\partial\psi}{\partial\eta_{cc}}\frac{\partial\eta_{cc}}{\partial\theta}\Bigg)d\theta = \psi_\theta d\theta,\end{aligned} \tag{A.119}$$

which can be recognised as the trace:

$$\mathrm{Tr}\left(\frac{\partial\psi}{\partial\boldsymbol{\eta}}\boldsymbol{\delta\eta}\right) = \mathrm{Tr}\left[\begin{pmatrix} \frac{\partial\psi}{\partial\eta_{aa}} & \frac{\partial\psi}{\partial\eta_{ab}} & \frac{\partial\psi}{\partial\eta_{ac}} \\ \frac{\partial\psi}{\partial\eta_{ba}} & \frac{\partial\psi}{\partial\eta_{bb}} & \frac{\partial\psi}{\partial\eta_{bc}} \\ \frac{\partial\psi}{\partial\eta_{ca}} & \frac{\partial\psi}{\partial\eta_{cb}} & \frac{\partial\psi}{\partial\eta_{cc}} \end{pmatrix}\begin{pmatrix} \frac{\partial\eta_{aa}}{\partial\theta} & \frac{\partial\eta_{ab}}{\partial\theta} & \frac{\partial\eta_{ac}}{\partial\theta} \\ \frac{\partial\eta_{ba}}{\partial\theta} & \frac{\partial\eta_{bb}}{\partial\theta} & \frac{\partial\eta_{bc}}{\partial\theta} \\ \frac{\partial\eta_{ca}}{\partial\theta} & \frac{\partial\eta_{cb}}{\partial\theta} & \frac{\partial\eta_{cc}}{\partial\theta} \end{pmatrix}d\theta\right]. \tag{A.120}$$

Therefore, relation (A.116) becomes:

$$\mathrm{Tr}\big(\boldsymbol{J}^{-1}\boldsymbol{T}\big(\boldsymbol{J}^T\big)^{-1}\boldsymbol{\delta\eta}\big) = \rho_x \mathrm{Tr}\left(\frac{\partial\psi}{\partial\boldsymbol{\eta}}\boldsymbol{\delta\eta}\right). \tag{A.121}$$

This relation must hold for any arbitrary symmetric matrix $\boldsymbol{\eta}$, which results in:

$$\boldsymbol{J}^{-1}\boldsymbol{T}\big(\boldsymbol{J}^T\big)^{-1} = \rho_x \frac{\partial\psi}{\partial\boldsymbol{\eta}}. \tag{A.122}$$

The Cauchy stress matrix $\boldsymbol{T}$ can be isolated by leftmulitplying with the Jacobian matrix $\boldsymbol{J}$ and rightmulitplying with its transpose $\boldsymbol{J}^T$:

$$\boldsymbol{T} = \rho_x \boldsymbol{J} \frac{\partial \psi}{\partial \boldsymbol{\eta}} \boldsymbol{J}^T. \tag{A.123}$$

By introducing $\phi = \rho_a \psi$ as the strain energy per unit initial volume, the above becomes:

$$\boldsymbol{T} = \left(\frac{\rho_x}{\rho_a}\right) \boldsymbol{J} \frac{\partial \phi}{\partial \boldsymbol{\eta}} \boldsymbol{J}^T, \tag{A.124}$$

which upon substituting definition (A.52) yields:

$$\boldsymbol{T} = \frac{1}{\det(\boldsymbol{J})} \boldsymbol{J} \frac{\partial \phi}{\partial \boldsymbol{\eta}} \boldsymbol{J}^T. \tag{2.38}$$

According to the principle of material frame indifference, the strain-energy density $\phi(\boldsymbol{\eta})$ of an isotropic material depends on the three strain invariants only [22, Ch. 4.1] [8, Eq. 1.46]. From the definition of these strain invariants follows that I_1 is of the first order, I_2 of the second order and I_3 is of the third order with respect to the strain. The strain-energy density function can be written as:

$$\phi = \phi_0 + \phi_1 + \phi_2 + \phi_3 + \dots \tag{2.40}$$

where ϕ_0 is independent of $\boldsymbol{\eta}$. From (2.38) it follows that the strain energy enters the expression of the stress matrix $\boldsymbol{T}$ only through its derivative with respect to $\boldsymbol{\eta}$. Therefore, the term ϕ_0 is irrelevant for the stresses. The linear terms in the elements of $\boldsymbol{\eta}$ are collected in ϕ_1 which are represented as a multiple of I_1:

$$\phi_1 = pI_1. \tag{A.125}$$

The quadratic terms in the elements of $\boldsymbol{\eta}$ are collected in ϕ_2 which are represented as a linear combination of I_1^2 and I_2:

$$\phi_2 = \frac{\lambda + 2\mu}{2} I_1^2 - 2\mu I_2, \tag{A.126}$$

where the second-order coefficients λ and μ are defined as the first and second Lamé parameter, respectively. Similarly, ϕ_3 contains the cubic terms in the elements of $\boldsymbol{\eta}$ which are represented as a linear combination of I_1^3, $I_1 I_2$ and I_3

$$\phi_3 = \frac{l + 2m}{3} I_1^3 - 2mI_1 I_2 + nI_3, \tag{A.127}$$

where the third-order coefficients l, m, n are defined as the Murnaghan constants.

The derivatives of the terms of the power series with respect to the strain matrix $\boldsymbol{\eta}$ can be determined by making use of the chain rule of differentiation. For the first term ϕ_1, this yields:

$$\frac{\partial \phi_1}{\partial \boldsymbol{\eta}} = p \frac{\partial I_1}{\partial I_1} \frac{\partial I_1}{\partial \boldsymbol{\eta}}, \tag{A.128}$$

where the derivative of the first strain invariant,

$$I_1 = \mathrm{Tr}(\boldsymbol{\eta}) = \eta_{aa} + \eta_{bb} + \eta_{cc}, \tag{A.129}$$

with respect to the strain matrix is defined as:

$$\frac{\partial I_1}{\partial \boldsymbol{\eta}} = \begin{pmatrix} \frac{\partial I_1}{\partial \eta_{aa}} & \frac{\partial I_1}{\partial \eta_{ab}} & \frac{\partial I_1}{\partial \eta_{ac}} \\ \frac{\partial I_1}{\partial \eta_{ba}} & \frac{\partial I_1}{\partial \eta_{bb}} & \frac{\partial I_1}{\partial \eta_{bc}} \\ \frac{\partial I_1}{\partial \eta_{ca}} & \frac{\partial I_1}{\partial \eta_{cb}} & \frac{\partial I_1}{\partial \eta_{cc}} \end{pmatrix} = \begin{pmatrix} 1 & 0 & 0 \\ 0 & 1 & 0 \\ 0 & 0 & 1 \end{pmatrix}. \tag{A.130}$$

Therefore, relation (A.128) becomes:

$$\frac{\partial \phi_1}{\partial \boldsymbol{\eta}} = p\boldsymbol{E_3}. \tag{A.131}$$

For the second term ϕ_2, this yields:

$$\frac{\partial \phi_2}{\partial \boldsymbol{\eta}} = \frac{\lambda + 2\mu}{2}\frac{\partial I_1^2}{\partial I_1}\frac{\partial I_1}{\partial \boldsymbol{\eta}} - 2\mu\frac{\partial I_2}{\partial I_2}\frac{\partial I_2}{\partial \boldsymbol{\eta}}, \tag{A.132}$$

where the derivative of the second strain invariant,

$$I_2 = \mathrm{Tr}(\mathrm{co}\,\boldsymbol{\eta}) = (\eta_{bb}\eta_{cc} - \eta_{bc}\eta_{cb}) + (\eta_{aa}\eta_{cc} - \eta_{ac}\eta_{ca}) + (\eta_{aa}\eta_{bb} - \eta_{ab}\eta_{ba}), \tag{A.133}$$

with respect to the strain matrix is defined as:

$$\frac{\partial I_2}{\partial \boldsymbol{\eta}} = \begin{pmatrix} \frac{\partial I_2}{\partial \eta_{aa}} & \frac{\partial I_2}{\partial \eta_{ab}} & \frac{\partial I_2}{\partial \eta_{ac}} \\ \frac{\partial I_2}{\partial \eta_{ba}} & \frac{\partial I_2}{\partial \eta_{bb}} & \frac{\partial I_2}{\partial \eta_{bc}} \\ \frac{\partial I_2}{\partial \eta_{ca}} & \frac{\partial I_2}{\partial \eta_{cb}} & \frac{\partial I_2}{\partial \eta_{cc}} \end{pmatrix} = \begin{pmatrix} \eta_{bb} + \eta_{cc} & -\eta_{ba} & -\eta_{ca} \\ -\eta_{ab} & \eta_{aa} + \eta_{bb} & -\eta_{cb} \\ -\eta_{ac} & -\eta_{bc} & \eta_{aa} + \eta_{bb} \end{pmatrix}. \tag{A.134}$$

The same expression, written in terms of the strain matrix, can be derived with:

$$\begin{aligned} I_1\boldsymbol{E_3} - \boldsymbol{\eta} &= \begin{pmatrix} \eta_{aa} + \eta_{bb} + \eta_{bb} - \eta_{aa} & 0 - \eta_{ab} & 0 - \eta_{ac} \\ 0 - \eta_{ba} & \eta_{aa} + \eta_{bb} + \eta_{bb} - \eta_{bb} & 0 - \eta_{bc} \\ 0 - \eta_{ca} & 0 - \eta_{cb} & \eta_{aa} + \eta_{bb} + \eta_{bb} - \eta_{cc} \end{pmatrix} \\ &= \begin{pmatrix} \eta_{bb} + \eta_{cc} & -\eta_{ba} & -\eta_{ca} \\ -\eta_{ab} & \eta_{aa} + \eta_{bb} & -\eta_{cb} \\ -\eta_{ac} & -\eta_{bc} & \eta_{aa} + \eta_{bb} \end{pmatrix} = \frac{\partial I_2}{\partial \boldsymbol{\eta}}. \end{aligned} \tag{A.135}$$

Upon substitution of the above in relation (A.132), the following is obtained:

$$\frac{\partial \phi_2}{\partial \boldsymbol{\eta}} = (\lambda + 2\mu)I_1\boldsymbol{E_3} - 2\mu(I_1\boldsymbol{E_3} - \boldsymbol{\eta}) = \lambda I_1\boldsymbol{E_3} + 2\mu\boldsymbol{\eta}. \tag{A.136}$$

The derivative of ϕ_3 with respect to $\boldsymbol{\eta}$ equals:

$$\frac{\partial \phi_3}{\partial \boldsymbol{\eta}} = \frac{l + 2m}{3}\frac{\partial I_1^3}{\partial I_1}\frac{\partial I_1}{\partial \boldsymbol{\eta}} - 2m\left(\frac{\partial I_1}{\partial \boldsymbol{\eta}}I_2 + \frac{\partial I_2}{\partial \boldsymbol{\eta}}I_1\right) + n\frac{\partial I_3}{\partial I_3}\frac{\partial I_3}{\partial \boldsymbol{\eta}}, \tag{A.137}$$

where the derivative of the third strain invariant,

$$I_3 = \det(\boldsymbol{\eta}) = \eta_{aa}(\eta_{bb}\eta_{cc} - \eta_{cb}\eta_{bc}) - \eta_{ab}(\eta_{ba}\eta_{cc} - \eta_{ca}\eta_{bc}) + \eta_{ac}(\eta_{ba}\eta_{cb} - \eta_{ca}\eta_{bb}), \tag{A.138}$$

with respect to the strain matrix is defined as:

$$\frac{\partial I_3}{\partial \boldsymbol{\eta}} = \begin{pmatrix} \frac{\partial I_3}{\partial \eta_{aa}} & \frac{\partial I_3}{\partial \eta_{ab}} & \frac{\partial I_3}{\partial \eta_{ac}} \\ \frac{\partial I_3}{\partial \eta_{ba}} & \frac{\partial I_3}{\partial \eta_{bb}} & \frac{\partial I_3}{\partial \eta_{bc}} \\ \frac{\partial I_3}{\partial \eta_{ca}} & \frac{\partial I_3}{\partial \eta_{cb}} & \frac{\partial I_3}{\partial \eta_{cc}} \end{pmatrix} = \begin{pmatrix} \begin{vmatrix} \eta_{bb} & \eta_{bc} \\ \eta_{cb} & \eta_{cc} \end{vmatrix} & \begin{vmatrix} \eta_{ca} & \eta_{cc} \\ \eta_{ba} & \eta_{bc} \end{vmatrix} & \begin{vmatrix} \eta_{ba} & \eta_{bb} \\ \eta_{ca} & \eta_{cb} \end{vmatrix} \\ \begin{vmatrix} \eta_{cb} & \eta_{cc} \\ \eta_{ab} & \eta_{ac} \end{vmatrix} & \begin{vmatrix} \eta_{aa} & \eta_{ac} \\ \eta_{ca} & \eta_{cc} \end{vmatrix} & \begin{vmatrix} \eta_{ca} & \eta_{cb} \\ \eta_{aa} & \eta_{ab} \end{vmatrix} \\ \begin{vmatrix} \eta_{ab} & \eta_{ac} \\ \eta_{bb} & \eta_{bc} \end{vmatrix} & \begin{vmatrix} \eta_{ba} & \eta_{bc} \\ \eta_{aa} & \eta_{ac} \end{vmatrix} & \begin{vmatrix} \eta_{aa} & \eta_{ab} \\ \eta_{ba} & \eta_{bb} \end{vmatrix} \end{pmatrix} = \mathrm{co}\,\boldsymbol{\eta}. \tag{A.139}$$

Therefore, relation (A.137) can be formulated as:

$$\frac{\partial I_3}{\partial \boldsymbol{\eta}} = (l+2m)I_1^2\boldsymbol{E_3} - 2m\left[I_2\boldsymbol{E_3} + I_1\left(I_1\boldsymbol{E_3} - \boldsymbol{\eta}\right)\right] + n\ \mathrm{co}\,\boldsymbol{\eta} = \left(lI_1^2 - 2mI_2\right)\boldsymbol{E_3} + 2mI_1\boldsymbol{\eta} + n\ \mathrm{co}\,\boldsymbol{\eta}. \quad \text{(A.140)}$$

Upon substitution of the derivative of the strain energy into relation (2.38), the expression for the Cauchy stress matrix $\boldsymbol{T}$ becomes:

$$\boldsymbol{T} = \frac{1}{\det(\boldsymbol{J})}\boldsymbol{J}\left(p\boldsymbol{E_3} + (\lambda I_1\boldsymbol{E_3} + 2\mu\boldsymbol{\eta}) + \left(lI_1^2 - 2mI_2\right)\boldsymbol{E_3} + 2mI_1\boldsymbol{\eta} + n\ \mathrm{co}\,\boldsymbol{\eta}\right)\boldsymbol{J}^T. \quad (2.42)$$

For zero strain it holds that $\boldsymbol{\eta}$ becomes a zero matrix, resulting in the strain invariants being zero and the Jacobian matrix $\boldsymbol{J}$ becoming orthogonal. In this case, the expression for the initial stress,

$$\boldsymbol{T_0} = p\boldsymbol{E_3} = \begin{pmatrix} p & 0 & 0 \\ 0 & p & 0 \\ 0 & 0 & p \end{pmatrix}, \quad (2.43)$$

is obtained where p denotes a strain-independent hydrostatic stress.

A.5. Connection between stress and wave velocity

This section acts as a link between Murnaghan's description of the stress and Hughes and Kelly's formulations of the wave velocity of a stressed medium. By adopting the index notation and rewriting the expression of the strain energy [11], the wave equation is obtained. The formulations of the wave velocity, expressed in terms of the stress and the Murnaghan constants, follows from the wave equation.

A.5.1. Cauchy's first law of motion

Through the principle of virtual work, a system of equations of equilibrium is obtained:

$$\left(\boldsymbol{\nabla_x}\,\boldsymbol{T}\right)^T + \rho_x\boldsymbol{X_x} = \boldsymbol{0}, \quad (2.32)$$

which, upon introducing an inertia term, yields Cauchy's first law of motion:

$$\left(\boldsymbol{\nabla_x}\,\boldsymbol{T}\right)^T + \rho_x\boldsymbol{X_x} = \rho_x\ddot{\boldsymbol{x}}, \quad (2.44)$$

where $\ddot{\boldsymbol{x}}$ denotes the 3 x 1 vector containing the second time derivatives of the final coordinates, i.e. their accelerations. Note that this expression is the Eulerian form of Cauchy's first law of motion. The Cauchy stress matrix $\boldsymbol{T}$ is describes the stress, occurring after a deformation, acting on the deformed medium. However, in some cases it is more convenient to use an alternative stress description which is related to the initial configuration, of which the element definitions are assumed to be known. This alternative stress description can be obtained by assuming a portion of a force $\boldsymbol{df}$ acting on both the initial and final scalar element of area, like depicted in Figure A.5.

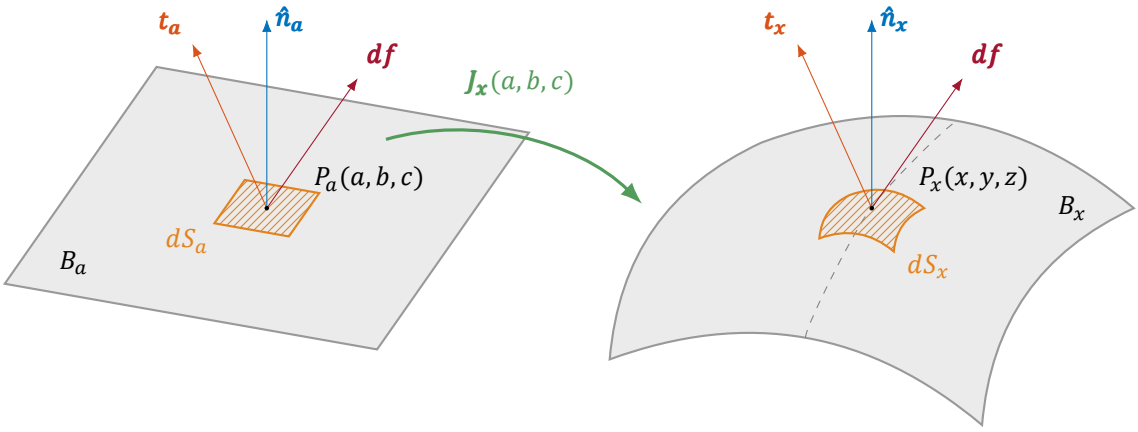

Figure A.5: Visualisation of the initial and final scalar elements of area and their respective force vectors.

The portion of the force $\boldsymbol{df}$ can be described with two equivalent expressions:

$$\boldsymbol{t_a} dS_a = \boldsymbol{df} = \boldsymbol{t_x} dS_x, \tag{2.45}$$

where $\boldsymbol{t_a}$ denotes the traction vector acting on the initial scalar element of area dS_a. The traction vector $\boldsymbol{t_x}$ is related to the Cauchy stress matrix through the Cauchy stress equation. Similarly, the traction $\boldsymbol{t_a}$ can be expressed in terms of a stress description such that equation (2.45) becomes:

$$\boldsymbol{\sigma}^T \hat{\boldsymbol{n}}_{\boldsymbol{a}} dS_a = \boldsymbol{df} = \boldsymbol{T}^T \hat{\boldsymbol{n}}_{\boldsymbol{x}} dS_x, \tag{2.46}$$

which, upon substitution of definition (A.15), can be simplified to:

$$\boldsymbol{\sigma}^T \boldsymbol{dS^a} = \boldsymbol{T}^T \boldsymbol{dS^x}, \tag{A.141}$$

where, $\boldsymbol{\sigma}$ denotes the nominal stress matrix which describes the stress, occurring after a deformation, acting on the undeformed medium. Both matrix elements of area can be related to each other through Nanson's formula (A.43):

$$\boldsymbol{dS^x} = \det(\boldsymbol{J})\, \boldsymbol{J}^{-T} \boldsymbol{dS^a}. \tag{A.142}$$

Therefore, relation (A.141) can be written as:

$$\boldsymbol{\sigma}^T \boldsymbol{dS^a} = \boldsymbol{T}^T \det(\boldsymbol{J})\, \boldsymbol{J}^{-T} \boldsymbol{dS^a}. \tag{A.143}$$

Upon substitution of definition (2.38), the above becomes:

$$\boldsymbol{\sigma}^T = \det(\boldsymbol{J}) \left(\frac{1}{\det(\boldsymbol{J})}\, \boldsymbol{J} \frac{\partial \phi}{\partial \boldsymbol{\eta}}\, \boldsymbol{J}^T \right) \boldsymbol{J}^{-T}, \tag{A.144}$$

which can be simplified to:

$$\boldsymbol{\sigma}^T = \boldsymbol{J} \frac{\partial \phi}{\partial \boldsymbol{\eta}}. \tag{A.145}$$

Here, $\boldsymbol{\sigma}^T = \boldsymbol{P}$ is defined as the first Piola-Kirchoff stress tensor, which describes the stress acting on the undeformed body. It should be noted that $\boldsymbol{\sigma}$ and $\boldsymbol{P}$ are symmetric, only and only if, the Jacobian matrix $\boldsymbol{J}$ is symmetric as well. The nominal stress matrix $\boldsymbol{\sigma}$ is then defined as:

$$\boldsymbol{\sigma} = \frac{\partial \phi}{\partial \boldsymbol{\eta}}\, \boldsymbol{J}^T. \tag{2.47}$$

By using the law of conservation of mass, $\rho_a dV_a = \rho_x dV_x$, expression (2.44) can be rewritten such that the Lagrangian form of Cauchy's first law of motion is obtained:

$$\left(\boldsymbol{\nabla_a}\, \boldsymbol{\sigma}\right)^T + \rho_a \boldsymbol{X_a} = \rho_a \ddot{\boldsymbol{x}}, \tag{2.48}$$

where $\left(\boldsymbol{\nabla_a}\, \boldsymbol{\sigma}\right)^T$ denotes the divergence of the nominal stress $\boldsymbol{\sigma}$ with respect to the initial coordinates and $\boldsymbol{X_a}$ – the initial mass forces.

A.5.2. Elastic coefficients

In order to solve for this equation of motion, it is convenient to introduce the index notation. For the purpose of this index notation it is necessary to rewrite the formulation of the strain energy,

$$\phi = pI_1 + \frac{\lambda + 2\mu}{2} I_1^2 - 2\mu I_2 + \frac{l + 2m}{3} I_1^3 - 2mI_1 I_2 + nI_3, \tag{A.146}$$

as a power series of the traces of the strain matrix $\boldsymbol{\eta}$. From relation (A.67) it is clear that the first strain invariant $I_1 = \mathrm{Tr}(\boldsymbol{\eta})$. When writing out the expression (A.70) it is possible to express the second strain invariant I_2 as:

$$I_2 = \mathrm{Tr}(\mathrm{co}\, \boldsymbol{\eta}) = \tfrac{1}{2}\Big(\mathrm{Tr}(\boldsymbol{\eta})^2 - \mathrm{Tr}(\boldsymbol{\eta}^2)\Big). \tag{A.147}$$

By using a similar approach for expression (A.73), the third strain invariant I_3 can be rewritten to:

$$I_3 = \det(\boldsymbol{\eta}) = \tfrac{1}{3}\Big(\tfrac{1}{2}\mathrm{Tr}(\boldsymbol{\eta})^3 - \tfrac{3}{2}\mathrm{Tr}(\boldsymbol{\eta})\mathrm{Tr}(\boldsymbol{\eta}^2) + \mathrm{Tr}(\boldsymbol{\eta}^3)\Big). \tag{A.148}$$

Upon substitution of these new found expressions in (A.146), the strain energy can be formulated as:

$$\begin{aligned}\phi(\boldsymbol{\eta}) = p\mathrm{Tr}(\boldsymbol{\eta}) + \frac{\lambda+2\mu}{2}\mathrm{Tr}(\boldsymbol{\eta})^2 - 2\mu\Big[\tfrac{1}{2}\Big(\mathrm{Tr}(\boldsymbol{\eta})^2 - \mathrm{Tr}(\boldsymbol{\eta}^2)\Big)\Big] + \frac{l+2m}{3}\mathrm{Tr}(\boldsymbol{\eta})^3 \\ - 2m\mathrm{Tr}(\boldsymbol{\eta})\Big[\tfrac{1}{2}\Big(\mathrm{Tr}(\boldsymbol{\eta})^2 - \mathrm{Tr}(\boldsymbol{\eta}^2)\Big)\Big] + \tfrac{1}{3}n\Big(\tfrac{1}{2}\mathrm{Tr}(\boldsymbol{\eta})^3 - \tfrac{3}{2}\mathrm{Tr}(\boldsymbol{\eta})\mathrm{Tr}(\boldsymbol{\eta}^2) + \mathrm{Tr}(\boldsymbol{\eta}^3)\Big).\end{aligned} \tag{A.149}$$

Assuming that the strain energy is minimal when there is zero strain, the linear term can be neglected. Elaborating further relation (A.149) then yields:

$$\phi(\boldsymbol{\eta}) = \frac{\lambda}{2}\mathrm{Tr}(\boldsymbol{\eta})^2 + \mu\mathrm{Tr}(\boldsymbol{\eta}^2) + \Big(m - \tfrac{1}{2}n\Big)\mathrm{Tr}(\boldsymbol{\eta})\mathrm{Tr}(\boldsymbol{\eta}^2) + \frac{\Big(l - m + \frac{1}{2}n\Big)}{3}\mathrm{Tr}(\boldsymbol{\eta})^3 + \frac{n}{3}\mathrm{Tr}(\boldsymbol{\eta}^3). \tag{A.150}$$

From now on the index notation will be adopted. By writing out the powers of the trace $\mathrm{Tr}(\boldsymbol{\eta})$, it can be found that they can be represented with the following:

$$\begin{aligned}\mathrm{Tr}(\boldsymbol{\eta}) &= \delta_{ij}\eta_{ij} \\ \mathrm{Tr}(\boldsymbol{\eta})^2 &= \delta_{ij}\delta_{kl}\eta_{ij}\eta_{kl} \\ \mathrm{Tr}(\boldsymbol{\eta})^3 &= \delta_{ij}\delta_{kl}\delta_{mn}\eta_{ij}\eta_{kl}\eta_{mn},\end{aligned} \tag{A.151}$$

where δ_{ij} denotes the Kronecker delta,

$$\delta_{ij} = \begin{cases} 1 & ; \quad \text{for} \quad i = j \\ 0 & ; \quad \text{else} \end{cases}, \tag{2.54}$$

and $i, j, k, l, m, n \in \{1, 2, 3\}$. The index notation of the traces of the power of the strain matrix must include all possible combinations of strain components η_{ij}. The trace of the squared strain matrix, $\mathrm{Tr}(\boldsymbol{\eta}^2)$, then becomes:

$$\mathrm{Tr}(\boldsymbol{\eta}^2) = I_{ijkl}\eta_{ij}\eta_{kl}, \tag{A.152}$$

whereas the trace of the cubed strain matrix, $\mathrm{Tr}(\boldsymbol{\eta}^3)$, becomes:

$$\mathrm{Tr}(\boldsymbol{\eta}^3) = \tfrac{1}{4}\Big(\delta_{ik}I_{jlmn} + \delta_{il}I_{jkmn} + \delta_{jk}I_{ilmn} + \delta_{jl}I_{ikmn}\Big)\eta_{ij}\eta_{kl}\eta_{mn}, \tag{A.153}$$

where I_{ijkl} denotes the fourth-order tensor which is defined as:

$$I_{ijkl} = \tfrac{1}{2}\Big(\delta_{ik}\delta_{jl} + \delta_{il}\delta_{jk}\Big). \tag{2.53}$$

The linear combination $\mathrm{Tr}(\boldsymbol{\eta})\mathrm{Tr}(\boldsymbol{\eta}^2)$ can then be written as:

$$\mathrm{Tr}(\boldsymbol{\eta})\mathrm{Tr}(\boldsymbol{\eta}^2) = \tfrac{1}{3}\Big(\delta_{ij}I_{klmn} + \delta_{kl}I_{mnij} + \delta_{mn}I_{ijkl}\Big)\eta_{ij}\eta_{kl}\eta_{mn}. \tag{A.154}$$

By using these newfound expressions the strain energy (A.150) can be written as a power series of elastic coefficients:

$$\phi = \tfrac{1}{2!}C_{ijkl}\eta_{ij}\eta_{kl} + \tfrac{1}{3!}C_{ijklmn}\eta_{ij}\eta_{kl}\eta_{mn} + \dots \tag{2.50}$$

where the fourth-order tensor C_{ijkl} is defined as:

$$C_{ijkl} = \lambda\delta_{ij}\delta_{kl} + 2\mu I_{ijkl} \tag{2.51}$$

and the sixth-order tensor C_{ijklmn} is defined as:

$$\begin{aligned}C_{ijklmn} = 2\Big(l - m + \tfrac{1}{2}n\Big)\delta_{ij}\delta_{kl}\delta_{mn} + 2\Big(m - \tfrac{1}{2}n\Big)\Big(\delta_{ij}I_{klmn} + \delta_{kl}I_{mnij} + \delta_{mn}I_{ijkl}\Big) \\ + \tfrac{1}{2}n\Big(\delta_{ik}I_{jlmn} + \delta_{il}I_{jkmn} + \delta_{jk}I_{ilmn} + \delta_{jl}I_{ikmn}\Big).\end{aligned} \tag{2.52}$$

A.5.3. Expansion of the nominal stress tensor

By transposing relation (A.56), it possible to express the Jacobian matrix $\boldsymbol{J}^T$ as:

$$\boldsymbol{J}^T = \begin{pmatrix} x_a & y_a & z_a \\ x_b & y_b & z_b \\ x_c & y_c & z_c \end{pmatrix} = \begin{pmatrix} u_a + 1 & v_a & w_a \\ u_b & v_b + 1 & w_b \\ u_c & v_c & w_c + 1 \end{pmatrix}, \tag{A.155}$$

which, upon generalising, yields the gradient tensor

$$J_{i\alpha} = \frac{\partial u_i}{\partial a_\alpha} + \delta_{i\alpha}. \tag{2.56}$$

The nominal stress matrix $\boldsymbol{\sigma}$ can then be written into the simplified index notation with:

$$\sigma_{\beta q} = \frac{\partial \phi}{\partial \eta_{\alpha\beta}} J_{\alpha q}, \tag{2.49}$$

where η_{kl} denotes the Lagrangian strain tensor which follows from relations (A.61) and (A.62):

$$\eta_{kl} = \frac{1}{2}\left(\frac{\partial u_l}{\partial a_k} + \frac{\partial u_k}{\partial a_l} + \frac{\partial u_i}{\partial a_k}\frac{\partial u_i}{\partial a_l}\right). \tag{2.55}$$

Relation (2.49) can be expanded by substituting definitions (2.50) and (2.56):

$$\sigma_{\beta q} = \left(\frac{\partial u_\alpha}{\partial a_q} + \delta_{\alpha q}\right)\frac{\partial}{\partial \eta_{\alpha\beta}}\left(\frac{1}{2!}C_{ijkl}\eta_{ij}\eta_{kl} + \frac{1}{3!}C_{ijklmn}\eta_{ij}\eta_{kl}\eta_{mn} + \dots\right), \tag{A.156}$$

which, after applying the chain rule of differentiation, becomes:

$$\begin{aligned} \sigma_{\beta q} \approx & \left(\frac{\partial u_\alpha}{\partial a_q} + \delta_{\alpha q}\right)\left[\frac{1}{2}\left(C_{ijkl}\frac{\partial \eta_{ij}}{\eta_{\alpha\beta}}\eta_{kl} + C_{ijkl}\eta_{ij}\frac{\partial \eta_{kl}}{\eta_{\alpha\beta}}\right)\right. \\ & \left. + \frac{1}{3!}\left(C_{ijklmn}\frac{\partial \eta_{ij}}{\eta_{\alpha\beta}}\eta_{kl}\eta_{mn} + C_{ijklmn}\eta_{ij}\frac{\partial \eta_{kl}}{\eta_{\alpha\beta}}\eta_{mn} + C_{ijklmn}\eta_{ij}\eta_{kl}\frac{\partial \eta_{mn}}{\eta_{\alpha\beta}}\right)\right] \\ = & \left(\frac{\partial u_\alpha}{\partial a_q} + \delta_{\alpha q}\right)\left[\frac{1}{2}\left(C_{\alpha\beta kl}\eta_{kl} + C_{ij\alpha\beta}\eta_{ij}\right)\right. \\ & \left. + \frac{1}{3!}\left(C_{\alpha\beta klmn}\eta_{kl}\eta_{mn} + C_{ij\alpha\beta mn}\eta_{ij}\eta_{mn} + C_{ijkl\alpha\beta}\eta_{ij}\eta_{kl}\right)\right]. \end{aligned} \tag{2.57}$$

Upon substitution of relation (2.55) and using the fact that the fourth-order elastic tensors are symmetric, i.e. $C_{ij\alpha\beta} = C_{\alpha\beta ij}$, the nominal stress tensor becomes:

$$\begin{aligned} \sigma_{\beta q} \approx & \left(\frac{\partial u_\alpha}{\partial a_q} + \delta_{\alpha q}\right)\left\{\frac{1}{2}C_{\alpha\beta kl}\left(\frac{\partial u_l}{\partial a_k} + \frac{\partial u_k}{\partial a_l} + \frac{\partial u_r}{\partial a_k}\frac{\partial u_r}{\partial a_l}\right)\right. \\ & + \frac{1}{3!}\left[\frac{1}{4}C_{\alpha\beta klmn}\left(\frac{\partial u_l}{\partial a_k} + \frac{\partial u_k}{\partial a_l} + \frac{\partial u_r}{\partial a_k}\frac{\partial u_r}{\partial a_l}\right)\left(\frac{\partial u_n}{\partial a_m} + \frac{\partial u_m}{\partial a_n} + \frac{\partial u_s}{\partial a_m}\frac{\partial u_s}{\partial a_n}\right)\right. \\ & + \frac{1}{4}C_{ij\alpha\beta mn}\left(\frac{\partial u_j}{\partial a_i} + \frac{\partial u_i}{\partial a_j} + \frac{\partial u_r}{\partial a_i}\frac{\partial u_r}{\partial a_j}\right)\left(\frac{\partial u_n}{\partial a_m} + \frac{\partial u_m}{\partial a_n} + \frac{\partial u_s}{\partial a_m}\frac{\partial u_s}{\partial a_n}\right) \\ & \left.\left. + \frac{1}{4}C_{ijkl\alpha\beta}\left(\frac{\partial u_j}{\partial a_i} + \frac{\partial u_i}{\partial a_j} + \frac{\partial u_r}{\partial a_i}\frac{\partial u_r}{\partial a_j}\right)\left(\frac{\partial u_l}{\partial a_k} + \frac{\partial u_k}{\partial a_l} + \frac{\partial u_r}{\partial a_k}\frac{\partial u_r}{\partial a_l}\right)\right]\right\}. \end{aligned} \tag{A.157}$$

By neglecting the terms of the third order and higher in $\frac{\partial u_i}{\partial a_j}$, relation (A.157) expands to:

$$\begin{aligned}\sigma_{\beta q} \approx{}& \frac{1}{2}C_{q\beta kl}\left(\frac{\partial u_l}{\partial a_k}+\frac{\partial u_k}{\partial a_l}\right)+\frac{1}{2}C_{q\beta kl}\frac{\partial u_r}{\partial a_k}\frac{\partial u_r}{\partial a_l}+\frac{1}{2}C_{\alpha\beta kl}\left(\frac{\partial u_l}{\partial a_k}\frac{\partial u_\alpha}{\partial a_q}+\frac{\partial u_k}{\partial a_l}\frac{\partial u_\alpha}{\partial a_q}\right)\\ &+\frac{1}{3!}\left[\frac{1}{4}C_{q\beta klmn}\left(\frac{\partial u_l}{\partial a_k}\frac{\partial u_n}{\partial a_m}+\frac{\partial u_l}{\partial a_k}\frac{\partial u_m}{\partial a_n}+\frac{\partial u_k}{\partial a_l}\frac{\partial u_n}{\partial a_m}+\frac{\partial u_k}{\partial a_l}\frac{\partial u_m}{\partial a_n}\right)\right.\\ &+\frac{1}{4}C_{ijq\beta mn}\left(\frac{\partial u_j}{\partial a_i}\frac{\partial u_n}{\partial a_m}+\frac{\partial u_j}{\partial a_i}\frac{\partial u_m}{\partial a_n}+\frac{\partial u_i}{\partial a_j}\frac{\partial u_n}{\partial a_m}+\frac{\partial u_i}{\partial a_j}\frac{\partial u_m}{\partial a_n}\right)\\ &\left.+\frac{1}{4}C_{ijklq\beta}\left(\frac{\partial u_j}{\partial a_i}\frac{\partial u_l}{\partial a_k}+\frac{\partial u_j}{\partial a_i}\frac{\partial u_k}{\partial a_l}+\frac{\partial u_i}{\partial a_j}\frac{\partial u_l}{\partial a_k}+\frac{\partial u_i}{\partial a_j}\frac{\partial u_k}{\partial a_l}\right)\right].\end{aligned} \tag{A.158}$$

Through multiplications with the Kronecker delta in the expression above, the indices of the partial derivatives of the displacements with respect to the initial coordinates can be manipulated. By doing this, all terms can be rewritten in the same derivatives:

$$\begin{aligned}\sigma_{ji} \approx{}& C_{ijkl}\frac{\partial u_k}{\partial a_l}+\frac{1}{2}C_{ijln}\delta_{km}\frac{\partial u_k}{\partial a_l}\frac{\partial u_m}{\partial a_n}+\frac{1}{2}C_{jnkl}\delta_{nm}\delta_{in}\frac{\partial u_k}{\partial a_l}\frac{\partial u_m}{\partial a_n}\\ &+\frac{1}{2}C_{jlmn}\delta_{lk}\delta_{il}\frac{\partial u_k}{\partial a_l}\frac{\partial u_m}{\partial a_n}+\frac{1}{2}C_{ijklmn}\frac{\partial u_k}{\partial a_l}\frac{\partial u_m}{\partial a_n},\end{aligned} \tag{A.159}$$

which after elaborating further can be simplified to:

$$\sigma_{ji} = C_{ijkl}\frac{\partial u_k}{\partial a_l}+\frac{1}{2}M_{ijklmn}\frac{\partial u_k}{\partial a_l}\frac{\partial u_m}{\partial a_n}+\ldots, \tag{2.58}$$

where the sixth-order tensor M_{ijklmn} is defined as:

$$M_{ijklmn} = C_{ijklmn}+C_{ijln}\delta_{km}+C_{jnkl}\delta_{im}+C_{jlmn}\delta_{ik}. \tag{2.59}$$

According to the theory of infinitesimal deformations, the higher-order strains are much less than the first-order strains. For these small deformations the initial and final coordinates are assumed to be equal. Therefore, upon omitting the higher-order strain terms, the linearised nominal stress tensor is obtained:

$$\sigma_{ji} \approx C_{ijkl}\frac{\partial u_k}{\partial x_l}. \tag{2.60}$$

A.5.4. Wave equation

Now that expression of the nominal stress tensor is obtained, it is possible to rewrite the Lagrangian form of Cauchy's first law of motion. First it is assumed there is small dynamic deformation $\boldsymbol{u}^{(1)}$ superposed on the large static deformation $\boldsymbol{u}^{(0)}$. The total deformation is then defined as:

$$\boldsymbol{u} = \boldsymbol{u}^{(0)}+\boldsymbol{u}^{(1)} = \boldsymbol{x}'-\boldsymbol{a}, \tag{2.62}$$

where $\boldsymbol{x}'$ denotes the new position after this dynamic deformation has occurred:

$$\boldsymbol{x}' = \begin{pmatrix}x'\\ y'\\ z'\end{pmatrix} = \begin{pmatrix}u^{(1)}+x\\ v^{(1)}+y\\ w^{(1)}+z\end{pmatrix}, \tag{2.63}$$

or, equivalently, in index notation:

$$x_i' = u_i^{(1)}+x_i. \tag{2.64}$$

After rewriting relation (2.48) with the index notation and neglecting the mass forces, the Lagrangian form of Cauchy's first law of motion in this new position reads:

$$\frac{\partial \sigma_{ji}}{\partial a_j} = \rho_a \frac{\partial x_i'}{\partial t^2}, \tag{2.65}$$

which, upon substituting relation (2.64) and elaborating the time-dependent part, becomes:

$$\rho_a \frac{\partial u_i^{(1)}}{\partial t^2} - \frac{\partial \sigma_{ji}}{\partial a_j} = 0. \tag{2.66}$$

The space-dependent part can be expressed in terms of the final coordinates x_k by rewriting the partial derivative with respect to the initial coordinates a_j. Through the application of the chain rule of differentiation the following holds:

$$\begin{aligned} \frac{\partial}{\partial a_j} &= \frac{\partial}{\partial x_k}\frac{\partial x_k}{\partial a_j} \\ &= \frac{\partial}{\partial x_k}\frac{\partial}{\partial a_j}\left(a_k + u_k^{(0)}\right) \\ &= \frac{\partial}{\partial x_k}\left(\frac{\partial a_k}{\partial a_j} + \frac{\partial u_k^{(0)}}{\partial a_j}\right) \\ &= \frac{\partial}{\partial x_j} + \frac{\partial u_k^{(0)}}{\partial a_j}\frac{\partial}{\partial x_k}. \end{aligned} \tag{A.160}$$

After repeating the same elaboration for $\frac{\partial u_k^{(0)}}{\partial a_j}$, the above becomes:

$$\frac{\partial}{\partial a_j} = \frac{\partial}{\partial x_j} + u_{k,j}^{(0)}\frac{\partial}{\partial x_k} + \ldots, \tag{2.67}$$

where $u_{k,j}^{(0)}$ denotes the short notation for the derivative of $u_k^{(0)}$ with respect to x_j.

Now, the space-dependent part of (2.66) can be expanded by substituting definition (2.58):

$$\begin{aligned} \frac{\partial \sigma_{ji}}{\partial a_j} &\approx \frac{\partial \sigma_{ji}}{\partial x_j} + u_{p,j}^{(0)}\frac{\partial \sigma_{ji}}{\partial x_p} \\ &\approx C_{ijkl}\frac{\partial}{\partial x_j}\left(\frac{\partial u_k}{\partial x_l} + u_{q,l}^{(0)}\frac{\partial u_k}{\partial x_q}\right) + u_{p,j}^{(0)}C_{ijkl}\frac{\partial}{\partial x_j}\left(\frac{\partial u_k}{\partial x_l} + u_{q,l}^{(0)}\frac{\partial u_k}{\partial x_q}\right) \\ &\quad + \frac{1}{2}M_{ijklmn}\frac{\partial}{\partial x_j}\left[\left(\frac{\partial u_k}{\partial x_l} + u_{q,l}^{(0)}\frac{\partial u_k}{\partial x_q}\right)\left(\frac{\partial u_m}{\partial x_n} + u_{r,n}^{(0)}\frac{\partial u_m}{\partial x_r}\right)\right] + u_{p,j}^{(0)}\frac{1}{2}M_{ijklmn}\frac{\partial}{\partial x_j}\left[\ldots\right] \\ &\quad + \ldots \end{aligned} \tag{2.69}$$

which, upon using the chain rule of differentiation, becomes:

$$\begin{aligned} \frac{\partial \sigma_{ji}}{\partial a_j} \approx\ & C_{ijkl}\left(\frac{\partial^2 u_k}{\partial x_j \partial x_l} + u_{q,l}^{(0)}\frac{\partial^2 u_k}{\partial x_j \partial x_q} + u_{q,lj}^{(0)}\frac{\partial u_k}{\partial x_q}\right) \\ & + u_{p,j}^{(0)}C_{ijkl}\left(\frac{\partial^2 u_k}{\partial x_p \partial x_l} + u_{q,l}^{(0)}\frac{\partial^2 u_k}{\partial x_p \partial x_q} + u_{q,lp}^{(0)}\frac{\partial u_k}{\partial x_q}\right) \\ & + \frac{1}{2}M_{ijklmn}\left[\left(\frac{\partial^2 u_k}{\partial x_j \partial x_l} + u_{q,l}^{(0)}\frac{\partial^2 u_k}{\partial x_j \partial x_q} + u_{q,lj}^{(0)}\frac{\partial u_k}{\partial x_q}\right)\left(\frac{\partial u_m}{\partial x_n} + u_{r,n}^{(0)}\frac{\partial u_m}{\partial x_r}\right)\right. \\ & \left. + \left(\frac{\partial u_k}{\partial x_l} + u_{q,l}^{(0)}\frac{\partial u_k}{\partial x_q}\right)\left(\frac{\partial^2 u_m}{\partial x_j \partial x_n} + u_{r,n}^{(0)}\frac{\partial^2 u_m}{\partial x_j \partial x_r} + u_{r,nj}^{(0)}\frac{\partial u_m}{\partial x_r}\right)\right] \\ & + u_{p,j}^{(0)}\frac{1}{2}M_{ijklmn}\frac{\partial}{\partial x_j}\left[\ldots\right] + \ldots \end{aligned} \tag{A.161}$$

If it is assumed that the total stress σ_{ji} has contributions from both the static displacement, $\sigma_{ji}^{(0)}\left(u_k^{(0)}\right)$, and from the additional dynamic displacement, $\sigma_{ji}^{(1)}\left(u_k^{(1)}\right)$, then it follows that:

$$\frac{\partial \sigma_{ji}(u_k)}{\partial a_j} = \frac{\partial \sigma_{ji}^{(0)}\left(u_k^{(0)}\right)}{\partial a_j} + \frac{\partial \sigma_{ji}^{(1)}\left(u_k^{(1)}\right)}{\partial a_j}. \tag{A.162}$$

Substituting the above in relation (2.66) yields:

$$\rho_a \frac{\partial u_i^{(1)}}{\partial t^2} - \left(\frac{\partial \sigma_{ji}^{(0)}\left(u_k^{(0)}\right)}{\partial a_j} + \frac{\partial \sigma_{ji}^{(1)}\left(u_k^{(1)}\right)}{\partial a_j} \right) = 0, \tag{A.163}$$

from which follows that if the medium is at rest, i.e. $\boldsymbol{u}^{(1)} = \mathbf{0}$:

$$\frac{\partial \sigma_{ji}^{(0)}\left(u_k^{(0)}\right)}{\partial a_j} = 0. \tag{A.164}$$

Therefore, relation (A.161) can be further elaborated by expanding the total displacement $u_k = u_k^{(0)} + u_k^{(1)}$ and omitting the terms that are solely depending on the static displacement $u_k^{(0)}$.

By assuming that the second-order derivatives of the static displacements and the multiplications between derivatives of the dynamic displacements are insignificant, relation (A.161) simplifies to:

$$\begin{aligned}
\frac{\partial \sigma_{ji}}{\partial a_j} \approx\ & C_{ijkl}\left(\frac{\partial^2 u_k^{(1)}}{\partial x_j \partial x_l} + u_{q,l}^{(0)} \frac{\partial^2 u_k^{(1)}}{\partial x_j \partial x_q} \right) + u_{p,j}^{(0)} C_{ijkl}\left(\frac{\partial^2 u_k^{(1)}}{\partial x_p \partial x_l} \right) \\
& + \frac{1}{2} M_{ijklmn}\left[\left(\frac{\partial^2 u_k^{(1)}}{\partial x_j \partial x_l} + u_{q,l}^{(0)} \frac{\partial^2 u_k^{(1)}}{\partial x_j \partial x_q} \right)\left(u_{m,n}^{(0)} + \frac{\partial u_m^{(1)}}{\partial x_n} + u_{r,n}^{(0)} \frac{\partial u_m^{(1)}}{\partial x_r} \right) \right. \\
& \left. + \left(u_{k,l}^{(0)} + \frac{\partial u_k^{(1)}}{\partial x_l} + u_{q,l}^{(0)} \frac{\partial u_k^{(1)}}{\partial x_q} \right)\left(\frac{\partial^2 u_m^{(1)}}{\partial x_j \partial x_n} + u_{r,n}^{(0)} \frac{\partial^2 u_m^{(1)}}{\partial x_j \partial x_r} \right) \right] + \dots \\
\approx\ & C_{ijkl}\left(\frac{\partial^2 u_k^{(1)}}{\partial x_j \partial x_l} + u_{q,l}^{(0)} \frac{\partial^2 u_k^{(1)}}{\partial x_j \partial x_q} \right) + u_{p,j}^{(0)} C_{ijkl}\left(\frac{\partial^2 u_k^{(1)}}{\partial x_p \partial x_l} \right) \\
& + \frac{1}{2} M_{ijklmn}\left(u_{m,n}^{(0)} \frac{\partial^2 u_k^{(1)}}{\partial x_j \partial x_l} + u_{k,l}^{(0)} \frac{\partial^2 u_m^{(1)}}{\partial x_j \partial x_n} \right) + \dots,
\end{aligned} \tag{A.165}$$

which can be further elaborated by substituting definition (2.59) and manipulating the indices of the partial derivatives:

$$\begin{aligned}
\frac{\partial \sigma_{ji}}{\partial a_j} \approx\ & C_{ijkl}\left(\frac{\partial^2 u_k^{(1)}}{\partial x_j \partial x_l} + u_{q,l}^{(0)} \frac{\partial^2 u_k^{(1)}}{\partial x_j \partial x_q} \right) + u_{p,j}^{(0)} C_{ijkl}\left(\frac{\partial^2 u_k^{(1)}}{\partial x_p \partial x_l} \right) \\
& + \frac{1}{2}\left(C_{ijklmn} + C_{ijln}\delta_{km} + C_{jnkl}\delta_{im} + C_{jlmn}\delta_{ik} \right)\left(u_{m,n}^{(0)} \frac{\partial^2 u_k^{(1)}}{\partial x_j \partial x_l} + u_{k,l}^{(0)} \frac{\partial^2 u_m^{(1)}}{\partial x_j \partial x_n} \right) \\
\approx\ & \left(C_{ijkl} + C_{ijkq} u_{l,q}^{(0)} + C_{ipkl} u_{j,p}^{(0)} \right) \frac{\partial^2 u_k^{(1)}}{\partial x_j \partial x_l} \\
& + \frac{1}{2}\left[C_{ijklmn}\left(u_{m,n}^{(0)} + \delta_{km}\delta_{ln} u_{k,l}^{(0)} \right) + C_{ijln}\left(u_{k,n}^{(0)} + \delta_{ln} u_{k,l}^{(0)} \right) \right. \\
& \left. + C_{jnkl}\left(u_{i,n}^{(0)} + \delta_{ik}\delta_{ln} u_{k,l}^{(0)} \right) + C_{jlmn}\left(\delta_{ik} u_{m,n}^{(0)} + \delta_{ik}\delta_{km}\delta_{ln} u_{k,l}^{(0)} \right) \right] \frac{\partial^2 u_k^{(1)}}{\partial x_j \partial x_l}.
\end{aligned} \tag{A.166}$$

Relation (A.166) can be simplified by elaborating the Kronecker delta and factorising the second-order spatial derivative:

$$\begin{aligned}\frac{\partial \sigma_{ji}}{\partial a_j} \approx & \left(C_{ijkl} + C_{ijkq}u_{l,q}^{(0)} + C_{ipkl}u_{j,p}^{(0)}\right)\frac{\partial^2 u_k^{(1)}}{\partial x_j \partial x_l} \\ & + \frac{1}{2}\Big[C_{ijklmn}\left(u_{m,n}^{(0)} + u_{m,n}^{(0)}\right) + C_{ijln}\left(u_{k,n}^{(0)} + u_{k,n}^{(0)}\right) \\ & + C_{jnkl}\left(u_{i,n}^{(0)} + u_{i,n}^{(0)}\right) + C_{jlmn}\left(\delta_{ik}u_{m,n}^{(0)} + \delta_{ik}u_{m,n}^{(0)}\right)\Big]\frac{\partial^2 u_k^{(1)}}{\partial x_j \partial x_l} \\ \approx & \Big(C_{ijkl} + C_{ijkq}u_{l,q}^{(0)} + C_{ipkl}u_{j,p}^{(0)} + C_{ijklmn}u_{m,n}^{(0)} + C_{ijln}u_{k,n}^{(0)} + C_{jnkl}u_{i,n}^{(0)} \\ & + C_{jlmn}\delta_{ik}u_{m,n}^{(0)}\Big)\frac{\partial^2 u_k^{(1)}}{\partial x_j \partial x_l},\end{aligned} \tag{A.167}$$

which, upon substitution in the Lagrangian form of Cauchy's first law of motion (2.66), yields:

$$\rho_a \frac{\partial^2 u_i^{(1)}}{\partial t^2} - B_{ijkl}\frac{\partial^2 u_k^{(1)}}{\partial x_j \partial x_l} = 0. \tag{2.71}$$

where the fourth-order tensor,

$$B_{ijkl} = C_{ijkl} + \delta_{ik}C_{jlqr}u_{q,r}^{(0)} + C_{rjkl}u_{i,r}^{(0)} + C_{irkl}u_{j,r}^{(0)} + C_{ijrl}u_{k,r}^{(0)} + C_{ijkr}u_{l,r}^{(0)} + C_{ijklmn}u_{m,n}^{(0)}, \tag{2.72}$$

denotes the effective elastic moduli.

A.5.5. Wave velocity

By dividing both sides of relation (2.71) by the initial mass density ρ_a, the wave equation is obtained:

$$\frac{\partial^2 u_i^{(1)}}{\partial t^2} - c_{ji}^2\frac{\partial^2 u_k^{(1)}}{\partial x_j \partial x_l} = 0, \tag{2.73}$$

where the second-order tensor,

$$c_{ji} = \sqrt{\frac{B_{ijkl}}{\rho_a}}, \tag{2.74}$$

denotes the velocity of a wave polarising in the i-direction while propagating in the j-direction.

A longitudinal wave propagating along the x-direction is considered, for which relation (2.73) becomes

$$\frac{\partial^2 u^{(1)}}{\partial t^2} - c_{xx}^2\frac{\partial^2 u^{(1)}}{\partial x^2} = 0, \tag{2.75}$$

where the expression for the wave velocity is

$$c_{xx} = \sqrt{\frac{B_{1111}}{\rho_a}}. \tag{A.168}$$

The fourth-order tensor B_{1111} can be expanded by using relation (2.72) and the following definition:

$$u_{k,j}^{(0)} = \frac{\partial u_k^{(0)}}{\partial x_j} = \begin{cases} e_{jk} & ; \quad \text{for} \quad j = k \\ 0 & ; \quad \text{else} \end{cases}, \tag{2.68}$$

where e_{jk} denotes the first-order approximation of the strain. After collecting similar terms, B_{1111} becomes:

$$B_{1111} = C_{1111} + \left(5C_{1111} + C_{111111}\right)u_{1,1}^{(0)} + \left(C_{1122} + C_{111122}\right)u_{2,2}^{(0)} + \left(C_{1133} + C_{111133}\right)u_{3,3}^{(0)}, \tag{A.169}$$

where the fourth-order tensors can be defined according to relation (2.51):

$$\begin{aligned} C_{1111} &= \lambda + 2\mu \\ C_{1122} &= C_{1133} = \lambda. \end{aligned} \tag{A.170}$$

The sixth-order tensors can be formulated by using relation (2.52):

$$\begin{aligned} C_{111111} &= 2\left(l - m + \tfrac{1}{2}n\right) + 6\left(m - \tfrac{1}{2}n\right) + 2n \\ C_{111122} &= C_{111133} = 2\left(l - m + \tfrac{1}{2}n\right) + 2\left(m - \tfrac{1}{2}n\right). \end{aligned} \tag{A.171}$$

The fourth-order tensor B_{1111} can then be further elaborated to:

$$B_{1111} = \lambda + 2\mu + \left(5\lambda + 10\mu + 2l + 4m\right)e_{xx} + \left(2l + \lambda\right)e_{yy} + \left(2l + \lambda\right)e_{zz}. \tag{A.172}$$

By factorising common terms, the above becomes:

$$B_{1111} = \lambda + 2\mu + \left(2l + \lambda\right)e + \left(4\lambda + 4m + 10\mu\right)e_{xx}, \tag{A.173}$$

where e is defined as the volumetric strain:

$$e = e_{xx} + e_{yy} + e_{zz}. \tag{2.77}$$

Then the wave velocity c_{xx}, expressed in terms of the uniaxial strains, becomes:

$$c_{xx} = \sqrt{\frac{\lambda + 2\mu + \left(2l + \lambda\right)e + \left(4\lambda + 4m + 10\mu\right)e_{xx}}{\rho_a}}. \tag{2.76}$$

The wave velocity can be written in terms of any of the orthogonal uniaxial stresses by using the definition of the linearised nominal stress (2.60):

$$\sigma_{ji} \approx C_{ijkl}\frac{\partial u_k^{(0)}}{\partial x_l}. \tag{2.60}$$

For a uniaxial stress in the i-direction, σ_{ii}, the above yields:

$$\begin{aligned} \sigma_{ii} &= C_{iikl}\frac{\partial u_k^{(0)}}{\partial x_l} \\ &= \left\{\lambda\delta_{ii}\delta_{kl} + 2\mu\left[\tfrac{1}{2}\left(\delta_{ik}\delta_{il} + \delta_{il}\delta_{ik}\right)\right]\right\}\frac{\partial u_k^{(0)}}{\partial x_l}, \end{aligned} \tag{A.174}$$

which, after elaborating the Kronecker delta terms, becomes:

$$\sigma_{ii} = \left(3\lambda + 2\mu\right)\frac{\partial u_k^{(0)}}{\partial x_l}. \tag{A.175}$$

Upon substituting definition (2.68), the above can be simplified to:

$$\sigma_{ii} = \left(3\lambda + 2\mu\right)e. \tag{2.78}$$

The uniaxial strains can be related to each other through Poison's ratio ν. Both the first and second Lamé parameter can be expressed in terms of ν:

$$\lambda = \frac{E\nu}{(1+\nu)(1-2\nu)}\ ; \quad \mu = \frac{E}{2(1+\nu)}, \tag{A.176}$$

where E denotes the Young's modulus. Both expressions can be isolated for the Young's modulus, which makes it possible to express the Poison's ratio in terms of the Lamé parameters:

$$\nu = \frac{\lambda}{2(\mu + \lambda)}. \tag{A.177}$$

The volumetric strain can now be rewritten in terms of one single uniaxial strain e_{ii} of the form[1]:

$$e = e_{xx} + e_{yy} + e_{zz} = e_{xx} - 2\nu e_{xx} = e_{xx}(1 - 2\nu), \tag{A.178}$$

which upon substituting (A.177) can be further elaborated to

$$e = e_{xx}\frac{\mu}{\lambda + \mu}. \tag{A.179}$$

Rewriting relation (2.76) in terms of the uniaxial strain e_{xx} yields:

$$c_{xx} = \sqrt{\frac{\lambda + 2\mu + (2l + \lambda)e_{xx}\frac{\mu}{\lambda + \mu} + (4\lambda + 4m + 10\mu)e_{xx}}{\rho_a}}, \tag{A.180}$$

which can be expanded by factorising the common terms:

$$c_{xx} = \sqrt{\frac{\lambda + 2\mu + e_{xx}\frac{\mu}{\lambda + \mu}\left[2l + \lambda + \frac{\lambda + \mu}{\mu}(4\lambda + 4m + 10\mu)\right]}{\rho_a}}. \tag{2.76}$$

Upon substitution of the linearised nominal stress σ_{xx}, the expression of the wave velocity becomes:

$$c_{xx}{}^{\sigma_{xx}} = \sqrt{\frac{\lambda + 2\mu \pm \frac{\sigma_{xx}}{3K}\left[2l + \lambda + \frac{\lambda + \mu}{\mu}(4\lambda + 4m + 10\mu)\right]}{\rho_a}}, \tag{2.79}$$

where $+\sigma_{xx}$ implies a tensile stress and $-\sigma_{xx}$ a compressive stress. The bulk modulus is denoted with $K = \lambda + \frac{2}{3}\mu$. Using a similar approach for the uniaxial stresses σ_{yy} and σ_{zz}, yields:

$$\begin{aligned} c_{xx}{}^{\sigma_{yy}} &= \sqrt{\frac{\lambda + 2\mu \pm \frac{\sigma_{yy}}{3K}\left[2l + \lambda - \frac{\lambda}{2\mu}(4\lambda + 4m + 10\mu)\right]}{\rho_a}} \\ c_{xx}{}^{\sigma_{zz}} &= \sqrt{\frac{\lambda + 2\mu \pm \frac{\sigma_{zz}}{3K}\left[2l + \lambda - \frac{\lambda}{2\mu}(4\lambda + 4m + 10\mu)\right]}{\rho_a}}, \end{aligned} \tag{A.181}$$

respectively.

For a transverse wave, polarising in the y-direction while propagating along the x-direction, the wave equation (2.73) becomes:

$$\frac{\partial^2 v^{(1)}}{\partial t^2} - c_{xy}^2\frac{\partial^2 v^{(1)}}{\partial x^2} = 0, \tag{2.82}$$

for which the expression for the wave velocity is:

$$c_{xy} = \sqrt{\frac{B_{2121}}{\rho_a}}. \tag{A.182}$$

The fourth-order tensor B_{2121} is then equal to:

$$B_{2121} = \mu + (\lambda + 2\mu + 2\mu + m)e_{xx} + (\lambda + 2\mu + m)e_{yy} + (\lambda + m - \tfrac{1}{2}n)e_{zz}, \tag{A.183}$$

[1]Note that this is only valid for isotropic materials for which ν is independent of the direction.

which can be expanded by factorising the common terms:

$$B_{2121} = \mu + (\lambda + m)e + 4\mu e_{xx} + 2\mu e_{yy} - \frac{1}{2}ne_{zz}. \tag{A.184}$$

The expression of the wave velocity c_{xy} then becomes:

$$c_{xy} = \sqrt{\frac{\mu + (\lambda + m)e + 4\mu e_{xx} + 2\mu e_{yy} - \frac{1}{2}ne_{zz}}{\rho_a}}. \tag{A.185}$$

The transverse-wave velocity of a medium which is stressed parallel to the propagation direction can be described with:

$$c_{xy}{}^{\sigma_{xx}} = \sqrt{\frac{\mu \pm \frac{\sigma_{xx}}{3K}\left(m + \frac{\lambda n}{4\mu} + 4\lambda + 4\mu\right)}{\rho_a}}. \tag{2.83}$$

When the medium is stressed parallel to the polarisation direction, the transverse-wave velocity becomes:

$$c_{xy}{}^{\sigma_{yy}} = \sqrt{\frac{\mu \pm \frac{\sigma_{yy}}{3K}\left(m + \frac{\lambda n}{4\mu} + \lambda + 2\mu\right)}{\rho_a}} \tag{A.186}$$

For a medium which is stressed perpendicular to both the propagation direction and the polarisation direction, the transverse-wave velocity is defined as:

$$c_{xy}{}^{\sigma_{zz}} = \sqrt{\frac{\mu \pm \frac{\sigma_{zz}}{3K}\left[\lambda + m - \frac{\lambda + \mu}{\mu}\left(\frac{3\mu\lambda}{\lambda + \mu} + \frac{1}{2}n\right)\right]}{\rho_a}}. \tag{A.187}$$

B

Side notes M.A. Biot

The intermediate steps and the corresponding side notes, which are needed to understand the derivations which have been made in the book and the papers of Biot, are elaborated here.

B.1. Equilibrium equations for the stress field

This sections covers the derivation of the dynamic equilibrium in the final configuration. This dynamic equilibrium, which lays the foundation for the wave equation, is obtained through Newton's second law of motion in both the initial and the final configuration.

B.1.1. Newton's second law of motion in rest

The initial-stress components are orientated according to the assumed sign conventions. Figure B.1 displays these stresses, which should make equilibrium in the x and y-direction.

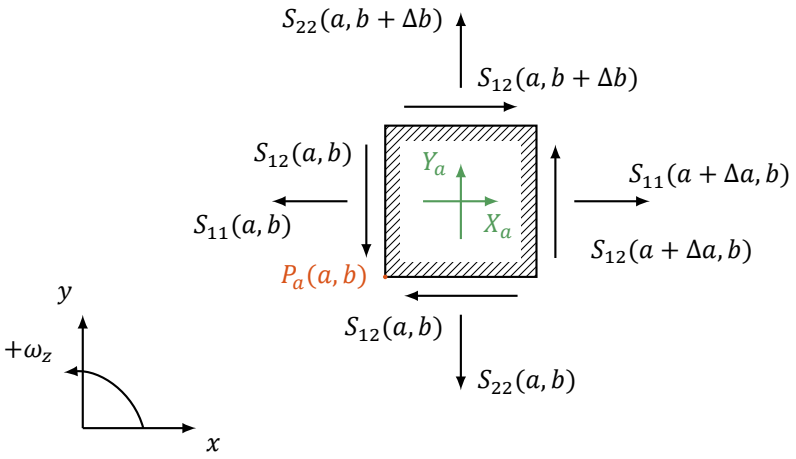

Figure B.1: Initial stresses acting on a square with dimensions $\Delta a, \Delta b$, including the assumed sign conventions.

Newton's second law of motion in the x and y-direction then reads:

$$\begin{aligned} -S_{11}(a,b)\Delta b - S_{12}(a,b)\Delta a + S_{11}(a+\Delta a,b)\Delta b + S_{12}(a,b+\Delta b)\Delta a + \rho_a X_a \Delta a \Delta b = 0 \\ -S_{22}(a,b)\Delta a - S_{12}(a,b)\Delta b + S_{22}(a,b+\Delta b)\Delta a + S_{12}(a+\Delta a,b)\Delta b + \rho_a Y_a \Delta a \Delta b = 0, \end{aligned} \tag{B.1}$$

respectively. By dividing the above by the area of the square, $\Delta a \Delta b$, the following is found:

$$\begin{aligned} \frac{S_{11}(a+\Delta a,b) - S_{11}(a,b)}{\Delta a} + \frac{S_{12}(a,b+\Delta b) - S_{12}(a,b)}{\Delta b} + \rho_a X_a = 0 \\ \frac{S_{12}(a+\Delta a,b) - S_{12}(a,b)}{\Delta a} + \frac{S_{22}(a,b+\Delta b) - S_{22}(a,b)}{\Delta b} + \rho_a Y_a = 0, \end{aligned} \tag{B.2}$$

which, upon evaluating $\lim_{\Delta a,\Delta b\to 0}$, can be recognised as the definition of a derivative for small changes. Therefore, the equilibrium conditions become:

$$\begin{aligned}\frac{\partial S_{11}}{\partial a}+\frac{\partial S_{12}}{\partial b}+\rho_a X_a&=0\\ \frac{\partial S_{12}}{\partial a}+\frac{\partial S_{22}}{\partial b}+\rho_a Y_a&=0,\end{aligned} \tag{3.1}$$

where ρ_a denotes the initial mass density and X_a, Y_a – the components of the initial mass force, expressed in units of acceleration.

B.1.2. Transformation rule of the stress tensor

The stresses acting on the element along the rotated axes x', y' can be rotated back such that they are orientated along the x, y axes. Biot mentions in his paper *"Theory of elasticity with large displacements and rotations"* [3] that this can be realised by using the tensor transformation relation:

$$\boldsymbol{\sigma}' = \boldsymbol{R}\boldsymbol{\sigma}\boldsymbol{R}^T. \tag{B.3}$$

Here, $\boldsymbol{R}$ is defined as the 2 x 2 rotation matrix which is a function of any rotation ω around the three orthogonal axes. The 2 x 2 matrices $\boldsymbol{\sigma}$ and $\boldsymbol{\sigma}'$ denote the nominal stress tensor related to the original and rotated axes, respectively:

$$\boldsymbol{\sigma}' = \begin{pmatrix}\sigma_{xx} & \sigma_{xy}\\ \sigma_{xy} & \sigma_{yy}\end{pmatrix};\quad \boldsymbol{R} = \begin{pmatrix}\cos(\omega) & -\sin(\omega)\\ \sin(\omega) & \cos(\omega)\end{pmatrix};\quad \boldsymbol{\sigma} = \begin{pmatrix}S_{11}+s_{11} & S_{12}+s_{12}\\ S_{12}+s_{12} & S_{22}+s_{22}\end{pmatrix}. \tag{B.4}$$

Note that for any arbitrary small angle ω, the trigonometric functions can be approximated such that the following holds:

$$\begin{aligned}\sin(\omega)&\approx\omega\\ \cos(\omega)&\approx 1.\end{aligned} \tag{B.5}$$

With this approximation, all terms in relation (B.3) of the second order and higher in the rotation angle will be discarded, which yields:

$$\begin{aligned}\sigma_{xx}&=S_{11}+s_{11}-2(S_{12}+s_{12})\omega_z\\ \sigma_{yy}&=S_{22}+s_{22}+2(S_{12}+s_{12})\omega_z\\ \sigma_{xy}&=S_{12}+s_{12}+(S_{11}-S_{22})\omega_z+(s_{11}-s_{22})\omega_z,\end{aligned} \tag{B.6}$$

where ω_z denotes the rotation around the z-axis. Since both the rotation angle ω_z and the incremental-stress components s_{ij} depend on the strain, their multiplication will result in higher-order terms. Therefore, the stresses σ_{xx}, σ_{yy} and σ_{xy}, approximated to the first order, become:

$$\begin{aligned}\sigma_{xx}&=S_{11}+s_{11}-2S_{12}\omega_z\\ \sigma_{yy}&=S_{22}+s_{22}+2S_{12}\omega_z\\ \sigma_{xy}&=S_{12}+s_{12}+(S_{11}-S_{22})\omega_z.\end{aligned} \tag{3.5}$$

B.1.3. Expansion of the partial derivatives with respect to the final configuration

The differentials of the final coordinates (x, y) are defined as:

$$\begin{aligned}dx&=\frac{\partial x}{\partial a}da+\frac{\partial x}{\partial b}db\\ dy&=\frac{\partial y}{\partial a}da+\frac{\partial y}{\partial b}db,\end{aligned} \tag{B.7}$$

which can be written in matrix notation with

$$\boldsymbol{dx} = \boldsymbol{J}\boldsymbol{da}, \tag{B.8}$$

where $\boldsymbol{da}$ and $\boldsymbol{dx}$ denote the 2 x 1 vectors containing the differentials of the initial and final coordinates, respectively. The quantity $\boldsymbol{J}$ denotes the non-singular 2 x 2 Jacobian matrix containing the derivatives of the final coordinates (x, y) with respect to the initial coordinates (a, b):

$$\boldsymbol{J} = \begin{pmatrix} \frac{\partial x}{\partial a} & \frac{\partial x}{\partial b} \\ \frac{\partial y}{\partial a} & \frac{\partial y}{\partial b} \end{pmatrix}. \tag{3.9}$$

The vector $\boldsymbol{da}$ can be isolated by left-multiplying equation (B.8) by the inverse of $\boldsymbol{J}$:

$$\boldsymbol{J}^{-1}\boldsymbol{dx} = \boldsymbol{da}, \tag{B.9}$$

where $\boldsymbol{J}^{-1}$ is defined as:

$$\boldsymbol{J}^{-1} = \frac{1}{\det(\boldsymbol{J})} \begin{pmatrix} \frac{\partial y}{\partial b} & -\frac{\partial x}{\partial b} \\ -\frac{\partial y}{\partial a} & \frac{\partial x}{\partial a} \end{pmatrix}. \tag{B.10}$$

Upon substituting definition (B.10) into relation (B.9), the differentials da and db become:

$$\begin{aligned} da &= \frac{1}{\det(\boldsymbol{J})} \left(\frac{\partial y}{\partial b} dx - \frac{\partial x}{\partial b} dy \right) \\ db &= \frac{1}{\det(\boldsymbol{J})} \left(-\frac{\partial y}{\partial a} dx + \frac{\partial x}{\partial a} dx \right), \end{aligned} \tag{B.11}$$

respectively. The partial derivatives of the initial coordinates with the respect to the final coordinates are obtained by dividing relation (B.11) by the differentials dx and dy. For the derivative $\frac{\partial a}{\partial x}$ this yields:

$$\frac{\partial a}{\partial x} = \frac{1}{\det(\boldsymbol{J})} \left(\frac{\partial y}{\partial b} \frac{dx}{dx} - \frac{\partial x}{\partial b} \frac{dy}{dx} \right). \tag{B.12}$$

Since the derivatives of the final coordinates with respect to each other are zero, the above can simplified to:

$$\frac{\partial a}{\partial x} = \frac{1}{\det(\boldsymbol{J})} \frac{\partial y}{\partial b} \frac{dx}{dx}, \tag{B.13}$$

which, by using $y = b + v$, becomes:

$$\begin{aligned} \frac{\partial a}{\partial x} &= \frac{1}{\det(\boldsymbol{J})} \frac{\partial (b + v)}{\partial b} \\ &= \frac{1}{\det(\boldsymbol{J})} \left(1 + \frac{\partial v}{\partial b} \right). \end{aligned} \tag{B.14}$$

A similar approach can be used to find the expressions of the other derivatives, which eventually yields:

$$\begin{aligned} \frac{\partial a}{\partial x} &= \frac{1}{\det(\boldsymbol{J})} \left(1 + \frac{\partial v}{\partial b} \right) \quad ; \quad \frac{\partial a}{\partial y} = -\frac{1}{\det(\boldsymbol{J})} \frac{\partial u}{\partial b} \\ \frac{\partial b}{\partial x} &= -\frac{1}{\det(\boldsymbol{J})} \frac{\partial v}{\partial a} \quad ; \quad \frac{\partial b}{\partial y} = \frac{1}{\det(\boldsymbol{J})} \left(1 + \frac{\partial u}{\partial a} \right). \end{aligned} \tag{3.8}$$

B.1.4. Newton's second law of motion after deformation

The dynamic equilibrium is established through the Newton's second law of motion at the point $P_x(x, y)$:

$$\begin{aligned} \frac{\partial \sigma_{xx}}{\partial x} + \frac{\partial \sigma_{xy}}{\partial y} + \rho_x X_x &= \rho_x \frac{\partial^2 u}{\partial t^2} \\ \frac{\partial \sigma_{xy}}{\partial x} + \frac{\partial \sigma_{yy}}{\partial y} + \rho_x Y_x &= \rho_x \frac{\partial^2 v}{\partial t^2}, \end{aligned} \tag{3.6}$$

where ρ_x denotes the final mass density and X_x, Y_x – the components of the final mass force. By making use of the chain rule of differentiation the above can be written as:

$$\begin{aligned}\frac{\partial\sigma_{xx}}{\partial a}\frac{\partial a}{\partial x}+\frac{\partial\sigma_{xx}}{\partial b}\frac{\partial b}{\partial x}+\frac{\partial\sigma_{xy}}{\partial a}\frac{\partial a}{\partial y}+\frac{\partial\sigma_{xy}}{\partial b}\frac{\partial b}{\partial y}+\rho_x X_x=\rho_x\frac{\partial^2 u}{\partial t^2}\\ \frac{\partial\sigma_{xy}}{\partial a}\frac{\partial a}{\partial x}+\frac{\partial\sigma_{xy}}{\partial b}\frac{\partial b}{\partial x}+\frac{\partial\sigma_{yy}}{\partial a}\frac{\partial a}{\partial y}+\frac{\partial\sigma_{yy}}{\partial b}\frac{\partial b}{\partial y}+\rho_x Y_x=\rho_x\frac{\partial^2 v}{\partial t^2},\end{aligned} \tag{B.15}$$

which, upon substitution of the definitions (3.8) and the definition of the Jacobian determinant (2.39), becomes:

$$\begin{aligned}\left(\frac{\rho_x}{\rho_a}\right)\left[\frac{\partial\sigma_{xx}}{\partial a}\left(1+\frac{\partial v}{\partial b}\right)-\frac{\partial\sigma_{xx}}{\partial b}\frac{\partial v}{\partial a}-\frac{\partial\sigma_{xy}}{\partial a}\frac{\partial u}{\partial b}+\frac{\partial\sigma_{xy}}{\partial b}\left(1+\frac{\partial u}{\partial a}\right)\right]+\rho_x X_x=\rho_x\frac{\partial^2 u}{\partial t^2}\\ \left(\frac{\rho_x}{\rho_a}\right)\left[\frac{\partial\sigma_{xy}}{\partial a}\left(1+\frac{\partial v}{\partial b}\right)-\frac{\partial\sigma_{xy}}{\partial b}\frac{\partial v}{\partial a}-\frac{\partial\sigma_{yy}}{\partial a}\frac{\partial u}{\partial b}+\frac{\partial\sigma_{yy}}{\partial b}\left(1+\frac{\partial u}{\partial a}\right)\right]+\rho_x Y_x=\rho_x\frac{\partial^2 v}{\partial t^2}.\end{aligned} \tag{B.16}$$

The dynamic equilibrium can be simplified by multiplying both sides with the Jacobian determinant, $\det(\boldsymbol{J})=\left(\frac{\rho_a}{\rho_x}\right)$. For convenience, the following notations are used for the first-order strains:

$$\begin{aligned}e_{xx}&=\frac{\partial u}{\partial a}\\ e_{yy}&=\frac{\partial v}{\partial b}\\ e_{xy}&=\frac{1}{2}\left(\frac{\partial v}{\partial a}+\frac{\partial u}{\partial b}\right).\end{aligned} \tag{3.11}$$

By factorising the stress components, relation (B.16) becomes:

$$\begin{aligned}\frac{\partial\sigma_{xx}}{\partial a}+\frac{\partial\sigma_{xy}}{\partial b}+e_{yy}\frac{\partial\sigma_{xx}}{\partial a}+e_{xx}\frac{\partial\sigma_{xy}}{\partial b}-(e_{xy}-\omega_z)\frac{\partial\sigma_{xy}}{\partial a}-(e_{xy}+\omega_z)\frac{\partial\sigma_{xx}}{\partial b}+\rho_a X_x=\rho_a\frac{\partial^2 u}{\partial t^2}\\ \frac{\partial\sigma_{xy}}{\partial a}+\frac{\partial\sigma_{yy}}{\partial b}+e_{yy}\frac{\partial\sigma_{xy}}{\partial a}+e_{xx}\frac{\partial\sigma_{yy}}{\partial b}-(e_{xy}-\omega_z)\frac{\partial\sigma_{yy}}{\partial a}-(e_{xy}+\omega_z)\frac{\partial\sigma_{xy}}{\partial b}+\rho_a Y_x=\rho_a\frac{\partial^2 v}{\partial t^2}.\end{aligned} \tag{3.10}$$

Now all the terms of this new formulation of the dynamic equilibrium will be treated and evaluated. The mass forces $\rho_a X_a$, $\rho_a Y_a$ can be approximated at the point $P_x(x,y)$ by using a Taylor expansion in two dimensions:

$$f(x,y)=f(a,b)+\frac{\partial f(a,b)}{\partial a}\frac{(x-a)}{1!}+\frac{\partial f(a,b)}{\partial b}\frac{(y-b)}{1!}+\dots \tag{B.17}$$

By considering only the first-order terms, the Taylor expansion for the initial mass force $\rho_a X_a$ becomes:

$$\begin{aligned}\rho_a X_a&=\rho_a\left(X_x+\frac{\partial X_x}{\partial a}\frac{(a-x)}{1!}+\frac{\partial X_x}{\partial b}\frac{(b-y)}{1!}\right)\\ &=\rho_a X_x-\rho_a u\frac{\partial X_x}{\partial a}-\rho_a v\frac{\partial X_x}{\partial b}.\end{aligned} \tag{B.18}$$

Upon isolating the mass force at the point $P_x(x,y)$, the following holds for both directions:

$$\begin{aligned}\rho_a X_x&=\rho_a X_a+\rho_a u\frac{\partial X_x}{\partial a}+\rho_a v\frac{\partial X_x}{\partial b}\\ \rho_a Y_x&=\rho_a Y_a+\rho_a u\frac{\partial Y_x}{\partial a}+\rho_a v\frac{\partial Y_x}{\partial b}.\end{aligned} \tag{B.19}$$

The derivatives of the stress components can be evaluated by substituting the relations (3.5). For the stress component σ_{xx} this results in:

$$\begin{aligned}\frac{\partial \sigma_{xx}}{\partial a} &= \frac{\partial s_{11}}{\partial a} + \frac{\partial S_{11}}{\partial a} - 2\omega_z \frac{\partial S_{12}}{\partial a} - 2S_{12}\frac{\partial \omega_z}{\partial a} \\ \frac{\partial \sigma_{xx}}{\partial b} &= \frac{\partial s_{11}}{\partial b} + \frac{\partial S_{11}}{\partial b} - 2\omega_z \frac{\partial S_{12}}{\partial b} - 2S_{12}\frac{\partial \omega_z}{\partial b}.\end{aligned} \tag{B.20}$$

Similarly, the derivatives of the stress component σ_{yy} become:

$$\begin{aligned}\frac{\partial \sigma_{yy}}{\partial a} &= \frac{\partial s_{22}}{\partial a} + \frac{\partial S_{22}}{\partial a} + 2\omega_z \frac{\partial S_{12}}{\partial a} + 2S_{12}\frac{\partial \omega_z}{\partial a} \\ \frac{\partial \sigma_{yy}}{\partial b} &= \frac{\partial s_{22}}{\partial b} + \frac{\partial S_{22}}{\partial b} + 2\omega_z \frac{\partial S_{12}}{\partial b} + 2S_{12}\frac{\partial \omega_z}{\partial b},\end{aligned} \tag{B.21}$$

whereas those of the stress component σ_{xy} become:

$$\begin{aligned}\frac{\partial \sigma_{xy}}{\partial a} &= \frac{\partial s_{12}}{\partial a} + \frac{\partial S_{12}}{\partial a} + \omega_z \frac{\partial}{\partial a}(S_{11} - S_{22}) + (S_{11} - S_{22})\frac{\partial \omega_z}{\partial a} \\ \frac{\partial \sigma_{xy}}{\partial b} &= \frac{\partial s_{12}}{\partial b} + \frac{\partial S_{12}}{\partial b} + \omega_z \frac{\partial}{\partial b}(S_{11} - S_{22}) + (S_{11} - S_{22})\frac{\partial \omega_z}{\partial b}.\end{aligned} \tag{B.22}$$

Next, these derivatives together with relations (B.19) are substituted into relations (3.10). Since the strains are approximated to the first order, all multiplications which result in higher-order terms are neglected. After substitution, the dynamic equilibrium in the x-direction yields:

$$\begin{aligned}&\frac{\partial s_{11}}{\partial a} + \frac{\partial S_{11}}{\partial a} - 2\omega_z \frac{\partial S_{12}}{\partial a} - 2S_{12}\frac{\partial \omega_z}{\partial a} + \frac{\partial s_{12}}{\partial b} + \frac{\partial S_{12}}{\partial b} + (S_{11} - S_{22})\frac{\partial \omega_z}{\partial b} \\ &\quad + \omega_z\left(\frac{\partial S_{11}}{\partial b} - \frac{\partial S_{22}}{\partial b}\right) + e_{yy}\frac{\partial S_{11}}{\partial a} + e_{xx}\frac{\partial S_{12}}{\partial b} - (e_{xy} - \omega_z)\frac{\partial S_{12}}{\partial a} - (e_{xy} + \omega_z)\frac{\partial S_{11}}{\partial b} \\ &\quad + \rho_a X_a + \rho_a u\frac{\partial X_x}{\partial a} + \rho_a v\frac{\partial X_x}{\partial b} = \rho_a \frac{\partial^2 u}{\partial t^2}.\end{aligned} \tag{B.23}$$

By rewriting the equilibrium conditions (3.1), the initial mass forces can be expressed in terms of the initial stresses:

$$\begin{aligned}\rho_a X_a &= -\frac{\partial S_{11}}{\partial a} - \frac{\partial S_{12}}{\partial b} \\ \rho_a Y_a &= -\frac{\partial S_{12}}{\partial a} - \frac{\partial S_{22}}{\partial b}.\end{aligned} \tag{B.24}$$

Rearranging and factorising the terms containing the rotation ω_z, results in:

$$\begin{aligned}&\frac{\partial s_{11}}{\partial a} + \frac{\partial s_{12}}{\partial b} + \rho_a u\frac{\partial X_x}{\partial a} + \rho_a v\frac{\partial X_x}{\partial b} + \omega_z\left(-\frac{\partial S_{12}}{\partial a} - \frac{\partial S_{22}}{\partial b}\right) - 2S_{12}\frac{\partial \omega_z}{\partial a} \\ &\quad + (S_{11} - S_{22})\frac{\partial \omega_z}{\partial b} + e_{yy}\frac{\partial S_{11}}{\partial a} + e_{xx}\frac{\partial S_{12}}{\partial b} - e_{xy}\left(\frac{\partial S_{12}}{\partial a} + \frac{\partial S_{11}}{\partial b}\right) \\ &\quad + \omega_z\left(-\frac{\partial S_{12}}{\partial a} + \frac{\partial S_{11}}{\partial b} + \frac{\partial S_{12}}{\partial a} - \frac{\partial S_{11}}{\partial b}\right) = \rho_a \frac{\partial^2 u}{\partial t^2}.\end{aligned} \tag{B.25}$$

After simplifying even further, the same approach can be used for the y-direction. The final result is the dynamic equilibrium, expressed in terms of the initial-stress components S_{ij} and the incremental-stress components s_{ij}, along the x, y-direction:

$$\begin{aligned}
&\frac{\partial s_{11}}{\partial a} + \frac{\partial s_{12}}{\partial b} + \rho_a u \frac{\partial X_x}{\partial a} + \rho_a v \frac{\partial X_x}{\partial b} + \rho_a \omega_z Y_a - 2S_{12}\frac{\partial \omega_z}{\partial a} \\
&\quad + (S_{11} - S_{22})\frac{\partial \omega_z}{\partial b} + e_{yy}\frac{\partial S_{11}}{\partial a} + e_{xx}\frac{\partial S_{12}}{\partial b} - e_{xy}\left(\frac{\partial S_{12}}{\partial a} + \frac{\partial S_{11}}{\partial b}\right) = \rho_a \frac{\partial^2 u}{\partial t^2} \\
&\frac{\partial s_{12}}{\partial a} + \frac{\partial s_{22}}{\partial b} + \rho_a u \frac{\partial Y_x}{\partial a} + \rho_a v \frac{\partial Y_x}{\partial b} - \rho_a \omega_z X_a + 2S_{12}\frac{\partial \omega_z}{\partial b} \\
&\quad + (S_{11} - S_{22})\frac{\partial \omega_z}{\partial a} + e_{yy}\frac{\partial S_{12}}{\partial a} + e_{xx}\frac{\partial S_{22}}{\partial b} - e_{xy}\left(\frac{\partial S_{22}}{\partial a} + \frac{\partial S_{12}}{\partial b}\right) = \rho_a \frac{\partial^2 v}{\partial t^2},
\end{aligned} \tag{3.12}$$

respectively.

B.2. Connection between initial-stress and wave velocity

This section deals with the relation between the initial-stress components S_{ij} and the expressions of the wave velocity. Through the principle of virtual work, a link between the initial-stress components and the elastic coefficients can be established. Upon expanding the dynamic equilibrium, the wave equation is obtained from which the formulations of the wave velocities, expressed in terms of the elastic coefficients, follow.

B.2.1. Virtual work principle

After deformation and rotation, a cube with unit dimensions is transformed into a parallelogram. In this parallelogram a unit sized square is cut out, whose stress field is displayed in Figure B.2.

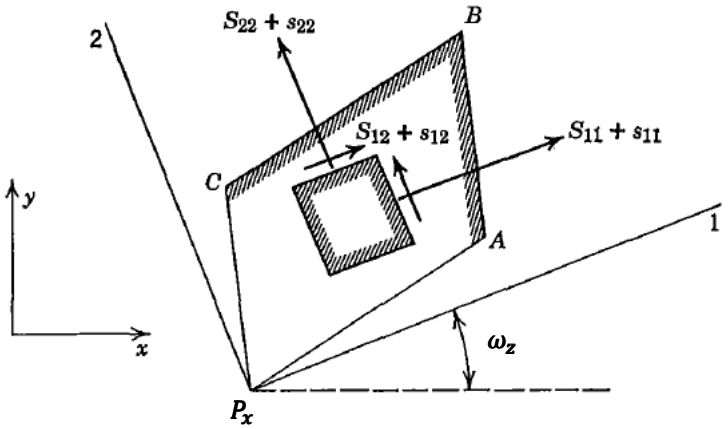

Figure B.2: Stress field of a unit cube after rotation and deformation [5] (edited).

These stress components s_{ij} acting on the square are related to the element of area before deformation. For the purpose of the virtual work principle, it is convenient to introduce Cauchy stress components T_{ij} which are related to the element of area after deformation. This can be done by considering a portion of a force $\boldsymbol{df}$ acting on an element with dimensions dx', dy' like depicted in Figure B.3.

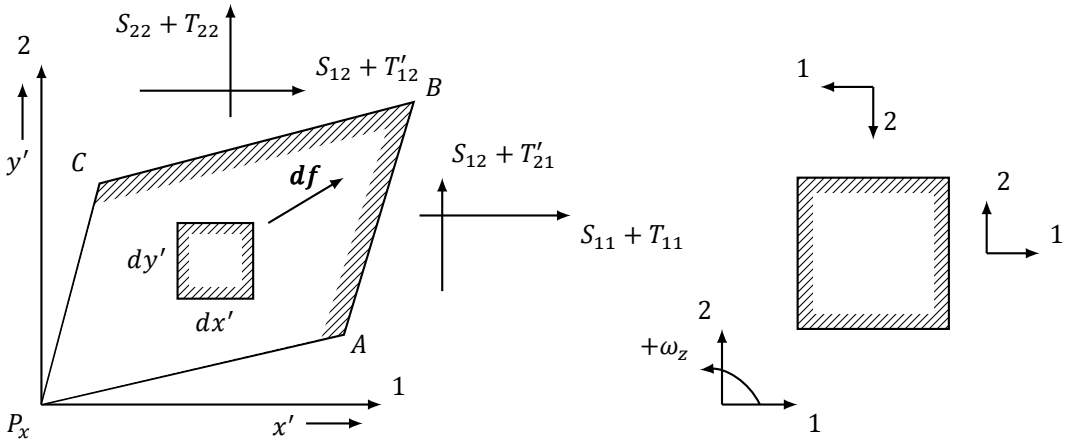

Figure B.3: The positive definition of the local coordinate system along the boundaries of the element dx', dy', according to the counterclockwise integration.

According to the chosen sign convention, the total force $\boldsymbol{f}$ is defined positive when $\boldsymbol{df}$ is integrated along the sides of the element in a counterclockwise direction. This results in the components of the force $\boldsymbol{df}$, along directions 1 and 2, to be defined as[1]:

$$\begin{aligned} df_1 &= (S_{11} + s_{11})dy' - (S_{12} + s_{12})dx' \\ df_2 &= (S_{12} + s_{12})dy' - (S_{22} + s_{22})dx'. \end{aligned} \tag{B.26}$$

The coordinates of the points A, B and C of the parallelogram can be expressed in terms of the strain components and are displayed in table B.1.

Table B.1: The coordinates of points A, B, C in terms of the strain components ϵ_{ij}.

Points of the parallelogram	Horizontal coordinate x'	Vertical coordinate y'
A	$1 + \epsilon_{11}$	ϵ_{12}
B	$1 + \epsilon_{11} + \epsilon_{12}$	$1 + \epsilon_{22} + \epsilon_{12}$
C	ϵ_{12}	$1 + \epsilon_{22}$

The forces on the sides of the parallelogram can now be defined by integrating the force df_i along the edges in a counterclockwise direction. This results in the following:

$$\begin{aligned} S_{11} + T_{11} &= \int_A^B df_1 \\ S_{12} + T'_{21} &= \int_A^B df_2 \\ S_{12} + T'_{12} &= \int_B^C df_1 \\ S_{22} + T_{22} &= \int_B^C df_2. \end{aligned} \tag{B.27}$$

These relations can be elaborated by using (B.26) and the coordinates from table B.1. For the first expression this results in:

[1]The minus sign of the forces acting on the plane dx' is due to the positive definition of its the local coordinate system with respect to the global coordinate system, as has been depicted in Figure B.3

$$\begin{aligned} S_{11} + T_{11} &= \int_A^B (S_{11} + s_{11})dy' - \int_A^B (S_{12} + s_{12})dx' \\ &= (S_{11} + s_{11})y'\Big|_A^B - (S_{12} + s_{12})x'\Big|_A^B \\ &= (S_{11} + s_{11})(1 + \epsilon_{22}) - (S_{12} + s_{12})\epsilon_{12}. \end{aligned} \tag{B.28}$$

After using a similar approach for the expressions and rearranging the terms, the following definitions are obtained:

$$\begin{aligned} T_{11} &= s_{11} + (S_{11} + s_{11})\epsilon_{22} - (S_{12} + s_{12})\epsilon_{12} \\ T'_{21} &= s_{12} + (S_{12} + s_{12})\epsilon_{22} - (S_{22} + s_{22})\epsilon_{12} \\ T'_{12} &= s_{12} + (S_{12} + s_{12})\epsilon_{11} - (S_{11} + s_{11})\epsilon_{12} \\ T_{22} &= s_{22} + (S_{22} + s_{22})\epsilon_{11} - (S_{12} + s_{12})\epsilon_{12}, \end{aligned} \tag{B.29}$$

which can be simplified by neglecting the higher-order terms:

$$\begin{aligned} T_{11} &= s_{11} + S_{11}\epsilon_{22} - S_{12}\epsilon_{12} \\ T'_{21} &= s_{12} + S_{12}\epsilon_{22} - S_{22}\epsilon_{12} \\ T'_{12} &= s_{12} + S_{12}\epsilon_{11} - S_{11}\epsilon_{12} \\ T_{22} &= s_{22} + S_{22}\epsilon_{11} - S_{12}\epsilon_{12}. \end{aligned} \tag{B.30}$$

It should be noted that the Cauchy stress tensor is supposed to be symmetric. This rule of symmetry follows from the demand that the total torque, caused by the shear stresses, should be zero. However, due to the inclusion of the initial-stress components this symmetry is lost, i.e. T'_{12} and T'_{21}, are not equal anymore. However, for the purpose of the principle of virtual work it is actually their average which is relevant:

$$T_{12} = \tfrac{1}{2}(T'_{12} + T'_{21}). \tag{B.31}$$

By using a first-order approximation of the strain components ϵ_{ij} and relation (B.31), the expressions (B.30) become:

$$\begin{aligned} T_{11} &= s_{11} + S_{11}e_{yy} - S_{12}e_{xy} \\ T_{22} &= s_{22} + S_{22}e_{xx} - S_{12}e_{xy} \\ T_{12} &= s_{12} + \tfrac{1}{2}S_{12}(e_{xx} + e_{yy}) - \tfrac{1}{2}(S_{11} + S_{22})e_{xy}. \end{aligned} \tag{B.32}$$

The total virtual work, exerted by the stresses acting across the deformed area, is defined as:

$$\delta V = (S_{11} + T_{11})\delta\epsilon_{11} + (S_{22} + T_{22})\delta\epsilon_{22} + (2S_{12} + T'_{12} + T'_{21})\delta\epsilon_{12}. \tag{B.33}$$

Knowing that the terms T_{ij} are already of the first order, the expression for the virtual work can be simplified by multiplying these stress components with the first-order approximation of the strain components e_{ij}. After substituting relation (B.31), the expression for the virtual work becomes:

$$\delta V = T_{11}\delta e_{xx} + T_{22}\delta e_{yy} + 2T_{12}\delta e_{xy} + S_{11}\delta\epsilon_{11} + S_{22}\delta\epsilon_{22} + 2S_{12}\delta\epsilon_{12}. \tag{B.34}$$

This expression has to be an exact differential in order to prove the existence of a strain energy potential. This condition is expressed in the following relations:

$$\begin{aligned} \frac{\partial T_{11}}{\partial e_{yy}} &= \frac{\partial T_{22}}{\partial e_{xx}} \\ \frac{\partial T_{11}}{\partial e_{xy}} &= 2\frac{\partial T_{12}}{\partial e_{xx}} \\ \frac{\partial T_{22}}{\partial e_{xy}} &= 2\frac{\partial T_{12}}{\partial e_{yy}}. \end{aligned} \tag{B.35}$$

The incremental-stress components T_{ij} can be expressed linearly in terms of the first-order approximation of the strains:

$$\begin{aligned} T_{11} &= C_{1111}e_{xx} + C_{1122}e_{yy} + 2C_{1112}e_{xy} \\ T_{22} &= C_{2211}e_{xx} + C_{2222}e_{yy} + 2C_{2212}e_{xy} \\ T_{12} &= C_{1211}e_{xx} + C_{1222}e_{yy} + 2C_{1212}e_{xy}. \end{aligned} \tag{B.36}$$

These relations must satisfy the conditions (B.35), which results in symmetry in the coefficients C_{ijkl}:

$$\begin{aligned} C_{1122} &= C_{2211} \\ C_{1112} &= C_{1211} \\ C_{2212} &= C_{1222}. \end{aligned} \tag{B.37}$$

Note that the incremental-stress components s_{ij} are also linear related to the strains. When substituting relations (B.32) into expressions (B.36), the stress components s_{ij} can be expressed in terms of the coefficients C_{ijkl}:

$$\begin{aligned} s_{11} &= C_{1111}e_{xx} + (C_{1122} - S_{11})e_{yy} + (2C_{1112} + S_{12})e_{xy} \\ s_{22} &= (C_{2211} - S_{22})e_{xx} + C_{2222}e_{yy} + (2C_{2212} + S_{12})e_{xy} \\ s_{12} &= (C_{1211} - \tfrac{1}{2}S_{12})e_{xx} + (C_{1222} - \tfrac{1}{2}S_{12})e_{yy} + (2C_{1212} + \tfrac{1}{2}S_{11} + \tfrac{1}{2}S_{22})e_{xy}. \end{aligned} \tag{B.38}$$

When comparing expressions (3.13) and (B.38), a relation between the the elastic coefficients B_{ijkl} and the initial stress components S_{ij} can be found:

$$\begin{aligned} &B_{1111} = C_{1111} && B_{1122} = C_{1122} - S_{11} && B_{1112} = C_{1112} + \tfrac{1}{2}S_{12} \\ &B_{2211} = C_{2211} - S_{22} && B_{2222} = C_{2222} && B_{2212} = C_{2212} + \tfrac{1}{2}S_{12} \\ &B_{1211} = C_{1211} - \tfrac{1}{2}S_{12} && B_{1222} = C_{1222} - \tfrac{1}{2}S_{12} && B_{1212} = C_{1212} + \tfrac{1}{4}S_{11} + \tfrac{1}{4}S_{22}. \end{aligned} \tag{B.39}$$

Upon substituting the symmetry relations (B.37), expression (B.39) can be simplified to:

$$\begin{aligned} B_{1122} + S_{11} &= B_{2211} + S_{22} \\ B_{1112} - \tfrac{1}{2}S_{12} &= B_{1211} + \tfrac{1}{2}S_{12} \\ B_{2212} - \tfrac{1}{2}S_{12} &= B_{1222} + \tfrac{1}{2}S_{12}. \end{aligned} \tag{3.14}$$

B.2.2. Wave equation

For the purpose of expanding the theory to the third dimension, it is convenient to make use of the index notation. Conform this notation system, the indices abide to the following:

$$i, j, k, l \in \{1, 2, 3\}. \tag{3.15}$$

The dynamic-equilibrium conditions (3.12) can then be simplified to [5]:

$$\frac{\partial s_{ij}}{\partial a_j} + \rho_a \Delta X_i - \rho_a \omega_{ik} X_k(x_l) - \rho_a e X_i(x_l) + S_{jk}\frac{\partial \omega_{ik}}{\partial a_j} + S_{ik}\frac{\partial \omega_{jk}}{\partial a_j} - e_{jk}\frac{\partial S_{ik}}{\partial a_j} = \rho_a \frac{\partial^2 u_i}{\partial t^2}, \tag{3.16}$$

where $e = e_{xx} + e_{yy} + e_{zz}$ denotes the volumetric strain. The strain components and the rotations are defined as:

$$\begin{aligned} e_{ij} &= \frac{1}{2}\left(\frac{\partial u_i}{\partial a_j} + \frac{\partial u_j}{\partial a_i}\right) \\ \omega_{ij} &= \frac{1}{2}\left(\frac{\partial u_i}{\partial a_j} - \frac{\partial u_j}{\partial a_i}\right), \end{aligned} \tag{3.17}$$

respectively, where the initial coordinates and the displacements are denoted with:

$$\begin{aligned} a_i &= (a_1, a_2, a_3) = (a, b, c) \\ u_i &= (u_1, u_2, u_3) = (u, v, w), \end{aligned} \tag{3.18}$$

respectively. From the above it follows that the rotation angles ω_{ij} are anti-symmetric. Their notation can be simplified by specifying the axis of rotation:

$$\begin{aligned} \omega_{11} &= 1 & \omega_{12} &= -\omega_z & \omega_{13} &= \omega_y \\ \omega_{21} &= \omega_z & \omega_{22} &= 1 & \omega_{23} &= -\omega_x \\ \omega_{31} &= -\omega_y & \omega_{32} &= \omega_x & \omega_{33} &= 1. \end{aligned} \tag{3.19}$$

The quantity ΔX_i denotes the increment in mass force per unit mass from the initial location to the displaced location and is defined as:

$$\Delta X_i = u_j \frac{\partial X_i(a_l)}{\partial a_j}, \tag{3.18}$$

where $X_i(a_l)$ denotes the initial mass force. The incremental-stress components s_{ij} can be rewritten as:

$$s_{ij} = Z_{ijkl} e_{kl} - S_{ij} e. \tag{3.21}$$

The fourth-order tensor Z_{ijkl} is defined as:

$$Z_{ijkl} = B_{ijkl} + S_{ij}\delta_{kl}. \tag{3.22}$$

where δ_{kl} denotes the Kronecker delta. The relations (3.14) then become:

$$B_{ijkl} + S_{ij}\delta_{kl} = B_{klij} + S_{kl}\delta_{ij}. \tag{3.23}$$

By setting the conditions for the initial-stress components, it is possible to examine the corresponding behaviour of elastic waves. This can be done by solving the dynamic-equilibrium relations (3.16). In order to study the influence of the initial-stress components on the wave velocity, a stressed cube is considered. A uniform initial-stress state in the principal directions along the x, y, z axes is assumed . This results in the spatially independent initial-stress components which are depicted in Figure B.4.

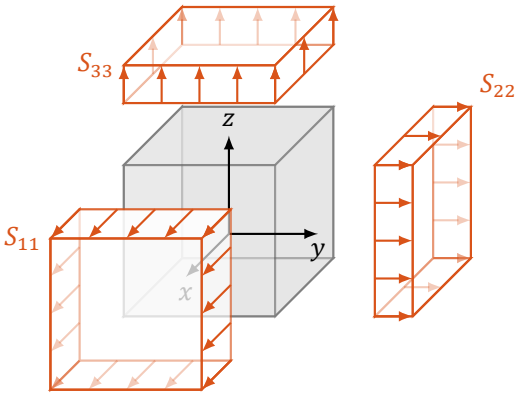

Figure B.4: Initial tensile stresses acting on a cube, including the assumed sign conventions.

Since the stresses are orientated along the three principal axes it follows from relations (3.1) that the mass forces $X_i(a_l)$ should be zero. Relation (3.16) then yields the following three dynamic-equilibrium conditions:

$$\begin{aligned}
&\frac{\partial s_{11}}{\partial x}+\frac{\partial s_{12}}{\partial y}+\frac{\partial s_{13}}{\partial z}+\left(S_{11}-S_{22}\right)\frac{\partial \omega_z}{\partial y}+\left(S_{33}-S_{11}\right)\frac{\partial \omega_y}{\partial z}=\rho_a\frac{\partial^2 u}{\partial t^2}\\
&\frac{\partial s_{12}}{\partial x}+\frac{\partial s_{22}}{\partial y}+\frac{\partial s_{23}}{\partial z}+\left(S_{11}-S_{22}\right)\frac{\partial \omega_z}{\partial x}+\left(S_{22}-S_{33}\right)\frac{\partial \omega_x}{\partial z}=\rho_a\frac{\partial^2 v}{\partial t^2}\\
&\frac{\partial s_{13}}{\partial x}+\frac{\partial s_{23}}{\partial y}+\frac{\partial s_{33}}{\partial z}+\left(S_{33}-S_{11}\right)\frac{\partial \omega_y}{\partial x}+\left(S_{22}-S_{33}\right)\frac{\partial \omega_x}{\partial y}=\rho_a\frac{\partial^2 w}{\partial t^2}.
\end{aligned} \tag{3.24}$$

For the first equation, $i=1$, the incremental-stress components s_{1j} can be elaborated with relation (3.21):

$$\begin{aligned}
s_{11}&=Z_{1111}e_{xx}+Z_{1122}e_{yy}+Z_{1133}e_{zz}+2Z_{1112}e_{xy}+2Z_{1113}e_{xz}+2Z_{1123}e_{yz}-S_{11}e\\
s_{12}&=Z_{1211}e_{xx}+Z_{1222}e_{yy}+Z_{1233}e_{zz}+2Z_{1212}e_{xy}+2Z_{1213}e_{xz}+2Z_{1223}e_{yz}\\
s_{13}&=Z_{1311}e_{xx}+Z_{1322}e_{yy}+Z_{1333}e_{zz}+2Z_{1312}e_{xy}+2Z_{1313}e_{xz}+2Z_{1323}e_{yz}.
\end{aligned} \tag{B.40}$$

After the substituting the definition of the first-order strain components e_{ij}, the derivatives of the stress components are of the form:

$$\begin{aligned}
\frac{\partial s_{11}}{\partial x}=&\left(Z_{1111}-S_{11}\right)\frac{\partial^2 u}{\partial x^2}+\left(Z_{1122}-S_{11}\right)\frac{\partial^2 v}{\partial x\partial y}+\left(Z_{1133}-S_{11}\right)\frac{\partial^2 w}{\partial x\partial z}\\
&+Z_{1112}\left(\frac{\partial^2 v}{\partial x^2}+\frac{\partial^2 u}{\partial x\partial y}\right)+Z_{1113}\left(\frac{\partial^2 w}{\partial x^2}+\frac{\partial^2 u}{\partial x\partial z}\right)+Z_{1123}\left(\frac{\partial^2 w}{\partial x\partial y}+\frac{\partial^2 v}{\partial x\partial z}\right).
\end{aligned} \tag{B.41}$$

The derivatives of the other stress components can be elaborated in a similar manner. The set of wave equations is obtained by substituting the spatial derivatives of the stress components together with the definition of the rotation angles ω_{ij} into relation (3.24).

The shape of this set of wave equations is depending on the type of waves which are being assumed. The wave forms which have been assumed for each wave equation are displayed in Figure B.5.

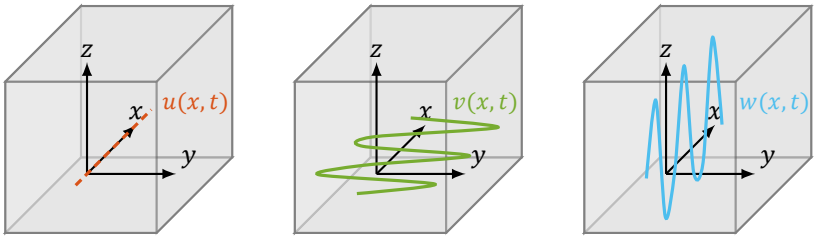

Figure B.5: Graphical representation of the assumed wave forms for each wave equation.

When considering these solutions, the set of wave equations eventually becomes:

$$\begin{aligned}
\rho_a\frac{\partial^2 u}{\partial t^2}-\left(Z_{1111}-S_{11}\right)\frac{\partial^2 u}{\partial x^2}&=0\\
\rho_a\frac{\partial^2 v}{\partial t^2}-\left(Z_{1212}+\tfrac{1}{2}S_{11}-\tfrac{1}{2}S_{22}\right)\frac{\partial^2 v}{\partial x^2}&=0\\
\rho_a\frac{\partial^2 w}{\partial t^2}-\left(Z_{1313}+\tfrac{1}{2}S_{11}-\tfrac{1}{2}S_{33}\right)\frac{\partial^2 w}{\partial x^2}&=0.
\end{aligned} \tag{3.25}$$

B.2.3. Wave velocity

The expressions of the wave velocities, expressed in terms of the initial-stress components, are obtained by dividing both sides of the three wave equations from relation (3.25) by the initial mass density ρ_a:

$$\begin{aligned}\frac{\partial^2 u}{\partial t^2} - {c_{xx}}^2 \frac{\partial^2 u}{\partial x^2} &= 0\\ \frac{\partial^2 v}{\partial t^2} - {c_{xy}}^2 \frac{\partial^2 v}{\partial x^2} &= 0\\ \frac{\partial^2 w}{\partial t^2} - {c_{xz}}^2 \frac{\partial^2 w}{\partial x^2} &= 0,\end{aligned} \tag{3.26}$$

where c_{xx}, c_{xy} and c_{xz} denote the wave velocities of waves propagating in the x-direction while polarising in the x, y and z-direction, respectively. By using relation (3.22), these wave velocities of the stressed medium can be expanded to:

$$\begin{aligned}{c_{xx}}^{S_{11}} &= \sqrt{\frac{B_{1111} + S_{11} - S_{11}}{\rho_a}}\\ {c_{xy}}^{S_{11};S_{22}} &= \sqrt{\frac{B_{1212} + \frac{1}{2}S_{11} - \frac{1}{2}S_{22}}{\rho_a}}\\ {c_{xz}}^{S_{11};S_{33}} &= \sqrt{\frac{B_{1313} + \frac{1}{2}S_{11} - \frac{1}{2}S_{33}}{\rho_a}}.\end{aligned} \tag{B.42}$$

These expressions can be further elaborated by introducing the material coefficient matrix $\boldsymbol{B}$. For an isotropic material the following holds:

$$\boldsymbol{B} = \begin{pmatrix} B_{1111} & B_{1122} & B_{1133} & B_{1112} & B_{1123} & B_{1113} \\ B_{2211} & B_{2222} & B_{2233} & B_{2212} & B_{2223} & B_{2213} \\ B_{3311} & B_{3322} & B_{3333} & B_{3312} & B_{3323} & B_{3313} \\ B_{1211} & B_{1222} & B_{1233} & B_{1212} & B_{1223} & B_{1213} \\ B_{2311} & B_{2322} & B_{2333} & B_{2312} & B_{2323} & B_{2313} \\ B_{1311} & B_{1322} & B_{1333} & B_{1312} & B_{1323} & B_{1313} \end{pmatrix} = \begin{pmatrix} \lambda+2\mu & \lambda & \lambda & 0 & 0 & 0 \\ \lambda & \lambda+2\mu & \lambda & 0 & 0 & 0 \\ \lambda & \lambda & \lambda+2\mu & 0 & 0 & 0 \\ 0 & 0 & 0 & \mu & 0 & 0 \\ 0 & 0 & 0 & 0 & \mu & 0 \\ 0 & 0 & 0 & 0 & 0 & \mu \end{pmatrix}. \tag{B.43}$$

The coefficients λ and μ denote the first and second Lamé parameter, respectively. With this definition of the material coefficient matrix it is now possible to expand the expressions for the wave velocities to:

$$\begin{aligned}{c_{xx}}^{S_{11}} &= \sqrt{\frac{\lambda + 2\mu}{\rho_a}}\\ {c_{xy}}^{S_{11};S_{22}} &= \sqrt{\frac{\mu + \frac{1}{2}S_{11} - \frac{1}{2}S_{22}}{\rho_a}}\\ {c_{xz}}^{S_{11};S_{33}} &= \sqrt{\frac{\mu + \frac{1}{2}S_{11} - \frac{1}{2}S_{33}}{\rho_a}}.\end{aligned} \tag{3.27}$$

C

Wave propagation under a stress state

The occurrence of a stress state influences the wave propagation of a medium. The intermediate steps needed to derive the formulations which describe these influences are elaborated here.

C.1. Wave propagation in a bending rod

In his work, Biot attempts to demonstrate the influence of the initial-stress state on the elastic wave propagation within a three-dimensional medium by generalising the model of a bending rod subjected to an axial force. This section covers the derivation of the equation of motion of this model and the analysis of the influence of the axial force on the wave propagation inside the bending rod.

C.1.1. Equation of motion

The equation of motion for a rod with a bending stiffness EI and a mass density ρ is derived through the combination of three types of equations. The first type is the kinematic relation which links different elements of motion of a body to each other. For an infinitesimal bending element the kinematic relation links the beam deflection $w(x)$ to the rotation $\phi(x)$ and the rotation to the curvature $\kappa(x)$:

$$\begin{aligned} \phi(x) &= -\frac{\partial w(x)}{\partial x} \\ \kappa(x) &= \frac{\partial \phi(x)}{\partial x}, \end{aligned} \tag{C.1}$$

respectively. Here, x denotes the direction of the axis of the rod and its deflection is in the z-direction. The second type is the constitutive relation, linking the internal forces to elements of motion. In a bending element, the constitutive relation describe the connection between the bending moment $M(x)$ and the curvature:

$$M(x) = EI\kappa(x). \tag{C.2}$$

The third type are the equilibrium equations, consisting of the equilibrium of the forces acting on the infinitesimal bending rod like depicted in Figure C.1.

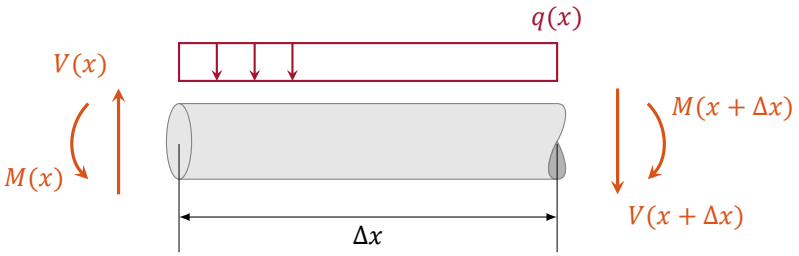

Figure C.1: Free-body diagram of an infinitesimal bending-rod element.

The vertical force equilibrium is obtained through Newton's second law of motion:

$$-V(x)+q\Delta x+V(x+\Delta x)=\rho\Delta x\frac{\partial^2 w(x,t)}{\partial t^2}, \tag{C.3}$$

which upon division by Δx becomes:

$$\frac{V(x+\Delta x)-V(x)}{\Delta x}=\rho\frac{\partial^2 w(x,t)}{\partial t^2}-q. \tag{C.4}$$

By taking the limit of Δx going to zero, the following is obtained:

$$\lim_{\Delta x\to 0}\frac{V(x+\Delta x)-V(x)}{\Delta x}=\lim_{\Delta x\to 0}\left(\rho\frac{\partial^2 w(x,t)}{\partial t^2}-q\right), \tag{C.5}$$

which, upon using the definition of the derivative, can be simplified to:

$$\frac{\partial V(x)}{\partial x}=\rho\frac{\partial^2 w(x,t)}{\partial t^2}-q. \tag{C.6}$$

The moment equilibrium at the location x reads:

$$-M(x)-V(x)\Delta x+\frac{1}{2}q\left(\Delta x\right)^2+M(x+\Delta x)=0. \tag{C.7}$$

After dividing both sides of the equation by Δx and subsequently taking its limit going to zero, the following is obtained:

$$\frac{\partial M(x)}{\partial x}=V(x). \tag{C.8}$$

By substituting the kinematic relations (C.1) into the constitutive relation (C.2) and the moment equilibrium (C.8) into the vertical force equilibrium (C.6), two second-order partial differential equations are obtained:

$$\begin{aligned} M(x)&=-EI\frac{\partial^2 w(x,t)}{\partial x^2}\\ \frac{\partial^2 M(x)}{\partial x^2}&=\rho\frac{\partial^2 w(x,t)}{\partial t^2}-q. \end{aligned} \tag{C.9}$$

These second-order partial differential equations can in turn be substituted in each other to form another partial differential equation. Upon assuming that the bending rod is prismatic, i.e. EI is constant, the fourth-order partial differential equation reads:

$$EI\frac{\partial^4 w(x,t)}{\partial x^4}+\rho\frac{\partial^2 w(x,t)}{\partial t^2}=q. \tag{C.10}$$

Figure C.2 displays the free-body diagram of a bending rod subjected to an axial compression P.

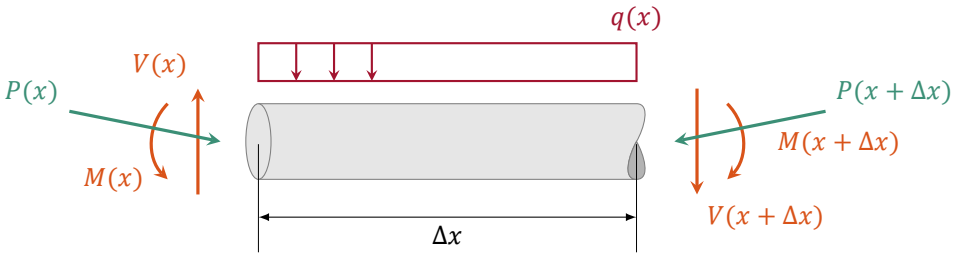

Figure C.2: Free-body diagram of an infinitesimal bending-rod element subjected to an axial compression.

Due the axial compression, a fourth equation is introduced. This equation is a geometrical relation, linking the axial force to its horizontal and vertical components. For the vertical component it holds that:

$$V_p = H\frac{\partial w(x,t)}{\partial x}, \tag{C.11}$$

whereas the horizontal component becomes:

$$H = P\cos\alpha. \tag{C.12}$$

By assuming that the rotation angle is infinitesimal, i.e. $\alpha \lll 1$, it holds, by definition, that $\cos\alpha \approx 1$:

$$H \approx P. \tag{C.13}$$

Therefore, the vertical component can be expressed as:

$$V_p = P\frac{\partial w(x,t)}{\partial x}. \tag{C.14}$$

The inclusion of the axial compression influences the vertical force equilibrium such that relation (C.6) becomes:

$$\frac{\partial V(x)}{\partial x} = \rho\frac{\partial^2 w(x,t)}{\partial t^2} + \frac{\partial V_p(x)}{\partial x} - q. \tag{C.15}$$

Upon substituting the moment equilibrium (C.8) in the new vertical equilibrium (C.15), the fourth-order partial differential equation reads:

$$EI\frac{\partial^4 w(x,t)}{\partial x^4} + P\frac{\partial^2 w(x,t)}{\partial x^2} + \rho\frac{\partial^2 w(x,t)}{\partial t^2} = q. \tag{C.16}$$

This equation of motion can be used to analyse the wave propagation within a bending rod subjected to an axial compression.

C.1.2. Influence of the axial load on the frequency

The free oscillations of the bending rod ($q = 0$) can be examined by considering the homogeneous solution,

$$w(x,t) = W(x)e^{i\omega t}, \tag{C.17}$$

which, upon substitution in relation (C.16), yields:

$$EI\frac{\partial^4}{\partial x^4}\left(W(x)e^{i\omega t}\right) + P\frac{\partial^2}{\partial x^2}\left(W(x)e^{i\omega t}\right) + \rho\frac{\partial^2}{\partial t^2}\left(W(x)e^{i\omega t}\right) = 0. \tag{C.18}$$

By evaluating the derivatives, the above is further elaborated to:

$$EI\frac{d^4W(x)}{dx^4} + P\frac{d^2W(x)}{dx^2} - \rho\omega^2 W(x) = 0. \tag{4.4}$$

The influence of the axial compression on the frequency ω, and thus the wave velocity, can be observed through the substitution of the fundamental mode shape,

$$W(x) = A\sin\left(\frac{\pi x}{l}\right), \tag{4.9}$$

in the fourth-order differential equation (4.4):

$$\begin{aligned} EI\frac{d^4}{dx^4}\left[A\sin\left(\frac{\pi x}{l}\right)\right] + P\frac{d^2}{dx^2}\left[A\sin\left(\frac{\pi x}{l}\right)\right] - \rho\omega^2 A\sin\left(\frac{\pi x}{l}\right) = 0 \\ A\sin\left(\frac{\pi x}{l}\right)\left[EI\left(\frac{\pi}{l}\right)^4 - P\left(\frac{\pi}{l}\right)^2 - \rho\omega^2\right] = 0 \Longrightarrow EI\left(\frac{\pi}{l}\right)^4 - P\left(\frac{\pi}{l}\right)^2 - \rho\omega^2 = 0. \end{aligned} \tag{C.19}$$

From this, the frequency can be expressed in terms of the axial compression with:

$$\begin{aligned}\omega &= \sqrt{\frac{EI}{\rho}\left(\frac{\pi}{l}\right)^4 - \frac{P}{\rho}\left(\frac{\pi}{l}\right)^2} \\ &= \left(\frac{\pi}{l}\right)^2 \sqrt{\frac{EI}{\rho} - \frac{P}{\rho}\left(\frac{l}{\pi}\right)^2}.\end{aligned} \tag{C.20}$$

The above can be further elaborated with:

$$\begin{aligned}\frac{\omega}{2\pi} &= \frac{\pi}{2l^2}\sqrt{\frac{EI}{\rho} - \frac{P}{\rho}\left(\frac{l}{\pi}\right)^2} \\ &= \frac{\pi}{2l^2}\sqrt{\frac{EI}{\rho}\left(1 - \frac{P}{EI}\frac{l^2}{\pi^2}\right)},\end{aligned} \tag{C.21}$$

which can be simplified to:

$$\frac{\omega}{2\pi} = \frac{c}{\lambda} = \frac{\pi}{2l^2}\sqrt{\frac{EI}{\rho}\left(1 - \frac{P}{P_c}\right)}, \tag{4.10}$$

where λ denotes the wavelength and P_c – the buckling load:

$$P_c = \frac{EI\pi^2}{l^2}. \tag{4.11}$$

If the axial load is assumed to be a tensile force, $T = -P$, and the bending stiffness of the rod is reduced to zero, relation (C.21) becomes:

$$\frac{\omega}{2\pi} = \frac{c}{\lambda} = \frac{1}{2l}\sqrt{\frac{T}{\rho}}, \tag{4.12}$$

which describes the frequency of a string under tension.

C.2. Acoustoelastic effect

The relation between the wave velocity and the stress applied to a medium is denoted as the acoustoelastic effect. Based on the expressions found by Hughes and Kelly [13], Lillamand et al. [18] have derived a linear relation between the relative wave-velocity change of a medium and the stress applied on this medium. This section covers the derivation of the linearised formulation of the acoustoelastic effect.

C.2.1. Reformulation of the wave velocity

For the purpose of finding an expression for the acoustoelastic effect, it is convenient to revise the formulation of the wave velocity of a stressed medium. As has been shown in Chapter 2, the longitudinal-wave velocity of medium which is stressed parallel to its propagation direction is defined as:

$$c_{xx}{}^{\sigma_{xx}} = \sqrt{\frac{\lambda + 2\mu \pm \frac{\sigma_{xx}}{3K}\left[2l + \lambda + \frac{\lambda+\mu}{\mu}(4\lambda + 4m + 10\mu)\right]}{\rho_a}}. \tag{2.79}$$

This expression can be written as a summation of stress-independent part and a stress-dependent part:

$$c_{xx}{}^{\sigma_{xx}} = \sqrt{\frac{\lambda + 2\mu}{\rho_a} \pm \frac{2l + \lambda + \frac{\lambda+\mu}{\mu}(4\lambda + 4m + 10\mu)}{3K\rho_a}\sigma_{xx}}, \tag{C.22}$$

where the stress-independent part denotes the initial wave velocity,

$$c_{xx}{}^{0} = \sqrt{\frac{\lambda + 2\mu}{\rho_a}}. \tag{C.23}$$

Upon factorising $c_{xx}{}^{0}$ in relation (C.22), the wave velocity of the stressed medium can be expressed in terms of the initial wave velocity:

$$\begin{aligned} c_{xx}{}^{\sigma_{xx}} &= \sqrt{\frac{\lambda + 2\mu}{\rho_a}} \sqrt{1 \pm \frac{2l + \lambda + \frac{\lambda + \mu}{\mu}(4\lambda + 4m + 10\mu)}{3K(\lambda + 2\mu)} \sigma_{xx}} \\ &= c_{xx}{}^{0} \sqrt{1 \pm \frac{2l + \lambda + \frac{\lambda + \mu}{\mu}(4\lambda + 4m + 10\mu)}{3K(\lambda + 2\mu)} \sigma_{xx}}. \end{aligned} \tag{C.24}$$

C.2.2. Relative wave-velocity change

When considering the wave velocity as a function of the stress σ_{xx}, the expression above can be approximated within the proximity of a stress with:

$$c_{xx}{}^{\sigma_{xx}}(\sigma_{xx}) = c_{xx}{}^{\sigma_{xx}}(a) + \frac{\partial c_{xx}{}^{\sigma_{xx}}(a)}{\partial \sigma_{xx}}(\sigma_{xx} - a). \tag{C.25}$$

The linearisation at zero stress, i.e. $a = 0$, gives an accurate approximation of the wave velocity subjected to stresses. Upon substituting expression (C.24) in relation (C.25) and using $a = 0$, the following is eventually obtained:

$$c_{xx}{}^{\sigma_{xx}} \approx c_{xx}{}^{0} \left(1 + \frac{2l + \lambda + \frac{\lambda + \mu}{\mu}(4\lambda + 4m + 10\mu)}{6K(\lambda + 2\mu)} \sigma_{xx}\right). \tag{C.26}$$

The above can be written in a more general form with the index notation:

$$c_{ij}{}^{\sigma_{kl}} = c_{ij}{}^{0}\left(1 + A_{ijkl}\sigma_{kl}\right), \tag{4.17}$$

where the fourth-order tensor A_{ijkl} denotes the acoustoelastic constant. This expression can be further elaborated to:

$$\Delta c_{ij}(\sigma_{kl}) = A_{ijkl}\sigma_{kl}, \tag{4.18}$$

where Δc_{ij} denotes the relative wave-velocity change:

$$\Delta c_{ij} = \frac{c_{ij}{}^{\sigma_{kl}} - c_{ij}{}^{0}}{c_{ij}{}^{0}}. \tag{4.19}$$

By repeating relation (C.26) for other waveforms, the different expressions for the acoustoelastic constants are determined. These expressions can be assembled in the following matrix:

$$\boldsymbol{A} = \begin{pmatrix} A_{xxxx} & A_{xxyy} & A_{xxzz} & A_{xxxy} & A_{xxxz} & A_{xxyx} & A_{xxyz} & A_{xxzx} & A_{xxzy} \\ A_{yyxx} & A_{yyyy} & A_{yyzz} & A_{yyxy} & A_{yyxz} & A_{yyyx} & A_{yyyz} & A_{yyzx} & A_{yyzy} \\ A_{zzxx} & A_{zzyy} & A_{zzzz} & A_{zzxy} & A_{zzxz} & A_{zzyx} & A_{zzyz} & A_{zzzx} & A_{zzzy} \\ A_{xyxx} & A_{xyyy} & A_{xyzz} & A_{xyxy} & A_{xyxz} & A_{xyyx} & A_{xyyz} & A_{xyzx} & A_{xyzy} \\ A_{xzxx} & A_{xzyy} & A_{xzzz} & A_{xzxy} & A_{xzxz} & A_{xzyx} & A_{xzyz} & A_{xzzx} & A_{xzzy} \\ A_{yxxx} & A_{yxyy} & A_{yxzz} & A_{yxxy} & A_{yxxz} & A_{yxyx} & A_{yxyz} & A_{yxzx} & A_{yxzy} \\ A_{yzxx} & A_{yzyy} & A_{yzzz} & A_{yzxy} & A_{yzxz} & A_{yzyx} & A_{yzyz} & A_{yzzx} & A_{yzzy} \\ A_{zxxx} & A_{zxyy} & A_{zxzz} & A_{zxxy} & A_{zxxz} & A_{zxyx} & A_{zxyz} & A_{zxzx} & A_{zxzy} \\ A_{zyxx} & A_{zyyy} & A_{zyzz} & A_{zyxy} & A_{zyxz} & A_{zyyx} & A_{zyyz} & A_{zyzx} & A_{zyzy} \end{pmatrix}. \tag{4.20}$$

The entries of this matrix are defined differently according to the theories of both Murnaghan and Biot. For Murnaghan's theory, a total of five different combinations of stress orientation and wave orientation is found, resulting in five different expressions for the acoustoelastic constants:

$$\boldsymbol{A_{Murnaghan}} = \begin{pmatrix} \Upsilon & \Phi & \Phi \\ \Phi & \Upsilon & \Phi \\ \Phi & \Phi & \Upsilon \\ \mathrm{X} & \Psi & \Omega \\ \mathrm{X} & \Omega & \Psi \\ \Psi & \mathrm{X} & \Omega \\ \Omega & \mathrm{X} & \Psi \\ \Psi & \Psi & \mathrm{X} \\ \Omega & \Psi & \mathrm{X} \end{pmatrix}, \tag{4.21}$$

where the acoustoelastic constants are defined as:

$$\begin{aligned} \Upsilon &= \frac{2l + \lambda + \frac{\lambda + \mu}{\mu}(4\lambda + 4m + 10\mu)}{6K(\lambda + 2\mu)} \\ \Phi &= \frac{2l + \lambda - \frac{\lambda}{2\mu}(4\lambda + 4m + 10\mu)}{6K(\lambda + 2\mu)} \\ \mathrm{X} &= \frac{m + \frac{\lambda n}{4\mu} + 4\lambda + 4\mu}{6K\mu} \\ \Psi &= \frac{m + \frac{\lambda n}{4\mu} + \lambda + 2\mu}{6K\mu} \\ \Omega &= \frac{\lambda + m - \frac{\lambda + \mu}{\mu}\left(\frac{3\mu\lambda}{\lambda + 2\mu} + \frac{1}{2}n\right)}{6K\mu}. \end{aligned} \tag{4.22}$$

For Biot's theory, the matrix is defined as:

$$\boldsymbol{A_{Biot}} = \frac{1}{4\mu}\begin{pmatrix} 0 & 0 & 0 \\ 0 & 0 & 0 \\ 0 & 0 & 0 \\ 1 & -1 & 0 \\ 1 & 0 & -1 \\ -1 & 1 & 0 \\ 0 & 1 & -1 \\ -1 & -1 & 1 \\ 0 & -1 & 1 \end{pmatrix}. \tag{4.23}$$

D

Preliminary experiments

For the purpose of obtaining reliable results, it is important to perform several preliminary experiments. During these experiments, the material parameters of the test specimens are validated. In order for the specimens to be representative, their initial wave velocity as well as their elastic parameters should be within the range of the theoretical estimated values. In addition, the proper working of the ultrasonic transducers must be verified. This has been done by searching for the centre frequency and ensuring that the emitted wave signal has a significant amplitude.

D.1. Initial wave velocity

For the purpose of verifying the proper working of the ultrasonic transducers, some elementary measurements have been performed. During these measurements, the initial wave velocity of the specimens were estimated through handpicking with the ToF method. Here, a distinction has been made between the large transducers and the small transducers. For these measurements S-wave transducers have been used. The round shaped housing of these transducers, however, create boundary effects which result in additional P-wave motion. This enables the identification of both the P -and S-wave arrivals of the specimens.

D.1.1. Large transducers

The large transducers have been applied on the flat sides of the cylindrical specimens. Subsequently a signal is emitted along the height of the specimens. Table D.1 displays a summary of the specimens which have been used for these measurements.

Table D.1: Test specimens used for the acoustic measurements and their respective dimensions.

Specimen	Type	Height h [mm]	Diameter d [mm]	Mass m [g]
CP-1	Cement paste	71.78	32.66	123.05
CC-2	Concrete	70.53	29.82	111.92
CP-3	Cement paste	70.02	32.20	116.17
CC-4	Concrete	64.48	29.79	101.80

The P -and S-wave arrivals of these specimens have then been identified with the ToF method, like depicted in Figure D.1. The arrival of the P-wave, t_P, is indicated by the first break of the wave whereas the arrival of the S-wave, t_S, is indicated by the abrupt increase in amplitude. The initial P -and S-wave velocities are then determined from these identified arrival times with

$$\begin{aligned} c_P &= \frac{h}{t_P} \\ c_S &= \frac{h}{t_S}, \end{aligned} \tag{D.1}$$

respectively.

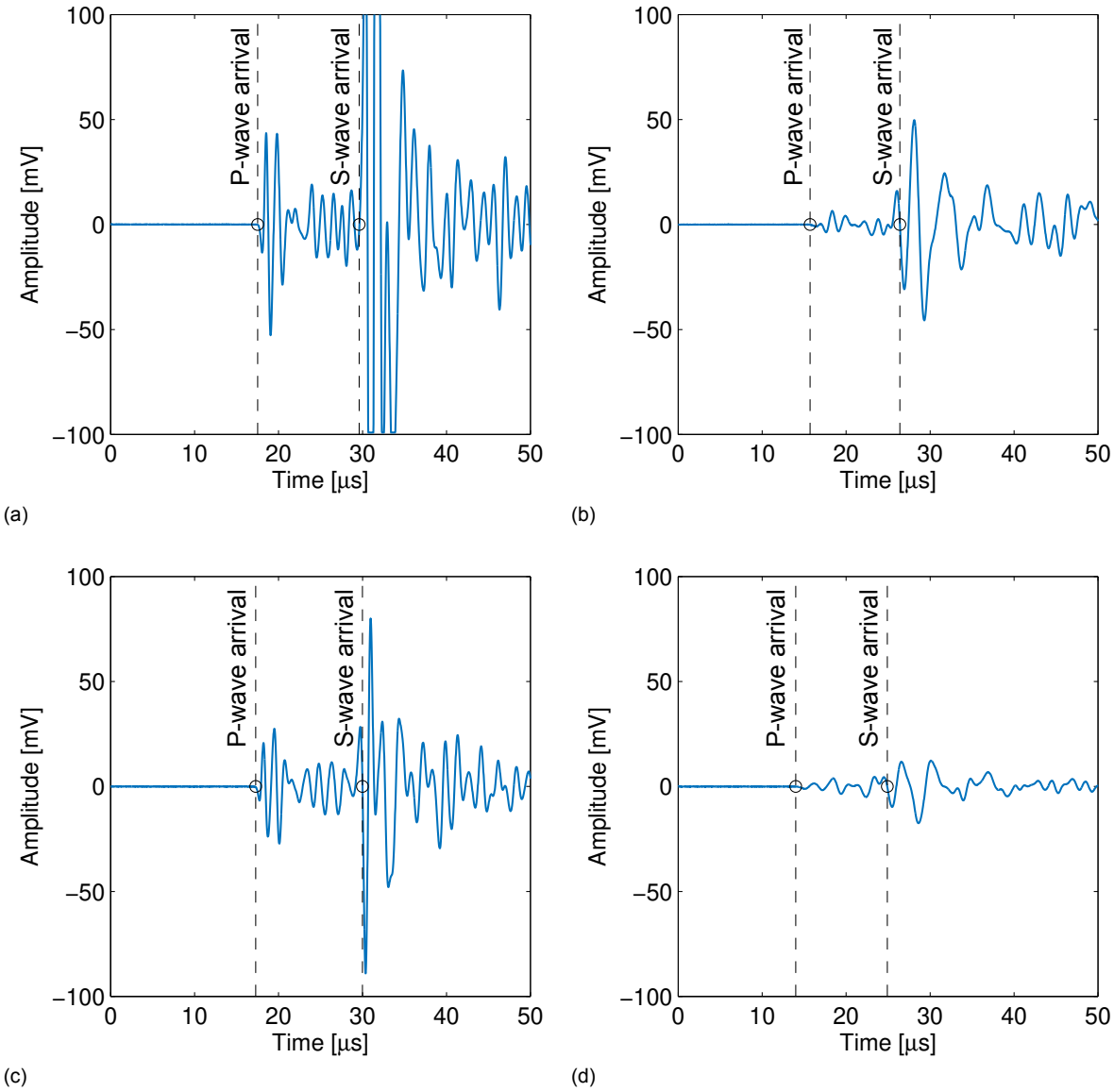

Figure D.1: Identification of the arrival times with the ToF method. Signals emitted along the axial direction by the large transducers at a frequency of 1 MHz. (a) Specimen CP-1. (b) Specimen CC-2. (c) Specimen CP-3. (d) Specimen CC-4.

The identified arrival times and the corresponding wave velocities following from the large transducers are displayed in Table D.2.

Table D.2: Identified arrival times and initial wave velocities of the specimens along the axial direction.

Specimen	Arrival t_P [µs]	Arrival t_S [µs]	P-wave velocity c_P [m/s]	S-wave velocity c_S [m/s]
CP-1	17.50	29.60	4102	2425
CC-2	15.70	26.40	4492	2672
CP-3	17.20	30.00	4071	2334
CC-4	14.00	24.90	4606	2590
Theoretically estimated values			4000	2500

From the data in Table D.2 it can be concluded that the initial wave velocities of the specimens are within the proximity of the expected theoretical values. Furthermore, it can be observed that the initial wave velocities of the concrete specimens are larger than those of the cement-paste specimens.

D.1.2. Small transducers

Similar to the large transducers, the small transducers have been applied at the flat sides of the specimens. In addition, they have also been applied on the curved sides of the cylindrical specimens. The latter enables the measurement of the initial wave velocity along the radial direction of the specimens. For these measurements, wave signals have been emitted along both height and the diameter of specimen CP-1. Figure D.2 displays the time signatures and the identification of the arrivals in the axial and radial direction, respectively.

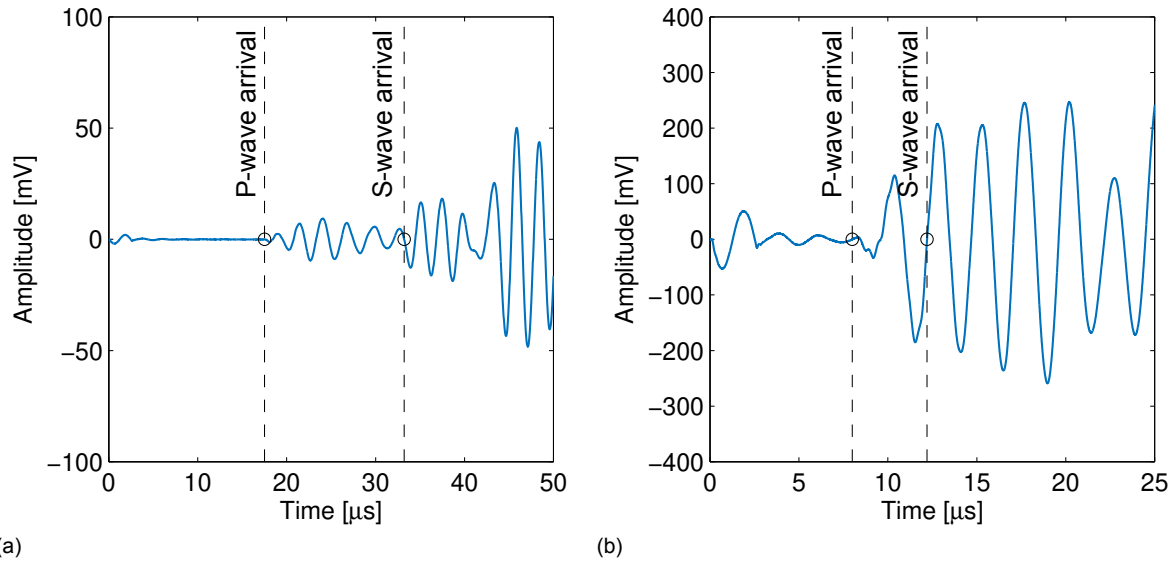

Figure D.2: Identification of the arrival times with the ToF method. Signals emitted through specimen CP-1 by the small transducers at a frequency of 400 kHz. (a) Signal along the axial direction. (b) Signal along the radial direction.

The identified arrival times and the corresponding wave velocities following from the small transducers are displayed in Table D.3.

Table D.3: Identified arrival times and initial wave velocities of signals emitted through specimen CP-1 by the small transducers.

Propagation direction	Arrival t_P [µs]	Arrival t_S [µs]	P-wave velocity c_P [m/s]	S-wave velocity c_S [m/s]
Axial	17.50	33.22	4102	2161
Radial	8.00	12.20	4083	2677
Theoretically estimated values			4000	2500

From the amplitudes of the time signatures in Figure D.2 it can be concluded that the small transducers function properly. By comparing the identified initial wave velocities of specimen CP-1 (Figures D.2 and D.3), it is observed that the initial P-wave velocities are coherent. The initial S-wave velocities, however, show less coherence. This can be attributed due to the uncertain S-wave arrival, resulting from the interference of P -and PS-wave reflections.

D.2. Uniaxial compression

The second-order elastic parameters are determined through the cyclic uniaxial compression of the specimens. During this load cycle, the specimens are loaded from 0 to 20 MPa with a partial unloading to 10 MPa. Following from this uniaxial compression are the stress-strain diagrams, depicted in Figure D.3. The axial strain is based on the measurement from the vertical LVDT, which includes the deformation of the setup. Therefore, in order to obtain the actual axial strain of the specimen, the data from the vertical LVDT must be calibrated.

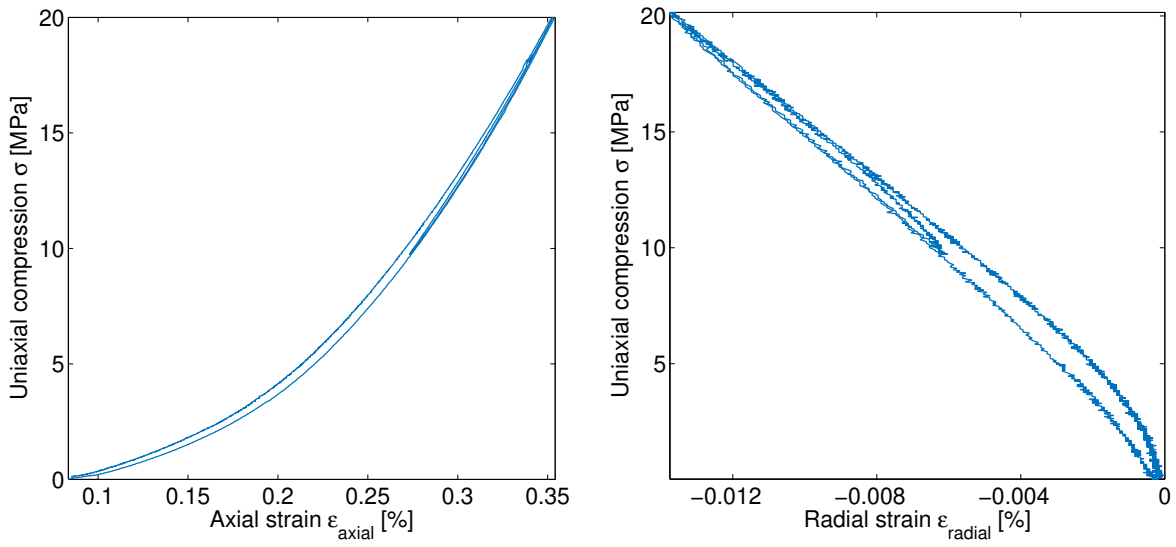

(a) (b)

Figure D.3: Stress-strain diagrams of specimen CP-3 from the uniaxial compression. Data acquired from cyclic loading ranging from 0 to 20 MPa. (a) Strain measured by the vertical LVDT. (b) Strain measured by the circumferential LVDT.

D.2.1. Calibration

The strain displayed in Figure D.3a contains some deformation following from the setup. In order to calibrate this data, an aluminum cylinder has been subjected to the same uniaxial compression as the test specimens. Figure D.4 displays a photo of the aluminum cylinder in the experimental setup as well as the resulting force-displacement diagram.

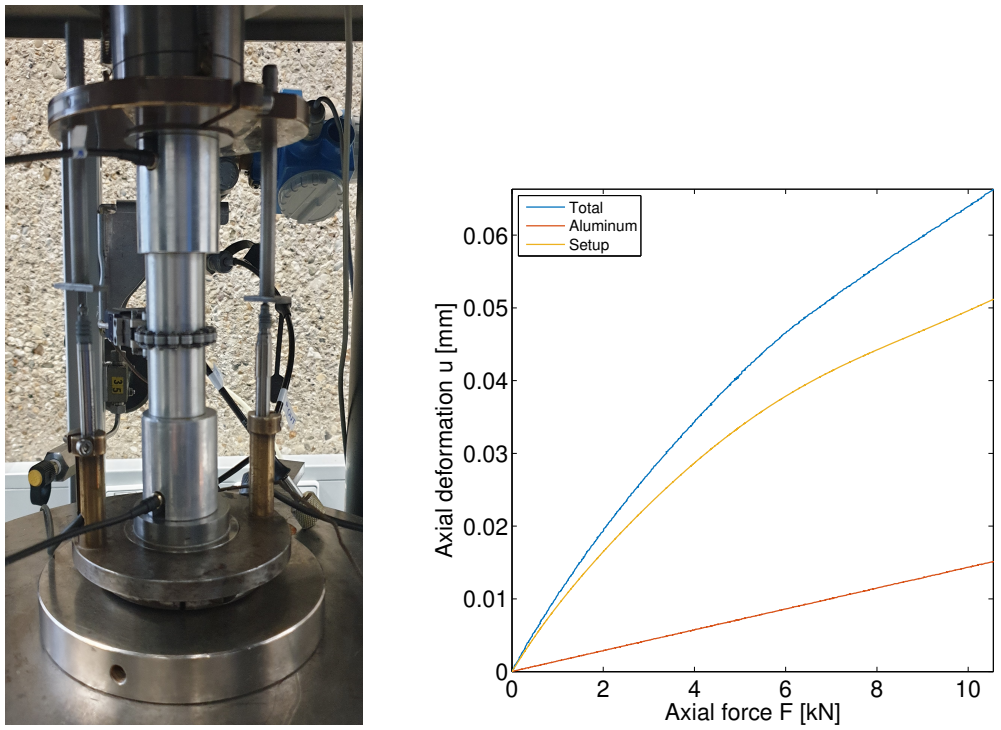

(a) (b)

Figure D.4: Uniaxial compression of an aluminum cylinder for the purpose of calibrating the axial deformation measurements; h = 70.12 mm, d = 29.84 mm, E = 70 GPa. (a) Photo of the calibration setup. (b) Force-displacement graph following from the uniaxial compression of the aluminum cylinder: second loading branch from 10 MPa to 20 MPa (graph shifted to the origin).

Since the material parameters of this aluminum cylinder are known, it is possible to determine the axial deformation of the setup with:

$$u_{setup} = u_{total} - u_{aluminum}. \tag{D.2}$$

Here, the axial deformation of the aluminum, $u_{aluminum}$, is obtained through Hooke's law:

$$u_{aluminum} = \frac{Fh}{EA}, \tag{D.3}$$

where A denotes the surface area of the ground plane of the cylinder.

D.2.2. Second-order elastic parameters

The raw data from the vertical LVDT has been calibrated by removing the axial deformation of the setup. The Young's moduli of the specimens have then been determined through the tangent to the stress-strain diagrams, like depicted in Figure D.5.

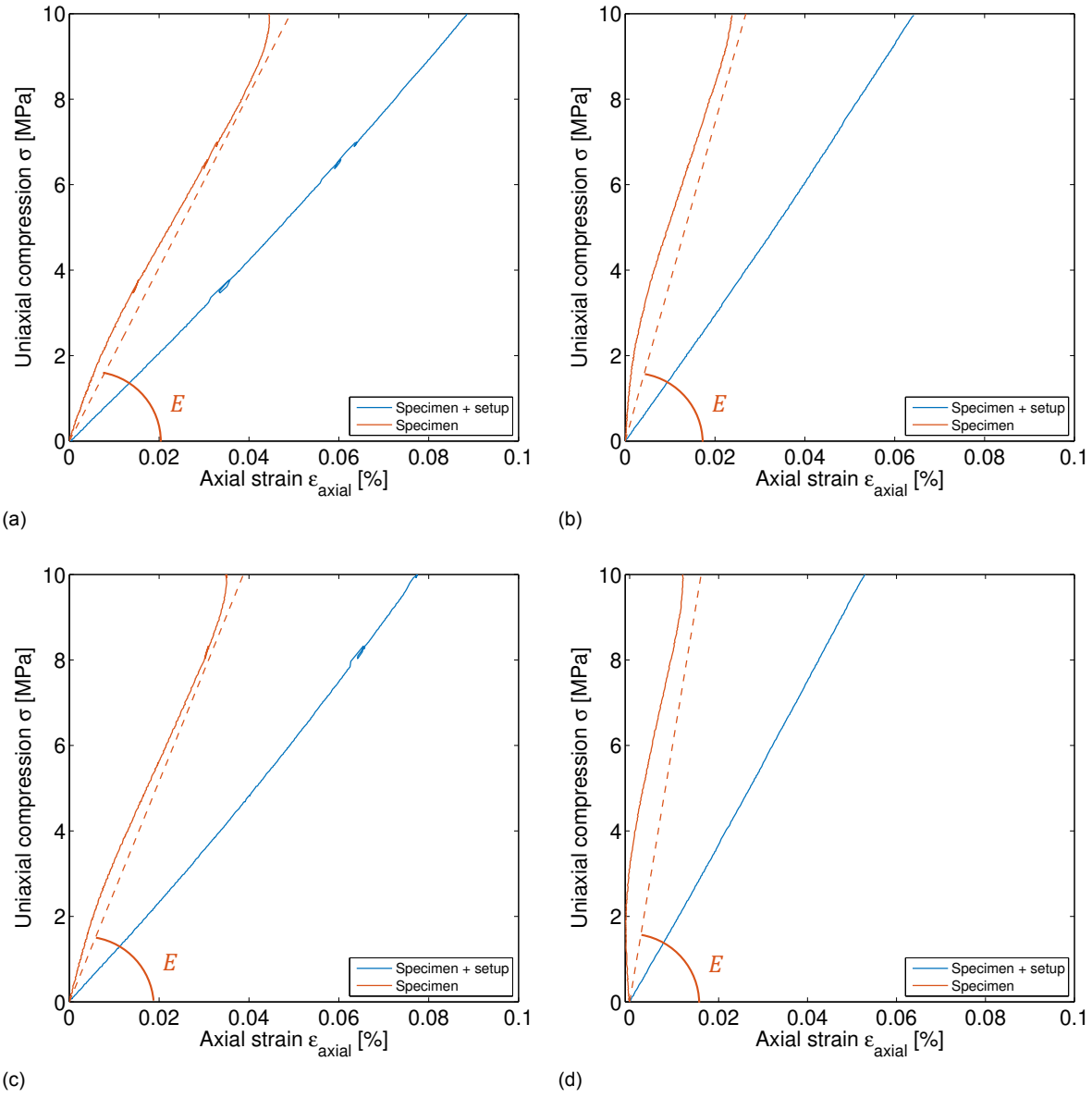

Figure D.5: Stress-strain graphs after the calibration: second loading branch from 10 MPa to 20 MPa (graph shifted to the origin). (a) Specimen CP-1. (b) Specimen CC-2B. (c) Specimen CP-3. (d) Specimen CC-4B.

The axial strain and radial strain of the specimens are then used to determine Poisson's ratio of the specimens:

$$\nu = -\frac{\epsilon_{radial}}{\epsilon_{axial}}. \tag{D.4}$$

Figure D.6 displays the development of Poisson's ratio as the compression on the test specimens increases.

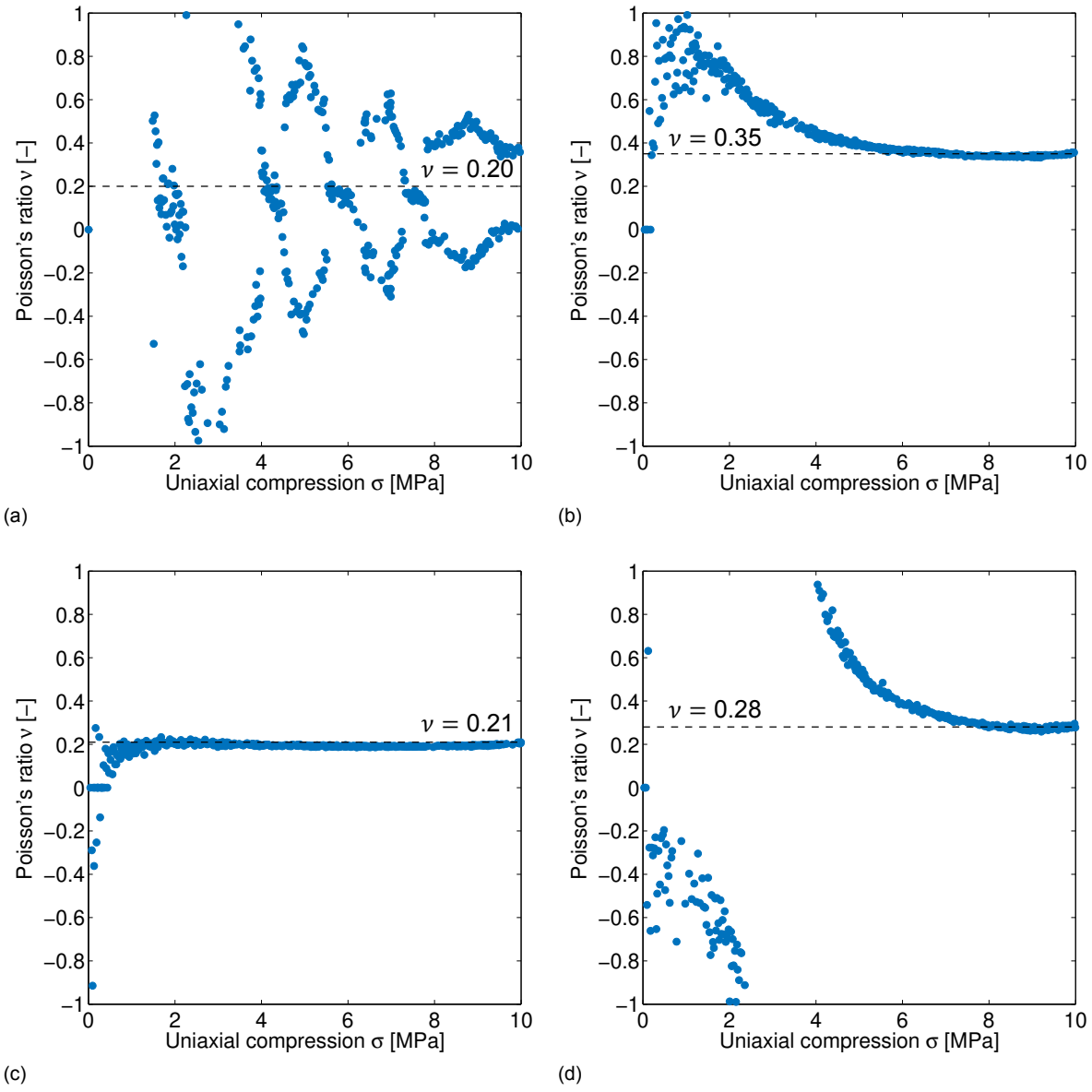

Figure D.6: Development of Poisson's ratio as compression increases: second loading branch from 10 MPa to 20 MPa (graph shifted to the origin). (a) Specimen CP-1. (b) Specimen CC-2B. (c) Specimen CP-3. (d) Specimen CC-4B.

The strange scatter witnessed in Figure D.6a is caused by the poor attachment of the circumferential LVDT during the uniaxial compression of specimen CP-1. In spite of this inaccurate data, it can be observed that the outliers are approximately centered around $\nu = 0.20$. The large value for Poisson's ratio of specimen CC-2B could be attributed to a local inhomogeneity of the specimen which was close to the circumferential LVDT.

Both the Young's moduli and Poisson's ratio of the final test specimens have been summarised in Table D.4.

Table D.4: Overview of the final test specimens and their second-order elastic parameters.

Specimen	Young's modulus E [GPa]	Poisson's ratio ν [$-$]	λ [GPa]	μ [GPa]
CP-1	20.30	0.20	5.64	8.46
CC-2B	37.25	0.35	32.19	13.80
CP-3	25.80	0.21	7.72	10.66
CC-4B	51.10	0.28	25.40	19.96
Expected values	20-40	0.20		

E

MATLAB script: Stretching Technique

E.1. Stretching code

```
function [EPS,CC,COEF_CORR,ERROR]=stretching_code(data,ref,time,epsilon,
    time_window,DTAU,message)

% Input parameters:

% data        : Matrix of n data signals of N samples [N x n]
% ref         : Reference signal [N x 1]
% time        : Time axis [N x 1]
% epsilon     : Range of stretching [min:step:max]
% time_window: Time window boundaries in samples (positive integer)
% DTAU        : Zero lag time (origin of stretching)

% Output parameters:

% EPS         : Stretching factors [n x 1]
% CC          : Maximum cross-correlation coefficients [n x 1]
% COEF_CORR   : Cross-correlation coefficients [N x n]
% ERROR       : Error

%% Code

ERROR=0;
if exist('data','var')==0;disp('error : no input data');CC=0;EPS=0;ERROR
    =1;return;end
if exist('ref','var')==0;ref=mean(data,2);end
if exist('message','var')==0;message='?-?';end
if exist('DTAU','var')==0;DTAU=0;disp('defaustretching_LCPCIt DTAU=0');end
%if exist('fe','var')==0;fe=1;disp('default sampling freq=1 Hz');end
if exist('time_window','var')==0;time_window=[1:size(data,1)];disp('
    default time window = full record');end
if exist('epsilon','var')==0;epsilon=[-1e-2:1e-4:1e-2];disp('default
    epsilon range=[-10^{-2} 10^{-2}] with 10^{-4} step');end

CC=zeros(size(data,2),1);
EPS=zeros(size(data,2),1);

string_disp=['processing strech ' message];

```

```
COEF_CORR=zeros(length(epsilon),size(data,2));
for EPS_index=1:length(epsilon)
    time2=(time+DTAU)*(1+epsilon(EPS_index)); % Stretched time axis
    synt=interp1(time,ref,time2,'spline');

    for DATE_index=1:size(data,2)
        temp=corrcoef(synt(time_window),data(time_window,DATE_index));
        COEF_CORR(EPS_index,DATE_index)=temp(2);
    end

end
COEF_CORR;
[CC b]=max(COEF_CORR);CC=CC';
EPS=epsilon(b)';
```

E.2. Cross-correlation

```
%% Script for performing cross-correlation to determine the relative wave
    velocity change
%
% Uses the following function:
%
% data_raw.m            : Loads the n data signals of N samples [n x N]
% stretching_code.m     : Calculates the cross-correlation of reference
    and data

%% Load the data

% Define the input parameters of the data_raw.m function

test = 'fin';
transducer = 'small';
orientation = 'axial';
wavetype = 'S';
frequency = '400kHz';
sample = 'cement paste 3';

% Run the data_raw.m functions

[n, name, TDM_raw, E_raw, TA, FA, df, sigma] = data_raw(test, transducer,
    orientation, wavetype, frequency, sample);

% Define the input parameters of the stretching_code.m function

data = TDM_raw.';                   % Transposes the data signals into
    column vectors
ref = data(1,:);                    % The reference signal is the first
    trace of the data
time = TA.';                        % Transposes the time axis into a
    column vector
epsilon = [-10e-2:1e-4:10e-2];      % Range of stretching from -10 to 10%
t_start = 25;                       % Start of time window at 25
    microseconds
t_end = 40;                         % End of time window at 40
    microseconds

t1 = find(TAc>=t_start,1,'first');  % Datapoint of first boundary
```

```
33 t2 = find(TAc>=t_end,1,'first');      % Datapoint of last boundary
34 time_window = t1:t2;                  % Time window interval in datapoints
35 DTAU = 0;                             % Origin of the stretching/stressing
36
37 % Run the stretching_code.m function
38
39 [EPS,CC,COEF_CORR,ERROR]=stretching_code(data,ref,time,epsilon,time_window
       ,DTAU);
```

Bibliography

[1] Keiiti Aki and Paul G. Richards. *Quantitative seismology*, volume II. University Science Books, Mill Valley, second edition, 1980. ISBN 9781891389634.

[2] Teodor M. Atanackovic and Ardeshir Guran. *Theory of Elasticity for Scientists and Engineers*. Birkhäuser, Boston, 2000. ISBN 9781461213307.

[3] Maurice A. Biot. Theory of Elasticity with Large Displacements and Rotations. *Proceedings of the Fifth International Congress of Applied Mechanics*, (3):117 – 122, 1938. URL http://www.pmi.ou.edu/Biot2005/papers/FILES/031.PDF.

[4] Maurice A. Biot. The influence of initial stress on elastic waves. *Journal of Applied Physics*, 11(8):522–530, 1940. ISSN 00218979. doi: 10.1063/1.1712807. URL https://hal.archives-ouvertes.fr/hal-01368866/document.

[5] Maurice A. Biot. *Mechanics of Incremental Deformations*, volume 280. New York, 1965. doi: 10.1016/0016-0032(65)90053-0. URL https://olemiss.edu/sciencenet/poronet/biot.pdf.

[6] Anders Brandt. *Noise and Vibration Analysis : Signal Analysis and Experimental Procedures*. John Wiley & Sons Ltd., Chichester, 1 edition, 2011. ISBN 9780470746448.

[7] Léon Brillouin. Sur les tensions de radiation. *Annales de Physique*, 10(4):528–586, 1925. ISSN 0003-4169. doi: 10.1051/anphys/192510040528.

[8] Renye Cai. *Original strain energy density functions for modeling of anisotropic soft biological tissue*. PhD thesis, l'Université Bourgogne Franche-Comté, 2017. URL https://tel.archives-ouvertes.fr/tel-01870267/document.

[9] Inc. Chegg. Piezoelectric Effect, 2020. URL https://www.chegg.com/learn/physics/introduction-to-physics/piezoelectric-effect.

[10] J.S. Chitode. *Digital Signal Processing*. Technical Publications Pune, Pune, 1st edition, 2008. ISBN 9788184314243.

[11] Simen Eldevik. *Measurement of non-linear acoustoelastic effect in steel using acoustic resonance*. PhD thesis, University of Bergen, 2014.

[12] Patrik Fröjd and Peter Ulriksen. Frequency selection for coda wave interferometry in concrete structures. *Ultrasonics*, 80:1–8, 9 2017. ISSN 0041624X. doi: 10.1016/j.ultras.2017.04.012. URL https://linkinghub.elsevier.com/retrieve/pii/S0041624X17301798.

[13] D. S. Hughes and J. L. Kelly. Second-Order elastic deformation of solids. *Physical Review*, 92(5):1145–1149, 1953. ISSN 0031899X. doi: 10.1103/PhysRev.92.1145.

[14] Iv-Infra. Hoe proefbelasten van bruggen miljardeninvesteringen voor vervanging kan voorkomen, 2018. URL https://iv-groep.nl/nl/over-iv/blog/2018/proefbelasten.

[15] C Kevinly, F Zhang, Y Yang, D Draganov, and C Weemstra. A study on monitoring multi-scale concrete members with coda-wave interferometry using embedded transducers. In *Bridge Maintenance, Safety, Management, Life-Cycle Sustainability and Innovations*, pages 2413–2418. 2021. doi: 10.1201/9780429279119-330.

[16] Eva O.L. Lantsoght, Yuguang Yang, Cor van der Veen, Ane de Boer, and Dick A. Hordijk. Ruytenschildt Bridge: Field and laboratory testing. *Engineering Structures*, 128:111–123, 2016. ISSN 18737323. doi: 10.1016/j.engstruct.2016.09.029. URL http://dx.doi.org/10.1016/j.engstruct.2016.09.029.

[17] Eric Larose and Stephen Hall. Monitoring stress related velocity variation in concrete with a 2×10−5 relative resolution using diffuse ultrasound. *The Journal of the Acoustical Society of America*, 125(4):1853–1856, 2009. ISSN 0001-4966. doi: 10.1121/1.3079771. URL https://hal.archives-ouvertes.fr/hal-00352370/document.

[18] Ivan Lillamand, Jean Franois Chaix, Marie Aude Ploix, and Vincent Garnier. Acoustoelastic effect in concrete material under uni-axial compressive loading. *NDT and E International*, 43(8):655–660, 2010. ISSN 09638695. doi: 10.1016/j.ndteint.2010.07.001.

[19] A.V. Metrikine and A.W.C.M. Vrouwenvelder. *Structural Dynamics CT 4140: Part 2 - Wave Dynamics (Lecture notes)*. Delft, 2005.

[20] Gabriele Milone. *Numerical study of Stress Identification in Concrete using Coda-Wave Interferometry (MSc thesis)*. 2019. URL https://webthesis.biblio.polito.it/12328/1/tesi.pdf.

[21] Francis D. Murnaghan. Finite Deformations of an Elastic Solid. *American Journal of Mathematics*, 59(2):235–260, 1937.

[22] Francis D. Murnaghan. *Finite Deformation of an Elastic Solid*, volume 2. London, 1951. doi: https://doi.org/10.2307/3611182. URL https://archive.org/details/in.ernet.dli.2015.141741/page/n135/mode/1up.

[23] Carnot L. Nogueira and Kevin L. Rens. Acoustoelastic response of concrete under uniaxial compression. *ACI Materials Journal*, 116(3):21–33, 2019. ISSN 0889325X. doi: 10.14359/51714462.

[24] T. Planès and E. Larose. A review of ultrasonic Coda Wave Interferometry in concrete. *Cement and Concrete Research*, 53:248–255, 2013. ISSN 00088846. doi: 10.1016/j.cemconres.2013.07.009. URL http://dx.doi.org/10.1016/j.cemconres.2013.07.009.

[25] J.M.J Spijkers, A.W.C.M. Vrouwenvelder, and E.C. Klaver. *Structural Dynamics CT 4140: Part 1 - Structural Vibrations (Lecture notes)*. Delft, 2005.

[26] J.F.A.M. van Hoof. *One- and two-dimensional wave propagation in solids (MSc thesis)*. Eindhoven, 1994. URL https://pure.tue.nl/ws/files/46929429/639912-1.pdf.